



Bioengineering: Stratifying the Immune Response to Biomaterials

Amy Elizabeth Mawdesley

Translational and Clinical Research Institute

Newcastle University

July 2020

Thesis submitted in partial fulfilment of the requirements for the degree of Doctor of
Philosophy

Abstract

Early failure of Metal-on-Metal (MoM) joint implants is often due to adverse reaction to metal debris (ARMD). These MoM implants are composed of a cobalt-chromium (CoCr) alloy which generates nanoscale particles and metal ions. Cobalt ions can activate the innate immune receptor, Toll-like receptor 4 (TLR4), increasing secretion of inflammatory cytokines/chemokines.

For this study, CoCr particles were generated in a multi-directional pin-on-plate wear simulator and characterised for use in cell treatments. In human THP-1 macrophages, CoCr particles were found to increase secretion of pro-inflammatory chemokines and cytokines including IL-8, CCL2, CCL3, CCL4 and IL-1 β . The gene expression of *IL-8* and *CCL3* was also up-regulated in response to CoCr particles. The expression of these markers was found to be largely TLR4-dependent as a small molecule TLR4 antagonist, CLI-095, significantly reduced these observed effects.

Further investigation demonstrated that CoCr particles can also increase expression of the adhesion molecules *ICAM-1* and *VCAM-1* in the human endothelial cell line, HMEC-1. Furthermore, CoCr particle stimulation in HMEC-1 cells led to increased neutrophil migration in a chemotaxis assay. In periprosthetic tissue retrieved from patients undergoing hip and knee revision surgery, there was evidence of immune cell infiltration and the presence of macrophages and T cells.

THP-1 macrophages were also treated with aluminium and zirconium oxides which are commonly used in ceramic hip implants. Both treatments resulted in significant TLR4-dependent increases to *IL-8*, *CCL2*, *CCL3* and *CCL4* gene expression and protein secretion. Use of ATP to mimic 'danger' signalling following initial priming with ceramics caused significant increases to IL-1 β expression.

These data demonstrate that CoCr particles and ceramic oxides can induce an immune response by up-regulating the expression of pro-inflammatory chemokines by a mechanism that appears to be largely TLR4-dependent. This study demonstrates a potential role for innate immunological mechanisms in the development of ARMD in patients with failed prosthetic joint implants.

Acknowledgements

Firstly, I would like to give thanks to my supervisors Professor Alison Tyson-Capper, Professor John Kirby and Professor Joanne Tipper for their fantastic support throughout the entirety of this project and for encouraging me to make the most out of the last four years. It has been a hugely enjoyable experience. Special thanks must also go to Dr Helen Lawrence who I am incredibly grateful to have worked with during my previous MRes and who helped shape this project as well as providing invaluable experience for myself moving forward. I would also like to thank the Medical Research Council (MRC) for funding this project and the number of opportunities provided throughout.

My time at the University of Leeds learning a 'new trade' of engineering was made so much more of an easier and enjoyable experience thanks to Dr Saurabh Lal and everyone else who welcomed me at the Institute of Medical and Biological Engineering. I must also extend particular thanks to Professor Joanne Tipper for supporting me with this aspect of my project.

I would also like to thank both Professor David Deehan and Mr Jim Holland for always offering their support, clinical knowledge and helping set up the collection of patient tissue samples which were used in this project. I would also like to thank Dr Barry Toole for processing and analysing the samples used for inductively coupled plasma mass spectrophotometry. Additionally, I am thankful to Dr Jonathan Scott for the collection and isolation of neutrophils which were used in the chemotaxis assays for this study. I am very grateful to Dr Jem Palmer for helping me with pretty much any technical issue I have had along the way as well as providing countless number of cells for culturing.

Thank you to all members of the Tyson-Capper lab group both past and present, Hannah, Soulaf, Sami, Vic and Shannon, you have all been great to work with and have always been there to either laugh with or listen to my rants when science just never seems to go quite right! I will miss working with you all. I would like to especially thank Shannon Jamieson whose hard work on the ceramic-mediated inflammatory response during her MRes project contributed to an important part of this thesis.

Extended thanks also go to the Kirby/Ali lab group who have been great friends and colleagues over the years. I am particularly grateful to Georgie and Chelsea, I could not have done this without either of you and your company for regular coffee/wine.

To my parents, I cannot thank you enough for everything you do for me, it means the world. In everything I do, I know that you are behind me all the way. Thank you for all the encouragement and for Dad telling me to be a scientist!

My final thanks go to Iain, you have truly been a rock for me over the past three years and have shown the upmost patience with me during final year stresses! I am so grateful for your love and support. I am sure you will be just as glad as I am to have this one ticked off. Hope you enjoy the read.

Contents

Abstract.....	iii
Acknowledgements.....	iv
List of Figures	xv
List of Tables	xx
Abbreviations.....	xxi
Chapter 1 : Introduction	1
1.1 Total Joint Replacements	1
1.1.1 Total hip replacement.....	1
1.1.2 Biomaterials in joint replacements.....	2
1.1.3 Change in patient demographics.....	3
1.1.4 The move towards Metal-on-Metal implants.....	5
1.1.5 Current status of biomaterials used in total hip replacements	6
1.2 Wear of Total Joint Replacements.....	9
1.2.1 Cobalt-chromium wear particles.....	11
1.2.2 Ceramic wear	12
1.3 Adverse Reaction to Metal Debris	13
1.3.1 Formation of inflammatory pseudotumours.....	14
1.3.2 Cobalt and chromium ion levels in patients with metal-on-metal prostheses	16
1.3.3 Osteolysis.....	17
1.3.4 Aseptic lymphocytic vasculitis-associated lesions (ALVAL)	19
1.4 Immune Response to Wear Debris.....	20
1.4.1 Innate immune system	20
1.4.2 Function of monocytes, macrophages and neutrophils	21
1.4.3 Phagocytosis of wear debris particles	22
1.4.4 Cytokines and chemokines as inflammatory mediators	25

1.5	Metal Ions Activate Toll-like Receptors	27
1.5.1	Nickel ions and TLR4.....	27
1.5.2	Cobalt ions and TLR4	29
1.5.3	Toll-like receptor 4	29
1.5.4	LPS activation of TLR4	30
1.5.5	Wear debris particles and TLR4	33
1.6	Consequences of TLR4 Activation.....	33
1.6.1	Cytokine and chemokine secretion	34
1.6.2	Enhanced phagocytosis.....	35
1.6.3	Process of leukocyte extravasation, adhesion and migration	35
1.7	The Inflammasome Response	38
1.7.1	NLRP3 activation	40
1.7.2	Consequences of NLRP3 activation	41
1.7.3	Metal ions, wear debris and the inflammasome.....	42
1.8	Future of Biomaterials in Joint Replacements.....	42
1.9	Summary.....	44
1.10	Hypothesis and Aims	44
1.11	Objectives	45
Chapter 2 : Materials and Methods		46
2.1	Cell Culture	46
2.1.1	Summary of cell lines used.....	46
2.1.2	Cell Maintenance	47
2.1.3	Cryopreservation of cells	47
2.1.4	Thawing and reseeded of cell lines.....	48
2.1.5	Mycoplasma testing	48
2.1.6	THP-1 differentiation.....	48
2.2	Cell Stimulation	49

2.2.1	Lipopolysaccharide	49
2.2.2	Negative control	49
2.2.3	Cobalt ions	49
2.3	TLR4 Signalling Inhibitors.....	50
2.3.1	CLI-095	50
2.3.2	MAB-tlr4.....	50
2.3.2.1	Mouse IgG1 isotype control antibody.....	50
2.4	Investigating the Inflammasome Response	50
2.4.1	ATP	50
2.5	Cell Viability	51
2.5.1	Trypan blue staining.....	51
2.5.2	XTT assay	51
2.6	Transmission Electron Microscopy (TEM)	52
2.7	Quantification of Gene Expression	52
2.7.1	RNA isolation	52
2.7.2	cDNA synthesis.....	54
2.7.3	Quantitative real-time polymerase chain reaction	54
2.8	Protein Quantification	55
2.8.1	Enzyme-linked immunosorbent assay (ELISA)	55
2.9	Statistical Analysis.....	57
Chapter 3 : Generation, Isolation and Characterisation of Clinically-relevant Cobalt Chromium Wear Particles		58
3.1	Introduction.....	58
3.2	Aims and Objectives.....	61
3.2.1	Objectives	61
3.3	Specific Materials	62
3.4	Specific Methods	62

3.4.1	Generation of CoCr particles using a six-station pin-on-plate wear simulator.....	62
3.4.1.1	Cleaning of rig components and CoCr pins and plates	62
3.4.1.2	Assembly of six-station pin-on-plate wear simulator	63
3.4.1.3	Linear bearing tray	64
3.4.1.4	Assembly of pin holder.....	65
3.4.1.5	Final assembly	65
3.4.2	Generation of sterile CoCr particles using a single-station pin-on-plate wear simulator.....	66
3.4.2.1	General preparation and cleaning of rig components.....	66
3.4.2.2	Assembly of single station pin-on-plate wear simulator.....	67
3.4.2.3	Sterility testing of retrieved lubricant	69
3.4.3	Scanning electron microscopy (SEM).....	70
3.4.3.1	Preparation of cobalt-chromium particles for SEM analysis from six station pin-on-plate wear simulator	70
3.4.3.2	Isolation of cobalt-chromium particles for SEM analysis from single-station pin-on-plate wear simulator	71
3.4.3.3	Imaging and characterisation of cobalt-chromium particles.....	73
3.4.3.4	Energy dispersive x-ray spectroscopy analysis of cobalt-chromium particles	74
3.4.3.5	Cobalt-chromium particle characterisation	74
3.4.4	Preparation of particles for cell culture studies	74
3.4.5	Endotoxin testing of generated CoCr particles	75
3.4.5.1	Endotoxin kit components	76
3.4.5.2	Sample preparation.....	76
3.4.5.3	Reagent preparation	76
3.4.5.4	Assay procedure	77
3.4.6	Inductively coupled plasma mass spectroscopy (ICP-MS)	78

3.5	Results	79
3.5.1	Generation of cobalt-chromium wear particles using the six- and single station pin-on-plate wear simulator	79
3.5.2	Characterisation of cobalt-chromium particles generated using a six-station pin-on-plate wear simulator	79
3.5.3	Characterisation of isolated cobalt-chromium particles generated using a single-station pin-on-plate wear simulator	83
3.5.4	Microbiological testing of generated CoCr particles from single-station pin-on-plate wear simulator	86
3.5.5	Endotoxin testing.....	86
3.5.6	Release of cobalt and chromium ions from CoCr particles.....	88
3.6	Discussion	91
3.6.1	Conclusions.....	95
Chapter 4 : Role of the Toll-like Receptor 4 Signalling Pathway and Inflammasome in the Inflammatory Response to CoCr Particles		96
4.1	Introduction.....	96
4.2	Aims and Objectives.....	97
4.2.1	Objectives	97
4.3	Specific Methods	98
4.3.1	Cell treatments	98
4.3.2	Meso Scale Discovery (MSD) multiplex cytokine analysis	98
4.3.2.1	MSD Components	100
4.3.2.2	Preparation of U-PLEX plate	101
4.3.2.3	Preparation of standards and samples	101
4.3.2.4	Preparation of detection antibody solution.....	102
4.3.3	Phagocytosis assay	102
4.4	Results	104
4.4.1	Effect of CoCr particles on cell viability	104

4.4.1.1	Trypan blue staining.....	104
4.4.1.2	XTT proliferation assay	106
4.4.2	Internalisation of CoCr particles by THP-1 cells.....	110
4.4.3	Phagocytic capability of THP-1 cells.....	115
4.4.4	Validation of cytokines and chemokines as a marker of inflammatory responses to CoCr particles	118
4.4.4.1	MSD assay.....	118
4.4.4.2	Effect of CoCr particles on inflammatory gene expression.....	122
4.4.5	Effect of TLR4 inhibition on CoCr-mediated cytokine release.....	126
4.4.6	Effect of TLR4 inhibition on CoCr-mediated inflammatory gene expression	131
4.4.7	Effect of anti-TLR4 neutralising antibody on the inflammatory response to CoCr particles	132
4.4.7.1	Optimisation of MAb-tlr4.....	133
4.4.8	Mouse macrophage inflammatory response to CoCr particles	135
4.4.8.1	CCL3 Dose response.....	135
4.4.8.2	Effect of TLR4 inhibition on CCL3 protein secretion.....	136
4.4.9	Monocyte inflammatory response to CoCr particles	137
4.4.9.1	Naïve THP-1 cells	137
4.4.10	Effect of CoCr particles on the inflammasome	141
4.4.10.1	Protein and gene expression of IL-1 β	141
4.5	Discussion.....	145
4.5.1	Future work.....	157
4.5.2	Conclusion.....	158
Chapter 5 : Functional Effects of CoCr particles <i>in vitro</i> and Translation to Patient Tissue Following Hip and Knee Revision Surgery.....		
5.1	Introduction	159

5.2	Aims and Objectives.....	160
5.2.1	Objectives	160
5.3	Specific Methods	162
5.3.1	Chemotaxis assay.....	162
5.3.2	Haematoxylin and eosin (H&E) staining.....	165
5.3.3	Immunohistochemistry	165
5.3.3.1	Dual colour immunohistochemistry.....	167
5.3.4	Cell migration assay.....	168
5.4	Results	169
5.4.1	Effect of CoCr particles on human microvascular endothelial cells.....	169
5.4.1.1	Cell viability.....	169
5.4.1.2	XTT proliferation assay.....	170
5.4.1.3	Internalisation of CoCr particles.....	171
5.4.2	Effect of CoCr particles on adhesion molecule expression	173
5.4.3	CoCr particle-mediated neutrophil migration.....	174
5.4.4	Periprosthetic soft tissue analysis from patients undergoing hip and knee revision surgeries.....	175
5.4.4.1	Patient clinical information.....	176
5.4.4.2	Histological findings of periprosthetic soft tissue following revision surgery, H&E staining	178
5.4.4.3	Histological findings of periprosthetic soft tissue following revision surgery, IHC staining.....	183
5.4.4.4	Are T cells present in periprosthetic tissues proliferative?.....	188
5.4.5	CoCr particles effect on cell migration of MG63 cells.....	190
5.5	Discussion	193
5.5.1	Future work	199
5.5.2	Conclusion	200

Chapter 6 : Investigating the Biological Effects of Ceramic Oxides	201
6.1 Introduction	201
6.2 Aims and Objectives	202
6.2.1 Objectives.....	202
6.3 Specific Materials.....	203
6.3.1 Ceramic oxides.....	203
6.3.1.1 Aluminium oxide.....	203
6.3.1.2 Zirconium(IV) oxide	203
6.4 Results.....	204
6.4.1 TEM images of ceramic oxide nanopowders	204
6.4.2 Effect of ceramic oxides on THP-1 cell viability	206
6.4.2.1 Trypan blue staining.....	206
6.4.2.2 XTT proliferation assay	209
6.4.3 Uptake of ceramic oxides by macrophage and endothelial cells.....	211
6.4.3.1 THP-1 cells.....	211
6.4.3.2 HMEC-1 cells	215
6.4.4 Effect of ceramic oxides on THP-1 cells	217
6.4.4.1 Inflammatory and chemotactic protein secretion	217
6.4.4.2 Inflammatory and chemotactic gene expression	219
6.4.5 The role of TLR4 in ceramic oxide-mediated inflammation.....	221
6.4.6 Mouse macrophage inflammatory response to CoCr particles	224
6.4.6.1 CCL3 dose response	224
6.4.6.2 Effect of TLR4 inhibition on CCL3 protein secretion.....	225
6.4.7 The role of the inflammasome in ceramic oxide-mediated inflammation	226
6.5 Discussion.....	231
6.5.1 Future work.....	236

6.5.2 Conclusion	237
Chapter 7 : Concluding Discussion.....	238
7.1 Aims and Outcomes	238
7.2 Overall Conclusions.....	240
7.3 Final Discussion	241
7.4 Study Limitations	244
7.5 Clinical Implications	246
7.6 Future Directions	247
Appendix A	250
Appendix B	252
Publications, presentations and awards.....	253
References	255

List of Figures

Figure 1.1 Total hip replacement prosthesis	3
Figure 1.2 Total number of primary hip replacement procedures in England and Wales.....	4
Figure 1.3 Metal-on-Metal hip resurfacing versus the total hip replacement.....	6
Figure 1.4 Biomaterials used in total hip replacements and demographics of patients receiving implants.	8
Figure 1.5 Bone resorption process.....	18
Figure 1.6. Phagocytosis process.	24
Figure 1.7 TLR4 pathway.	32
Figure 1.8 Leukocyte adhesion and migration.	37
Figure 1.9 The NLRP3 inflammasome.	39
Figure 2.1 RNA gel electrophoresis.....	53
Figure 3.1 Microscopy images comparing CoCr wear particles generated on pin-on-plate simulator versus commercial CoCr particles	59
Figure 3.2 Components of the six-station pin-on-plate wear simulator	63
Figure 3.3 Components of single station pin-on-plate wear simulator.....	67
Figure 3.4 Assembly of pin holder for single-station pin-on-plate wear simulator	68
Figure 3.5 Fully assembled single pin-on-plate wear simulator.....	69
Figure 3.6 Plating out serum onto bacterial growth plates using standard method	70
Figure 3.7 CoCr particle isolation method	73
Figure 3.8 SEM images of CoCr particles generated on six-station pin-on-plate wear simulator	80
Figure 3.9 SEM image of CoCr particles generated on six-station pin-on-plate wear simulator	80
Figure 3.10 SEM images of CoCr particles generated on six-station pin-on-plate wear simulator	81
Figure 3.11 SEM image of CoCr particles generated on six-station pin-on-plate wear simulator	81
Figure 3.12 Frequency distribution of CoCr particles generated using a six-station pin-on-plate wear simulator	82
Figure 3.13 Energy dispersive x-ray spectroscopy analysis of nanoscale CoCr particles.....	83
Figure 3.14 SEM image of isolated CoCr particles generated using a single-station pin-on-plate wear simulator	84
Figure 3.15 SEM image of isolated CoCr particles generated using a single-station pin-on-plate wear simulator	84

Figure 3.16 SEM image of isolated CoCr particles generated using a single-station pin-on-plate wear simulator	85
Figure 3.17 Frequency distribution of isolated CoCr particles generated using a single-station pin-on-plate wear simulator	86
Figure 3.18 Standard curve for the quantitation of endotoxin	87
Figure 3.19 Cobalt and chromium ion release from CoCr particle dose between 0.05 and 50µm³ CoCr particles per cell response at 24 hours	89
Figure 3.20 Time course showing cobalt and chromium release from CoCr particles	89
Figure 3.21 Comparison of CoCr particles and CoCl₂ ion concentration over time	90
Figure 4.1 MSD multiplex method and set up	100
Figure 4.2 Cell line viability CoCr particle dose response at 24 hours determined by trypan blue staining.....	105
Figure 4.3 Cell line viability CoCr particle dose response at 48 hours determined by trypan blue staining.....	106
Figure 4.4 Proliferation of THP-1 cells following exposure to stimulants for 24 hours.....	108
Figure 4.5 Proliferation of THP-1 cells following exposure to stimulants for 48 hours.....	109
Figure 4.6 Transmission electron microscopy of untreated THP-1 cells	111
Figure 4.7 Transmission electron microscopy of THP-1 cells treated with CoCr particles	112
Figure 4.8 Transmission electron microscopy displaying aggregates of CoCr particles within phagosomes of THP-1 cells	113
Figure 4.9 Transmission electron microscopy displaying THP-1 intracellular structures following CoCr particle treatment.....	114
Figure 4.10 Transmission electron microscopy using high magnification to visualise and characterise individual CoCr particles	115
Figure 4.11 Optimisation of pHrodo™ Red E. coli BioParticles® phagocytosis assay, dose and time response in activated THP-1 cells	117
Figure 4.12 CoCr particle dose response in THP-1 cells, assessment of inflammatory proteins – significant changes.....	120
Figure 4.13 CoCr particle dose response in THP-1 cells, assessment of inflammatory proteins – non-significant changes	122
Figure 4.14 IL-8 gene expression following CoCr particle dose response	123
Figure 4.15 IL-8 gene expression following CoCr particle treatment time course	125
Figure 4.16 CCL3 gene expression following CoCr particle treatment time course	126

Figure 4.17 Effect of TLR4 inhibition in CoCr particle treated THP-1 cells, assessment of inflammatory proteins - significant changes	130
Figure 4.18 Effect of TLR4 inhibition in CoCr particle treated THP-1 cells, assessment of inflammatory proteins - non-significant changes.....	131
Figure 4.19 Effect of TLR4 inhibition in CoCr particle treated THP-1 cells, assessment of IL-8 gene expression.....	132
Figure 4.20 Optimisation of MAb-tlr4 in LPS-stimulated THP-1 cells	134
Figure 4.21 CoCr particle dose response in mouse J774 cells - assessment of CCL3 protein expression	136
Figure 4.22 Effect of TLR4 inhibition in CoCr particle treated J774 cells, assessment of CCL3 protein expression	137
Figure 4.23 CoCr particle dose response in naive THP-1 monocytic cells - assessment of IL-8 and CCL3 protein expression	139
Figure 4.24 Effect of TLR4 inhibition in CoCr particle treated naive THP-1 monocytic cells, assessment of IL-8 and CCL3 protein expression.....	140
Figure 4.25 IL-1 β gene and protein expression following CoCr particle and ATP treatment in THP-1 cells.....	142
Figure 4.26 IL-1 β gene and protein expression following LPS treatment and CoCr particle stimulation in THP-1 cells	144
Figure 5.1 Neutrophil chemotaxis protocol.....	163
Figure 5.2 Migratory neutrophil counting using absolute count bright beads by flow cytometry	164
Figure 5.3 HMEC-1 cell viability following CoCr particle treatment determined by trypan blue staining	169
Figure 5.4 Proliferation of HMEC-1 cells following exposure to CoCr particles	170
Figure 5.5 Transmission electron microscopy of untreated HMEC-1 cells	172
Figure 5.6 Transmission electron microscopy of CoCr particle treated HMEC-1 cells	173
Figure 5.7 Effect of CoCr particles on ICAM1 and VCAM1 expression.....	174
Figure 5.8 Trans-endothelial chemotaxis of neutrophils towards IL-8 following stimulation of HMEC-1 with CoCr particles.....	175
Figure 5.9 Representative H&E images illustrating inflammatory infiltration I	179
Figure 5.10 Representative H&E images illustrating inflammatory infiltration II	180
Figure 5.11 Representative H&E images illustrating inflammatory infiltration III	181
Figure 5.12 Representative H&E images illustrating inflammatory infiltration IV	182
Figure 5.13 Representative IHC images illustrating T lymphocyte population I	184

Figure 5.14 Representative IHC images illustrating T lymphocyte population II	185
Figure 5.15 Representative IHC images illustrating macrophage population I	186
Figure 5.16 Representative IHC images illustrating macrophage population II	187
Figure 5.17 Representative images of CD3 and Ki67 dual coloured IHC staining	189
Figure 5.18 Effect of treatment with CoCr particles and CoCl₂ on wound closure and migration in MG63 cells I	191
Figure 5.19 Effect of treatment with CoCr particles and CoCl₂ on wound closure and migration in MG63 cells II	192
Figure 6.1 Transmission electron microscopy using high magnification to visualise and characterise individual aluminium oxide particles	205
Figure 6.2 Transmission electron microscopy using high magnification to visualise and characterise individual zirconium oxide particles	206
Figure 6.3 THP-1 cell viability Al₂O₃ and ZrO₂ dose response at 24 hours determined by trypan blue staining	208
Figure 6.4 Proliferation of THP-1 cells following exposure to Al₂O₃ and ZrO₂ for 24 hours	210
Figure 6.5 Transmission electron microscopy of THP-1 cells treated with Al₂O₃	212
Figure 6.6 Transmission electron microscopy displaying aggregates of Al₂O₃ within vacuoles of THP-1 cells	213
Figure 6.7 Transmission electron microscopy of THP-1 cells treated with ZrO₂	214
Figure 6.8 Transmission electron microscopy displaying aggregates of ZrO₂ within phagosomes of THP-1 cells	215
Figure 6.9 Transmission electron microscopy of HMEC-1 cells treated with Al₂O₃	216
Figure 6.10 Transmission electron microscopy of HMEC-1 cells treated with ZrO₂	217
Figure 6.11 Al₂O₃ and ZrO₂ particle dose response in THP-1 cells, assessment of inflammatory proteins	219
Figure 6.12 Al₂O₃ and ZrO₂ particle dose response in THP-1 cells, assessment of inflammatory gene expression	221
Figure 6.13 Effect of TLR4 inhibition in Al₂O₃ and ZrO₂ treated THP-1 cells, assessment of IL-8 gene and protein expression	223
Figure 6.14 Al₂O₃ and ZrO₂ dose response in mouse J774 cells - assessment of CCL3 protein expression	225
Figure 6.15 Effect of TLR4 inhibition in Al₂O₃ and ZrO₂ treated J774 cells, assessment of CCL3 protein expression	226

Figure 6.16 IL-1β gene and protein expression following Al₂O₃ or ZrO₂ stimulation and ATP treatment in THP-1 cells	228
Figure 6.17 IL-1β gene and protein expression following LPS treatment and Al₂O₃ or ZrO₂ stimulation in THP-1 cells	230
Figure 7.1 Working model.....	244

List of Tables

Table 1.1 Risk of revision 10 years post total hip replacement by gender, age and implant material.	10
Table 2.1 Taqman gene expression assays	55
Table 2.2 ELISA reagent concentrations	56
Table 2.3 DuoSet ELISA ancillary reagent kit	57
Table 3.1 The components required for the assembly of the six-station pin-on-plate wear simulator	64
Table 3.2 Pierce LAL chromogenic endotoxin quantitation kit contents and reagent preparation	76
Table 3.3 Endotoxin concentrations taken from lubricants of six-station pin-on-plate wear simulator	87
Table 3.4 Endotoxin concentrations taken from lubricants of single-station pin-on-plate wear simulator	88
Table 4.1 Cytokines and chemokines measured for multiplex analysis and their functions	99
Table 4.2 Components of U-PLEX MSD assay	100
Table 4.3 Protein secretion of inflammatory markers of interest following CoCr particle treatment in THP-1 cells with and without the addition of TLR4 inhibitor (CLI-095)	128
Table 4.4 Protein secretion of inflammatory markers of interest following CoCl₂ treatment in THP-1 cells with and without the addition of TLR4 inhibitor (CLI-095)	129
Table 5.1 Primary antibodies used in immunohistochemistry	167
Table 5.2 Summary of patient clinical information	177

Abbreviations

ADP	Adenosine diphosphate
Al₂O₃	Aluminium oxide
ALVAL	Aseptic lymphocytic vasculitis-associated lesions
ANOVA	Analysis of variance
APES	3-aminopropyltriethoxysilane
ARMD	Adverse reaction to metal debris
ASC	Apoptosis-associated speck-like protein containing a CARD
ASR	Articular surface replacement
ATP	Adenosine triphosphate
ATZ	Alumina-toughened zirconia
BSA	Bovine serum albumin
CARD	Caspase recruitment domain
CCL-	Chemokine ligand-
CCR	C-C Chemokine receptor
CD	Cluster of differentiation
cDNA	Complementary DNA
CoC	Ceramic-on-Ceramic
CoCl₂	Cobalt hexahydrate
CoCr	Cobalt-Chromium
CoCrMo	Cobalt-Chromium-Molybdenum
CoP	Ceramic-on-Polyethylene
CXCL	Chemokine (C-X-C motif) ligand
DAB	3'-diaminobenzidine
DAMPs	Danger-associated molecular patterns
DEPC	Diethyl pyrocarbonate
DMSO	Dimethyl sulphoxide
DNA	Deoxyribonucleic acid
DPX	Dibutylphthalate polystyrene xylene
EDTA	Ethylenediaminetetraacetic acid
EDX	Energy dispersive x-ray spectroscopy
EGF	Epidermal growth factor

ELISA	Enzyme-linked immunosorbent assay
EMEM	Eagle's modified essential medium
FACs	Fluorescence activated cell sorting
FBS	Foetal bovine serum
FFPE	Formalin-fixed paraffin-embedded
GM-CSF	Granulocyte macrophage colony stimulating factor
H&E	Haematoxylin and eosin
HBA	Heated blood agar
HEK293	Human embryonic kidney cells
HEPES	4-(2-hydroxyethyl)-1-piperazineethanesulfonic acid
HMEC	Human microvascular endothelial cells
HMGB1	High mobility group box 1
HRP	Horseradish peroxidase
HSCs	Haematopoietic stem cells
HSP	Heat shock proteins
ICAM-1	Intercellular adhesion molecule 1
ICP-MS	Inductively coupled plasma-mass spectroscopy
IFNγ	Interferon gamma
IHC	Immunohistochemistry
IL-	Interleukin-
IRAK-M	Interleukin receptor-associated kinase-M
IRAK1	Interleukin-1 receptor associated kinase 1
IRF3	Interferon regulatory factor 3
LAL	Lyophilized amebocyte lysate
LBP	LPS-binding protein
LDH	Lactase dehydrogenase
LFA-1	Lymphocyte function-associated antigen
LPS	Lipopolysaccharide
LRR	Leucine-rich repeat
M-CSF	Macrophage colony stimulating factor
MAC-1	Macrophage antigen 1
MD2	Myeloid differentiation protein
MGCs	Multi-nucleated giant cells

MHC	Major histocompatibility complex
MHRA	Medicines & Healthcare products Regulatory Agency
MM6	MonoMac 6
MMP-1	Matrix metalloproteinase-1
MMPs	Matrix metalloproteinases
MoM	Metal-on-Metal
MoP	Metal-on-Polyethylene
MRI	Magnetic resonance imaging
mRNA	Messenger ribonucleic acid
MSD	Meso scale discovery
MyD88	Myeloid differentiation primary response 88
NA	Nutrient agar
NADPH	Nicotinamide adenine dinucleotide phosphate
NaOH	Sodium hydroxide
NFκB	Nuclear factor kappa-light-chain-enhancer of activated B cells
NK	Natural killer
NLRP	Nucleotide-binding oligomerisation domain, Leucine rich Repeat and Pyrin domain containing
NLRs	Nucleotide oligodimerisation domain-like receptors
NOD	Nucleotide-binding oligomerisation domain
OA	Osteoarthritis
OPG	Osteoprotegerin
P2X₇	P2X purinoceptor 7
PAMPs	Pathogen-associated molecular patterns
PBMCs	Peripheral blood mononuclear cells
PBS	Phosphate buffered saline
PBST	Phosphate buffered saline with tween
PECAM-1	Platelet endothelial cell adhesion molecule-1
PMA	Phorbol 12-myristate 13-acetate
pNA	p-nitroaniline
PRRs	Pattern recognition receptors
PYD	Pyrin domain

qRT-PCR	Quantitative real time polymerase chain reaction
RA	Rheumatoid arthritis
RANK	Receptor activator of nuclear kappa B
ROS	Reactive oxygen species
RPMI	Roswell park memorial institute medium
RT	Room temperature
SAB	Saboraud dextrose agar
SDS	Sodium dodecyl sulphate
SEAP	Secreted alkaline phosphatase
SEM	Scanning electron microscopy
SPT	Sodium polytungstate
STAT-6	Signal transducer and activator of transcription 6
TBS	Tris buffered saline
TEM	Transmission electron microscopy
TGFβ	Transforming growth factor beta
TH1	T helper 1
THR	Total hip replacement
TIR	Toll IL-1 resistance domain
TIRAP	TIR domain containing adaptor protein
TJR	Total joint replacement
TLR4	Toll-like receptor 4
TLRs	Toll-like receptors
TNFα	Tumour necrosis factor alpha
TPA	12-O-tetradecanoylphorbol-13-acetate
TRAF	TNF receptor associated factors
TRAM	TRIF-related adaptor molecule
TRIF	TIR-domain-containing adapter-inducing interferon- β
TWIK-2	Two-pore domain weak inwardly rectifying K ⁺ 2
UHMWPE	Ultra-high molecular weight polyethylene
VCAM-1	Vascular cell adhesion molecule 1
VLA-4	Very late antigen 4
ZrO₂	Zirconium oxide
ZTA	Zirconia toughened alumina

Chapter 1 : Introduction

1.1 Total Joint Replacements

The total joint replacement (TJR) is the leading treatment option for end-stage osteoarthritis (OA) with over 90% of hip replacements performed to treat OA (National Joint Registry for England, 2019). TJR is utilised when anti-inflammatory drugs or other pain relief is insufficient to alleviate patient symptoms (National Joint Registry for England, 2019). The pain associated with these OA is caused by the wear of cartilage which forms the articulating surface of joints. OA affects joints such as the hips, knees, elbows, ankles and shoulders, primarily causing considerable pain and discomfort in patients which ultimately debilitates their mobility. TJR is also utilised less commonly in other conditions such as rheumatoid arthritis (RA), fractures, dislocation and other diseases of the bone (National Joint Registry for England, 2019).

1.1.1 Total hip replacement

The total hip replacement (THR) involves replacing both the acetabulum, femoral head and a large portion of bone from the femur. The first breakthrough in modern joint replacements came in the 1960s when Sir John Charnley designed a Metal-on-Polyethylene (MoP) cemented hip prosthesis consisting of a small metal head and ultra-high molecular weight polyethylene (UHMWPE) cup (Knight *et al.*, 2011). The Charnley hip was successful in many patients and generally provided good long-term outcomes in relieving pain and improving quality of life through enhanced mobility (Nilsson and Isaksson, 2010; Choi *et al.*, 2012; Milosev *et al.*, 2012; Kiraly and Gondos, 2014). However, MoP devices tend to wear over time, which leads to what is known as 'aseptic loosening' of the implant. Therefore, patients inevitably require revision surgery in which the prosthesis is removed and replaced by a new implant. Revision surgery is far more complex than primary TJRs and can result in only modest clinical improvement and further complications, especially in younger patients (Karam *et al.*, 2012).

1.1.2 Biomaterials in joint replacements

The materials used to design THRs are constantly under development to provide lesser wear rates and most importantly, improve implant longevity. The different types of materials used in these implants are summarised in **Figure 1.1**. The first alumina ceramic implants were introduced in the 1970s as a 'stronger' alternative to the conventional polyethylene cup which had been previously used. However, despite some early positive outcomes, ceramic implants had a particularly high fracture rate which were extremely difficult to revise due to difficulties in removal of all parts of the shattered components. Ceramic implants also suffered from aseptic loosening over time, therefore offering little improvement from the conventional MoP design. Second generation ceramic implants were introduced during the 1980s, however, aseptic loosening continued to be problematic despite the incidence of fractures reducing. Therefore, the most widely used device at the time continued to be MoP designs which were becoming more associated over time with failure due to polyethylene wear osteolysis (destruction of bone tissue), resulting in aseptic loosening. Although MoP devices also failed for various other reasons including dislocations, in younger, more active patients, osteolysis was the predominant cause for revision. The longevity of any implant is dependent on several different factors; mostly involving the levels and type of activity taken by the patient and the weight of the individual. Both of these factors can potentially add extra pressure to the implant. However, the general degradation of the implant over time will still be a contributing factor to implant failure rates.

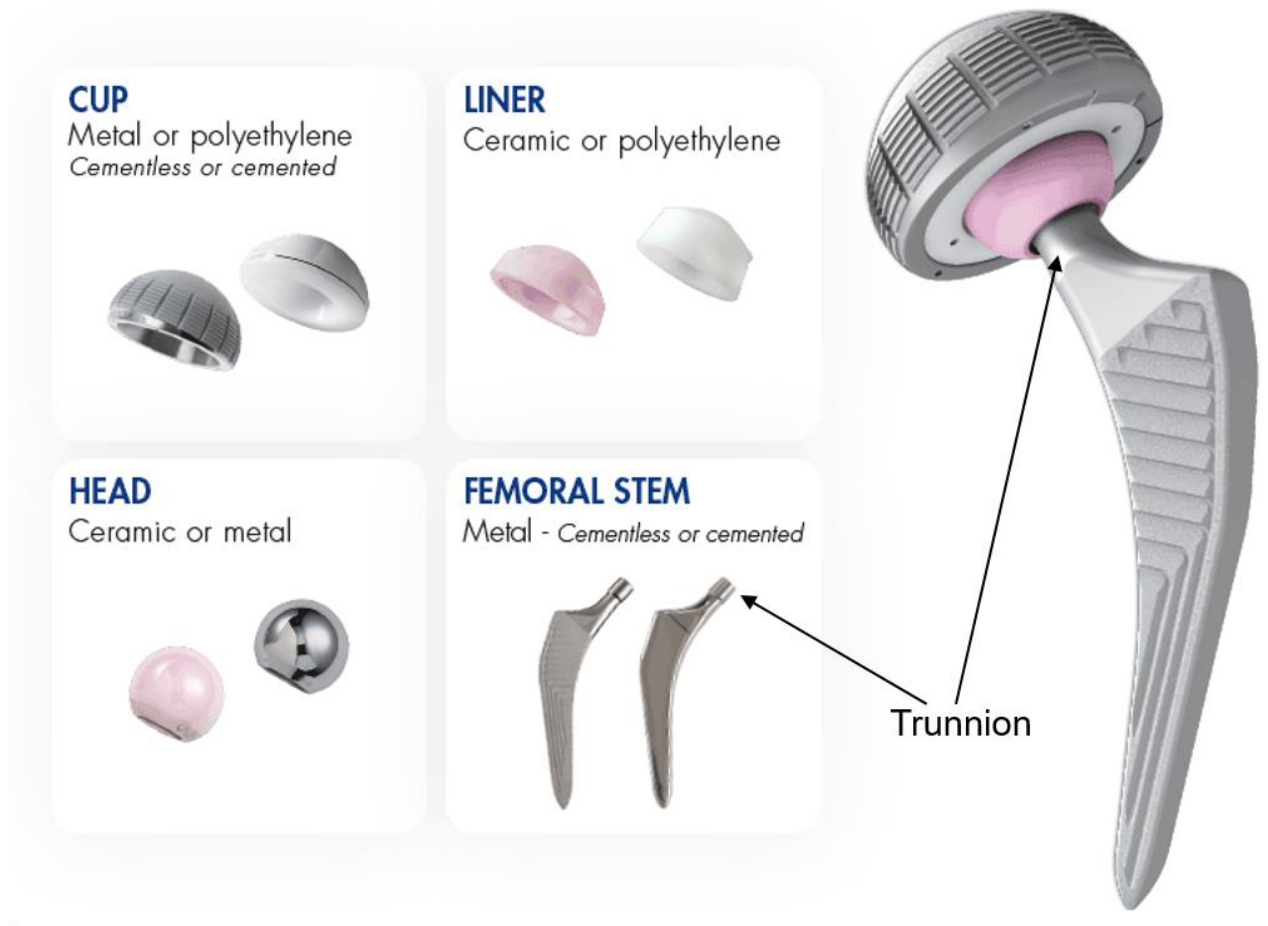


Figure 1.1 Total hip replacement prosthesis

Figure shows the structure and different materials which can be used in modern total hip replacement prostheses. Generally, the femoral stem will be fabricated from a titanium/metal alloy and the other component materials will vary. The cup of the implant is conventionally polyethylene but can also be metal. The head of the implant varies between ceramic and metal and the liner ceramic or polyethylene. Image obtained and adapted from <https://www.medacta.com/EN/hip-replacement>.

1.1.3 Change in patient demographics

The demographic of patients suffering from OA and the number requiring THRs has changed dramatically in recent years in England and Wales (National Joint Registry for England, 2019). Obesity rates are continually rising along with an ageing population which puts extra stress and pressure on hip joints. Furthermore, an active lifestyle is encouraged to help prevent obesity which can also lead to further damage to the hip joint and can result in further OA cases. These factors combined suggest that not only are cases of OA increasing, but patients are presenting with OA at a much younger age. The increasing number of OA cases is reflected in the increase of THRs which

are performed annually in England and Wales. The number has risen from 42,769 reported surgeries in 2004 to 92,874 in 2018 (**Figure 1.2**).

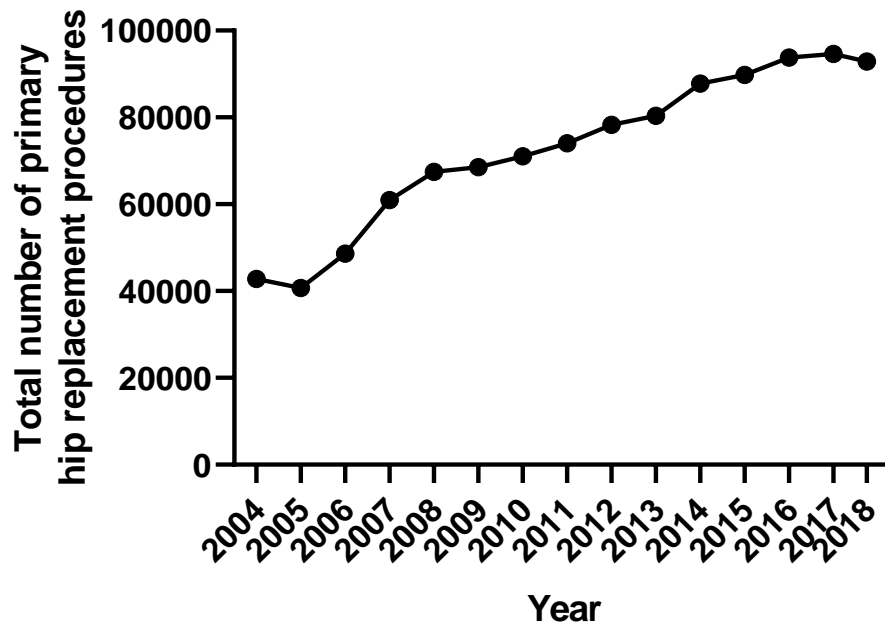


Figure 1.2 Total number of primary hip replacement procedures in England and Wales.

(National Joint Registry for England, 2019).

Although conventional MoP implants are successful in most patients, these prostheses were originally aimed at older patients with low activity levels. Therefore, the pressure put on MoP implants is manageable over a fairly long period of time (i.e. 10 to 15 years). However, if MoP devices are implanted in younger patients (i.e. under 60 years old) then the patient is far more likely to surpass this 10 to 15-year period. Younger patients will therefore inevitably require complicated revision surgery and the possibility of multiple revisions within their lifetime. Designers of implants began to focus on improvements to wear rates by producing prostheses that are low-wearing which led to the introduction of Metal-on-Metal (MoM) implants.

1.1.4 The move towards Metal-on-Metal implants

MoM implants consist of both components (the femoral head and acetabular cup) being fabricated from a metal alloy. MoM implants were initially introduced in the 1960s but the performance of these prostheses were mixed, with poor patient outcomes and relatively high failure rates (Brown *et al.*, 2002). Therefore, by the 1970s the use of MoM implants was scarce, however, the clinical need for more durable materials remained. During the 1980s and early 1990s, a new generation of MoM implants were introduced which were made from a cobalt-chromium-molybdenum (CoCrMo) alloy. It was also around this time that MoM resurfacing prostheses were developed and became particularly popular in younger patients. MoM resurfacing implants were an attractive option for younger patients as it allowed improved preservation of the femoral head and neck and reduced dislocation (**Figure 1.3**). Another advantage of using MoM implants was due to the fact the materials used were thinner, so that a larger femoral head could be placed within the same sized acetabular cup. Larger head sizes helped to address the problems associated with dislocation and offered greater stability for the patient.

Initial reports of MoM implants were very positive and analysis indicated that there was potentially sixty times less wear when compared with conventional MoP devices (Cuckler, 2005). Apparent lower wear rates led to the number of MoM implants used dramatically rising during the early 2000s. However, it soon became apparent that there was a high failure rate in patients who had received either MoM resurfacing or total replacements. In fact, in 2010, the manufacturer of the Articular Surface Replacement (ASR), DePuy, voluntarily recalled the device from the market due to concerns regarding higher than expected short-term revision rates (Langton *et al.*, 2011a; Bernthal *et al.*, 2012). Around the same time, The Medicines and Healthcare Products Regulatory Agency (MHRA) issued specific guidelines regarding the monitoring of patients who had received MoM implants. The concern from the MHRA was regarding the presence of soft tissue reactions in patients who suffered with pain. Specifically, the MHRA advised that symptomatic patients should have their cobalt and chromium ion levels measured in the serum as well as Magnetic Resonance Imaging (MRI) scans. If either of these tests revealed abnormally high ion concentrations (anything higher than 7 parts per billion or 7µg/L) or any soft tissue reactions (i.e. fluid retention or tissue masses) then revision surgery would be considered. Using these

parameters as a 'diagnosis' was the beginning of what would be termed Adverse Reaction to Metal Debris (ARMD).



Figure 1.3 Metal-on-Metal hip resurfacing versus the total hip replacement.

Comparison of a hip resurfacing replacement (right side hip) with a total hip replacement (left side hip). In hip resurfacing the femoral stem is considerably shorter so preserves more of the patient's bone (Image taken from (Amarasekera and Griffin, 2012)).

1.1.5 Current status of biomaterials used in total hip replacements

Due to the problems associated with MoM implants discussed previously, there was a sharp decline in their use from 2008 onwards (see **Figure 1.4A.**). By 2011, the use of MoM implants was completely abrogated. Throughout time, MoP implants have consistently remained the most popular choice of implant materials. However, there is a clear clinical need for biomaterials which are long-lasting, with low wear rates and are low risk for potential immune responses to wear debris. As discussed previously, ceramics have been in use since the 1970s and efforts have been made since to improve the design and composition of these implants. Implants containing alumina

oxides were introduced due to its apparent hardness and low wear rates which was hoped to overcome previous issues of friction and wear. In 1995, the need for hard and low-wearing materials led to the development of the BIOLOX® Forte (CeramTec, Germany) as a material which was highly dense and pure ceramic. However, increased fracture rates remained a problem and thus zirconia was introduced to the material, Zirconia Toughened Alumina (ZTA) (17%). Zirconia provided further strength to the material whilst counteracting fracture and wear issues. The BIOLOX® Delta fabricated from ZTA was made commercially available by CeramTec in 2003.

The development of ZTA as a biomaterial has meant a gradual increase in the number of Ceramic-on-Polyethylene (CoP) implants used in primary surgeries (**Figure 1.4A**). Furthermore, the average age of patients receiving CoP implants is significantly less than those receiving conventional MoP implants, highlighting their importance to be utilised in younger, more active patients (**Figure 1.4B**). The use of Ceramic-on-Ceramic (CoC) implants in which both the femoral head and liner are fabricated from ZTA initially increased following the decline in MoM implant use. However, CoC implants continued to suffer from issues with ceramic liner fracture and also 'squeaking' of the implant which has since led to their more recent decline (Gallo *et al.*, 2012). Ultimately, the use of CoC has likely declined due to the success in longevity of CoP implants which is also a more cost-effective solution.

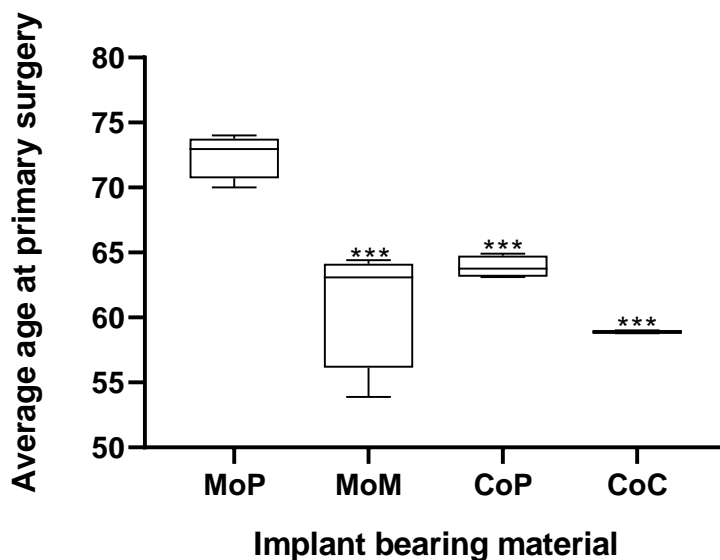
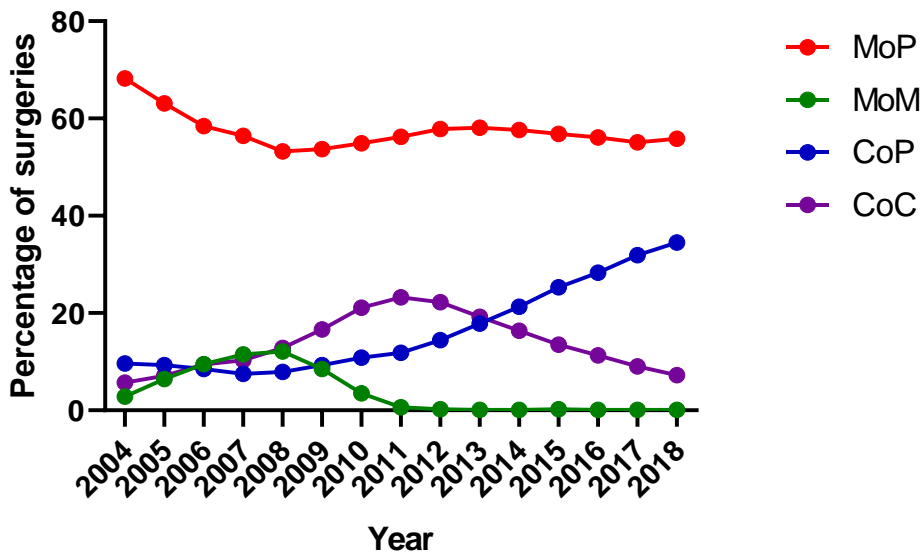


Figure 1.4 Biomaterials used in total hip replacements and demographics of patients receiving implants.

A) The percentage of different biomaterials used for bearing surfaces in primary total hip replacements. Metal-on-Polyethylene (MoP) consistently remains the most commonly used implant type. The use of Metal-on-Metal (MoM) increased between 2004 and 2008 and then rapidly declined due to issues associated with adverse reaction to metal debris. Ceramic-on-Polyethylene (CoP) implants have steadily increased during recent years whereas the use of Ceramic-on-Ceramic (CoC) implants initially increased following the decrease of MoM but due to problems with fracture have also decreased since 2011. **B)** The average age at primary surgery for each bearing implant type. Conventional MoP implants were most commonly used in older patients (70+ years) whereas MoM, CoP and CoC implants were most often utilised in younger patients (under 65 years) due to lesser wear rates (National Joint Registry for England, 2019).

1.2 Wear of Total Joint Replacements

Although MoM implants were initially designed to offer lesser wear rates when compared to conventional MoP devices, MoM implants with large femoral head diameters (>36mm) were reported to have higher wear rate due to 'edge loading'. Edge loading occurs as a result of decreased contact between the cup and head at the rim of the cup resulting in increased contact stress (Underwood *et al.*, 2012). Furthermore, general articulation of the joint and motion over time can also result in significant wear regardless of the materials used. However, the risk of revision with MoM implants, particularly in resurfacing surgeries, was significantly higher than any other type of implant which was a major factor in their decline of use (**Table 1.1**). Interestingly, female patients are also at a higher risk of implant failure compared to males especially in hip resurfacings and MoM implants. Females have also been shown to report higher levels of pain and are at greater risk of dislocation and aseptic loosening (Jameson *et al.*, 2012; Cvetanovich *et al.*, 2015). The relatively low risk of revision in CoP implants emphasises the reason why they are increasingly growing in popularity.

Table 1.1 Risk of revision 10 years post total hip replacement by gender, age and implant material.

Blue italics signify that fewer than 250 cases remained at risk at these time points.

Risk of revision at 10 years (%)		
MoP hip replacement		
Age (years)	Males	Females
<55	5.53	4.47
55-64	5.10	4.12
65-74	4.14	3.50
75+	3.64	3.49
MoM hip replacement		
<55	17.79	26.44
55-64	16.70	22.45
65-74	13.70	19.33
75+	8.70	9.59
MoM hip resurfacing		
<55	7.76	19.75
55-64	7.17	17.53
65-74	7.66	14.89
75+	<i>7.24</i>	<i>13.59</i>
CoP hip replacement		
<55	3.68	4.22
55-64	3.33	3.31
65-74	2.55	3.01
75+	2.95	3.04
CoC hip replacement		
<55	4.64	4.57
55-64	3.79	3.31
65-74	3.14	2.51
75+	<i>4.22</i>	2.92

The major concern with wear in MoM implants, is the release of cobalt-chromium (CoCr) wear debris particles and ions from the implant into the surrounding tissues and vasculature. In particular, cobalt ions are found at significantly higher levels in patient's serum than other metals used in MoM implants (i.e. chromium and molybdenum) (Witzleb *et al.*, 2006; Maurer-Ertl *et al.*, 2017). There have also been reports of CoCr accumulations observed in organs such as the kidney, spleen and liver, therefore the systemic effects that CoCr particles may cause is of obvious concern (Urban *et al.*, 2000; Abdel-Gadir *et al.*, 2016).

Most of the debris generated and released from MoM implants are from the two articulating bearing surfaces (Callaghan *et al.*, 2004). However, corrosion at the femoral head-neck junction or from the trunnion can occur (known as trunnionosis) (Whitehouse *et al.*, 2015) (**Figure 1.1**). The trunnion of the implant is typically manufactured from metal alloys including titanium, aluminium and CoCrMo. Therefore, trunnionosis and subsequent generation of debris is applicable to not only MoM implants but also MoP and ceramic devices. In fact, cases of ARMD have been reported in patients who have received either MoP or CoC implants (Matharu *et al.*, 2016; Waterson *et al.*, 2018).

Additionally, irrespective of the type of implant used, degradation of the device will occur over time which in turn will generate not only metal, but also polyethylene or ceramic nano- or micro-particles. Wear debris of any kind are then capable of circulating to surrounding tissues or more systemically. It is therefore no surprise that wear debris itself is one of the key factors in shortening the lifespan of prosthetic joints and increasing the number of revision surgeries.

1.2.1 Cobalt-chromium wear particles

Studies which have retrieved CoCr particles from the tissues of patients who have received MoM implants indicate that these tend to be nanoscale in size (Xia *et al.*, 2017). Xia *et al.* (2017) collected tissue from a total of 53 patients who had undergone revision surgery for ARMD. The investigators found that all particles were nanoscale in size, varying between 10-800nm and were mostly circular in morphology, irregular, with a few small needle-like particles. Differences observed in shape and morphology of particles could be due to the variations in particle isolation techniques from tissue

samples which are employed. Particle isolation methods can ultimately alter particle size, morphology and characteristics. Moreover, particle characteristics can effect *in vitro* investigations into cell toxicity as it is known that the size and shape of CoCr particles can affect cellular responses (Caicedo *et al.*, 2013; Posada *et al.*, 2015).

The biological effects that CoCr particles can elicit have been investigated in numerous studies. Previous studies have shown potential cell toxicity caused by CoCr nano- (i.e. under 1000nm) and micro-scale (i.e. anything over 1000nm) particles in various cell lines and peripheral blood mononuclear cells (PBMCs) as well as their ability to up-regulate inflammatory markers (Alarifi *et al.*, 2013; Nyga *et al.*, 2015; Wang *et al.*, 2016). In addition to CoCr wear debris particles, cobalt ions which are released from the CoCr alloy can also elicit toxic effects on cells as well as inducing apoptosis, necrosis and inflammatory responses (Huk *et al.*, 2004; Catelas *et al.*, 2005). One study investigated the biological effects of CoCr particles (supplied by DePuy), on a monocytic cell line. The CoCr particles used in this study generated significantly increased levels of cobalt ions and increased apoptotic gene markers in cells when treated with both particles and cobalt ions (Posada *et al.*, 2014). However, the exact mechanisms and pathways which are involved in these reactions remains poorly understood.

1.2.2 Ceramic wear

Generally, the survivorship of CoP and CoC implants have been relatively high (97% at 10 years) (D'Antonio *et al.*, 2012). The wear rates from ceramic bearings are particularly low when compared to other implant types which would explain their enhanced longevity. As discussed previously, efforts have been made to improve the design and composition of ceramic implants in more recent years. Implants containing ZTA e.g. the BIOLOX® Delta have grown in popularity. Furthermore, ZTA devices have been reported to generate fivefold less wear in comparison to alumina only implants (Al-Hajjar *et al.*, 2013). Previous studies using CoC simulators have shown varied results regarding the size distribution of generated alumina particles. Using transmission electron microscopy (TEM) and scanning electron microscopy (SEM) appeared to give differing results of either nanometre scale particles (5-90nm) or micrometre (0.05-3.2µm), respectively (Tipper *et al.*, 2002).

The primary concern with CoP and CoC implants have always centred on fracture rates. However, ceramic wear debris may not be as biologically inert as first believed or proposed. Biopsies taken from CoC implants demonstrated macrophage infiltration confirmed by immunohistochemical (IHC) staining (Mochida *et al.*, 2001). However, very few studies have investigated the biological effects of ceramic wear debris in comparison to CoCr *in vitro*. Furthermore, very few have used clinically relevant materials as it can be particularly difficult to generate high volumes of ceramic wear particles on simulators due to the materials durability. One report compared alumina ceramic wear particles with CoCr particles and found them to be only weakly genotoxic to human cells *in vitro* (Tsaousi *et al.*, 2010). Another study showed that macrophage-like cells treated with alumina ceramic particles secreted four-times more tumour necrosis factor alpha (TNF α) when compared with untreated controls (Sterner *et al.*, 2004). The investigators also concluded that there was no significant difference in TNF α secretion when cells were treated with sub-micron particles (0.6 μ m) or micron sized particles (2 μ m) (Sterner *et al.*, 2004). This finding was in agreement with a previous investigation which compared alumina ceramic particles with UHMWPE particles of the same size and demonstrated that the alumina particles were capable of inducing enhanced TNF α secretion and initiating apoptosis in mouse macrophage cells (Petit *et al.*, 2002). However, another study concluded that the size of alumina wear particles was in fact a crucial factor in determining subsequent biological responses. The investigators showed that smaller alumina particles generated in a hip simulator were mildly cytotoxic in histiocytic cells at a concentration of 50 μ m³ per cell (approximately 3% of cell by volume) but larger commercial alumina particles did not induce the same toxic effects (Germain *et al.*, 2003).

1.3 Adverse Reaction to Metal Debris

The symptoms associated with failed MoM joint replacements include soft tissue damage, bone destruction and in some cases, the formation of large visible masses known as pseudotumours (Pandit *et al.*, 2008). These symptoms collectively are termed ARMD, which cause pain, swelling and discomfort around the area of the joint whilst substantially affecting patient mobility and quality of life (Langton *et al.*, 2011b). Due to the symptoms described, ARMD is the primary reason for MoM implant failure and requirement for revision surgery. Compared to the failure of conventional implants

(e.g. dislocation, loosening and septic infection), ARMD differs significantly due to the progressive destructive nature of the disease along with soft tissue necrosis and its development in what appear to be well-functioning implants.

The exact underlying mechanisms behind ARMD are unknown and the unpredictable nature of its occurrence in patients makes it difficult to predict and diagnose. For example, high serum concentrations of metal ions do not necessarily lead to symptomatic patients and some patients with normal metal ion concentrations have been known to suffer from symptoms and show signs of ARMD (Langton *et al.*, 2013; van Lingen *et al.*, 2013).

Patients who present with ARMD will typically require revision surgery with an alternative implant to alleviate the symptoms described previously. Resolving ARMD with revision surgery explains the high failure rates which have been reported with MoM devices. However, revision surgery is associated with poorer outcomes compared to primary surgery as the bone is typically weaker. Some studies have suggested that half of revisions for ARMD suffered from complications and around a third underwent further surgery (Grammatopoulos *et al.*, 2009; Rajpura *et al.*, 2011; Munro *et al.*, 2014). Although the number of MoM implants being used has reduced dramatically since their peak in the early 2000s, there are potentially millions of people worldwide who have MoM devices implanted, therefore, it is important to gain a further understanding of ARMD. Furthermore, in implants most commonly used today, metals are still often used in other medical devices such as dental implants and spinal rods.

1.3.1 Formation of inflammatory pseudotumours

Inflammatory pseudotumours were first described following the observation of aseptic soft tissue masses around hip prostheses which were necrotic in nature and infiltrated with immune cells such as macrophages and lymphocytes (Pandit *et al.*, 2008). This original finding was identified in 17 female patients who had all received a MoM resurfacing implant with the pseudotumours observed being either solid or cystic (Pandit *et al.*, 2008). Metal wear debris was also observed within the tissue which suggested either a toxic reaction to excess metal wear debris or a hypersensitivity reaction. The main symptom associated with inflammatory pseudotumours is discomfort and pain, particularly in the groin area (Bosker *et al.*, 2012). However, other

patients also complain of instability which can ultimately lead to dislocation and some patients describe clicking sensations in the hip itself.

Whether the presentation of pseudotumours is associated with high wear levels and metal ion concentrations is highly debatable. For example, some studies have confirmed a correlation between higher wear levels, elevated serum metal ion concentrations and the prevalence of pseudotumours (Langton *et al.*, 2010; Davda *et al.*, 2011). However, other researchers have found that MoM implants with relatively low wear (less than 5µm per year) had a 40% chance of pseudotumour formation (Matthies *et al.*, 2012). Moreover, asymptomatic patients with pseudotumours have been observed, although these are still concerning and patients should be monitored regularly (Kwon *et al.*, 2011; Konan *et al.*, 2017). In addition to these findings, research has shown the incidence of pseudotumours does not differ between poor-functioning and well-functioning hips i.e. asymptomatic vs symptomatic (Hart *et al.*, 2012). Therefore, inflammatory pseudotumours are very difficult to predict and, similarly to serum metal ion concentrations and the development of ARMD, appear to be patient-specific.

Inflammatory pseudotumours do not appear to be unique to MoM articulations. There have been reported cases of pseudotumours developing from MoP implants (Scully and Teeny, 2013; Persson *et al.*, 2018). However, pseudotumours associated with MoP implants are usually concluded to be due to trunnion corrosion which is typically fabricated from metals so may account for reactions occurring in patients (Whitehouse *et al.*, 2015). Pseudotumours have also been observed to develop in patients who have received CoC and CoP implants i.e. without any CoCr bearing surfaces (Malem *et al.*, 2013; Campbell *et al.*, 2017; Serrano *et al.*, 2018). Most interestingly, in a particular case study with a CoC implant, there was complete absence of a CoCr stem, femoral head or source of cobalt metal ions/CoCr debris (Campbell *et al.*, 2017). Therefore, it is reasonable to presume that the pseudotumour formation was a direct consequence of ceramic debris/wear particles.

1.3.2 Cobalt and chromium ion levels in patients with metal-on-metal prostheses

Elevated levels of cobalt and chromium ions have been observed in the serum, urine, joint fluid and organs of patients with MoM implants (Sargeant *et al.*, 2006; De Smet *et al.*, 2008; Walter *et al.*, 2008; Langton *et al.*, 2010). Langton *et al.* (2010) found that cobalt (~1000µg/L to 10,000µg/L) ion levels in joint fluid can vary hugely in ARMD patients but are significantly higher than in asymptomatic patients. However, Langton *et al.* also observed that although the average cobalt ion serum concentration in ARMD cases was higher than in asymptomatic patients (29.5µg/L vs. 2.67µg/L), in some asymptomatic cases, significantly higher concentrations were recorded e.g. up to 228µg/L. De Smet *et al.* (2008) also found that the joint fluid levels of metal ions were at least an order of magnitude higher than those measured in patient serum (for example, 2185µg/L cobalt ions in joint fluid vs. 33.8µg/L in serum). However, De Smet *et al.* showed that there was a strong correlation between measured high levels of serum and joint fluid concentrations of metal ions in each patient which was associated with wear-scar depth. Another study was able to demonstrate that abnormal wear (greater than 3mm³ per year) was indicative of blood and serum cobalt ion concentration, with a concentration of larger than 4.5µg/L showing specificity and sensitivity of abnormal wear 95% and 94%, respectively (Sidaginamale *et al.*, 2013).

It was these findings within the literature that helped shape the MHRA guidelines regarding the 'safe' limit of cobalt and chromium ion serum concentrations (i.e. 7µg/L). However, in other studies, there have been conflicting results regarding large variations in reported ion concentrations (Davda *et al.*, 2011; Renner *et al.*, 2016). Variations observed in cobalt and chromium concentrations in both serum and synovial fluid can make ARMD very difficult to predict and can undermine the supposed 'cut off' point for safe levels, as determined by the MHRA. Furthermore, there have been reported cases of ARMD, pseudotumours and delayed type IV hypersensitivity reactions with ion concentrations below the MHRA threshold (Hallab *et al.*, 2010; Sampson and Hart, 2012). Differences observed between individual patients suggests that patient-specific responses to metal ions may be occurring rather than an adverse response developing once a certain concentration is reached.

1.3.3 Osteolysis

Osteolysis in the case of joint replacements is due to increased bone resorption triggered by signals from macrophages and inflammatory mediators e.g. cytokines. Cytokines have a profound effect on the function and interaction of osteoblasts (bone-forming), osteoclasts (bone-resorbing) and macrophages which all play a role in bone homeostasis. If there is a drive towards osteoclastogenesis, this leads to excessive bone-resorption, osteolysis and ultimately aseptic loosening of implants. Osteoclasts drive bone resorption by the secretion of acidic matrix metalloproteinases (MMPs) and can therefore be a direct cause of osteolysis in implant loosening. The differentiation of immune cells such as monocytes into osteoclasts is driven by factors such as $TNF\alpha$ and interleukin-1 (IL-1). For full differentiation to osteoclasts, cells require interactions with their cell surface Receptor Activator of Nuclear Kappa-B (RANK) with its ligand, RANKL, expressed by osteoblasts on the bone surface (**Figure 1.5**). Osteoprotegerin (OPG) can prevent osteoclastogenesis by binding to RANKL and preventing its interaction with RANK. Therefore, the ratio of RANKL to OPG can regulate osteoclast differentiation and the balance between bone formation and resorption. It has been shown that both cobalt and chromium metal ions can decrease OPG and therefore promote the differentiation of osteoclasts and further osteolysis (Zijlstra *et al.*, 2012). Several studies have demonstrated the expression of RANKL, OPG, and RANK in peri-implant tissues from cases of osteolysis (Haynes *et al.*, 2001; Holding *et al.*, 2006; Chen *et al.*, 2012).

Consistent with these findings, both CoCr particles and ions reduce proliferation of pre-osteoblasts as well as significantly elevating RANKL expression and inhibiting OPG expression (Yang *et al.*, 2019). In a study which investigated periprosthetic osteolysis of loosened hip implants, the authors found an over-expression of RANKL by osteoblasts as well as lower OPG/RANKL ratio in the synovial fluid of patients (Wang *et al.*, 2010).

Aseptic loosening due to osteolysis is the leading indication of all revision procedures and is also a hallmark of ARMD. Consequently, the effect of wear debris and particles on both osteoblasts and osteoclasts has been of interest to researchers. Cobalt ions and CoCr particles have been shown to down-regulate expression of members of the Transforming Growth Factor beta ($TGF-\beta$) signalling pathway (which promotes

osteoblast differentiation) in osteoblast cell lines as well as collagens which are regulated by TGF- β (Drynda *et al.*, 2018a; Drynda *et al.*, 2018b).

CoCr particles were compared to alumina ceramic particles in an investigation involving osteolytic markers (Klinder *et al.*, 2018). When human osteoblasts were treated with both types of particles, there was a direct induction of matrix metalloproteinase-1 (MMP-1) messenger ribonucleic acid (mRNA) but not active protein (Klinder *et al.*, 2018). This finding was interesting and conflicts previous reports which indicate that particle exposure is associated with increased MMP protein expression in macrophages and PBMCs (Jonitz-Heincke *et al.*, 2016; Jonitz-Heincke *et al.*, 2017). Other research comparing biomaterials concluded that CoCr particles were the most biologically active biomaterial in osteoblasts, increasing their secretion of MMP-1 significantly and reducing the synthesis of collagen (Lochner *et al.*, 2011). Zirconium appeared to generate the least amount of cellular biological effects (Lochner *et al.*, 2011).

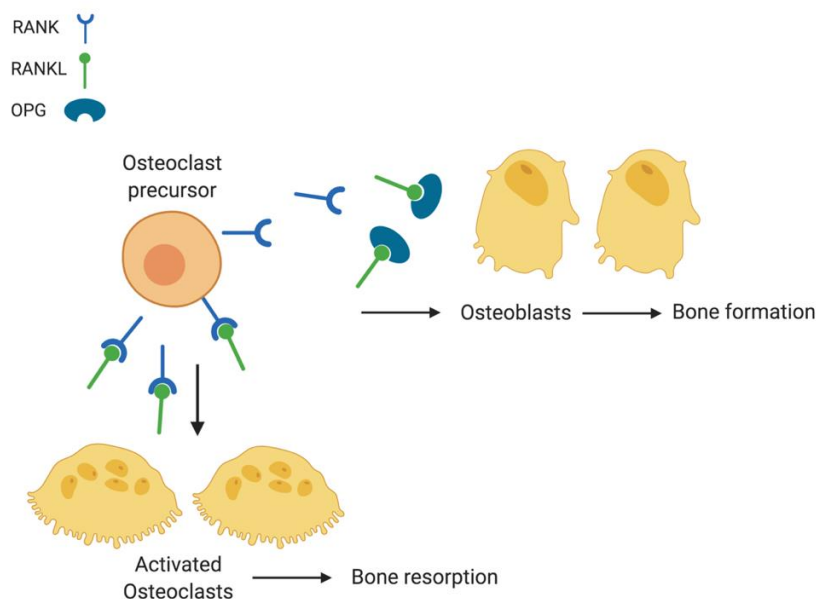


Figure 1.5 Bone resorption process.

The receptor RANK is expressed by osteoclast precursor cells and can bind to RANKL, which is expressed and can be secreted by cells such as osteoblasts. Following receptor binding of RANK and RANKL, multi-nucleated osteoclasts are formed which then drive osteoclastogenesis i.e. bone resorption. Osteoprotegerin (OPG) acts as a decoy molecule and can also bind to RANK to prevent osteoclast differentiation and therefore promote bone formation. The ratio of RANKL to OPG therefore regulates osteoclast differentiation and is vital for determining the balance between bone resorption and formation. Image created using Biorender.

1.3.4 Aseptic lymphocytic vasculitis-associated lesions (ALVAL)

The infiltration of lymphocytes present in the tissues of patients with ARMD suggests that the adaptive immune system may also be implicated in this reaction (Davies *et al.*, 2005; Blumenfeld *et al.*, 2010). The heavy lymphocytic infiltrate phenotype is termed by researchers and clinicians as Aseptic Lymphocytic Vasculitis-Associated Lesions (ALVAL). As the main features of ALVAL are lymphocytic in nature this led researchers to believe that early implant failure may occur due to delayed type IV hypersensitivity (Catelas *et al.*, 2015). Delayed hypersensitivity is characterised by a cell-mediated response controlled by T helper 1 (Th1) cells. Th1 can be activated by antigen-presenting cells i.e. metal ions or wear particles are potentially presented to T cells causing them to differentiate into a pro-inflammatory phenotype (Th1). Once stimulated, T cells proliferate and secrete 'lymphokines' (e.g. interleukin 2-6) which further attracts immune cells such as macrophages to the site of inflammation which can then become activated. In a chronic state of hypersensitivity this ultimately leads to mass cellular infiltrate of macrophages and potentially granuloma formation. It is known that CoCr wear debris particles from MoM implants can produce potentially high levels of cobalt and chromium metal ions which can act as haptens when combined with large carrier protein molecules (Thierse *et al.*, 2005). When wear debris particles are combined with haptens they can be presented by either dendritic cells or macrophages following phagocytosis to T cells and stimulate the adaptive immune response.

The pathological phenotype of a type IV hypersensitivity response would mostly be a heavy lymphocyte infiltrate, a macrophage response and possible tissue necrosis, all of which are hallmarks of ARMD. A similar response is observed in the case of contact dermatitis to nickel which is often termed as 'metal allergy' which is relatively common in the general population (around 5 to 10%) (Ahlstrom *et al.*, 2017).

However, whether hypersensitivity is the main or leading cause of ARMD is questionable. One study by Kwon *et al.* investigated the cellular response to cobalt, chromium and nickel between patients with or without inflammatory pseudotumours (Kwon *et al.*, 2010). Using a lymphocyte proliferation assay, they found that there was no difference in response from either patient group, suggesting that there may be other immune reactions taking place in response to metal ions or particles. Cytokine and

chemokine profiling in patient's serum and peri-implant tissues with aseptic loosening revealed increased levels of both classically innate immune proteins such as interleukin-1 beta (IL-1 β) and interleukin-8 (IL-8) but also the presence of interleukin-2 (IL-2) and interferon gamma (IFN- γ), indicating involvement of T cell mediated responses (Christiansen *et al.*, 2019). Therefore, it is likely that both the innate and adaptive immune systems are involved in this type of response.

1.4 Immune Response to Wear Debris

As previously discussed, wear debris is generated from all types of implants, regardless of the biomaterial used e.g. UHMWPE and ceramic. Although MoP implants generally have a long life-span when compared to MoM implants, one of the primary reasons they fail over time is due to osteolysis leading to aseptic loosening of the implant itself. It is suggested that polyethylene wear debris released from MoP implants are responsible for osteolysis due to chronic inflammation which therefore indicates that a possible immune response is occurring. Furthermore, the symptoms which accompany ARMD i.e. swelling, soft tissue necrosis and pseudotumour formation are all indicators of inflammation and role for the immune system.

It is important to note that all patients undergoing TJR surgeries will, to some extent, suffer from inflammation. However, inflammation following surgery tends to be acute whilst the patient starts to become mobile again (Chen *et al.*, 2016). In some patients, the immune system appears to be constantly activated resulting in chronic inflammation, leading to the symptoms previously described. It is suggested that wear debris plays a role in initiating immune responses following TJRs and in the case of ARMD, specifically CoCr particles and metal ions.

1.4.1 Innate immune system

The innate immune response is activated upon recognition of potentially harmful pathogens and is therefore termed 'the first line of defence'. It would therefore seem reasonable to assume it would be the innate immune system which would encounter and respond to wear debris primarily. Furthermore, one of the main type of cells which are involved in the innate immune response, macrophages, have been shown to be present in both the synovial fluid and soft tissue surrounding implants in patients with

adverse reactions (Mahendra *et al.*, 2009; Campbell *et al.*, 2010; Pajarinen *et al.*, 2010; Dapunt *et al.*, 2014a; Perino *et al.*, 2014). Additionally, in a study investigating polyethylene and titanium particle-induced osteolysis in mice, the response was found to be independent of lymphocytes, which are mostly associated with the adaptive immune response. Interestingly, other types of innate immune cells such as neutrophils and eosinophils are found in relatively low numbers in peri-implant tissues from failed MoM implants (Mahendra *et al.*, 2009; Perino *et al.*, 2014).

1.4.2 Function of monocytes, macrophages and neutrophils

The innate immune system is comprised of different cell types which all play a role in the initial stage of pathogen clearance. Innate immune cells include; eosinophils, neutrophils, monocytes/macrophages and basophils. As this study is investigating the innate immune response to biomaterials used in orthopaedic implants, the focus of this section will be on the development of immune cells most often implicated in ARMD; monocytes, macrophages and neutrophils.

Monocytes/Macrophages

Monocytes are derived from haematopoietic stem cells (HSCs) which undergo differentiation to common myeloid progenitor cells, monoblasts, pro-monocytes and finally monocytes. For this differentiation process to occur, several different growth factors are involved such as Macrophage Colony-Stimulating Factor (M-CSF) and Granulocyte Macrophage Colony-Stimulating Factor (GM-CSF). Once in circulation, monocytes can survey for any pathogens they may encounter and eventually can migrate to tissues where they differentiate into macrophages. Under certain conditions, monocytes can also differentiate into dendritic cells (DCs) (monocyte-derived DCs). *In vitro*, a combination of GM-CSF and interleukin-4 (IL-4) can stimulate differentiation of monocytes into monocyte-derived DCs.

The primary function of macrophages is to phagocytose potentially harmful pathogens. However, they are also capable of secreting both cytokines and chemoattractant subtypes, chemokines, which are involved in antigen presentation and activate the adaptive immune system. Numerous macrophages can also fuse together to form Multi-nucleated Giant Cells (MGCs). MGCs are thought to be critical in the role of aseptic loosening of prosthetic joints and osteolysis by promoting osteoclastogenesis

(Carli *et al.*, 2011). A study involving a 3-Dimensional peripheral tissue-equivalent model, consisting of a monolayer of endothelial cells supported by a collagen gel, showed that metal wear particles induce the formation of MGCs (Dutta *et al.*, 2015).

Macrophages residing in tissues express a range of Pattern Recognition Receptors (PRRs). PRRs are capable of recognising and responding to numerous exogenous danger pathogens, otherwise known as Pathogen-Associated Molecular Patterns (PAMPs) and endogenous 'alarmins' also known as Danger-Associated Molecular Patterns (DAMPs). Generally, upon recognition of PAMPs and DAMPs, the up-regulation of pro-inflammatory cytokines and chemokines are promoted which aid in pathogen clearance.

As previously discussed, monocytes and macrophages also play an important role in linking the innate and adaptive immune systems by functioning as APCs. Macrophages can phagocytose pathogens and present fragments to T cells which then initiates the adaptive immune response.

Neutrophils

HSCs are also capable of differentiating into neutrophils, using an alternative lineage to that of monocytes. Firstly they become myeloblasts, then promyelocytes and finally neutrophilic myelocytes (Hidalgo *et al.*, 2019). Mature neutrophils are established once intracellular granules are formed. Neutrophils are also released into the circulation but quickly migrate into tissues. The primary role of neutrophils is in the removal of potentially harmful pathogens from tissue. Neutrophils achieve pathogen clearance by a number of different processes including; phagocytosis, degranulation by the release of several granule stored factors such as MMPs, defensins and lysosomes and the release of Nicotinamide Adenine Dinucleotide Phosphate (NADPH) oxidase which in turn produces hydrogen peroxide and ultimately hypochlorous acid (Kolaczowska and Kubes, 2013).

1.4.3 Phagocytosis of wear debris particles

A major role for both macrophages and neutrophils is phagocytosis and many studies have investigated the role of these cells in phagocytosing wear debris particles (Nine *et al.*, 2014; Scharf *et al.*, 2014). The process of phagocytosis involves endocytosis in which the pathogen is engulfed by the plasma membrane and contained intracellularly

within a phagosome (**Figure 1.6**). The pathogen is degraded by either enzymes (e.g. NADPH oxidase, deoxyribonucleic acid (DNA)ses, lipases and proteases) or antimicrobial peptides when the phagosome comes into contact with lysosomes. These events also cause macrophages to become more activated, leading to increased cytokine and chemokine secretion. Furthermore, once digested, some pathogen antigens can be presented by antigen-presenting cells to then activate the adaptive immune system.

Phagocytosis

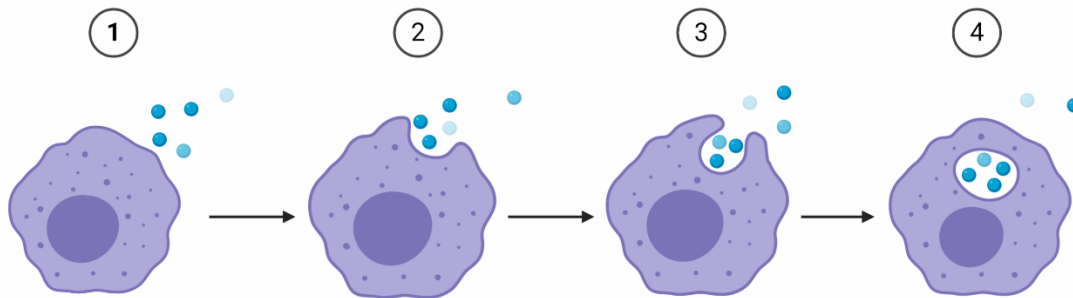


Figure 1.6. Phagocytosis process.

1) Pathogen comes into contact with phagocytic cell e.g. macrophage and binds to cell surface receptors. **2)** The macrophage begins to engulf the pathogen in the plasma membrane. **3)** Pathogen can now enter the cell by endocytosis. **4)** Pathogen is enclosed within a phagosome. Image created using Biorender.

Phagocytosed CoCr particles have been observed by histological examination and ultrastructural analysis of periprosthetic tissues recovered from patients with MoM implants. The ultrastructural analysis of CoCr particles as visualised by TEM demonstrated the presence of phagosomes with predominantly round and some rod-shaped CoCr particles which ranged from nanometer to micrometer in size (Scharf *et al.*, 2014). This is in agreement with other *in vitro* cellular studies in which osteoblasts were shown to phagocytose both UHMWPE and CoCr particles (Lohmann *et al.*, 2000). Papageorgiou *et al.* (2007a) demonstrated that both micron and nano-sized CoCr particles could be internalised by primary human fibroblasts and, in particular, nano-sized particles were observed within vacuoles whereas micron-sized particles were located in the cytoplasm, surrounding the nucleus. Another study has also shown the up-take and internalisation of CoCr nanoparticles in human peripheral leukocytes (Colognato *et al.*, 2008).

Studies have shown the potential for aluminium and zirconium ceramic particles to be engulfed by both primary fibroblasts and macrophages (Hashimoto and Imazato, 2015; Faye *et al.*, 2017). Phagocytosis of wear debris which is being chronically released from implants is likely to activate cells into an inflammatory state. Moreover, any

particles which are too large to be phagocytosed may also be causing similar effects and challenging the immune system. It has also been shown that once these CoCr particles are phagocytosed by macrophages, metal ions can be released such as cobalt and chromium which may also contribute to the inflammatory response (Scharf *et al.*, 2014).

Once any cell type has phagocytosed CoCr particles, then cells such as macrophages can become activated and actively secrete pro-inflammatory mediators such as cytokines and chemokines. Previous research has demonstrated that macrophages which are treated with wear particles, release a number of pro-inflammatory mediators such as IL-1 β , TNF α and IL-8 (Dalal *et al.*, 2012; Samelko *et al.*, 2013; Samelko *et al.*, 2016).

1.4.4 Cytokines and chemokines as inflammatory mediators

As previously discussed, following phagocytosis or in response to PAMPs and DAMPs, cytokines and chemokines are released from immune cells and play a critical role in driving inflammation. Cytokines are secreted proteins which play a major role in cell signalling and chemokines (a subset of cytokines) are mostly involved in chemotaxis, which controls the migration of cell types.

Both cytokines and chemokines are secreted from cells in response to potential dangers e.g. bacteria or viruses, and control cell migration, adhesion, proliferation, activation and maturation by binding to specific receptors on target cells. Other cell types which are not classically 'immune cells' are also known to secrete cytokines and chemokines such as fibroblasts and endothelial cells. Therefore, ARMD is potentially caused by the over-expression of persistent cytokine and chemokine release which results in chronic inflammation (Fahey *et al.*, 2014; Chu *et al.*, 2015).

Chemokines

Chemokines are classified based on their associated receptor, of which there are 19 known G-protein coupled receptors (Lodowski and Palczewski, 2009). These are further classified into 'CC' receptors or 'CXC' receptors and their chemokine ligands are therefore named based on this classification e.g. chemokine ligand 3/4 (CCL3/CCL4) or CXCL8 (IL-8) (Zlotnik and Yoshie, 2012). Generally, CC chemokines

attract monocytes/macrophages and a small subset of lymphocytes whereas CXC chemokines are chemotactic for neutrophils, although there are some exceptions. In the context of ARMD/aseptic loosening the main role of chemokines includes the migration of immune and inflammatory cells from the circulation to the periprosthetic tissues by creating a chemotactic gradient as well as apoptosis and angiogenesis.

Chemokines which are secreted by macrophages can affect which type of immune cells are attracted to the site of inflammation and therefore determine the cellular infiltrate found in tissues. It is known that in failed implants due to aseptic loosening, chemokine gene expression and protein expression is up-regulated in the peri-implant tissues e.g. CCL3, IL-8 and chemokine ligand 2 (CCL2) (Koulouvaris *et al.*, 2008; Nich *et al.*, 2013; Nich *et al.*, 2016). Furthermore, elevated IL-8 expression is directly correlated with short revision times from primary surgery (Jamsen *et al.*, 2017). Other examples where chemokines have been implicated in implant biomaterial studies include; titanium wear debris particles demonstrating an increased expression of CCL2, which is a chemoattractant for macrophages (Nakashima *et al.*, 1999). One study blocked the interaction of CCL2 with its receptor C-C chemokine receptor type 2 (CCR2) following exposure to UHMWPE particles in a mouse model and found a reduction in particle-induced osteolysis (Gibon *et al.*, 2012).

The local micro-environment can determine whether a macrophage is polarised to two different states or sub-classes; M1 or M2. The M1 subset is typically pro-inflammatory in phenotype and induced by lipopolysaccharide (LPS) and/or IFN γ . When activated, M1 macrophages induce pro-inflammatory cytokine release (e.g. TNF α and interleukin 6 (IL-6)) as well as chemokines (e.g. CCL2, CCL3, CCL4 and IL-8). M1 macrophages are the predominant subset found in cases of aseptic loosening of implants (Nich *et al.*, 2013). M2 macrophages are induced by various cytokines including interleukin-4 (IL-4), interleukin-13 (IL-13) and interleukin-10 (IL-10). M2 macrophages exhibit a more immunomodulatory phenotype and exert anti-inflammatory effects. A recent study described a new macrophage phenotype induced by CoCr wear particles which differed from typical M1 or M2 macrophages (Bijukumar *et al.*, 2020). The authors observed increased expression of M1 markers and decreased M2 markers. However, these CoCr particles induced macrophages also exhibited higher expression of signal transducer and activator of transcription 6 (STAT-6) (M2 marker) and lower cluster of

differentiation 86 (CD86) expression (M1 marker), suggesting a mixed phenotype (Bijukumar *et al.*, 2020).

1.5 Metal Ions Activate Toll-like Receptors

1.5.1 Nickel ions and TLR4

As previously discussed, hypersensitivity to nickel is relatively common with around an estimated 65 million people in Europe effected, or between 5-10% of the general population, with a higher prevalence observed in young females (Mattila *et al.*, 2001; Ahlstrom *et al.*, 2017). Hypersensitivity reaction occurs upon contact with nickel-containing items such as costume jewellery, body piercings and coins (Liden *et al.*, 2008). Under these circumstances, individuals can develop allergic contact dermatitis which is believed to be predominantly driven by the adaptive immune response involving antigen presentation to T lymphocytes by dendritic cells. However, for efficient sensitisation following re-exposure to contact allergens, a second pro-inflammatory stimulus is required. This unknown stimulus led to a ground-breaking study in 2010 by Schmidt *et al.* who began to investigate the mechanisms behind hypersensitivity to nickel (Schmidt *et al.*, 2010).

Nickel ions can stimulate the pro-inflammatory transcription factor Nuclear Factor Kappa-light-chain-enhancer of activated B cells (NF-κB) and subsequent release of inflammatory cytokines. Schmidt *et al* recognised that the gene profiling studies investigating pro-inflammatory responses associated with nickel ions appeared to be linked primarily with innate immunity (Viemann *et al.*, 2007). For an innate immune response to occur, membrane-bound and intracellular receptors (PRRs) are activated by immune signals (PAMPs and DAMPs). These receptors most commonly belong to families such as Toll-like Receptors (TLRs) or Nucleotide Oigodimerisation Domain (NOD)-like Receptors (NLR). The authors of this study therefore hypothesised that nickel ions could potentially activate these receptors and initiate an immune response (Schmidt *et al.*, 2010).

Firstly, Schmidt *et al* (2010) investigated which receptor family could be involved in the immune response to nickel ions. The authors decided to target Myeloid Differentiation primary response 88 (MyD88) which is an adaptor protein essential for TLR signalling pathways. Schmidt *et al.* found that depletion of MyD88 by RNA-mediated interference

in nickel ion-stimulated endothelial cells almost completely abolished the expression of IL-8. These findings suggested a potential role for TLRs in the observed response (Schmidt *et al.*, 2010).

LPS, or bacterial endotoxin, also up-regulates IL-8 expression in endothelial cells through activation of Toll-like Receptor 4 (TLR4). To evaluate whether TLR4 is implicated in nickel ion-mediated immune responses, Human Embryonic Kidney cells (HEK293) were transfected with human TLR4 and its co-receptor Myeloid Differentiation factor 2 (MD2) which are not endogenously expressed. Parental HEK293 cells did not respond to nickel ions or LPS, however, TLR4 and MD2 transfected cells responded to both stimuli, which demonstrates the ability of nickel ions to activate human TLR4 (Schmidt *et al.*, 2010).

Another important finding within this research was that the TLR4 response to nickel ions was species-specific. Schmidt *et al.* found that mouse cells such as bone marrow-derived macrophages or Raw264.7 macrophages did not produce TNF α when stimulated with nickel ions despite their sensitivity to LPS. The investigators predicted that non-conserved sequence motifs of human TLR4 could be responsible for the difference in species responses. To test this hypothesis, HEK293 cells were transfected with either human or mouse TLR4 as well as human MD2 and found that cells expressing mouse TLR4 and human MD2 did not secrete IL-8 in response to nickel ions. They also discovered that the differences between species is caused by a so-called 'histidine pocket' consisting of 3 histidine residues at positions 431, 456 and 458 in the human TLR4 sequence. Murine TLR4 lacks both H456 and H458 which means the 3 residues are unable to come together to form a binding site for nickel ions and as a result murine TLR4 cannot be activated by nickel ions. TLR4 activation was proven by a series of mutant deletion experiments which demonstrated that double mutation of H456 and H458 considerably decreased nickel ion-induced IL-8 production in numerous assays including western blots, flow cytometry and Enzyme-Linked Immunosorbent Assay (ELISA) (Schmidt *et al.*, 2010). This finding further explains why previous mouse models were unresponsive to nickel ions as murine TLR4 is lacking in these two crucial histidine residues (Sato *et al.*, 2007).

Due to its association with hypersensitivity reactions, nickel is rarely used in prosthetic implants or is present in small, trace amounts. As previously discussed, the main materials used in MoM implants are CoCr. Cobalt shares many similar properties to

nickel as they are adjacent transition metals on the periodic table. Importantly, it is known that both metals are capable of binding to histidine as cobalt and nickel columns are frequently used to isolate histidine-tagged proteins (Bornhorst and Falke, 2000). Therefore, it was hypothesised that perhaps cobalt ions could also bind directly to human TLR4 in a similar way to nickel ions and provide a possible link to ARMD.

1.5.2 Cobalt ions and TLR4

The first study conducted by Tyson-Capper *et al.* investigated the potential for cobalt ions to activate human and mouse TLR4 (Tyson-Capper *et al.*, 2013). The study design involved using both a human and mouse reporter cell line which contained a Secreted Alkaline Phosphatase (SEAP) reporter gene. Upon activation of NF κ B, the SEAP gene is induced and released from cells. Increased NF κ B activity results in further SEAP secretion which can be quantified using a colorimetric assay. In this set of experiments, the addition of cobalt ions only increased SEAP secretion in human TLR4-expressing reporter cells and not in murine TLR4-expressing reporter cells. These findings were therefore in agreement with the previous investigations by Schmidt *et al.* involving nickel ions and their ability to only activate the human form of TLR4 (Schmidt *et al.*, 2010). The findings regarding cobalt-mediated activation of human TLR4 have been further confirmed by other studies (Raghavan *et al.*, 2012; Potnis *et al.*, 2013; Oblak *et al.*, 2015; Lawrence *et al.*, 2016b). These studies have used human TLR4-specific inhibitors (e.g. monoclonal antibodies or CLI-095) which decrease the production of pro-inflammatory cytokines in macrophage cell models treated with cobalt ions (Lawrence *et al.*, 2014; Lawrence *et al.*, 2016b).

The fact that cobalt ions released from MoM implants potentially activate TLR4 provided a potential aetiology for ARMD and inflammation associated with these prostheses.

1.5.3 Toll-like receptor 4

TLR4 is an innate immune receptor belonging to the TLR family. TLRs are PRRs and form an essential part of initiating the innate immune response by recognising a variety of pathogens. There are currently 10 known TLRs which are either expressed on the cellular surface (TLR2, 4, 5, 6 and 10) or intracellularly (TLR3, 7, 8 and 9). Each TLR

recognises specific PAMPs which are expressed by individual pathogens. In the case of TLR4, its specific PAMP is LPS which is expressed in the cell wall of gram-negative bacteria. Furthermore, TLRs are also able to recognise a number of DAMPs for example, High Mobility Group Box 1 (HMGB1), a nuclear protein secreted by necrotic cells which can go on to activate TLR2, 4 and 9.

To become fully activated, TLR4 requires homodimerisation to allow the binding of adaptor proteins such as MyD88. Homodimerisation of the TLR4 receptor allows a downstream signalling cascade to occur which results in the activation of transcription factors such as NF κ B and Interferon Regulatory Factor 3 (IRF3). NF κ B regulates the transcription of both cytokines and chemokines such as IL-8 and TNF α . TLR activation also aids in the link between the innate and adaptive immune systems by promoting enhanced phagocytosis and antigen presentation to T cells. This study will focus mostly on TLR4, which is expressed by many different cell types such as macrophages and endothelial cells (Vaure and Liu, 2014).

1.5.4 LPS activation of TLR4

As discussed previously, LPS is the main ligand for TLR4. However, TLR4 can only become fully activated by LPS with the addition of accessory proteins such as LPS-Binding Protein (LBP), Cluster of Differentiation 14 (CD14) and MD2. LBP binds to LPS and forms a complex with CD14 which transfers LPS to MD2 which is complexed with TLR4. Once MD2/TLR4 binds with LPS, this initiates the homodimerisation of TLR4. It is known that the MD2 complex is crucial to LPS-mediated activation of TLR4 as MD2 deficient mice do not respond to LPS (Park and Lee, 2013).

TLR4 can recruit further adaptor proteins to initiate a signalling cascade by utilising its Toll IL-1 Resistance domain (TIR). The adaptor proteins which are recruited also contain TIRs and include, MyD88, TIR domain containing Adaptor Protein (TIRAP), TIR domain containing adaptor-inducing Interferon- β (TRIF) and TRIF-related Adaptor Molecule (TRAM) and can activate signalling pathways via Interleukin-1 Receptor Associated Kinase 1 (IRAK1) and TNF Receptor Associated Factors (TRAF) molecules as well as transcription factors such as NF κ B (Lu *et al.*, 2008). The recruitment of these adaptor proteins ultimately leads to the up-regulation of pro-

inflammatory cytokines and chemokines and promotes an immune response against LPS. The TLR4 pathway signalling pathway is outlined in **Figure 1.7**.

Although LPS is the main ligand described for TLR4 and the most frequently studied, there are known other stimulants of TLR4. As discussed earlier, HMGB1 is another of the more well-known ligands but various Heat Shock Proteins (HSPs), hyaluronans and fibrinogens are others (Erridge, 2010). However, it is debatable whether these 'DAMPs' are able to bind to TLR4 directly or whether they are potentially assisted by endotoxin contamination (Erridge, 2010). What has been established though, is that various stimuli can activate TLR4 other than LPS, whether this be PAMPs, DAMPs or in fact metal ions such as nickel and cobalt.

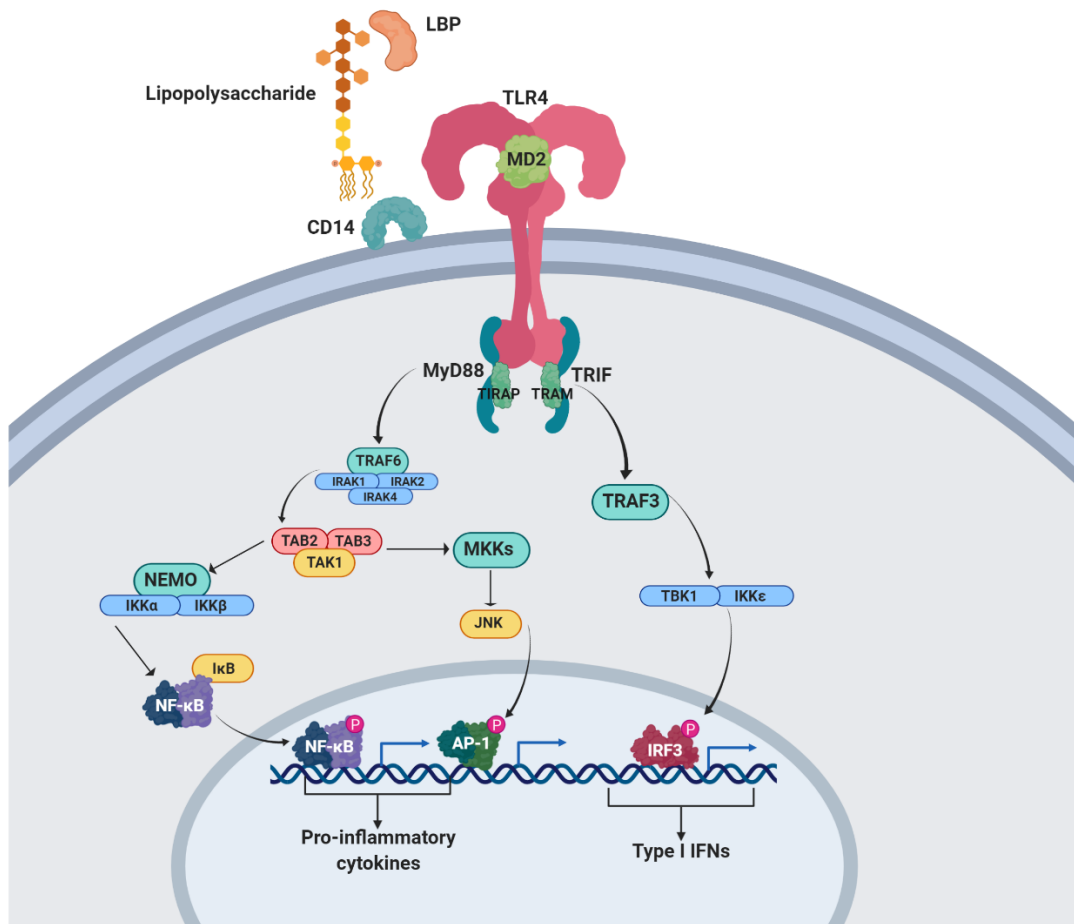


Figure 1.7 TLR4 pathway.

Lipopolysaccharide (LPS)-mediated activation of Toll-like receptor 4 (TLR4) requires several molecules including LPS binding protein (LBP), cluster differentiation 14 (CD14) and myeloid differentiation factor-2 (MD2). LBP is a protein which binds directly to LPS and facilitates the interaction between LPS and CD14. CD14 can either be anchored to the cell membrane or exist in its soluble form. CD14 transfers the LPS/LBP complex to MD2, which complexes with TLR4 itself and 'recognises' LPS. Following this recognition, TLR4 begins to recruit its downstream adaptors through interactions with Toll IL-1 Resistance (TIR) domains. The signalling cascade can either follow the Myeloid differentiation primary response 88 (MyD88)-dependent pathway or the MyD88-independent pathway (TIR-domain-containing adapter-inducing interferon- β (TRIF)). The MyD88-dependent pathway recruits several complexes and kinases. This ultimately leads to the activation of the transcription factors, nuclear factor- κ B (NF- κ B) and activator protein 1 (AP-1), leading to up-regulation of pro-inflammatory cytokines and chemokines. The TRIF pathway also recruits proteins and kinases. Following this downstream signalling the transcription factor interferon regulatory transcription factor (IRF3) is activated which results in the production of Type I interferons. Image created using Biorender.

1.5.5 Wear debris particles and TLR4

Few studies have investigated CoCr particles and their role in potentially activating TLR4, despite knowing that activation can occur through cobalt ions.

In the few studies that have investigated CoCr particles and the TLR4 pathway, the particles used have largely been commercially available and do not represent the most 'clinically relevant' model particles. Commercially available particles are usually either too large in size or uniform in shape (i.e. micrometre sized as opposed to nanometre and regular versus irregular shaped). One study investigated whether CoCr particles activated a monocytic cell line, PBMCs and an *in vivo* mouse model more predominantly through TLR4 or TLR2 (Samelko *et al.*, 2017). The authors concluded that in co-stimulation experiments with either LPS (TLR4 agonist) or PAM3CSK (TLR2 agonist) the osteolytic and inflammatory effect (measured by the secretion of TNF α and IL-1 β) of CoCr particles was greater in the TLR4 model (Samelko *et al.*, 2017). However, the same group also found that using a blocking TLR4-specific antibody in a monocytic cell line, did not significantly reduce the secretion of TNF α or IL-1 β following stimulation with CoCr particles (Samelko *et al.*, 2016). In contrast to these findings, another group investigated the effect of CoCr particles on a monocytic cell line in combination with a TLR4 blocking antibody as well as silencing of MyD88 (Potnis *et al.*, 2013). TLR4 inhibition prevented particle-induced NF κ B activation and significantly decreased IL-8 release. Furthermore, the gene expression of TLR4 in osteoblasts has been shown to be up-regulated when treated with CoCr particles (Jonitz-Heincke *et al.*, 2019).

After reviewing the literature, there appears to be no direct investigations into ceramics and their effect on the TLR4 pathway. However, titanium oxide (TiO₂) and zirconium oxide (ZrO₂) have been shown to up-regulate the expression of other TLRs (*TLR3 and TLR7*) (Lucarelli *et al.*, 2004). It is possible that these biomaterials may be activating alternative pathways which in turn up-regulate TLR expression.

1.6 Consequences of TLR4 Activation

Once activated by LPS (or other potential stimuli), TLR4 initiates an inflammatory response which is described in the following section.

1.6.1 Cytokine and chemokine secretion

The activation of transcription factors following TLR4 activation will determine which cytokines or chemokines are up-regulated and secreted. For example, NF κ B activation leads to the production of pro-inflammatory cytokines and chemokines such as IL-6, IL-8 and TNF α whereas IRF3 activation promotes interferon up-regulation (Honda *et al.*, 2006; Liu *et al.*, 2017). In the case of LPS activation of TLR4, a milieu of cytokines and chemokines are released which all combine to promote an effective inflammatory response (Guijarro-Munoz *et al.*, 2014).

IL-8 is a CXC chemokine most commonly secreted by macrophages and endothelial cells. As discussed in **section 1.4.4**, IL-8 has been associated with aseptic implant loosening due to its increased expression in the tissues of patients with loosened implants. Furthermore, IL-8 is a selected marker of inflammation and TLR4 activation in many cellular *in vitro* studies which have investigated cobalt ion and CoCr particle initiated immune responses (Lawrence *et al.*, 2014; Lawrence *et al.*, 2016b). The main function of IL-8 is to attract neutrophils to the site of inflammation. CCL2, CCL3 and CCL4 are all CC chemokines and are also up-regulated following TLR4 activation. CCL2, similarly to CCL3 and CCL4, can chemoattract monocytes, however, they are also capable of recruiting Natural Killer (NK) cells and T cells (Hughes and Nibbs, 2018).

TLR4 signalling must be tightly regulated so that the immune system can be returned to a physiological state and prevent causing harm such as sepsis which can lead to organ failure and potentially death. Regulation of TLR4 activation can occur by several mechanisms; down-regulating expression of TLR4, blocking interactions with soluble factors or decoy receptors and various inhibitory signalling molecules. One example of a soluble factor involved in the regulation of TLR4 signalling is the soluble form of TLR4 which has been shown to significantly reduce LPS-induced NF- κ B activation and subsequent cytokine production in a mouse macrophage cell line (Iwami *et al.*, 2000). Interleukin Receptor-Associated Kinase-M (IRAK-M) is an example of an inhibitory molecule, typically expressed by monocyte/macrophage cells. IRAK1 and IRAK4 are active kinases part of the signalling cascade initiated by TLR4 activation and IRAK-M inhibits their signalling thus negatively regulating TLR4 signalling (Kobayashi *et al.*,

2002). Mice deficient in IRAK-M display heightened inflammatory responses in response to LPS such as increased cytokine production and NF- κ B activation (Deng *et al.*, 2006).

1.6.2 Enhanced phagocytosis

Not only does activation of TLR4 lead to the production of the inflammatory cytokines and chemokines discussed, it can also promote phagocytosis by immune cells. For example, TLR4 knockout mice have reduced phagocytic capability when compared with wild type and macrophages treated with LPS have significantly increased rate of phagocytosis (Blander and Medzhitov, 2004; Anand *et al.*, 2007). The exact mechanisms by which phagocytic capability is enhanced following TLR4 activation is unclear. A recent study suggested that the adaptor protein TRAM is instrumental for the effective phagocytosis of *Escherichia coli* and *Staphylococcus aureus* (Skjesol *et al.*, 2019). Ultimately, the mechanisms which lead to enhanced phagocytosis likely differ dependent on the pathogen encountered.

1.6.3 Process of leukocyte extravasation, adhesion and migration

For an inflammatory immune response to be fully orchestrated, leukocytes such as monocytes or neutrophils from the circulation must enter tissue at the site of infection, injury or stress to ultimately aid tissue repair. TLRs are crucial for leukocyte migration to occur as they can recognise and bind to ligands from pathogens, activate immune cells and initiate the secretion of cytokines and chemokines which in turn activate endothelial cells within the microvasculature. The first step of leukocyte migration is the establishment of interactions with the leukocytes and endothelial cells through a series of steps; capturing, rolling, leukocyte arrest, crawling to sites of exit and transmigration through the endothelium (**Figure 1.8**).

Adhesion molecules expressed by both leukocytes and endothelial cells aid with the initial interaction between the two cell types. Selectins, expressed by endothelial cells e.g. E-selectin and P-selectin are up-regulated in response to inflammatory stimuli and initiate the capture of leukocytes in the circulation (McEver, 2015). As the leukocytes flow, with this transient interaction, they begin to roll across the endothelium which is slowed due to pulling of long membrane tethers. Integrins, expressed by the leukocytes

become activated and can bind to adhesion markers such as Intercellular Adhesion Molecule 1 (ICAM-1) and Vascular Cell Adhesion Molecule 1 (VCAM-1). ICAM-1 and VCAM-1 expression are up-regulated by endothelial cells in response to pro-inflammatory cytokines and allow firm adhesion to the rolling leukocytes. Leukocyte integrins are also activated in response to inflammatory stimuli such as chemokines and are crucial for firm adhesion to take place. The ligands for ICAM-1 binding are Lymphocyte Function-associated Antigen (LFA-1), expressed by all leukocytes and Macrophage antigen 1 (MAC-1) which is typically expressed by monocytes/macrophages. The integrin ligand for VCAM-1 is Very Late Antigen 4 (VLA-4), expressed by both lymphocytes and monocytes (Chigaev and Sklar, 2012). The expression of adhesion molecules is tightly regulated so that these processes only occur during pathogenic conditions. As discussed, pro-inflammatory cytokines such as IL-6 and TNF α , are secreted in response to pathogens which in turn cause the up-regulation of adhesion molecules and the activation of the endothelium (Zhang *et al.*, 2011). As activation of TLR4 results in cytokine production, LPS has been shown to directly influence the expression of ICAM-1 in an endothelial cell line (Sawa *et al.*, 2008). Moreover, following exposure of cobalt ions to myoblasts there is a significant increase in ICAM-1 expression which is further enhanced by the addition of monocytes (Laumonier *et al.*, 2019).

Once firm adhesion has become established, leukocytes are able to 'crawl' on the surface of blood vessels until they encounter suitable 'exit sites' and transmigrate through the endothelium into the tissue. The secretion of chemokines from macrophages located within the inflamed tissue creates a gradient for the leukocytes to migrate towards. However, cell surface receptors located at endothelial cell intercellular junctions are thought to also play a major role such as Platelet Endothelial Cell Adhesion Molecule-1 (PECAM-1) on both leukocytes and endothelial cells allowing the transmigration of leukocytes. The type of immune cell attracted to site of inflammation is dependent on the pathogen encountered and which profile of chemokines are secreted e.g. IL-8 attracts neutrophils or CCL3 and CCL4 will attract monocytes/macrophages. Chemokines are also capable of conformational changes to adhesion markers which contribute to the process of adhesion binding to leukocytes. Once the leukocytes have infiltrated the inflamed tissue, they are able to orchestrate further inflammatory immune responses such as phagocytosis and eventual clearance of the pathogen which initiated the response.

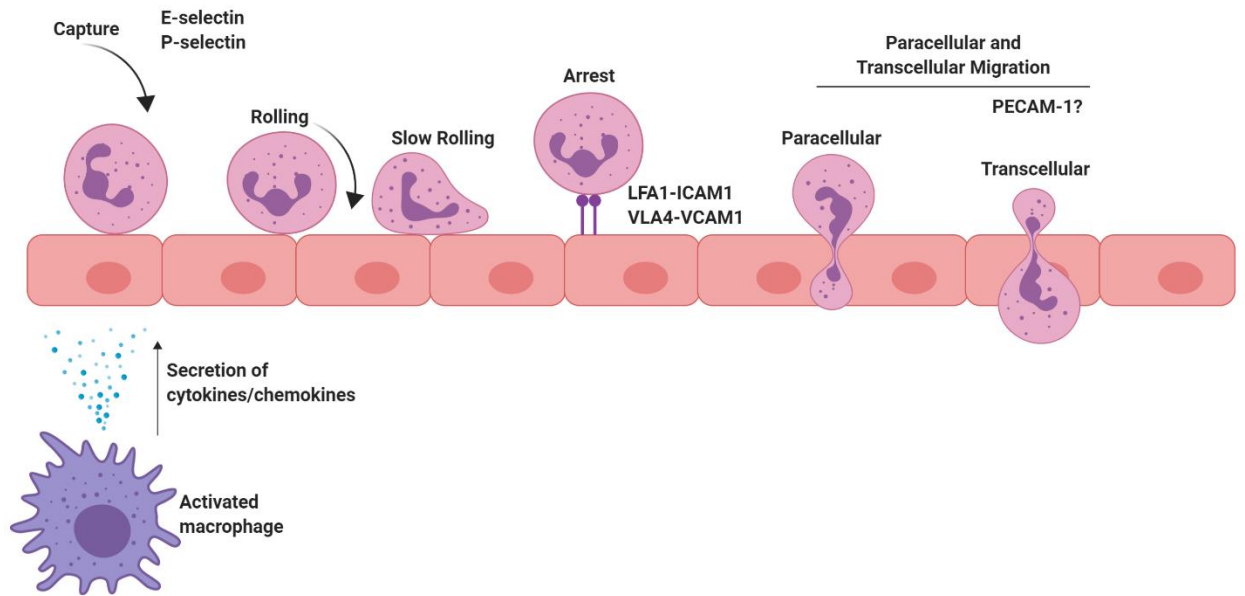


Figure 1.8 Leukocyte adhesion and migration.

Leukocyte extravasation is a process which involves a number of proteins and chemotactic stimuli. Firstly, the endothelium is activated by pro-inflammatory cytokines or chemokines released by activated immune cells such as macrophages. Endothelium activation causes the up-regulation of selectins on endothelial cells such as E-selectin and P-selectin which interact with molecules expressed on the surface of leukocytes. This transient interaction allows the leukocytes to roll across the endothelium until they become firmly bound to the endothelial adhesion markers ICAM-1 and VCAM-1 which attach to LFA-1 and VLA-4 expressed by leukocytes. The leukocyte can then either cross the endothelium by paracellular migration (between cell junctions) or transcellularly. It is not fully understood which proteins/molecules are involved in this process but PECAM-1 is believed to play an important role. Image created using Biorender.

1.7 The Inflammasome Response

Inflammasomes are intracellular multiprotein signalling complexes that are assembled upon recognition of pathogenic microorganisms and danger signals. Upon activation of inflammasomes, pro-inflammatory caspases can become cleaved and up-regulated. There are various distinct inflammasomes, all of which are assembled in response to both PAMPs and DAMPs within the cytosol. Upon recognition of these ligands; activation, oligomerisation and the recruitment of an adaptor protein, Apoptosis-associated Speck-like protein containing a CARD (ASC), follows. ASC consists of two domains: a Pyrin Domain (PYD) and a Caspase Recruitment Domain (CARD) which allow ASC to bridge the interaction between the inflammasome sensor and caspase 1 (Petrilli *et al.*, 2007). Ultimately, this interaction leads to the formation of active protease caspase 1, increased secretion of the pro-inflammatory cytokines IL-1 β and interleukin-18 (IL-18) and pyroptosis, a highly inflammatory form of cell death. Numerous receptors have been identified and confirmed to assemble inflammasomes. These include the Nucleotide-binding Oligomerisation Domain (NOD), Leucine-Rich Repeat (LRR)-containing protein (NLR) family members, NLRP1, NLRP3 and NLRC4. These 'canonical' inflammasomes are also complimented by the non-canonical pathway, which targets both caspase 4 and 5 in humans and can also induce pyroptosis (Kayagaki *et al.*, 2013).

The NLRP3 inflammasome has been investigated in relation to implant wear debris *in vitro* (Caicedo *et al.*, 2009; Samelko *et al.*, 2016). For example, a monocytic cell line treated with cobalt, chromium and nickel ions as well as CoCrMo alloy particles demonstrated an up-regulation of IL-1 β for all treatments which was caspase-1 dependent (Caicedo *et al.*, 2009). In agreement with this study, the NLRP3 pathway was shown to play a greater role in CoCr particle-mediated inflammation when compared to the TLR4 pathway by comparing the use of inhibitors for caspase-1 and TLR4, respectively (Samelko *et al.*, 2016). The NLRP3 signalling pathway is summarised in **Figure 1.9**.

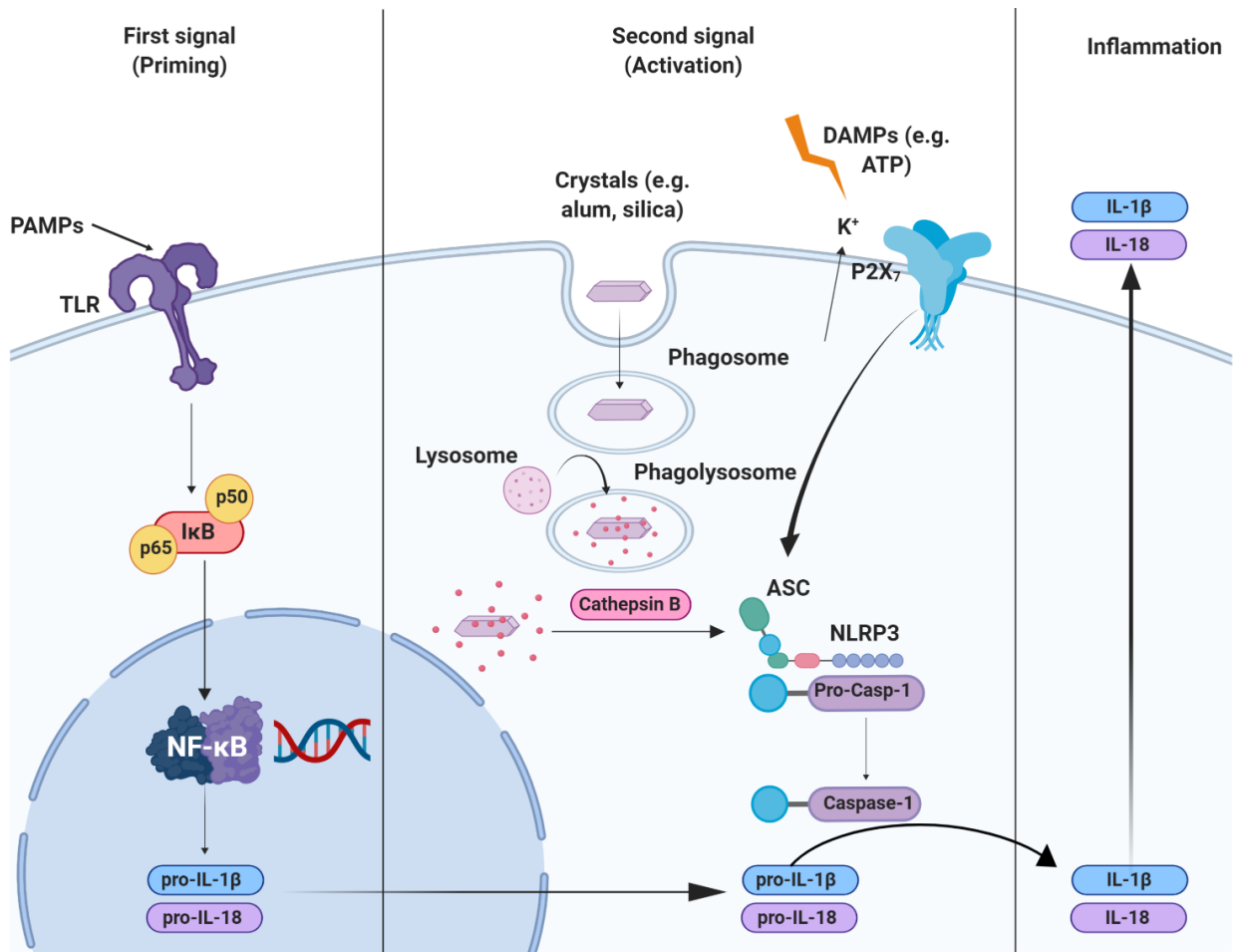


Figure 1.9 The NLRP3 inflammasome.

For NLRP3 to become fully activated 2 signals are required; priming and activation. The priming signal can be achieved through a plethora of PAMP signals e.g. LPS which acts through the toll-like receptors (TLRs) and leads to the activation of NF- κ B. This in turn results in the production of pro-IL-1 β and pro-IL-18 which remains cytosolic. The second activation signal remains rather more poorly understood however potassium (K^+) efflux and cathepsin B are possible activators of NLRP3. The effect of ATP is mediated by the purinergic P2X₇ receptor which causes K^+ efflux from the cytosol upon activation. The phagocytosis of crystals such as alum and silica can lead to lysosomal swelling, destabilisation and damage. This process releases cathepsin B, a lysosomal cysteine protease which is thought to then directly activate NLR3P3. Upon activation, NLRP3 can assemble with ASC which in turn induces pro-capase-1 dimerisation allowing auto-activation to the proteolytic form caspase-1. Caspase-1 is activated through interaction with ASC and can then cleave pro-IL-1 β and pro-IL-18 to their active form which is then secreted from the cell. Image created using Biorender.

1.7.1 NLRP3 activation

The NLRP3 inflammasome consists of 3 main components; a sensor (NLRP3), adaptor (ASC) and an effector (caspase 1). The domains that make up NLRP3 itself are an amino-terminal pyrin domain (PYD), a central NACHT domain and a carboxyl-terminal LRR domain. For NLRP3 to become fully activated, 2 steps are required; a priming step followed by activation. The priming stage is initiated in response to several different PAMPs which as previously stated, activate PRRs such as TLRs or through cytokines which activate NF- κ B which can lead to the up-regulation of NLRP3 components, caspase-1 and pro-IL-1 β (Bauernfeind *et al.*, 2009). The priming stage of NLRP3 activation is also involved in post-translational modifications such as ubiquitination and phosphorylation. However, the second activation step is required to induce full activation and the assembly of the inflammasome. Interestingly, unlike other inflammasomes, NLRP3 has many proposed activators such as bacterium, viruses and endogenous danger signals (i.e. DAMPs), however, the common factor with these activators is that they induce cellular stress although it is currently unknown the exact mechanisms NLRP3 facilitates to be able to sense stresses.

The second activating signal is believed to cause a number of signalling events which cause the full activation of NLRP3 such as efflux of potassium ions (K⁺) and lysosomal destabilisation. Once more, these events remain to be confirmed and may be overlapping. However, K⁺ efflux appears to be an important upstream signal for NLRP3 activation as Adenosine Triphosphate (ATP) and nigericin (which cause the depletion of K⁺) are known to induce the maturation of pro IL-1 β so that IL-1 β can be secreted (Perregaux and Gabel, 1994). These factors can activate the P2X purinoceptor 7 (P2X₇), a non-specific ligand-gated cation channel. However, upon stimulation, P2X₇ promotes sodium and calcium ion influx and interacts with the Two-pore domain Weak Inwardly rectifying K⁺ 2 (TWIK2) channel which ultimately promotes K⁺ efflux. Therefore, TWIK2 may play a more important role in K⁺ efflux and ultimately NLRP3 activation. This has recently been demonstrated by depleting *Kcnk6* (the gene encoding TWIK2) in macrophages which prevented NLRP3 activation and suppressed sepsis-induced lung inflammation in mice (Di *et al.*, 2018). Lysosomal destabilisation is another proposed signalling event to cause NLRP3 full activation and can be caused by the phagocytosis of particulates such as aluminium salts and silica crystals (Hornung *et al.*, 2008). Phagocytosis of crystals and salts induces lysosomal

acidification, swelling and finally rupture which causes the release of particulates into the cellular cytoplasm. The importance of lysosomal destabilisation has been demonstrated using cathepsin inhibitors which reside in the lysosome and cathepsin B has been shown to be released following lysosomal membrane degradation (Orlowski *et al.*, 2015). Once NLRP3 is fully activated, the assembly of the inflammasome can ensue i.e. with ASC and caspase-1 which leads to the production of mature IL-1 β and IL-18.

1.7.2 Consequences of NLRP3 activation

As discussed previously, pro IL-1 β is an inactive pre-cursor found in the cellular cytoplasm which is only released in its mature form following the activation of the inflammasome e.g. NLRP3. Therefore, pro IL-1 β is expressed following the initial 'priming' step and secretion occurs when the second activation step is induced. NLRP3 activation causes pro caspase-1 to become its active form and cleaves pro IL-1 β to its mature form, although the exact mechanisms that IL-1 β is then secreted from cells remains poorly understood. However, it has been established that IL-1 β secretion occurs prior to Lactate Dehydrogenase (LDH) release, therefore prior to cell death or pyroptosis (Brough and Rothwell, 2007). This method of IL-1 β secretion is also similar for the cleavage of pro-IL-18 by caspase-1 to its active form, IL-18. Both IL-1 β and IL-18 can be secreted by many different cell types but most typically by immune cells such as monocytes and macrophages. Mature IL-1 β is a pro-inflammatory cytokine and important mediator in a number of immune responses. For example, IL-1 β is involved in the recruitment of innate immune cells to the site of inflammation and modulates adaptive immune cells such as T cells. The function of mature IL-18 is rather different and plays an important role in the production of IFN- γ as well as controlling the cytotoxic activity and proliferation of NK cells and T cells. IL-18 can also promote the secretion of other cytokines such as TNF α and IL-8 and can therefore influence neutrophil migration and activation.

1.7.3 Metal ions, wear debris and the inflammasome

Previous studies have shown that metal ions such as cobalt, chromium and nickel are all able to trigger NLRP3 activation in macrophages (Caicedo *et al.*, 2009; Li and Zhong, 2014). However, the underlying mechanisms behind NLRP3 activation remains elusive although it is known that NLRP3 induction relies on NF- κ B activation which metal ions are known stimuli of. Moreover, DAMP signalling can activate NLRP3 such as Reactive Oxygen Species (ROS) production and lysosomal destabilisation which are all potential effects of metal ion stimulation. Studies have also demonstrated the production of IL-1 β in macrophage cell lines treated with metal ions *in vitro*, a hallmark of NLRP3 activation (Caicedo *et al.*, 2009). However, a recent study investigating metal ions and their effect on bone marrow-derived mouse macrophages found that cobalt ions did not induce IL-1 β secretion when using LPS as the 'priming' first signal (Ferko and Catelas, 2018). In contrast, another study showed that chromium ions acted as the second 'activation stimuli' in a model using THP-1 macrophages (Adam *et al.*, 2017). IL-1 β secretion was induced following priming with 12-O-tetradecanoylphorbol-13-acetate (TPA) (a known priming signal in THP-1 cells) and subsequent stimulation with chromium ions. The amount of IL-1 β secreted under these conditions was comparable with ATP (Adam *et al.*, 2017).

1.8 Future of Biomaterials in Joint Replacements

The current literature suggests that the causes of ARMD appear to be "immune regulated" leading to chronic inflammation in some patients receiving implants containing metals (Lawrence *et al.*, 2014). It has been well established that metal ions potentially released from these implants can activate the TLR4 pathway which may be partially responsible for reactions observed. However, few studies have used clinically relevant CoCr particles to investigate these effects. It is also important to establish which other immunological pathways may be involved i.e. the NLRP3 inflammasome and whether this is caused directly by wear debris particles or indirectly through activation of alternative pathways. Although the use of MoM implants has been almost completely abrogated, CoCr continues to be used in implants such as MoP prostheses. Therefore, these implants may lead to similar CoCr wear debris and as a result

potentially cause ARMD. Moreover, there are currently millions of patients worldwide who have received MoM implants which may suffer from ARMD in the future.

The lessons we have learned from MoM implants and any further biological understanding we can gain from investigating their effects can also be applied to different and increasingly used biomaterials such as ceramics. Although ceramics were originally believed to be bio-inert, the presence of a pseudotumour in a case of a patient with a CoC implant suggests otherwise (Campbell *et al.*, 2017).

1.9 Summary

In summary, MoM implants are believed to fail mostly due to ARMD which causes enhanced osteolysis, soft tissue necrosis, pseudotumour formation and pain meaning that implants need to be revised in a costly and complicated procedure. Furthermore, it seems that other implants such as MoP, CoP and CoC could also potentially cause similar effects which are yet to be fully understood or investigated. ARMD is driven by inflammation due to the presence of immune cells in periprosthetic tissue and the up-regulation of pro-inflammatory cytokines and chemokines in response to metal ions and wear debris. However, the exact mechanisms and immune pathways which initiate this response and the downstream signalling events remain unknown. It has previously been established that metal ions such as cobalt can activate the TLR4 pathway, which is usually activated by bacterial LPS. However, the effects of clinically relevant CoCr wear debris particles is less clear and whether any other pathways are involved i.e. the inflammasome and how much of a role these pathways play. Furthermore, the effect that other biomaterials used in ceramic implants e.g. alumina and zirconia have on the TLR4 pathway etc. has not been investigated despite their ever-growing popularity.

1.10 Hypothesis and Aims

This study therefore hypothesises that metal wear debris from joint implants can activate human TLR4 and subsequently the inflammasome which results in inflammatory responses accounting for the development of ARMD.

The aims of this study are to use *in vitro* cell models to demonstrate the potential inflammatory effect of clinically relevant CoCr particles and ceramic oxide nanopowders and assess the role of TLR4 and the inflammasome in these responses.

1.11 Objectives

A. To generate and characterise clinically relevant CoCr wear particles suitable for cell culture

Nanoscale particles were generated using a six-station pin-on-plate wear simulator using the alloy material which is used in MoM implants, CoCrMo. Particles were characterised using scanning electron microscopy (SEM) to establish their size and composition and then sterilised for use in cell culture treatments. Inductively couple plasma mass spectroscopy (ICP-MS) was used to confirm the concentration of cobalt and chromium ions released from the particles in cell culture medium.

B. To determine the role of TLR4 and the inflammasome in the inflammatory response to CoCr particles

A Meso Scale Discovery (MSD) multiplex cytokine/chemokine assay was conducted to investigate potential markers of CoCr-mediated inflammation in monocyte/macrophage cell lines. TLR4 inhibitors were employed to see whether they inhibited any of the observed effects. The inflammasome response to CoCr particles was also investigated by evaluating IL-1 β expression and secretion. The phagocytosis of CoCr particles by THP-1 cells investigated by transmission electron microscopy (TEM) and a phagocytosis assay.

C. To Investigate the functional effects of CoCr particles *in vitro* and the translation to patient tissue following hip and knee revision surgery

The effect of adhesion molecule expression was assessed in HMEC-1 endothelial cell. The migration of neutrophils was investigated using a transwell chemotaxis assay. Soft tissue was collected from patients undergoing revision TJR and stained for immune cell infiltration to further establish the migration of cells in an *in vivo* setting.

D. To investigate the biological effect of ceramic oxide nanopowders

The techniques and assays previously established were applied to two ceramic oxide nanopowders, aluminium and zirconia. Cell lines were treated with these ceramic oxide nanopowders to establish whether an inflammatory response occurred and whether this was TLR4 specific or involved activation of the inflammasome.

Chapter 2 : Materials and Methods

2.1 Cell Culture

Cell culture work was performed under sterile conditions using Class II Microbiological Safety Cabinets and aseptic technique employed at all times. Cells were incubated in a humidified atmosphere at 37°C and 5% CO₂ in tissue culture flasks with ventilated caps (Greiner, Austria).

2.1.1 Summary of cell lines used

MonoMac 6

MonoMac 6 (MM6) cells are a human monocytic cell line derived from acute monocytic leukaemia (provided by Dr Jem Palmer, Newcastle University, UK) and known to express TLR4 (previous research within group) as well as responding to bacterial LPS by secretion of inflammatory cytokines e.g. IL-8 (work undertaken as part of previous MRes project). MM6 cells were cultured in Roswell Park Memorial Institute Medium (RPMI)-1640 medium (Sigma Aldrich, USA) and supplemented with 10% foetal bovine serum (FBS), 2mM L-glutamine, 50U/ml penicillin and 50µg/ml streptomycin (Sigma Aldrich, USA).

THP-1

THP-1 cells are a human monocytic cell line derived from acute pre-monocytic leukaemia (ATCC® TIB-202™) and cultured in RPMI-1640 medium and supplemented with 10% FBS, 2mM L-glutamine, 50U/ml penicillin and 50µg/ml streptomycin.

J774

J774 cells are murine macrophages isolated from BALB/c mice (provided by Dr Jem Palmer, Newcastle University, UK) and were cultured in RPMI-1640 medium supplemented with 10% FBS, 2mM L-glutamine, 50U/ml penicillin and 50µg/ml streptomycin.

HMEC-1

Human microvascular endothelial cells (HMEC-1) are derived from dermal foreskin (ATCC® CRL-3243™, USA). Cells were cultured in MCDB131 medium (ThermoFisher

Scientific, UK) supplemented with 10% v/v FBS, 50U/ml penicillin, 50µg/ml streptomycin, 10ng/ml epidermal growth factor (EGF) and 1µg/ml hydrocortisone (all Sigma Aldrich, USA).

MG63

MG63 cells are human osteoblast-like cells isolated from an osteosarcoma of a 14 year old male (ATCC® CRL-1427™). MG63 cells were cultured in Eagle's Modified Essential Medium (EMEM) (Sigma Aldrich, USA) supplemented with 10% FBS, 2mM L-glutamine, 50U/ml penicillin and 50µg/ml streptomycin.

2.1.2 Cell Maintenance

Cell lines were cultured and experimented using aseptic technique within Class II Microbiological Safety Cabinets. Once cells reached around 80% confluency they were passaged using cell culture medium described in **section 2.1.1**.

Suspension cells (MM6 and THP-1) were centrifuged at 300g for 5 minutes, supernatant discarded and the pelleted cells re-suspended in pre-warmed (to 37°C) fresh complete culture medium.

Adherent cells (HMEC-1 and MG63) were washed with phosphate-buffered-saline (PBS) (Sigma Aldrich, USA) following removal of media. Cells were then detached using 2mM trypsin-ethylenediaminetetraacetic acid (EDTA) (Sigma Aldrich, USA) at 37°C, centrifuged at 300g for 5 minutes and re-suspended in complete media.

J774 cells are loosely adherent therefore sub-cultured by scraping to dislodge the cells, centrifuged at 300g for 5 minutes and re-suspended in complete media.

2.1.3 Cryopreservation of cells

Stocks of cells were maintained by routinely performing cell cryopreservation. Cells were frozen in cryovials at approximately $1 \times 10^6 \text{ ml}^{-1}$ cells in FBS with 10% v/v dimethyl sulphoxide (DMSO) (Sigma Aldrich, USA) at -80°C in a freezing container containing isopropanol overnight. They were then moved to liquid nitrogen for long-term storage.

2.1.4 Thawing and reseeded of cell lines

A cryovial containing approximately $1 \times 10^6 \text{ ml}^{-1}$ of all cell types was retrieved from liquid nitrogen and immediately thawed in a water bath at 37°C . The cells were then transferred to a sterile universal containing 10ml of sterile pre-warmed PBS to remove DMSO. The cell suspension was centrifuged at 300g for 5 minutes, PBS discarded and cell pellet re-suspended in 10ml of pre-warmed cell culture medium. This cell suspension was then transferred to a sterile cell culture flask (75cm^2) containing a further 5ml of fresh cell culture medium and stored in an incubator at 37°C and 5% CO_2 until approximately 80% confluent.

2.1.5 Mycoplasma testing

All cell lines were routinely tested for mycoplasma contamination using the MycoAlert™ Mycoplasma Detection Kit (Lonza, Switzerland). The kit tests cell supernatant by lysing any mycoplasma that is present and the released enzymes react with the MycoAlert™ Substrate which catalyses the conversion of adenosine diphosphate (ADP) to ATP. The ATP is catalysed by luciferase (in the MycoAlert™ Reagent) into a light signal. The ratio of ATP before and after addition of the MycoAlert™ Substrate is then calculated, which indicates the presence or absence of mycoplasma in the sample. A ratio of < 0.9 suggests the sample is mycoplasma free.

2.1.6 THP-1 differentiation

THP-1 cells are a suspension (non-adherent) monocytic cell line which can be differentiated to become non-polarised adherent macrophage-like cells (Chanput *et al.*, 2013). In this state the cells stop proliferating, change morphology, become more phagocytic and are in a more activated state i.e. release inflammatory mediators. THP-1 cells were treated with 5ng/ml phorbol 12-myristate 13-acetate (PMA) (PeproTech, USA) for 24 hours at 37°C , 5% CO_2 . The concentration of PMA selected was based on previous published studies and also work undertaken by fellow PhD student Miss Chelsea Griffiths, Newcastle University, UK (Park *et al.*, 2007). Following this time period, all THP-1 cells became adherent and were therefore deemed to be macrophage-like. To avoid over-activation of the cells prior to stimulation assays, cell

supernatant was discarded, cells washed with PBS and fresh complete culture medium was added and incubated for a resting period.

2.2 Cell Stimulation

2.2.1 Lipopolysaccharide

LPS is a known agonist of TLR4 and was used as a positive control throughout, it is also well established to mount an inflammatory response in the cell lines used in this study (Bosshart and Heinzelmann, 2016; Lawrence *et al.*, 2016b). TLR4-specific LPS (from *E. coli* serotype J5, Alexis Biochemicals, USA), which does not contain any other TLR agonists or contaminants which may activate TLRs was diluted in the appropriate complete culture medium for cell stimulation assays. A stock solution of 1000ng/ml was made and further diluted to a final working concentration between 10-1000ng/ml.

2.2.2 Negative control

During all cell stimulation studies, cells incubated in complete medium only were used as a negative control. Vehicle controls were included for reagents reconstituted in DMSO.

2.2.3 Cobalt ions

Cobalt hexahydrate (CoCl_2) (Sigma Aldrich, USA) was diluted in appropriate complete culture medium prior to cell stimulation. The concentrations selected for CoCl_2 were based on previous research within the group (Lawrence *et al.*, 2014; Lawrence *et al.*, 2016b). This varied between 0.025mM to 0.75mM which provides maximal cell responses without inducing cell toxicity. These concentrations are similar to other studies in similar cell lines and refined when comparing metal ion concentrations found in the serum and joint fluid of patients with failing MoM implants (De Smet *et al.*, 2008; Davda *et al.*, 2011; Holland *et al.*, 2012).

2.3 TLR4 Signalling Inhibitors

2.3.1 CLI-095

CLI-095 (Invivogen, USA) is a small molecule TLR4 antagonist which acts specifically by blocking signalling mediated by the intracellular domain of TLR4 (li *et al.*, 2006; Kawamoto *et al.*, 2008). A stock of CLI-095 was reconstituted in DMSO and then further diluted in complete culture medium to obtain a final stock concentration of 100µg/ml. A concentration of 1µg/ml was used in cell treatments as this dose had been previously optimised in similar cell lines to achieve effective inhibition whilst not affecting cell viability (Lawrence *et al.*, 2016a). In all experiments, cells were pre-treated with 1µg/ml CLI-095 for 6 hours prior to stimulation with TLR4 agonists.

2.3.2 MAb-tlr4

MAb-tlr4 (Invivogen, USA) is a human TLR4 specific IgG1 neutralising monoclonal antibody. MAb-tlr4 is from the W7C11 clone, although its exact binding site is unavailable. The antibody was reconstituted in 1ml of sterile water to obtain a concentration of 0.1mg/ml. Cells were pre-treated with between 0.5 and 10µg/ml MAb-tlr4 for 1 hour prior to simulation with TLR4 agonists.

2.3.2.1 Mouse IgG1 isotype control antibody

Mouse IgG1 isotype control antibody (Invivogen, USA), from the T8E5 clone, was used as a negative control in conjunction with MAb-tlr4 (an IgG1 monoclonal antibody). The isotype control was used at the maximal concentration of MAb-tlr4 used and cells treated for the same amount of time. The antibody was reconstituted in 1ml of sterile water to obtain a concentration of 0.1mg/ml.

2.4 Investigating the Inflammasome Response

2.4.1 ATP

Adenosine 5'-triphosphate disodium salt (ATP) (Invivogen, USA) is a potassium efflux agent which can trigger activation of the NLRP3 inflammasome in response to PAMPs such as LPS. It stimulates the caspase-1 dependent cleavage and secretion of IL-

1 β from LPS-stimulated cells (Mariathasan *et al.*, 2006). ATP was reconstituted in endotoxin-free water and the pH adjusted using 4 M sodium hydroxide (NaOH). Following priming of cells with LPS or other PAMP stimulants (e.g. potentially CoCr particles), 5mM ATP was added for 1 hour to stimulate IL-1 β maturation and secretion.

2.5 Cell Viability

2.5.1 Trypan blue staining

Cell viability was assessed using the trypan blue exclusion assay. A 1:1 dilution of trypan blue dye (ThermoFisher Scientific, UK) and cell suspension was added to a Luna disposable cell counting slide and cell viability counted and measured using a Luna II automated cell counter (both Logos Biosystems, South Korea). A cell with reduced viability will have a disrupted cell membrane so cannot exclude the dye. Therefore, these cells appear blue in colour. However, healthy cells with intact membranes can exclude the dye and appear clear. All cells were automatically counted and a cell viability percentage determined in relation to the total number of cells in the suspension.

2.5.2 XTT assay

The XTT (2,3-Bis-(2-Methoxy-4-Nitro-5-Sulfophenyl)-2H-Tetrazolium-5-Carboxanilide) assay kit (Roche, Switzerland) was used to determine the impact of THP-1 cell stimulation treatments on cell viability. The assay is based on the cleavage of yellow tetrazolium salt, XTT, to form an orange formazan dye, which only occurs in viable cells. Therefore, the more dye present then the more viable cells in each well/treatment. The dye formed is soluble in aqueous solutions and can be directly quantified using a standard spectrophotometer.

THP-1 cells were seeded in a clear, flat-bottomed 96 well plate at 5×10^4 cells/well in 100 μ l of complete cell culture medium and 5ng/ml PMA and incubated for 24 hours. Cells were subsequently washed with sterile PBS and fresh complete medium added to each well overnight. Cells were then stimulated with either LPS, CoCr particles or CoCl₂ at various concentrations for a further 24 hours. Following this period, 50 μ l of XTT with electron coupling reagent (final concentration 0.3mg/ml) was added to each

well and incubated at 37°C for between 2 and 24 hours. At 2, 4, 6 and 24 hours the plate was read at 450nm using a spectrophotometer.

2.6 Transmission Electron Microscopy (TEM)

Cross-sections of individual cells were used to generate TEM images so that intracellular features could be visualised and analysed. TEM microscopes use streams of electrons which are focused by magnetic condenser lenses onto a specific sample. This electron beam passes through the sample and electrons are scattered according to the density of the sample. For the samples to be imaged, detection of electrons is sensed by a fluorescent plate.

Stimulated THP-1 cells were collected in 1.5ml microcentrifuge tubes and centrifuged at 5,500g for 5 minutes. All traces of media were carefully removed and the cell pellet re-suspended in 1ml of 2% glutaraldehyde with 0.2M cacodylate to fix the cells. These were then handed to EM Research Services (Newcastle University, UK) for the remainder of sample processing. After fixation, samples were dehydrated through serial ethanol concentrations. Samples were then placed in propylene oxide as a transitional buffer before embedding in epoxy resin. Samples were then cut into ultra-thin sections (50-70nm) and stained with electron dense stains, typically heavy metals, to show cellular structures.

2.7 Quantification of Gene Expression

2.7.1 RNA isolation

Total RNA was isolated from stimulated cells using the Promega ReliaPrep RNA Miniprep Systems Kit (Promega, USA) following the manufacturer's protocol. Briefly, suspension cells were collected in a sterile 1.5ml microcentrifuge tubes, centrifuged, re-suspended in sterile PBS, further centrifuged then lysed in BL buffer containing 1% 1-Thioglycerol (BL+TG buffer). The cell pellet was further homogenised by a combination of vortexing and pipetting prior to the addition of isopropanol. Adherent cells were washed in sterile PBS before being directly lysed with BL+TG buffer in the cell culture plate, scraped using the end of a 1ml syringe and collected in a sterile microcentrifuge tube before the addition of isopropanol. The cell lysate for both

suspension and adherent cells was then transferred to ReliaPrep Minicolumns followed by a series of washing steps with RNA wash solution, centrifugation (at 8,000g) and a 15-minute incubation step with a DNase I incubation mix. This was followed by several further wash steps including with a column wash solution then the elution of RNA in nuclease-free water. Analysis of total RNA quantity and quality was determined by a NanoDrop One spectrophotometer (ThermoFisher Scientific, UK). Absorbance was read at 260nm, 280nm and 230nm, which measures nucleic acid, protein and organic solvent content, respectively. Thus, these values can be used to generate ratios which evaluate the purity of each RNA sample. A 260/280 ratio of between 1.8 and 2.2 indicates the sample was pure enough to use in future experiments. RNA was then stored at -80°C.

The integrity of RNA was assessed by gel electrophoresis on a 2% w/v agarose gel. Intact RNA is represented by two distinct bands; 28S and 18S ribosomal RNA units (**Figure 2.1**).

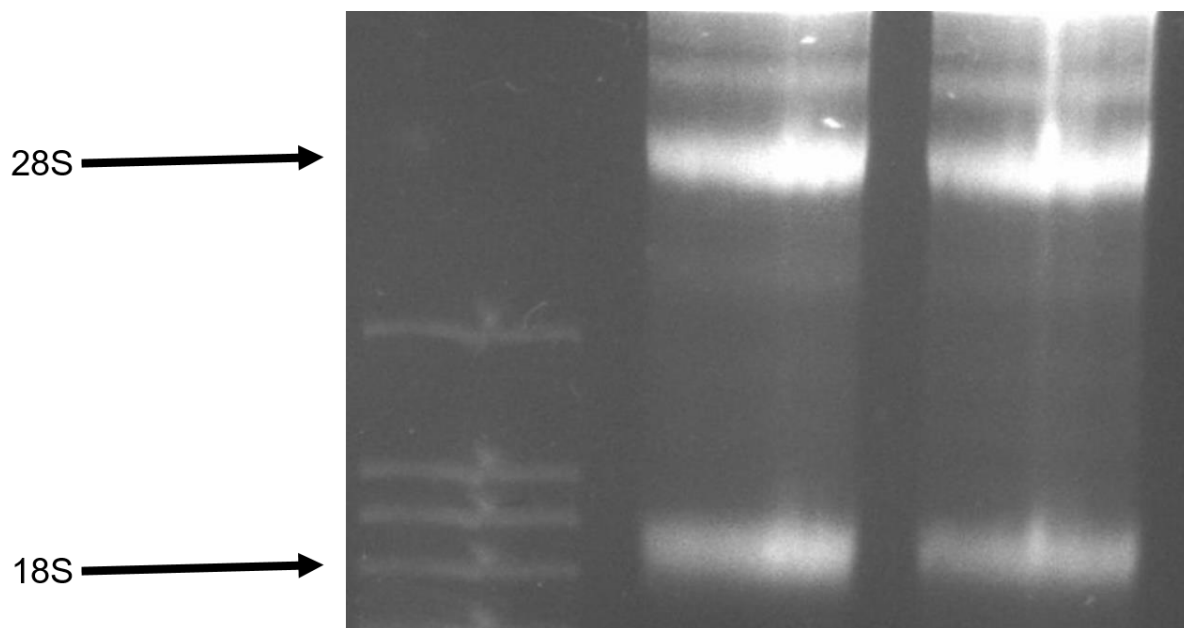


Figure 2.1 RNA gel electrophoresis

Isolated RNA was separated by electrophoresis on a 2% w/v agarose gel. The 28S and 18S bands are the two ribosomal subunits and show intact RNA.

2.7.2 cDNA synthesis

First strand complementary DNA (cDNA) was synthesised using the Bioline Tetro cDNA synthesis kit (Bioline, UK) using between 0.5µg and 1µg of total RNA. Each reaction contained the appropriate amount of RNA, 1µl of either Oligo (dT)₁₈ or Random hexamers, 1µl 10mM dNTP mix, 4µl 5x RT buffer, 1µl RiboSafe RNase inhibitor, 1µl Tetro Reverse Transcriptase (200u/µl) and diethyl pyrocarbonate (DEPC)-treated water up to a volume of 20µl. Reactions were incubated in a T100 thermocycler (BioRad, USA) at 45°C for 30 minutes and if using random hexamers, 10 minutes at 25°C followed by 45°C for 30 minutes. The reaction was terminated by incubating at 85°C for 5 minutes then immediately storing at 4°C before transferring to -20°C for long-term storage.

2.7.3 Quantitative real-time polymerase chain reaction

Quantitative real-time polymerase chain reaction (qRT-PCR) can be used to quantify changes in gene expression. qRT-PCR throughout this study was conducted using Taqman gene expression probes and reagents (**Table 2.1**). These probes contain both forward and reverse primers, in addition to Taqman probes. The probes are conjugated to a fluorescent reporter dye and a quencher which prevents fluorescence when the probe is intact. However, following cDNA replication, the probe is degraded by Taq polymerase and the fluorescence signal is released.

Each reaction contained 5µl of 2X Taqman gene expression mastermix, 2µl diluted cDNA template, 0.5µl Taqman gene expression probe and 2.5µl RNase-free water (all ThermoFisher Scientific, UK). For each primer used, a negative control containing RNase-free water was used in place of the diluted cDNA template. Unless otherwise stated, gene expression was normalised to either *18S* or *GAPDH* as a housekeeping gene.

A 10µl sample of the reaction mix was added in triplicate to a MicroAmp 96 well plate (ThermoFisher Scientific, UK) which was then ran on a StepOnePlus real-time PCR thermocycler (Applied Biosystems, USA). Reactions were incubated at 50°C for 2 minutes and 95°C for 10 minutes followed by 40 cycles of 95°C for 15 seconds and 60°C for 1 minute.

Relative gene expression values were quantified by normalising CT values of the target genes with CT values of the housekeeping gene using the $2^{-\Delta\Delta C_t}$ method.

Table 2.1 Taqman gene expression assays

TaqMan gene expression assays were purchased from ThermoFisher Scientific, UK

Target gene	Species	Assay ID
18S	Human	Hs03003631_g1
GAPDH	Human	Hs02758991_g1
IL-8	Human	Hs00174103_m1
CCL3	Human	Hs00234142_m1
IL-1β	Human	Hs01555410_m1
ICAM-1	Human	Hs01003372_m1
VCAM-1	Human	Hs01003372_m1

2.8 Protein Quantification

2.8.1 Enzyme-linked immunosorbent assay (ELISA)

ELISA is a technique used to quantify protein secretion, most commonly cytokines and chemokines. The ELISA kits used throughout this study were DuoSet sandwich ELISAs purchased from R&D Systems and performed according to the manufacturer's protocol. The DuoSet ELISA Ancillary Reagent Kit (R&D Systems, USA) provided all additional reagents required. The general overview and principle of the assay is described below.

Firstly, a clear polystyrene microplate (R&D Systems, USA) was coated with a capture antibody diluted in ELISA plate-coating buffer at room temperature (RT) overnight. The plate was then blocked with 1% bovine serum albumin (BSA) in PBS for 1 hour at RT to prevent non-specific binding. Supernatant from stimulated cells was collected in 1.5ml microcentrifuge tubes whilst processing cell lysates therefore no cells or debris would be present. Known standards and appropriately diluted supernatants were added in triplicate to the plate and incubated for 2 hours at RT. The detection antibody

was then added to the plate for 2 hours at RT, followed by the addition of Streptavidin-horseradish peroxidase (HRP) for 20 minutes at RT. The ELISA was developed using a 1:1 dilution of colour reagent A (hydrogen peroxide) and colour reagent B (tetramethylbenzidine) (R&D Ancillary Kit) and incubated at RT for 20 minutes or until the reaction had developed sufficiently. The solution was stopped with a stop solution (2N sulfuric acid) and plates then read at 450nm on a spectrophotometer. In between all steps (excluding the addition of stop solution) the plate was aspirated and washed 3 times using an automated plate washer (ThermoFisher Scientific, UK) and wash buffer (0.05% Tween 20 in PBS).

Reagent concentrations for the ELISAs used during this study are summarised in **Table 2.2.** and the reagents from the DuoSet ELISA Ancillary Reagent Kit summarised in **Table 2.3.**

Table 2.2 ELISA reagent concentrations

	IL-8	CCL3	CCL3 (mouse)	CCL4	CCL2	IL-10	IL-1 β
Capture Antibody (μg/ml)	4	0.4	0.4	1	1	2	4
Maximum Standard (pg/ml)	2000	500	500	1000	1000	2000	250
Detection Antibody (ng/ml)	20	200	100	50	25	75	200

Table 2.3 DuoSet ELISA ancillary reagent kit

	Description	Working concentration
ELISA Plate-Coating Buffer	Sterile-filtered 1X PBS	N/A
Reagent Diluent Concentrate	10% Bovine Serum Albumin (BSA) solution	1% BSA in PBS (dilute in deionised water)
Stop Solution	2N sulfuric acid	N/A
Colour Reagent A	Hydrogen peroxide	Mix together in equal volumes
Colour Reagent B	Tetramethylbenzidine	
Wash Buffer Concentrate	Concentrated solution of buffered surfactant with preservative	1 in 25 dilution in distilled water to prepare 1X wash buffer (0.05% Tween)

2.9 Statistical Analysis

Statistical analysis was performed using GraphPad Prism 8.0. All error bars represent standard deviation unless otherwise stated. The analysis method is described for each individual experiment, majority used were one-way analysis of variance (ANOVA). Statistical significance is shown as follows:

* $p < 0.05$

** $p < 0.01$

*** $p < 0.001$

Chapter 3 : Generation, Isolation and Characterisation of Clinically-relevant Cobalt Chromium Wear Particles

3.1 Introduction

As discussed in **Chapter 1**, CoCr particles which have been characterised from both retrieval and hip simulator studies are observed to be mostly nanoscale in size (Doorn *et al.*, 1998; Catelas *et al.*, 2003). The morphology of these particles also tend to be round in shape with a small number of needle-like shard particles as observed by TEM (Doorn *et al.*, 1998). To fully understand the biological responses to wear debris generated by orthopaedic implants it is important that particles used in cell culture experiments are comparable to those released from implants *in vivo*. Previous *in vitro* cell culture studies have also utilised commercially available particles (Dalal *et al.*, 2012; Caicedo *et al.*, 2013). However, these tend to be much larger in size (μm range) and mostly uniform in their morphology (**see Figure 3.1**). Therefore, researchers have developed various systems with increasing levels of complexity to produce or generate CoCr wear particles. These include; pin-on-plate simulators, whole joint simulators and retrieved particles isolated from patient tissue (Tipper *et al.*, 1999; Germain *et al.*, 2003; Papageorgiou *et al.*, 2014).

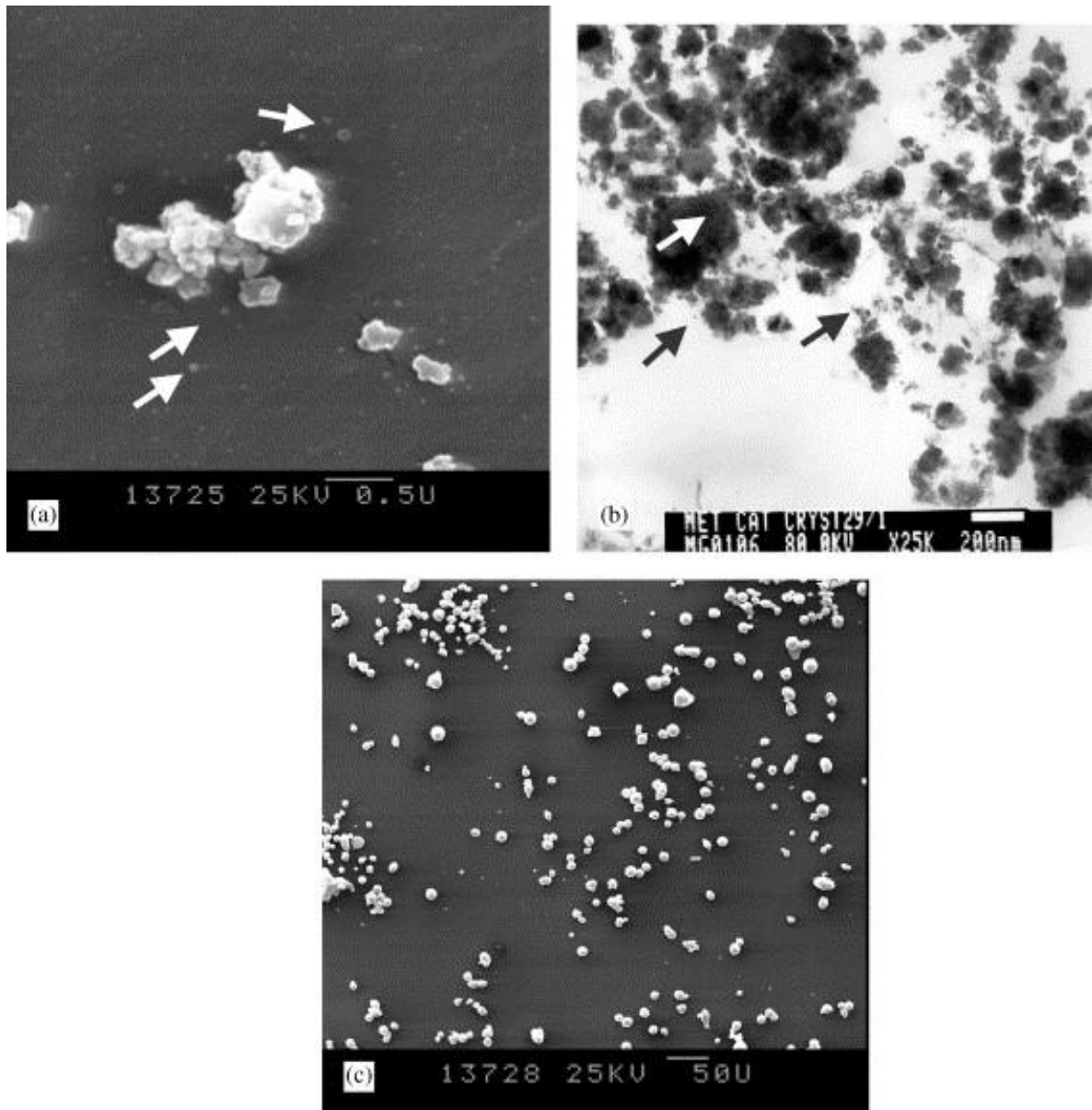


Figure 3.1 Microscopy images comparing CoCr wear particles generated on pin-on-plate simulator versus commercial CoCr particles

A) SEM image of CoCr particles generated by pin-on-plate simulator displaying large aggregates as well as smaller nanoscale individual particles as demonstrated by arrows. **B)** TEM image of CoCr particles generated by pin-on-plate simulator, small 10-20nm particles can be observed more clearly within the aggregates. **C)** SEM image of commercially available CoCr particles (supplied by Osprey Metals Ltd.) which displayed a uniform morphology of a much larger average size of $9.87 \pm 5.67 \mu\text{m}$ (all images taken from (Germain *et al.*, 2003)).

The lubricant in which the particles are generated, using simulators, also needs to be taken into consideration. If proteins are present in the sample, for example from cell culture media containing FBS, this can make visualisation of the particles under microscopy problematic and prevent accurate size distribution and characterisation of

the particles. Furthermore, isolation methods for CoCr particles generated in these lubricants are difficult as the material is unable to tolerate extreme changes to pH which can cause changes in morphology, aggregation or potential loss of particles (Catelas *et al.*, 2001). More recently, Lal *et al.* (2016) developed a novel particle isolation method employing enzymatic digestion with proteinase K followed by a density gradient using sodium polytungstate (SPT) (Lal *et al.*, 2016). The method was developed for the recovery of both ceramic and metal particles from lubricants containing serum and found to have no effect on size or morphology of the recovered particles.

Pin-on plate wear simulators utilise a technique that mimics the wear mechanisms of total hip replacement devices during what would be classed as a 'normal' gait cycle (Jin *et al.*, 2000). The simulator is multidirectional, with the plate moving linearly, whilst the pin rotates which replicates the movement of the femoral head within the acetabular cup of the hip joint. Sterile water can be used as the lubricant in this setting as it has been shown that these conditions lead to the generation of clinically relevant CoCr particles (in terms of their size and shape) and eliminates the requirement for a digestion protocol to isolate the particles (Germain *et al.*, 2003).

Therefore, for this study, a multidirectional pin-on-plate simulator was used to generate clinically relevant CoCr particles in sterile water which are similar in size, morphology and composition to those in the published literature. However, generating particles in sterile water is not necessarily the most accurate representation of what may be occurring *in vivo* or in patients. This is because the presence of proteins and other metabolites may affect wear rates and the composition of the particles produced. Moreover, the six-station pin-on-plate simulator which was to be utilised as part of this study is extremely difficult to run under sterile conditions due to the positioning of the rig. This means, that for cell culture studies, particles would have to be sterilised prior to use, and therefore, would lose released metal ions and other natural properties that may be altered during this process. For this reason, a single station pin-on-plate wear rig based within a class II biological safety cabinet, was also used to generate sterile CoCr particles with complete cell culture medium containing 25% FBS used as a lubricant. The method developed by Lal *et al.* (2016) for the isolation and recovery of metal wear debris from lubricants containing serum was employed due to its effectiveness and efficiency so that particles could be characterised prior to use (Lal

et al., 2016). The particles produced under these conditions would therefore offer a 'gold standard' which could ultimately be used for cell culture studies and potentially produce more meaningful conclusions.

3.2 Aims and Objectives

The aim of this chapter was to generate and isolate clinically-relevant CoCr wear particles to be used for subsequent investigation into their biological effects. Nanoscale particles were generated using a six-station pin-on-plate wear simulator using material with some alloy compositions used in MoM hip implants. The lubricant chosen in this instance was water, which removed the need for lubricant digestion. CoCr particles were also generated using a single station pin-on-plate wear simulator under sterile conditions. The lubricant used in these tests was cell culture medium containing 25% (v/v) FBS, therefore, digestion methods were employed to isolate the particles for further characterisation.

3.2.1 Objectives

- Generate clinically-relevant cobalt chromium wear particles using a six-station pin-on-plate wear simulator in sterile water, using high carbon CoCrMo alloy pins and plates
- Filter and characterise CoCr wear particles generated to determine particle size and morphology using SEM, EDX analysis and ImageJ
- Prepare generated CoCr wear particles for cell culture studies by sterilising and determining the concentration of particles
- Generate sterile clinically-relevant cobalt chromium wear particles using a single station pin-on-plate wear simulator in cell culture medium containing 25% (v/v) FBS, using high carbon CoCrMo alloy pins and plates
- Isolate particles generated in cell culture medium containing 25% (v/v) FBS using enzymatic digestion and a density gradient ultracentrifugation method

3.3 Specific Materials

Smooth, high carbon, CoCr alloy pins and plates were manufactured in house (School of Mechanical Engineering, University of Leeds) from a high carbon > 0.2% (w/w) CoCrMo alloy (ASTM F1537), which is the alloy used in surgical implants. The pins and plates were polished to a smooth contact surface of approximately 0.02-0.04 μ m and 0.01-0.02 μ m surface roughness, respectively.

The pins and plates were engraved with an identification number on the non-contact face to allow for continuity in the test rig. Prior to use, pins and plates were washed in household detergent before sonication for 10 minutes in 70% (v/v) isopropanol. Following on from this, the pin and plates were stored in a moisture controlled environment for at least 48 hours, and then weighed (repeated 3-5 times, accuracy \pm 5 μ g) prior to the test run.

3.4 Specific Methods

3.4.1 *Generation of CoCr particles using a six-station pin-on-plate wear simulator*

Clinically relevant CoCr wear particles were generated using a six-station pin-on-plate wear simulator. The simulator used was designed and manufactured within the School of Mechanical Engineering at University of Leeds. Smooth, high carbon, CoCr alloy pins and plates were used throughout to generate CoCr particles as described in **section 3.3**. Once generated, these wear particles were used *in vitro* to investigate the inflammatory response of cell lines to CoCr wear particles.

3.4.1.1 *Cleaning of rig components and CoCr pins and plates*

The entire components of the six-station rig were firstly immersed in household detergent with warm water for 15 minutes then individually scrubbed with a toothbrush. All metal components were sonicated in 70% (v/v) isopropanol for 10 minutes. All components were then immersed in 1% (v/v) Trigene (Scientific Laboratory Supplies, UK) for 20 minutes then thoroughly rinsed in distilled water before completely drying in disposable paper towels (**Figure 3.2**).

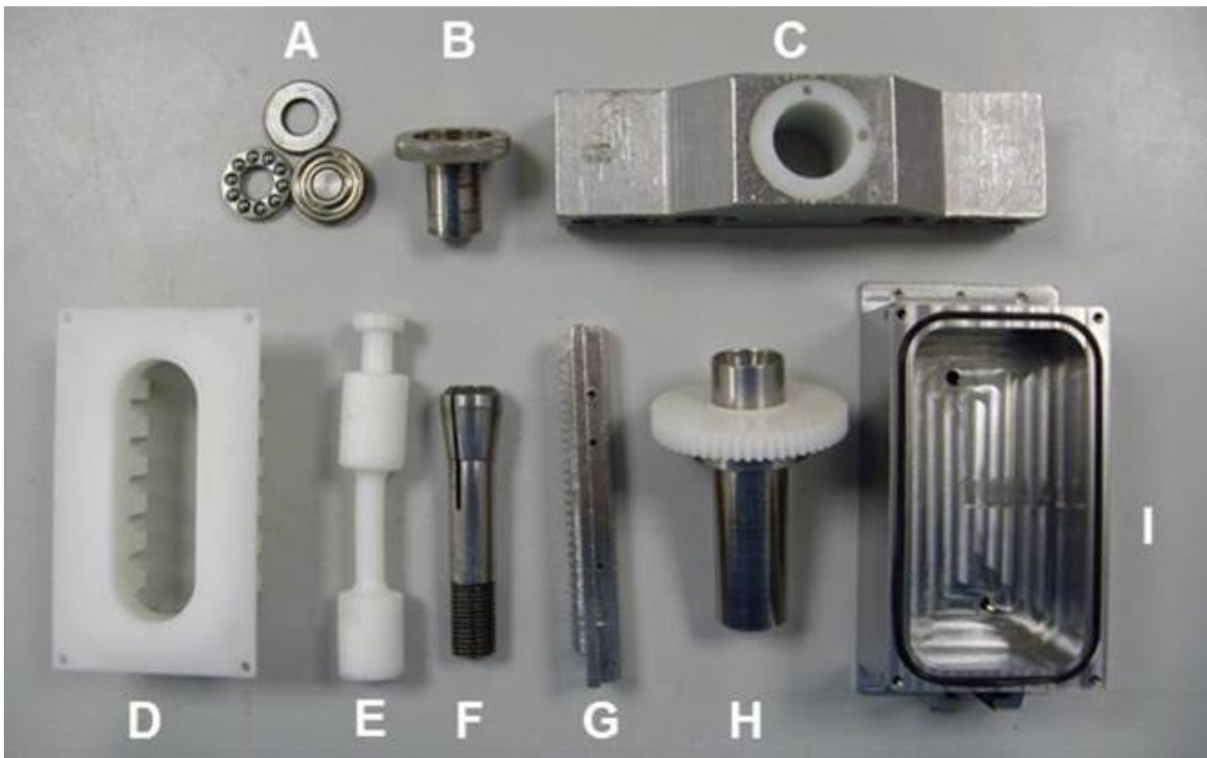


Figure 3.2 Components of the six-station pin-on-plate wear simulator

A) Ball bearing assembly components, **B)** threaded nut, **C)** bridge section, **D)** polymer baffle, **E)** connecting rod, **F)** collet, **G)** toothed rack, **H)** pin holder with polymer gear, **I)** stainless-steel bath with seal inside the side groove. Image taken from PhD thesis Craven, 2016 (Craven, 2016).

3.4.1.2 Assembly of six-station pin-on-plate wear simulator

The components required for the setup of the six-station pin-on-plate wear rig simulator are listed in **Table 3.1**.

Table 3.1 The components required for the assembly of the six-station pin-on-plate wear simulator

Assembly of pin/plate/load	Six station pin-on-plate wear simulator components
Assembly of plate in bath	Six stainless steel baths, six stainless steel bath inserts (cobalt chromium plates were fixed into these for test), six polymer baffles, six stainless steel toothed racks and six plastic sheets
Assembly of pin in holder	Six polymer gear wheels, four stainless steel bridges (spans all six stations), six stainless steel pin holders (collets), six collet outer sleeves, six threaded nuts and six stainless steel spacers
Screws, pins and bearings	12 large stainless steel screws, 12 short, small stainless steel screws, 24 long, small stainless steel screws, six pivot pins, 12 split pins, six ball bearing assemblies and six linear bearings
Additional equipment	Six polyethylene connecting rods, six cantilever arms, six weights, a range of Allen keys, spirit level, adjustable wrench, 50ml syringe, sterile deionised water, 150ml sterile collection pot

3.4.1.3 Linear bearing tray

Prior to the assembly of the six-station wear simulator, the pins and plates were individually numbered and the pairing of the pin and plates for each station remained constant throughout the tests. The orientation of the plate within the bath also remained the same. The linear bearing tray was assembled, whereby each plate was screwed into a separate bath using the short, small screws. A rubber seal was placed in the groove of the bath and a polymer baffle was secured into position using the long and small screws, covering the top of the bath with the polymer baffle. The toothed racks were screwed into position on the side of each bath. Each numbered bath was secured into place on the rig at the corresponding station number.

3.4.1.4 Assembly of pin holder

Each individual pin was placed in a collet, to ensure the pin protruded approximately 5mm. Different sized metal spacers were also inserted to ensure each pin protruded by roughly the same distance. The collet containing the pins was then placed into the pin holder, which was then placed into the corresponding bridge section and the threaded nut screwed in to place, fixing the pin into position in the collet. The polymer gear wheel was then fixed onto the top of the pin holder. The bridge apparatus was then transferred across to the support brackets within the simulator. The polymer wheel was aligned with the toothed rack at the side of each stainless-steel bath which allowed the rotation of the pin. It was important to check at this point that the motion was smooth between the two bearings. The bridge was secured by tightening clamps, clearance distances were checked between the threaded nut and the bridge and the pin-on-plate movement was also established.

3.4.1.5 Final assembly

The lubricant used was ultrapure deionised water and approximately 30 ml was added to each bath using a syringe. The pin holder was lifted slightly to ensure the presence of lubricant between the pin and plate prior to commencing the operation of the wear rig. The polymer connecting rods were slotted into place at the front of the baths and secured to the scotch yoke mechanism situated at the other end of the rod. The cantilever arms were secured into place using 2 split pins per arm and a single pivot pin. Using a spirit level and spanner, the pin on the cantilever arm was altered to ensure the arm was level. A ball bearing assembly was placed on top of the pin holder and a small amount of Vaseline® was applied around the washers to act as a lubricant (and allow rotation). The cycle counter on the rig was set to zero and the motor was turned on. The frequency was recorded and adjusted to 1 Hz or 60 cycles.min⁻¹, with a stroke length of 28 mm and a rotation $\pm 30^\circ$. A steel weight was then added to each of the cantilever arms to correspond to 80 N per station. The rig was operated for 3 weeks during the day (approximately 8 hours per day). Before switching off the rig at the end of each day, the speed was slowly reduced and the weights were removed. The lubricant was topped up each day to maintain sufficient lubrication. Upon completion of the pin-on-plate testing, the number of cycles was recorded and the rig was

dismantled. The lubricant containing the particle debris for each station was transferred into appropriately labelled sterile plastic pots and stored at -20°C.

3.4.2 Generation of sterile CoCr particles using a single-station pin-on-plate wear simulator

Sterile, clinically relevant CoCr wear particles were generated using a single station pin-on-plate wear simulator. The simulator used was designed and manufactured within the School of Mechanical Engineering at University of Leeds. Smooth, high carbon, CoCr alloy pins and plates were manufactured in house (School of Mechanical Engineering, University of Leeds) from a high carbon > 0.2% (w/w) CoCrMo alloy (ASTM F1537). Once generated, these wear particles were used *in vitro* to investigate the inflammatory response of cells to CoCr wear particles.

3.4.2.1 General preparation and cleaning of rig components

All components from the single station wear simulator were washed in household detergent in warm soapy water before being thoroughly rinsed with distilled water (**Figure 3.3**). The metal components were placed in a sonicating water bath in 70% (v/v) isopropanol for a minimum of 20 minutes then rinsed with copious amounts of distilled water and dried. These were then wrapped in tin foil and heated in an oven at 180°C for 4 hours to sterilise the components.

All lubricant samples and aliquots of ultrapure water were prepared in a class II laminar flow cabinet to ensure sterility. Sterile running of the test rig was performed in a class I laminar flow cabinet. All items including components were sprayed with 70% (v/v) ethanol before being placed inside the cabinet. Prior to each test, the cabinet was exposed to UV for 1 hour.

The serum lubricant was made up either the day before the rig was operated and stored at 4°C, or on the day of the test run. The lubricant consisted of RPMI 1640 media supplemented with 25% (v/v) FBS and was transferred into a sterile container. Sterile aliquots of ultrapure water were also prepared in sterile universals to be used to 'top up' the lubricant during the duration of the wear test.

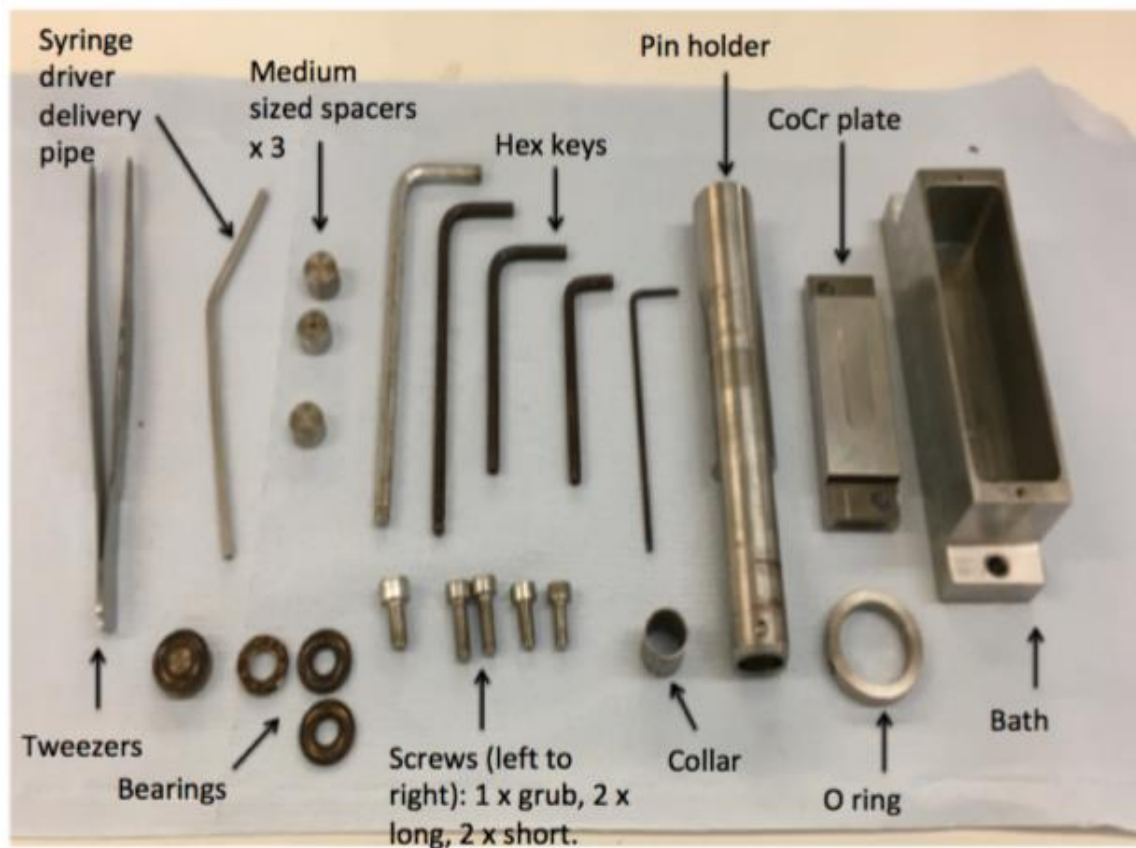


Figure 3.3 Components of single station pin-on-plate wear simulator

Image taken from PhD thesis, Yarrow-Wright 2018 (Yarrow-Wright, 2018).

3.4.2.2 Assembly of single station pin-on-plate wear simulator

Prior to assembly, the cabinet and rig base were cleaned with household detergent in warm water followed by 1% (w/v) Trigene and finally 70% (v/v) ethanol.

All components were assembled within a class I laminar flow cabinet. Using the components pictured in **Figure 3.3**, firstly, the plate screws were used to tighten the CoCr plate inside the bath, which was then placed into the rig where it was secured into position using the short screws. The O ring was inserted into the pin holder, the CoCr pin inserted into the O ring and tightened using the screw on the side of the pin holder. The assembled pin holder was fed through the arm of the rig and lowered by rotating the mechanism to ensure the flat sides of the pin holder were aligned with the bearings (**Figure 3.4**).

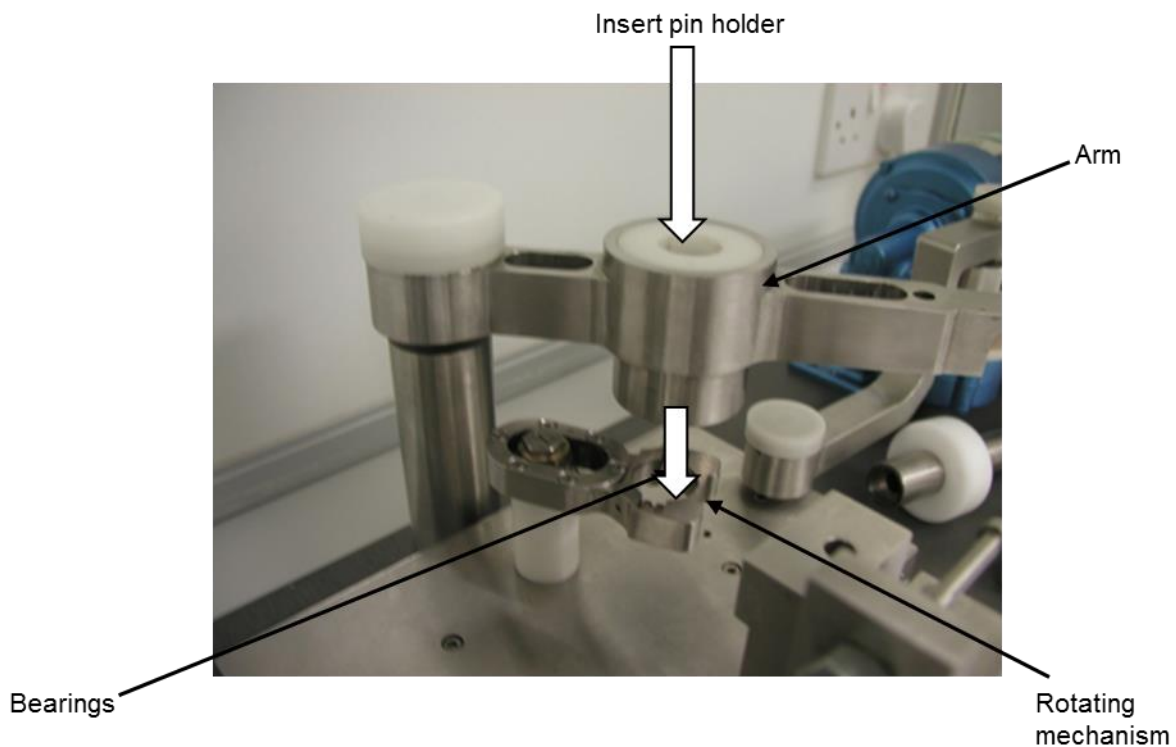


Figure 3.4 Assembly of pin holder for single-station pin-on-plate wear simulator

Image taken from PhD thesis, Yarrow-Wright 2018 (Yarrow-Wright, 2018).

Approximately, 30ml of RPMI 1640 medium (supplemented with 25% (v/v) FBS) was added to the bath using a sterile plastic syringe. The pin holder was then lifted to allow the lubricant to pass over all the surfaces. A load of 80N was applied using a weight positioned on the cantilever arm. The motor was switched on and the speed set to the equivalent of 1 Hz. The lubricant was topped up using ultrapure water throughout the duration of the test run. The final assembly of the rig is pictured in **Figure 3.5**.

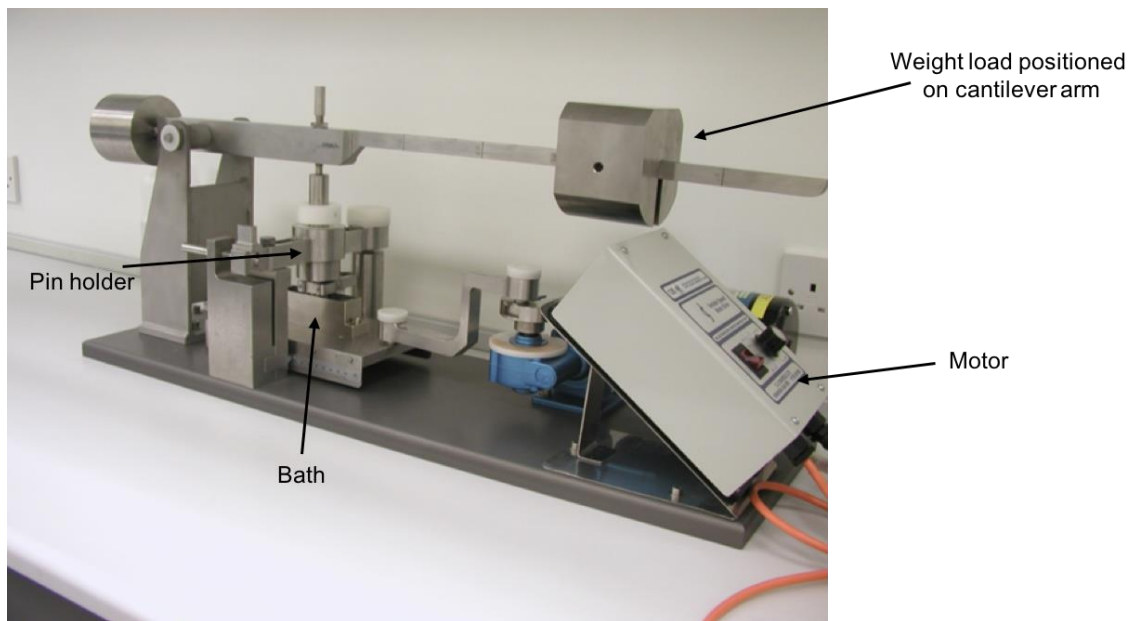


Figure 3.5 Fully assembled single pin-on-plate wear simulator

Image taken from PhD thesis, Yarrow-Wright 2018 (Yarrow-Wright, 2018).

The test was continuously run for 8 hours per day for 3 weeks and lubricant collected at the end of every week. Lubricant was removed using a sterile 50ml syringe and transferred to a sterile pot and stored at -20°C.

3.4.2.3 Sterility testing of retrieved lubricant

A sample of the collected lubricant from the single-station pin-on-plate wear simulator was tested for bacterial contamination by plating out on heated blood agar (HBA), sabouraud dextrose agar (SAB) and nutrient agar (NA) plates (all ThermoFisher Scientific, UK) using sterile technique (i.e. under the presence of a Bunsen burner flame). The lubricant was spread over the plates in a series of standard lines (**Figure 3.6**). Plates were incubated over a period of 24-72 hours at either 37°C (HBA and NA) or 30°C (SAB). Any bacteria present would colonise along the lines and confirm the presence of contamination.

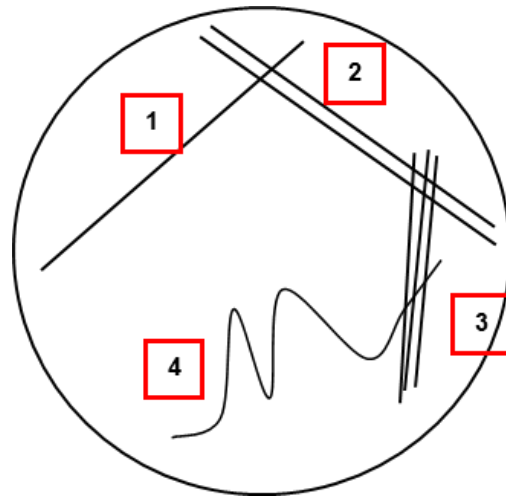


Figure 3.6 Plating out serum onto bacterial growth plates using standard method

3.4.3 Scanning electron microscopy (SEM)

The size, composition and morphology of the CoCr particles generated in **section 3.4.1 and section 3.4.2** were determined and analysed using SEM and energy dispersive x-ray spectroscopy (EDX) analysis.

3.4.3.1 Preparation of cobalt-chromium particles for SEM analysis from six station pin-on-plate wear simulator

CoCr particles generated from the six-station pin-on-plate wear simulator were filtered onto 0.015 μm pore size membranes using filtration glassware. The glassware was firstly washed thoroughly using household detergent and a bottle brush then rinsed a minimum of 3 times with distilled water, followed by a final rinse with ultrapure water. All filtration was performed in a class I laminar flow hood.

A 1mg.ml⁻¹ stock of CoCr particles was diluted in a further 5ml of sterile water. The diluted stock was sonicated for 30 minutes in a sonicating water bath whilst pipetting the solution before being filtered through a 0.015 μm pore size filter membrane. Prior to filtration, each membrane was cleaned by filtering 10ml of 70% (v/v) ethanol followed by 10ml of ultrapure water. Once the particle solution had passed through the filter, it was transferred to a petri dish and allowed to dry overnight at room temperature. A small section of the dried filter membrane was mounted on to a 2.5cm aluminium short

stub using an adhesive carbon tab and the edges of the filter coated with carbon paste. The CoCr particle samples were sputter coated with carbon to a thickness of 3nm.

3.4.3.2 Isolation of cobalt-chromium particles for SEM analysis from single-station pin-on-plate wear simulator

As the CoCr particles collected from the single-station pin-on-plate wear simulator were generated in lubricant containing serum an enzymatic digestion and density gradient ultracentrifugation method was employed in order to isolate and purify particles prior to their characterisation (**summarised in Figure 3.7**).

Firstly, the SW32Ti rotor buckets for centrifugation were cleaned thoroughly using hot water and detergent followed by drying the inner and outer surfaces using tissue paper. The centrifuge tubes (Beckman Coulter Ltd, UK) were also thoroughly cleaned using hot water and detergent before rinsing 3 times with filtered water and one final rinse using sterile water. All the centrifuge tubes were coated using siliconising fluid surfactant (Surfasil) (ThermoFisher Scientific, UK) using lint free cloths and tweezers. Specifically, the lint free cloth was wet with undiluted Surfasil solution then the inner surface of the centrifuge tube rubbed with the wet lint free cloth making sure the whole inner surface was covered. A dry lint free cloth was then using to rub the inner surfaces until dry. The tubes were rinsed with methanol then twice with sterile water prior to use. The lubricant retrieved from the simulator was vortexed 3 times for 10 seconds and the volume made up to 30ml by the addition of sterile water. Immediately after mixing, the lubricant was added to the centrifuge tubes and placed inside the SW32Ti rotor buckets and balanced using sterile water. The tubes were centrifuged at 160,000g for 3 hours at room temperature using a Beckman Optima L-90K ultra-centrifuge and SW32Ti rotor. Following centrifugation, the supernatant was carefully removed by aspiration leaving behind a volume of 3ml to re-suspend the pellet, located in the bottom of the tube.

The re-suspended pellets of particles containing proteins (from FBS) were subsequently added to 0.1M 4-(2-hydroxyethyl)-1-piperazineethanesulfonic acid (HEPES) buffer (Melford Laboratories, UK), 0.5% (w/v) sodium dodecyl sulphate (SDS) (Sigma Aldrich, USA) and 3mM calcium chloride, to a final volume of 5ml. For enzymatic digestion, 250µl of proteinase K (1mg.ml⁻¹) (ThermoFisher Scientific, UK)

was added then transferred to an incubator on an orbital shaker for 18 hours at 50°C. Following this time, the particle solution was sonicated for 10 minutes before the enzymatic digestion step was repeated by the addition of proteinase K (1mg.ml⁻¹) and further incubation for 22 hours at 50°C, whilst being shaken.

SPT gradients were prepared by sequentially layering 60% (v/v) SPT ($\rho=2.0$ g/cm³), 40% (v/v) SPT ($\rho=1.6$ g/cm³) and 20% (v/v) SPT ($\rho=1.2$ g/cm³) in thin wall polypropylene tubes (Beckman, UK). The digest was sonicated for 10 minutes before it was pipetted slowly on top of the SPT density gradient. The tubes were filled to the top by the addition of sterile water. The samples were centrifuged (Beckman Optima L-90K ultra-centrifuge and SW40 rotor) at 180,000g for 4 hours at room temperature. At this point, a protein band was observed between the 20% (v/v) and 40% SPT layers (v/v). The supernatant was carefully aspirated and discarded and the pellet of particles at the bottom of the tube was re-suspended in 1ml of sterile water, sonicated for 10 minutes before being transferred to clean pre-coated centrifuge tubes.

The recovered particles were washed 3 times in sterile water using Beckman Optima L-90K ultra-centrifuge and SW40 rotor at 180,000g for 1 hour at 37°C. Between each wash, the supernatant was collected and the particles were re-suspended in sterile water before sonication for 10 minutes. The particles finally pelleted at the bottom of the tube were re-suspended in sterile water and stored at -20°C for future analysis.

The isolated particles could then be filtered onto 0.015 μ m pore size membranes as described in **section 3.4.3.1.** for SEM analysis.

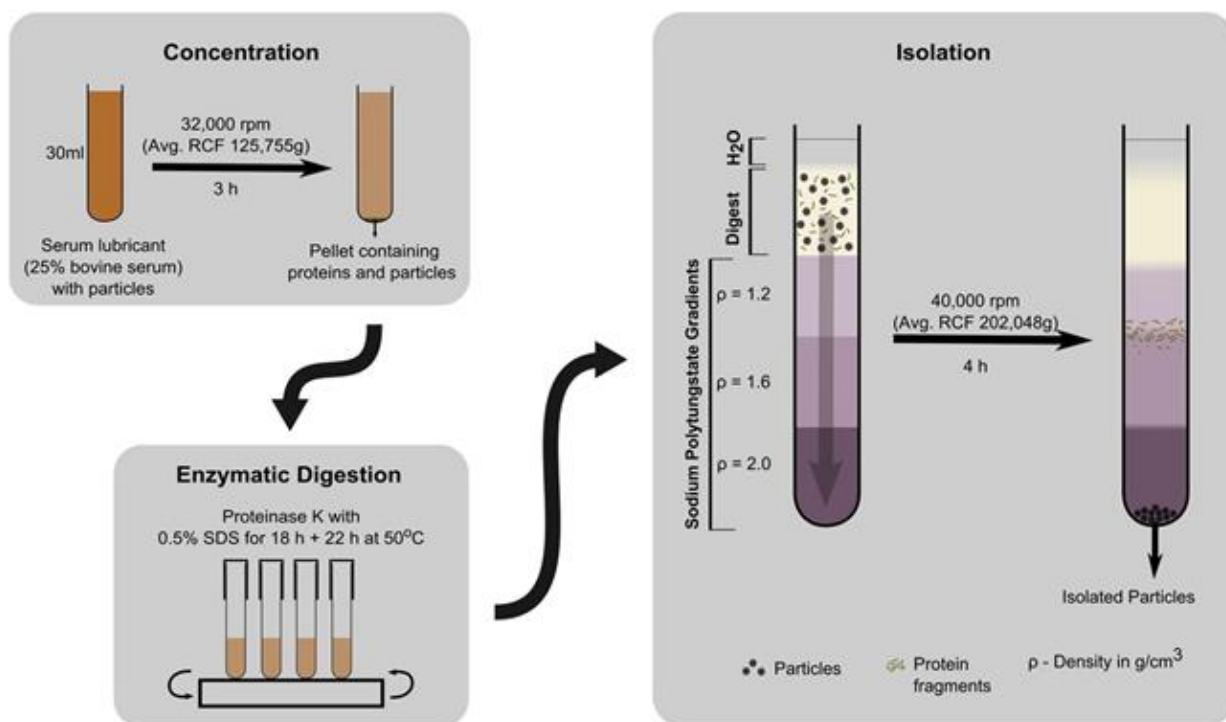


Figure 3.7 CoCr particle isolation method

The method employed for particle isolation can be divided into 3 main stages. **1)** The concentration stage involves pelleting the particles by centrifugation so that a smaller, more concentrated volume can be obtained. **2)** The enzymatic digestion stage involves the addition of Proteinase K for 22 hours which digests the proteins present from the serum. **3)** A density gradient is formed in the isolation stage by using sodium polytungstate and ultra-centrifugation to ultimately separate the isolated particles from the digested proteins (Lal *et al.*, 2016)

3.4.3.3 Imaging and characterisation of cobalt-chromium particles

The CoCr particles were visualised using a Hitachi SU8230 field emission gun electron microscope (FEGSEM) (University of Leeds) at a working distance of 3mm and an acceleration of 1kV. Images were taken at magnifications between x 30K and x 100K by Dr Saurabh Lal (Faculty of Engineering, University of Leeds). The images obtained were analysed using the image analysis software ImageJ, to measure the maximum length and area of the particles. Approximately 150 particles were characterised in total and only particles where the entire circumference could be observed were measured.

3.4.3.4 Energy dispersive x-ray spectroscopy analysis of cobalt-chromium particles

EDX spectroscopy analysis was performed to identify the elemental composition of CoCr particles collected on the filter membranes. This analysis was performed whilst taking the SEM images. Pin point analysis using numerous EDX detection points were selected from a range of CoCr particles, including aggregates.

3.4.3.5 Cobalt-chromium particle characterisation

The SEM images were analysed using ImageJ software to generate a size distribution for the particles generated. Each particle was sized manually by drawing around the perimeter of the particle. Particles were only included if the entire outer edge was viewable i.e. if the particles had aggregated these were not included. A minimum of 300 particles were analysed, pooled from all magnifications taken with the SEM. The size range was distributed between 0-150nm in 10nm increments and >150nm. The results were then presented as a percentage of the total number of particles which were sized.

3.4.4 Preparation of particles for cell culture studies

The exact volume of CoCr particles generated was calculated by completing the following. Firstly, the pins and plates were stored in a moisture controlled environment for at least 48 hours after the test run and then weighed (repeated 3-5 times, accuracy $\pm 5\mu\text{g}$) to determine the mass lost from both components. This mass loss was then combined to give a total mass loss (in mg) which could then be divided by the amount of lubricant retrieved to give a $\mu\text{g.ml}^{-1}$ stock solution.

The particle suspension was thawed and transferred into a glass flask which was then placed in an oven for 4 hours at 180°C to sterilise the particles, evaporate the water they were generated in and remove any potential endotoxin. The particles were re-suspended in 40ml RPMI cell culture medium (containing no other supplements) to give a final stock solution of approximately 2000-3000 $\mu\text{g.ml}^{-1}$ and stored at -20°C. Smaller stocks of approximately 200-300 $\mu\text{g.ml}^{-1}$ were stored to help avoid particle aggregation and repeated freeze-thawing.

Cells were cultured with CoCr particles at volumes of $0.5\mu\text{m}^3$, $5\mu\text{m}^3$ and $50\mu\text{m}^3$ per cell using the calculation specified in **Appendix A**. Previously published literature have determined these particle volumes for the use in cell viability assays in similar cell lines which were used in this study (Germain *et al.*, 2003; Papageorgiou *et al.*, 2007). Once thawed, particle suspensions were sonicated in an ultrasonic water bath for 5 minutes before being added to cells.

3.4.5 Endotoxin testing of generated CoCr particles

The presence of endotoxin in lubricants taken from both the six- and single-station pin-on-plate wear simulators was tested using the Pierce™ Chromogenic Endotoxin Quantitation Kit (ThermoFisher Scientific, UK) which accurately measures and detects the endotoxin, LPS, in samples using the amoebocyte lysate assay. The kit offers a highly sensitive endpoint with detection between 0.1 to 1 endotoxin units/ml (EU.ml⁻¹). One EU is equal to approximately 0.1 to 0.2 ng endotoxin/ml of solution. The amoebocyte lysate used in this assay is derived from the blood of the horseshoe crab which initiates several enzymatic reactions in the presence of endotoxin, including the activation of Factor C, B and pro-clotting enzyme. Once activated, this enzyme catalyses the release of p-nitroaniline (pNA) from a colourless chromogenic substrate (Ac-Ile-Glu-Ala-Arg-pNA), producing a yellow colour which can be stopped with the addition of acetic acid and measured on a spectrophotometer at 405nm. The intensity of developed colour is therefore proportional to the concentration of endotoxin present in any given sample and the concentration can be calculated using a standard curve.

3.4.5.1 Endotoxin kit components

Table 3.2 Pierce LAL chromogenic endotoxin quantitation kit contents and reagent preparation

Pierce LAL chromogenic endotoxin quantitation kit contents **Storage and preparation**

Lyophilized <i>E. coli</i> (0111:B4) Endotoxin Standard, 1 vial, 20 endotoxin units (EU)/vial	Stored at 4°C and reconstituted with 2ml endotoxin free water.
Lyophilized Amebocyte Lysate (LAL), 1 vial, 1.7 mL/vial upon reconstitution	Stored at 4°C and reconstituted with 1.7ml endotoxin free water.
Lyophilized Chromogenic Substrate, 1 vial, 3.4 mL/vial upon reconstitution	Stored at 4°C and reconstituted with 3.4ml endotoxin free water.
Endotoxin-Free Water, 1 vial, 50 mL	Stored at 4°C

3.4.5.2 Sample preparation

Generated CoCr particle samples were defrosted and 500µl from each sample transferred to an eppendorf. Samples were heated to 75°C for 30 minutes, vortexed then centrifuged at 13,000 g for 10 minutes. A volume of 0.5 µl supernatant from each sample was transferred to a new eppendorf and diluted with 49.5 µl endotoxin free water to achieve a 1:100 dilution as per the manufacturer's instructions to eliminate interference from undiluted serum.

3.4.5.3 Reagent preparation

3.4.5.3.1 Endotoxin standard

Standards of *E. coli* were prepared at room temperature by reconstituting in 2ml of endotoxin-free water to give a final concentration of 10 EU/ml. The solution was then vortexed vigorously for 15 minutes. Standards were prepared from this stock endotoxin by firstly adding 200µl of stock to 1800µl of endotoxin-free water to achieve a final concentration of 1 EU.ml⁻¹ (standard 1). Standard 2 (0.5 EU.ml⁻¹) was prepared by

taking 1000µl of standard 1 and diluting in a further 1000µl of endotoxin-free water. Standard 3 (0.25 EU.ml⁻¹) was prepared using 500µl of standard 1 diluted in 1500µl of endotoxin-free water and standard 4 (0.10 EU.ml⁻¹) by taking 200µl of standard 1 and diluting in 1800µl of endotoxin-free water. All standards were vortexed for 1 minute after mixing.

3.4.5.3.2 *Limulus Amebocyte Lysate reagent*

LAL reagent was reconstituted immediately before use with 1700µl of endotoxin-free water and swirled gently to dissolve.

3.4.5.3.3 *Chromogenic substrate*

The chromogenic substrate was reconstituted in 3.4ml of endotoxin-free water and pre-warmed at 37°C for 5 minutes before use.

3.4.5.4 *Assay procedure*

Before starting the assay procedure, all reagents were brought to room temperature and a 96 well plate heated to 37°C. The 96 well plate was maintained at 37°C in a heat block throughout the assay. A volume of 50µl of either standards, blanks (endotoxin-free water or RPMI media only) and diluted samples were added in triplicate to the 96 well plate followed by the addition of 50µl of LAL reagent and a timer was started. The plate was briefly removed from the heat block and mixed gently by tapping 10 times on the side of the plate before returning to the heat block and incubating for precisely 12 minutes. The reconstituted chromogenic substrate was pre-warmed for 5 minutes at 37°C and after exactly 12 minutes of incubation with the LAL reagent 100µl of chromogenic substrate added to each well. Again, the plate was briefly removed from the heat block and mixed gently by tapping 10 times on the side of the plate before returning to the heat block for 6 minutes. Following this 6-minute incubation period, 50µl of stop solution (25% (v/v) acetic acid) was added to each well and again the plate mixed by tapping as before. The plate was then immediately read at 405nm using a spectrophotometer. The blank readings were subtracted from all standards and samples and a standard curve prepared from the endotoxin standards (1, 0.5, 0.25 and 0.10

EU.ml⁻¹). The concentration of the samples were then determined using linear regression.

3.4.6 Inductively coupled plasma mass spectroscopy (ICP-MS)

ICP-MS was used to determine the cobalt (Co) and chromium (Cr) ion concentrations that were released from the CoCr particles using the concentrations to be investigated in cell culture assays (0.5µm³, 5µm³ and 50µm³ particles per cell) and over a period of 0 to 48 hours. ICP-MS analyses single elements within a sample by using an ionisation source that breaks the sample up into its integral elements and converts these elements into ions. An induction coil enables energy to 'couple' with ICP, normally composed of argon gases. The samples in liquid form must firstly be converted to aerosol form using a nebuliser which uses supersonic expansion of gas to create a fine mist from the liquid sample. A spray chamber then removes large droplets which could not be processed in the plasma. The samples are then digested in 2% (v/v) nitric acid which stabilises elements in their ionic form.

The particles at the above concentrations were incubated at 37⁰C in 5% (v/v) CO₂ in complete cell culture medium for 48 hours. Samples were collected at 0, 6, 12, 24 and 48 hours. Particle suspensions were centrifuged for 20 minutes at (16,800g) and the supernatants containing the released ions analysed using ICP-MS at the Department of Blood Sciences, Freeman Hospital, Newcastle upon Tyne by Dr Barry Toole.

3.5 Results

3.5.1 Generation of cobalt-chromium wear particles using the six- and single station pin-on-plate wear simulator

The aim of this chapter was to generate sufficient volumes of clinically-relevant cobalt chromium particles to be used in future cell culture studies. By running the pin-on-plate simulators for the durations discussed, a large volume of particles was generated under different conditions and were ample for the experiments planned as part of this project.

3.5.2 Characterisation of cobalt-chromium particles generated using a six-station pin-on-plate wear simulator

The characterisation in terms of size and morphology and the composition of the CoCr particles generated in the six-station pin-on-plate wear simulator were determined and analysed after filtration on 0.015 μ m filter membranes using SEM and EDX analysis as described in **section 3.4.3.1**. Image analysis was performed using ImageJ software to determine the diameter of the particles (minimum of 150 particles per sample). The morphology of the generated particles collected on the filter membranes are shown in **Figure 3.8** to **Figure 3.11**.

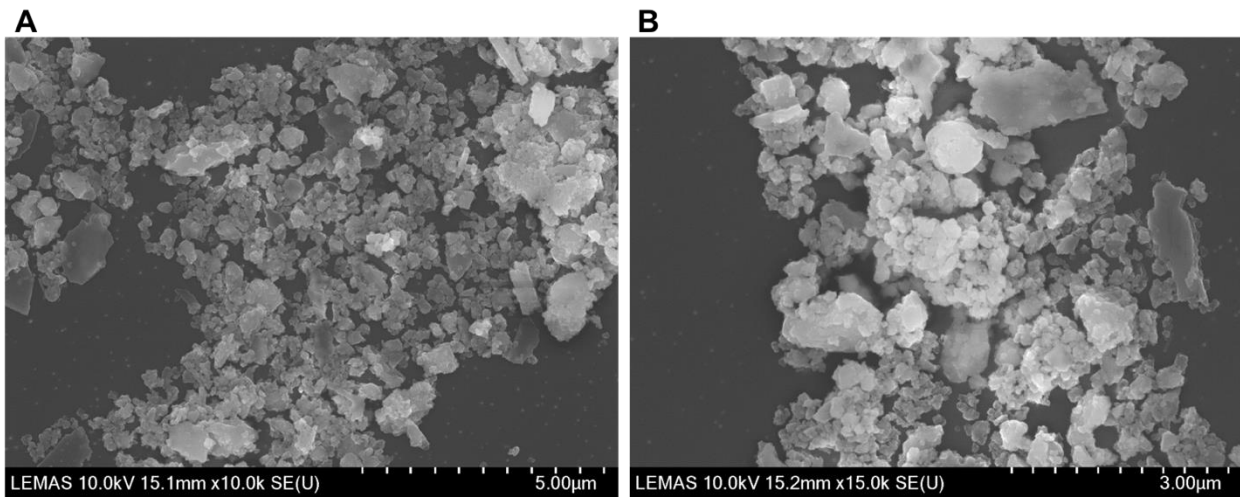


Figure 3.8 SEM images of CoCr particles generated on six-station pin-on-plate wear simulator

(A) x10K and (B) x15K magnification

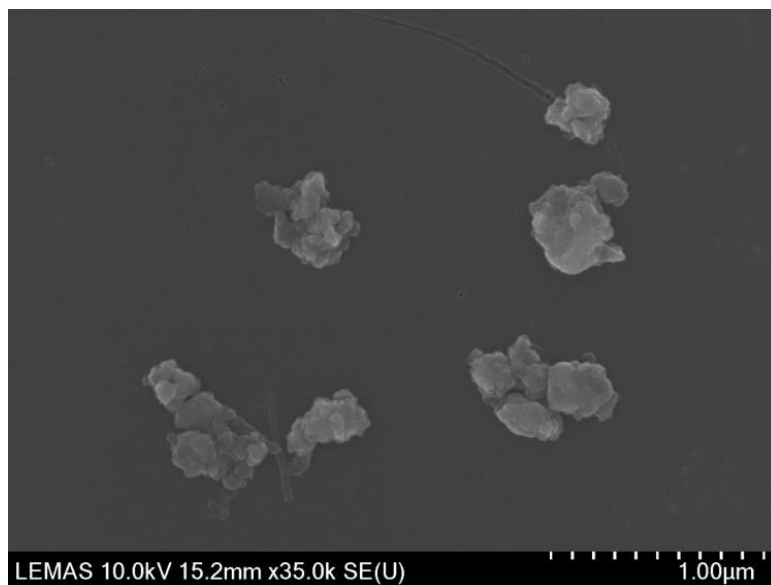


Figure 3.9 SEM image of CoCr particles generated on six-station pin-on-plate wear simulator

x35K magnification

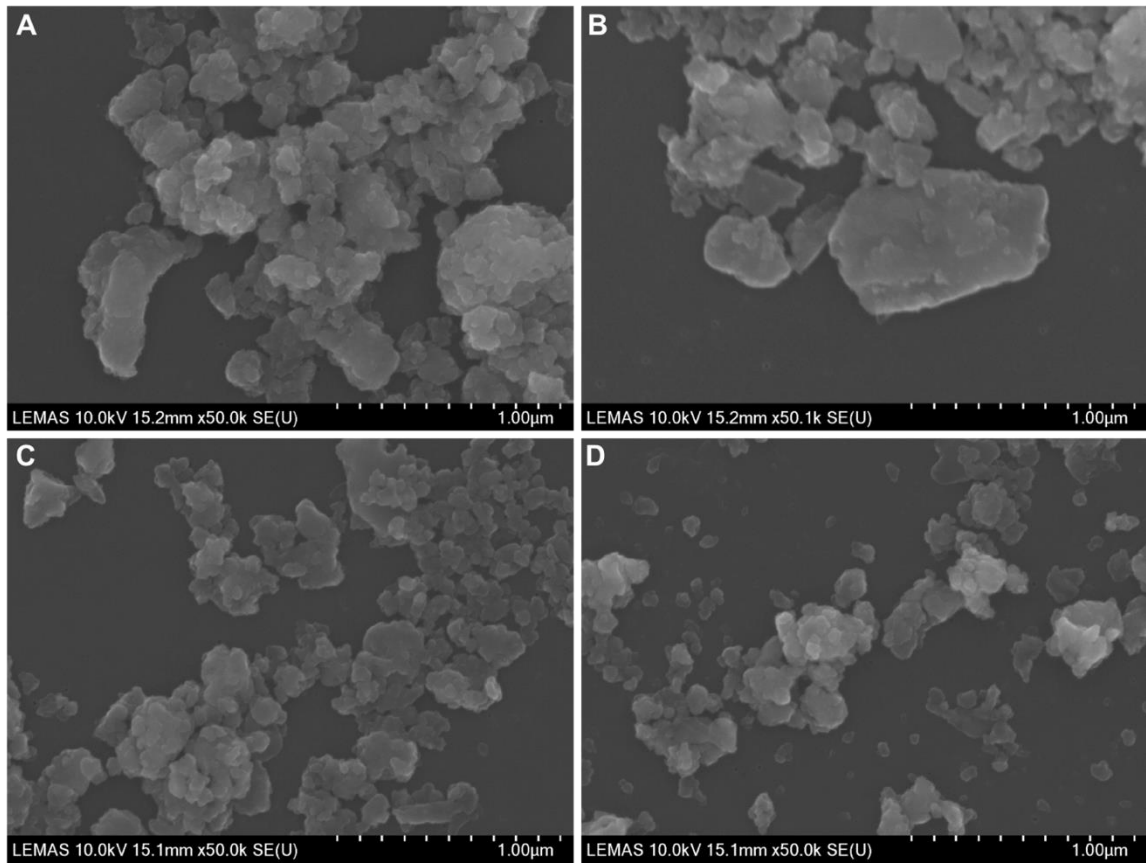


Figure 3.10 SEM images of CoCr particles generated on six-station pin-on-plate wear simulator

Images are representative of 4 different tests, x50K magnification.

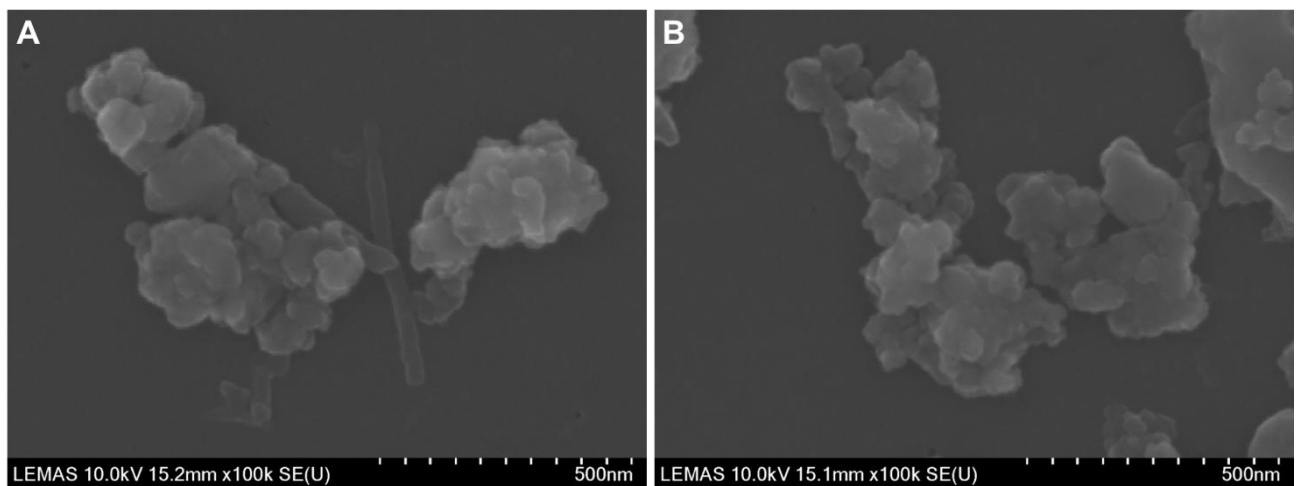


Figure 3.11 SEM image of CoCr particles generated on six-station pin-on-plate wear simulator

Images are representative of 4 different tests, x100K magnification.

Under low magnification (x10K and x15K) granular, micron sized CoCr particles were observed (**Figure 3.8**). However, these irregular particles which are larger in morphology appear to be due to agglomerations of particles from smaller nano-scale particles. As magnification increased it became clearer that the individual particles are in fact much smaller and the agglomerations make up the larger sized particles viewed (**Figure 3.10**). Furthermore, at higher magnifications (e.g. x100K), numerous round to oval shaped particles, uniform in their morphology, were observed and were nano-scale in size (**Figure 3.11**). There were no shard-like particles observed in these samples.

The size distribution of the particles collected on the filters was generated using ImageJ software. The percentage (calculated against the total number of particles observed i.e. minimum of 150 per sample) of CoCr particles which were <50nm in length was 42%, 47.3% were between 50 and 99nm in length and only 8.7% of particles generated were larger than 100nm in size (**Figure 3.12**).

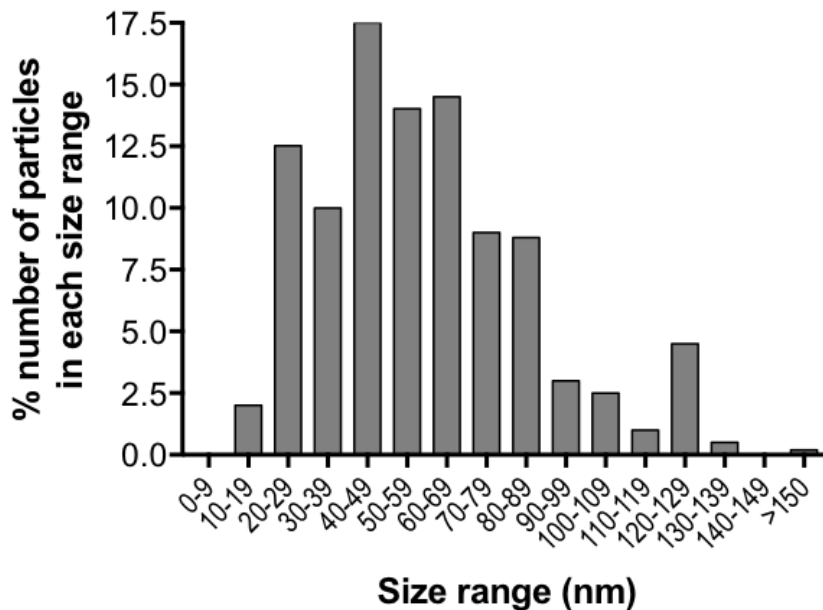


Figure 3.12 Frequency distribution of CoCr particles generated using a six-station pin-on-plate wear simulator

Particles were generated using a six-station pin-on-plate wear simulator, imaged using SEM and the percentage size distribution determined using ImageJ. At least 150 particles were characterised per sample.

The elemental composition of the CoCr particles was determined using EDX analysis as described in **section 3.4.3.4. (Figure 3.13)**. The EDX detection point was taken from within a particle agglomerate. The analysis revealed peaks of excitation for carbon, cobalt, chromium, phosphorous and oxygen. The high carbon content was due to the method for sample preparation which involved carbon coating of the sample for SEM imaging and subsequent EDX analysis. Therefore, the elemental composition was as expected and composed of Co, Cr and Mo elements.

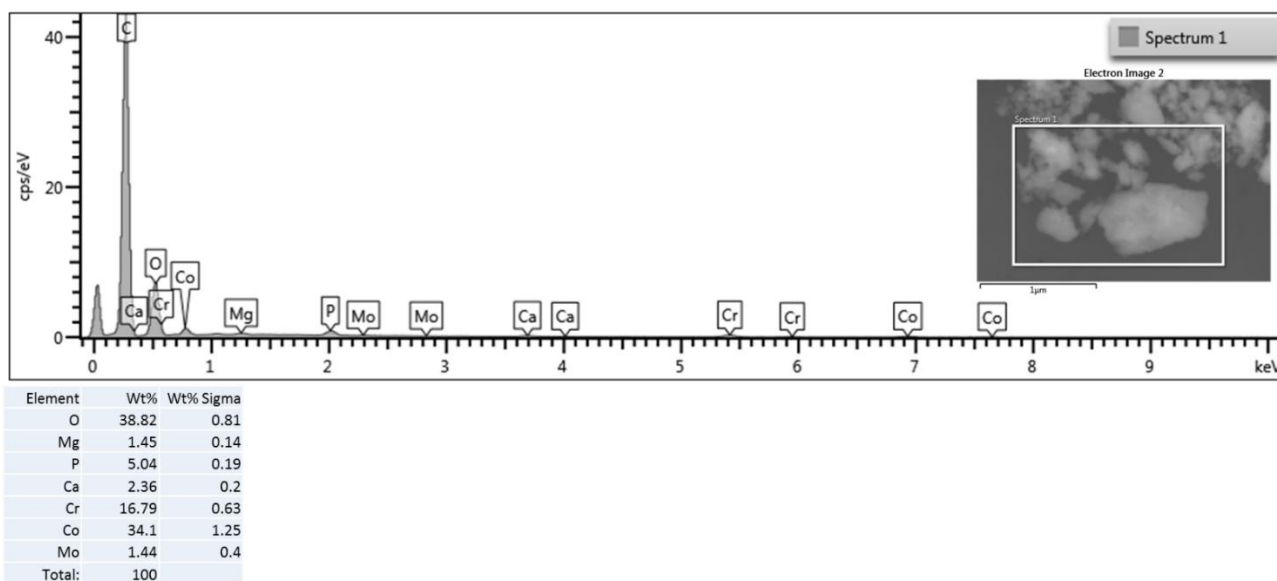


Figure 3.13 Energy dispersive x-ray spectroscopy analysis of nanoscale CoCr particles

Pin point energy dispersive x-ray spectroscopy was used to determine the elemental composition of generated CoCr particles. In this instance, the peak for carbon (C) is due to the coating of the particles for SEM analysis. There are other significant peaks at cobalt (Co) and chromium (Cr).

3.5.3 Characterisation of isolated cobalt-chromium particles generated using a single-station pin-on-plate wear simulator

The characterisation in terms of size and morphology and the composition of the CoCr particles generated in the sterile single-station pin-on-plate wear simulator, where RPMI media containing 25% (v/v) FBS was used as the lubricant, were firstly digested then determined and analysed after filtration on 0.015µm filter membranes using SEM and EDX analysis as described in **section 3.4.3.1**. Image analysis was performed using ImageJ software to determine the diameter of the particles (minimum of 150

particles per sample). The morphology of the generated particles collected on the filter membranes are shown in **Figure 3.14 to Figure 3.16**. These particles were isolated using the method described in **section 3.4.3.2**, and SEM imaging was used to confirm that the morphology of the particles were similar to those particles generated in sterile water described in **section 3.5.2**.

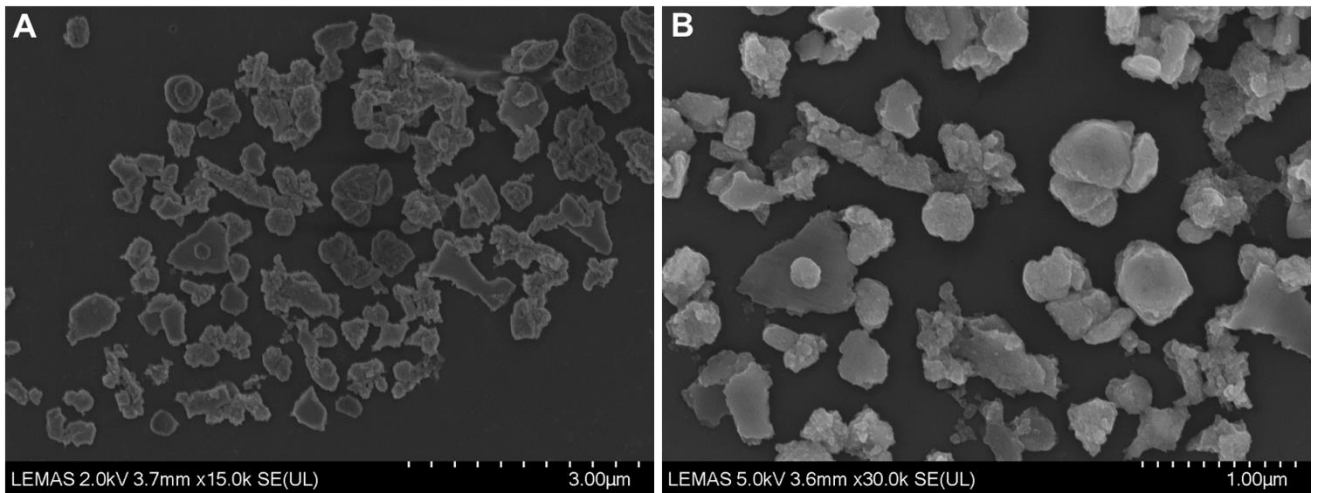


Figure 3.14 SEM image of isolated CoCr particles generated using a single-station pin-on-plate wear simulator

(A) x15K and (B) x30K magnification

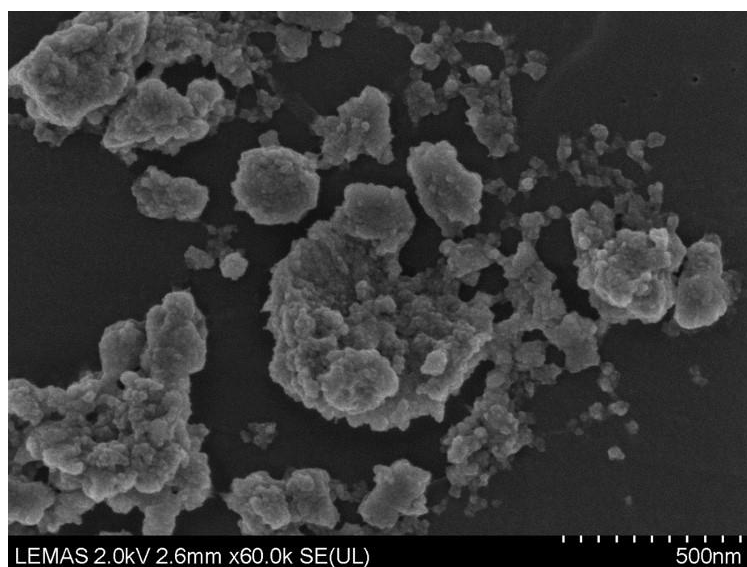


Figure 3.15 SEM image of isolated CoCr particles generated using a single-station pin-on-plate wear simulator

x60K magnification

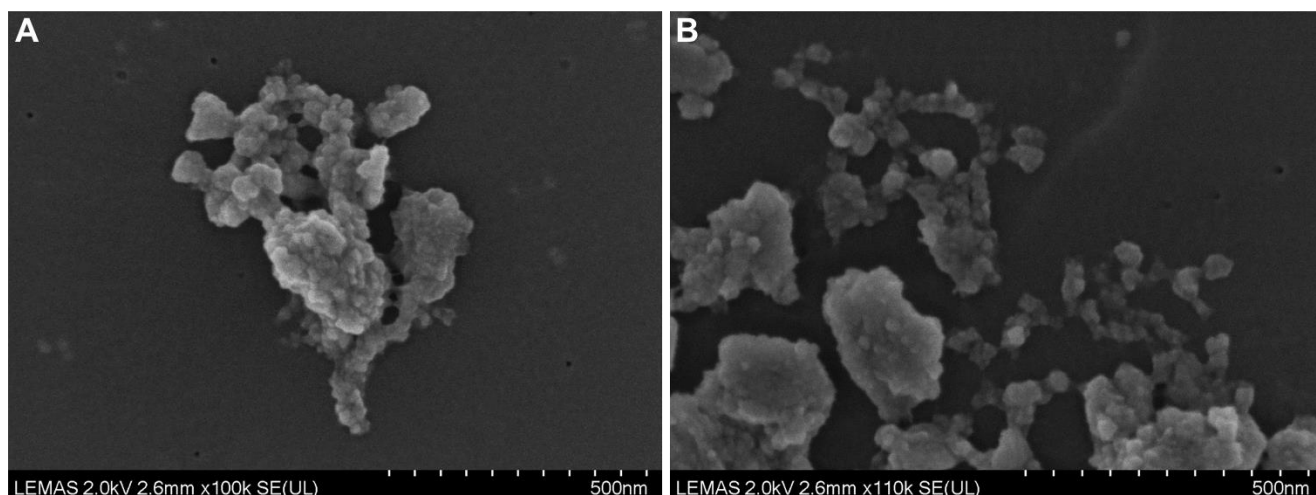


Figure 3.16 SEM image of isolated CoCr particles generated using a single-station pin-on-plate wear simulator

(A) x100K and (B) x110K magnification

The particles isolated from the single-station pin-on-plate wear simulator were similar in morphology to the particles generated using a six-station pin-on-plate simulator as previously described. Larger aggregates were observed at low magnification (x15K and 30K) (**Figure 3.14**), whereas smaller individual particles, although difficult to resolve were visible at higher magnifications (x100K and x110K) (**Figure 3.16**).

The size distribution of the particles which were isolated and then collected on the filters was generated using ImageJ software. The percentage (calculated against the total number of particles observed i.e. minimum of 150 per sample) of CoCr particles which were <50nm in length was 48%, 53.7% were between 50-99nm in length and only 3% of particles were larger than 100nm in size (**Figure 3.17**). Therefore, the size of the observed particles following isolation were similar to those that were generated using water as a lubricant.

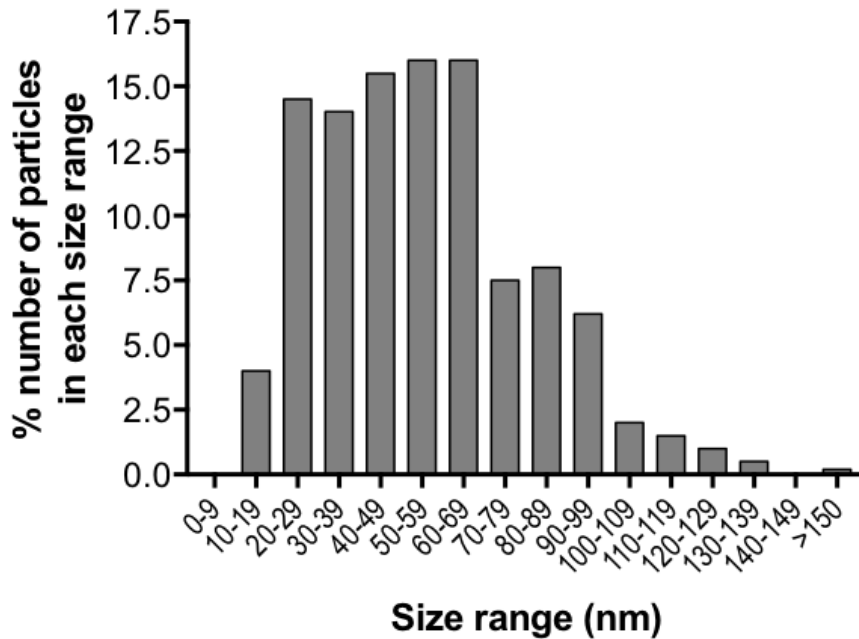


Figure 3.17 Frequency distribution of isolated CoCr particles generated using a single-station pin-on-plate wear simulator

Particles were generated using the single-station pin-on-plate wear simulator, isolated from their lubricant and imaged using SEM. The percentage size distribution was then determined using ImageJ. At least 150 particles were characterised per sample.

3.5.4 Microbiological testing of generated CoCr particles from single-station pin-on-plate wear simulator

Agar plates, as described in **section 3.4.2.3**, were used for the microbiological testing of sample lubricants from the single-station pin-on-plate wear simulator and incubated for up to 72 hours to assess for any contamination. All samples which were collected throughout the running of the wear rig came back clear i.e. no contamination was detected in any of the tests, and the lubricants were deemed sterile.

3.5.5 Endotoxin testing

Lubricants taken from both the six- and single-station pin-on-plate wear simulators were tested for endotoxin using the Pierce™ Chromogenic Endotoxin Quantitation Kit. A standard curve was also created using *E. coli* at concentrations ranging between 0.1 and 1 EU/ml⁻¹ (**Figure 3.18**). The endotoxin concentration of each sample could then be determined by extrapolating from the standard curve using a linear regression

equation. Previous research has shown that as little as 0.1 EU/ml⁻¹ of LPS/endotoxin can upregulate inflammatory gene expression in primary human monocytes (Oostingh *et al.*, 2011). **Table 3.3** and **Table 3.4** demonstrate the concentrations of endotoxin (EU/ml⁻¹) in CoCr lubricant samples taken from the six-station and single-station pin-on-plate wear simulators, respectively, extrapolated from the standard curve.

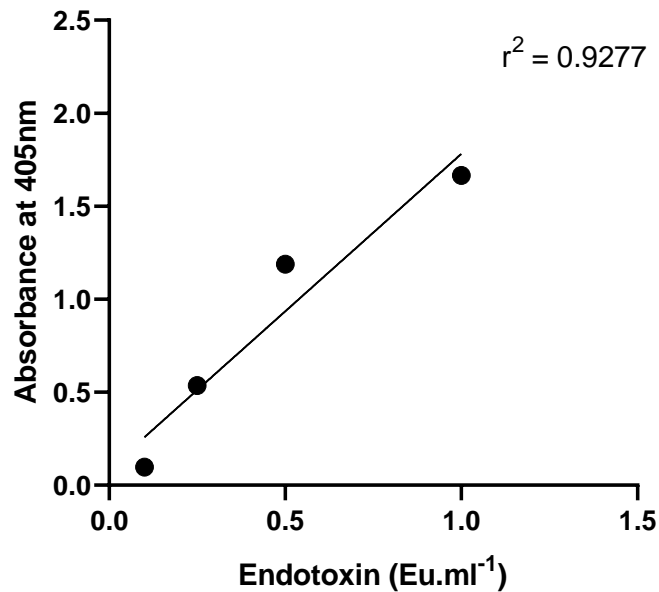


Figure 3.18 Standard curve for the quantitation of endotoxin

A standard curve was calculated using linear regression so that lubricant samples taken from wear testing could be tested for endotoxin and the optical densities extrapolated from the graph to determine the EU.ml⁻¹.

Table 3.3 Endotoxin concentrations taken from lubricants of six-station pin-on-plate wear simulator

Concentrations taken from triplicate values and standard deviation of the mean calculated

Source of lubricant	Eu.ml ⁻¹
Six station sample 1	0.088±0.21
Six station sample 2	0.211±0.11
Six station sample 3	0.025±0.31

Table 3.4 Endotoxin concentrations taken from lubricants of single-station pin-on-plate wear simulator

Concentrations taken from triplicate values and standard deviation of the mean calculated

Source of lubricant	Eu.ml ⁻¹
Single station sample 1	2.323±0.42
Single station sample 2	2.556±0.23

3.5.6 Release of cobalt and chromium ions from CoCr particles

In both cobalt and chromium ion measurement, there was a dose dependent increase in ion concentration as CoCr particle concentration increased reaching a peak of 1500µg/L and 350µg/L, respectively at 50µm³ per cell equivalent (**Figure 3.19A and Figure 3.19B**).

The largest concentration of CoCr particles (50µm³ per cell) was then used to determine cobalt and chromium ion release over a period of up to 48 hours (**Figure 3.20A and Figure 3.20B**). The results showed that following 24 hours, maximal concentration of both cobalt and chromium ions had been reached as at 48 hours there was very little difference between the two concentrations. For example, cobalt ion concentration after 24 hours ranged between 1292µg/L-1372µg/L and at 48 hours 1275µg/L-1447µg/L. This was similar for chromium ion concentrations which ranged between 519µg/L-569µg/L following 24 hours and 534µg/L-608µg/L at 48 hours.

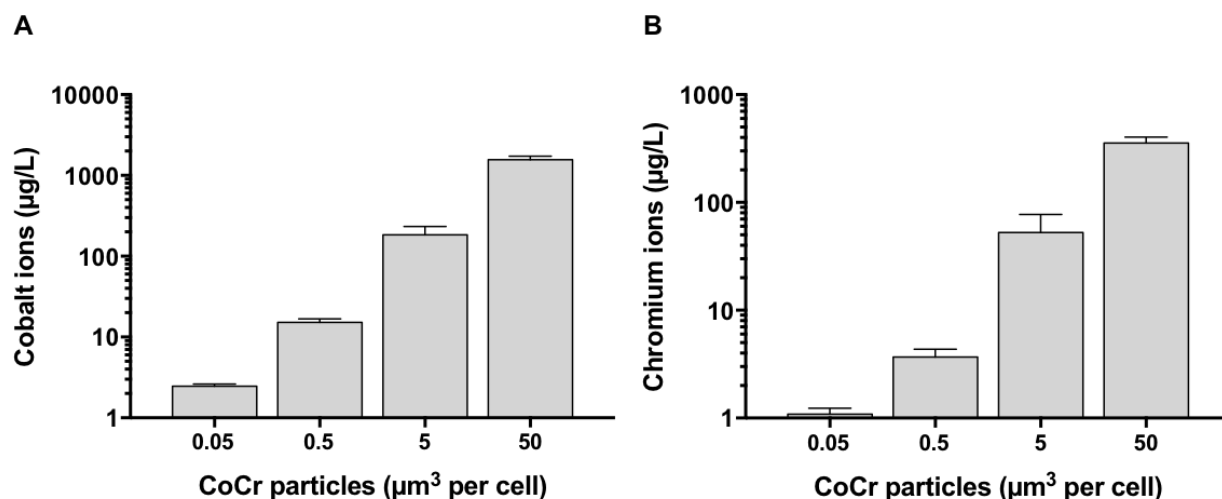


Figure 3.19 Cobalt and chromium ion release from CoCr particle dose between 0.05 and 50 μm^3 CoCr particles per cell response at 24 hours

Generated CoCr particles from a six-station pin-on-plate wear simulator were incubated in complete cell culture medium to determine the release of cobalt **(A)** and chromium **(B)** ions after 24 hours measured by ICP-MS. Data is representative of two independent experiments.

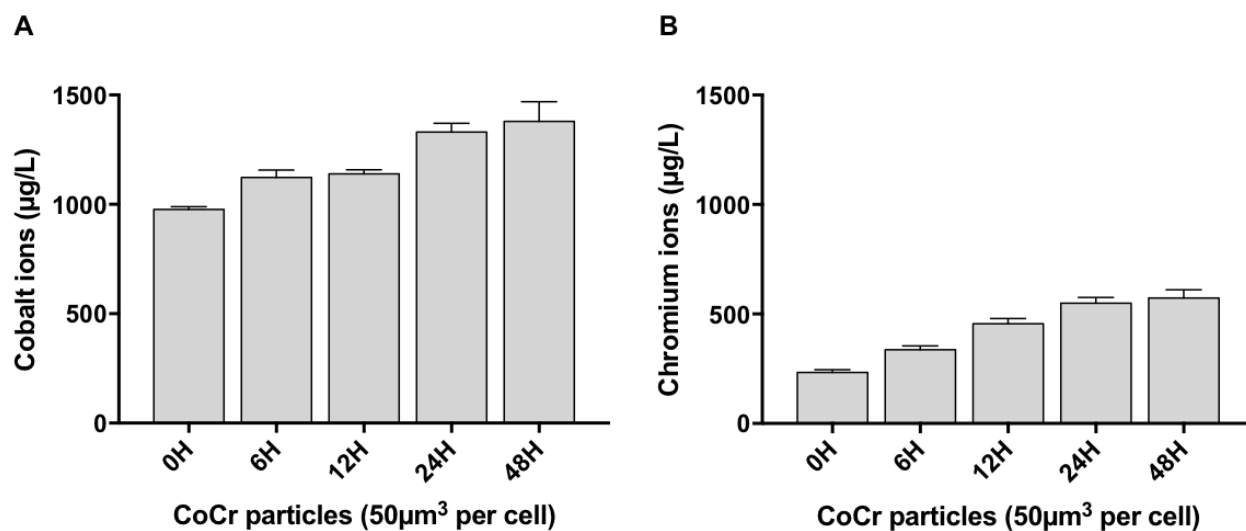


Figure 3.20 Time course showing cobalt and chromium release from CoCr particles

Generated CoCr particles from a six-station pin-on-plate wear simulator were incubated with the equivalent volume of 50 μm^3 particles per cell in complete cell culture medium to determine the release of cobalt **(A)** and chromium **(B)** ions between 0 and 48 hours measured by ICP-MS. Data is representative of two independent experiments.

To be able to investigate the differences in biological effect of both CoCr particles and cobalt ions alone it was important to determine the cobalt ion concentration to be used in cell treatments to compare responses. The concentration of cobalt ions released from $50\mu\text{m}^3$ particles per cell ($1500\mu\text{g/L}$) was converted into mM to approximately 0.025mM (or $25\mu\text{M}$) CoCl_2 . This concentration was added to complete RPMI media and incubated for 48 hours to determine the cobalt ion concentration by ICP-MS and ensure this was accurate compared to what was measured (**Figure 3.21**). As shown previously, the release of cobalt ions from CoCr particles increased between 0 and 24 hours, reaching a peak of $1500\mu\text{g/L}$. At 0 hours, cobalt ion concentration from CoCl_2 was larger when compared to CoCr particle treatment (approximately $1250\mu\text{g/L}$ versus $975\mu\text{g/L}$, respectively). CoCl_2 ion concentration did not change over time indicating that the concentration added remained consistent over 48 hours. Cobalt ion concentration in this instance reached a peak of $1243\mu\text{g/L}$ and was therefore similar to the concentration of cobalt ions released from the $50\mu\text{m}^3$ per cell dose of CoCr particles ($1378\mu\text{g/L}$).

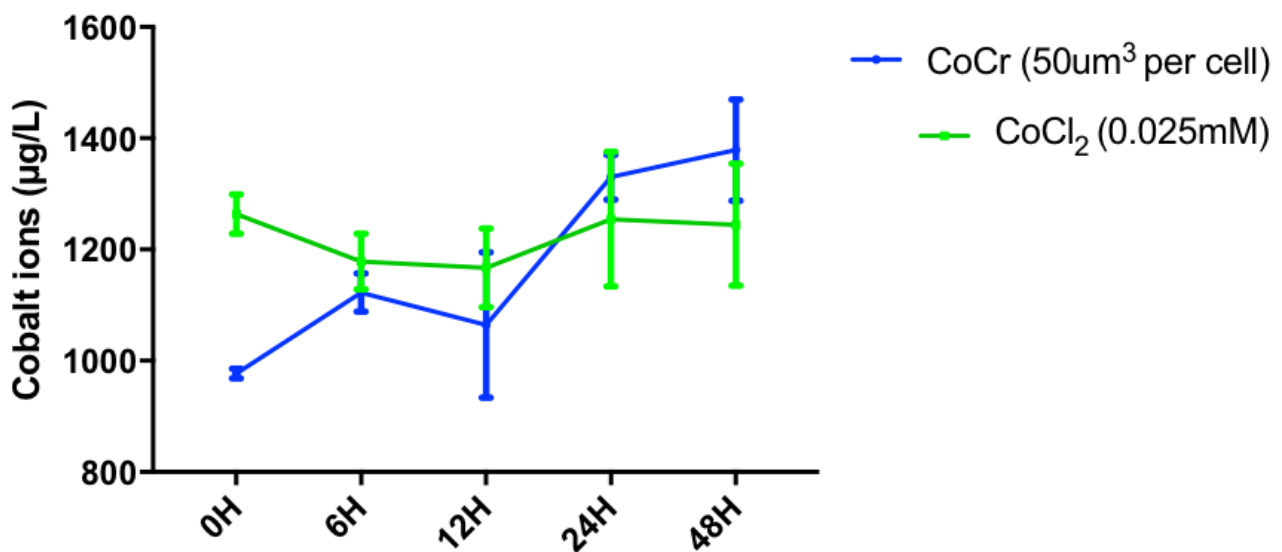


Figure 3.21 Comparison of CoCr particles and CoCl_2 ion concentration over time

The estimated dose of CoCl_2 (0.025mM) which was released by CoCr particles ($50\mu\text{m}^3$ per cell) after 24 hours was added to complete RPMI media and cobalt ion concentration measured by ICP-MS over a period of 0-48 hours. Data is representative of two independent experiments.

3.6 Discussion

For this part of the study, both a six- and single-station pin-on-plate wear simulator were used to generate CoCr particles, using smooth high carbon CoCrMo alloy pins and plates and using either sterile water or RPMI media (+ 25% (v/v) FBS) as a lubricant, respectively. In this instance, metal pins articulated against metal plates using multi-directional motion and generated wear particles over a total of 3 weeks, articulating at a frequency of 1 Hz under a load of 80N (to replicate the motions and loads of a typical hip joint). The CoCr particles generated could then be compared to previous studies to ensure they were of correct elemental composition, size and morphology. The six-station pin-on-plate wear simulator was utilised so that large volumes of CoCr particles could be generated in a relatively short time frame. The single-station wear simulator provided fewer, but potentially more clinically-relevant CoCr particles, due to the presence of proteins from the FBS included within the RPMI lubricant as well as cobalt and chromium ions that are released during the wear testing. The single-station simulator also provided a sterile environment to generate CoCr particles for cell culture studies. The sterility of these CoCr particles was confirmed by taking samples during the test run for microbiological analysis and also tested for endotoxin to ensure there was no contamination.

The use of these pin-on-plate wear simulators has been previously established in the literature to generate CoCr particles of a clinically-relevant size and morphology (Germain *et al.*, 2003). The benefit of generating CoCr particles in sterile water with the six-station simulator was that these could be simply characterised due to the lack of proteins in the lubricant. These particles could also be easily sterilised by heat-treating at 180°C for 4 hours which has been shown to effectively remove any endotoxin meaning they are suitable to be used in cell culture experiments (Germain *et al.*, 2003). However, it was also important to generate CoCr particles which would be more similar to those generated in an *in vivo* patient setting and hence the addition of serum into the lubricant was employed for the single-station simulator. This meant that the simulator had to be ran under aseptic conditions so that the lubricant containing the serum and potentially released cobalt and chromium ions could be maintained for cell culture studies as heat-treating for sterilisation leads to the evaporation and loss of the lubricant.

The CoCr particles generated in the six-station pin-on-plate wear simulator had an average size of 45nm. The size of generated particles did not significantly alter when characterising particles isolated from lubricant containing serum generated in the single-station wear simulator, which had an average size of 57nm. The particles produced were of a comparable size to those observed in tissues from patients with failed implants (i.e. the nanoscale range) and similar in size and morphology to those studies which have also used metal-on-metal wear and pin-on-plate simulators to produce CoCr wear particles for cell culture studies (Brown *et al.*, 2007; Papageorgiou *et al.*, 2014). However, it was particularly difficult to accurately measure the size of each individual particle due to the agglomeration and aggregation of particles. In another study which also used the six-station pin-on-plate wear simulator with water as the lubricant of choice, aggregated CoCr particles were also observed with an average size of 40-49nm (Behl *et al.*, 2013). In this study, efforts to prevent the formation of aggregates of CoCr particles were employed by using sonication for 10 minutes, as it has been shown that longer periods of sonication (more than 30 minutes) can in fact lead to further re-agglomeration (Chowdhury *et al.*, 2010). However, despite using a shorter sonication time, re-agglomeration of particles occurred relatively quickly and was therefore difficult to avoid completely. It is likely that CoCr particle aggregates are reflected in the tissues of patients with metal implants and have also been observed in the tissues of *in vivo* mouse models (Akbar *et al.*, 2012; Paulus *et al.*, 2019).

In a study which isolated CoCr particles from the tissue of 13 patients with MoM hip implants undergoing revision surgery investigators found that the morphology of these particles were mostly round but with some shard-like particles observed (Doorn *et al.*, 1998). This is in agreement with other retrieval studies which have isolated particles from explanted tissue in patients with MoM hip resurfacings (Xia *et al.*, 2011; Goode *et al.*, 2012). In this study, there did not appear to be any shard-like particles with all observed particles appearing to be round in their morphology. This appears to be similar to other simulator studies generating CoCr particles which also report round morphologies with the absence of shard-like particles (Brown *et al.*, 2007; Papageorgiou *et al.*, 2007; Paulus *et al.*, 2019). These findings may come down to which type of CoCr alloy is investigated, for example; cast or wrought alloys which can produce different particle morphologies (cast are known to produce shard-like particles). Wrought CoCr alloys possess higher strength in comparison to cast alloys

and therefore are more likely to be used in implants requiring increased strength properties and this was the alloy utilised in this study as well as the other simulator studies discussed. However, cast alloys are frequently used in some resurfacing devices e.g. Birmingham Hip Resurfacing. This would explain why some of the studies investigating tissue from patients who have received MoM hip implants have observed shard-like particles.

EDX analysis was employed to confirm the elemental composition of the generated CoCr particles. Both cobalt and chromium were detected at 34.1% and 16.79% (Wt%), respectively, and a small peak for molybdenum at 1.44% which demonstrated a consistent ratio of elements when compared with the clinical biomaterial used in CoCrMo implants. The importance of evaluating morphological and elemental composition of these particles is paramount prior to investigating cellular responses. This is because, particle volume, size and shape can alter consequent effects and to ensure particles are as close to being clinically relevant as possible (Papageorgiou *et al.*, 2007; Nine *et al.*, 2014). For example, nanoscale CoCr particles have been shown to cause more mitochondrial damage, more DNA damage and enhanced cytotoxicity in fibroblasts when compared to microscale CoCr particles (Papageorgiou *et al.*, 2007).

Furthermore, an effective particle isolation protocol which does not alter particle characteristics is equally important for particles generated in the presence of FBS. The use of these particles in cell culture assays will add further clinical relevance as the presence of proteins better mimics the *in vivo* setting. This isolation protocol must also be reproducible and efficient. Previous alkaline and acid digestion methods have proven to be inadequate in preventing alterations to particle characteristics and enzymatic digestion can also be inefficient and unreliable. However, a novel method for the isolation and recovery of metal wear debris from lubricants containing serum was employed in this study, which involved enzymatic digestion with proteinase K and density gradient ultracentrifugation methods (Lal *et al.*, 2016). The particles were then filtered onto 0.015µm pore sized filters and imaged using SEM. These particles did not appear to differ in size or morphology compared to the CoCr particles generated in sterile water from the six-station pin-on-plate wear simulator thus validating six-station pin-on-plate simulator and use of water as a lubricant.

Before CoCr particles could be used for *in vitro* cell culture experiments it was crucial to ensure the sterility of the particles generated from both the six- and single-station

pin-on-plate wear simulators. This is because this research focuses on inflammatory responses so it is important to establish that any responses observed are from the sample stimuli and not due to contaminant endotoxin/LPS. The lubricants collected from the six-station pin-on-plate wear simulator were generated under non-sterile conditions and were therefore subject to heat treatment to remove any potential endotoxin prior to testing with the Pierce™ Chromogenic Endotoxin Quantitation Kit. All possible efforts were made in the running of the single-station pin-on-plate wear simulator to keep conditions sterile so that this lubricant (cell culture media with and without the addition of FBS) could be directly used in future cell culture experiments and directly tested for endotoxin contamination. The results from the endotoxin quantitation demonstrated that 2 out of the 3 lubricants tested from the heat-treated six-station pin-on-plate wear simulators contained less than 0.1 EU/ml^{-1} with one sample slightly over this threshold at 0.211 EU/ml^{-1} . Therefore, it could be assumed that these samples were suitable for future cell culture experiments. Conversely, the lubricants taken from the single-station pin-on-plate wear simulator tested higher for endotoxin at concentrations of 2.3 and 2.5 EU/ml^{-1} . This was surprising given that these particles were generated under 'sterile conditions' and had passed initial microbiological testing checks using agar plates. To ensure the agar plates were working as expected, known sources of bacteria and fungi could have been used to streak the plates alongside lubricant testing. The higher levels of endotoxin were possibly due to serum contamination within the lubricant samples or could have been easily contaminated during the endotoxin testing itself. However, it does demonstrate the effectiveness of heat treatment in eliminating endotoxin from the particles generated in the six-station using water as the lubricant of choice.

It is likely that endotoxin binds easily on the surface of nanoparticles due to their highly reactive surfaces (Li and Boraschi, 2016). It is also possible that nanoparticles can interfere with the optical densities of LAL assays which has been cited in ISO regulations. The single-station samples were taken directly from the lubricant and therefore potentially contained a higher concentration of particles which could have explained the higher endotoxin concentrations. It is interesting that when samples of lubricant were taken during the running of the single-station for use in microbiological tests (agar plate streaking) that these all came back clear of any contamination. It is therefore possible that perhaps these sample lubricants became contaminated at a different stage perhaps in transfer to long term storage. In future, it is important to run

appropriate controls and ensure the same concentration of particles is used across test samples in LAL assays. Further experiments investigating the biological effects of CoCr particles on cell lines involved only using samples measuring under 0.1 EU/ml to ensure any inflammatory effects were due to CoCr particles and not potential endotoxin contamination.

The results from the ICP-MS investigating the release of cobalt and chromium ions from generated particles demonstrated that these ions are released in a dose dependent manner as well as gradually over a course of time (0-24 hours). There was no significant difference in ion release between 24 and 48 hours for both cobalt and chromium ions. This is in agreement with previous studies which have demonstrated that cobalt and chromium ion release from CoCr particles reached its maximum at 24 hours and did not significantly increase at 48 hours (Papageorgiou *et al.*, 2007; Behl *et al.*, 2013). It has been hypothesised that this is due to an oxidation film layer that is formed, preventing corrosion of particles and subsequent ion release. It was particularly important to establish the concentration of cobalt ions released from the generated CoCr particles to provide a further 'control' to future cell culture studies. By using the observed released cobalt ion concentration alongside CoCr treatments, this will help establish whether any inflammatory effects are due to cobalt ions alone or whether the effect is enhanced in the presence of the particles.

3.6.1 Conclusions

CoCr wear particles for use in cell culture studies were generated either in water from a six-station pin-on-plate wear simulator or in RPMI media (+25% (v/v) FBS) in a single-station simulator. The size and morphology of these particles were similar to those observed from patients who have received implants containing metals, therefore, they could be deemed clinically-relevant. The CoCr particles generated were vacuum filtered (particles generated in RPMI media containing FBS were firstly isolated using enzymatic digestion and density gradient methods) and characterised using SEM and elemental analysis confirmed using EDX. The number of particles produced were sufficient to complete all future cell culture assays to investigate the effect of CoCr wear particles on human cell lines.

Chapter 4 : Role of the Toll-like Receptor 4 Signalling Pathway and Inflammasome in the Inflammatory Response to CoCr Particles

4.1 Introduction

Chapter 3 described the generation of clinically relevant CoCr particles and the steps taken to characterise and prepare these particles to be utilised in cell culture treatments, *in vitro*. Previous work carried out within the group investigating inflammatory effects of cobalt ions have focussed on the use of monocytic/macrophage cell lines (Lawrence *et al.*, 2014; Lawrence *et al.*, 2016a; Lawrence *et al.*, 2016b). Therefore, in this study, the human MM6 and THP-1 cell lines as well as mouse J774 cells were used to optimise cell treatments with CoCr particles. Once the dose of particles was optimised, it was important to establish reliable and significant markers of inflammation following treatments. Specific immunological pathways such as TLR4 and the NLRP3 inflammasome were then subsequently targeted to elucidate their role in this inflammatory response. The TLR4 pathway was the main signalling pathway of interest based on our previous work using cobalt ions which are known to activate TLR4 and cause up-regulation of chemokines and cytokines, particularly IL-8 (Lawrence *et al.*, 2014; Lawrence *et al.*, 2016b). The inflammasome pathway, specifically NLRP3, was also investigated as researchers have suggested CoCr-mediated inflammation acts through a DAMP rather than a PAMP response so could therefore be caused by NLRP3 activation and subsequent up-regulation of IL-1 β (Samelko *et al.*, 2016).

The effect of CoCr particles on a mouse macrophage cell line (J774) was investigated to determine whether the particles could elicit a response in these cells and species. As previously discussed, it has been established that cobalt and nickel ions are unable to activate mouse TLR4 due to the lack of two conserved histidine residues found only in the human TLR4 amino-acid sequence to which metal ions bind, causing TLR4 activation. Therefore, if CoCr particles can activate J774 cells this would suggest that other alternative pathways may be involved.

It was important to first determine whether the dosage of particles used to treat cells caused cytotoxicity/cell death. It is known that high concentrations of cobalt ions can cause cytotoxicity and results from the previous chapter indicate that cobalt ions are released into cell culture medium from the generated CoCr particles to be used in this

study (Kwon *et al.*, 2009). It was therefore necessary to establish a dose sufficient to perpetuate an inflammatory effect without causing toxicity. Trypan blue staining was selected to measure cytotoxicity and an XTT assay to assess proliferation rate of cells.

Phagocytosis of CoCr particles was discussed in **section 1.4.3** and therefore as part of this study, TEM was used on activated THP-1 cells to analyse intracellular changes following stimulation with CoCr particles. Furthermore, in **section 1.6.2**, enhanced phagocytosis following TLR4 activation was also discussed so a phagocytosis assay was utilised to establish how treatment with CoCr particles can affect the phagocytic ability of macrophage cells.

4.2 Aims and Objectives

The aim of this chapter was to establish the effects of clinically relevant CoCr nanoscale particles in monocyte/macrophage cell lines by assessing toxicity and protein and gene expression of pro-inflammatory cytokines and chemokines known to be involved in ARMD and osteolytic responses. The TLR4 and NLRP3 inflammasome pathways were investigated to determine their potential role in these responses. Macrophage phagocytic capability was investigated by imaging cells by TEM following CoCr particle treatment as well as performing a phagocytosis assay.

4.2.1 Objectives

- To investigate the effect of CoCr particles on MM6, THP-1 and J774 cell viability
- To establish whether THP-1 cells can phagocytose CoCr particles
- To establish the effect of CoCr particles on the phagocytic ability of THP-1 cells
- To establish which proteins are significantly up-regulated in response to CoCr particles
- To investigate whether the use of TLR4-specific inhibitors can prevent the inflammatory response mediated by CoCr particles
- To investigate whether CoCr particles can activate the NLRP3 inflammasome complex

4.3 Specific Methods

4.3.1 Cell treatments

For all cell treatments using CoCr particles in this part of the study, sterilised particles generated in the six-station pin-on-plate wear simulator were used as described in **section 3.4.4**. These particles were used due to findings from endotoxin testing in **section 3.5.5**, which demonstrated potential endotoxin contamination in particles generated in the single-station pin-on-plate wear simulator.

4.3.2 Meso Scale Discovery (MSD) multiplex cytokine analysis

A Meso Scale Discovery (MSD) plate was used to measure changes in cytokine and chemokine expression in THP-1 cells treated with CoCr particles in the presence and absence of the TLR4 inhibitor, CLI-095. Specifically, 400,000 activated THP-1 cells were stimulated with varying concentrations of CoCr particles (0.5 to 50 μm^3 per cell) for 24 hours. For treatments including CLI-095, cells were pre-treated with 1 $\mu\text{g}/\text{ml}$ CLI-095 for 6 hours prior to stimulation.

MSD analysis offer many advantages over ELISAs such as, the sensitive measurement of up to 10 different cytokines or chemokines in one single sample, and a wide dynamic range whilst only requiring a small sample volume. This study used U-PLEX technology, which allows for the custom creation of any combination of up to 10 compatible markers to be analysed on the same plate. The following cytokines and chemokines were chosen due to their association with innate immune responses and due to data extrapolated from a previous PCR microarray of cobalt ion treated monocytes; IL-8, CCL2, CCL3, CCL4, CCL20, CXCL10, TNF α , IL-1 β , IL-10 and IL-13. The role of these cytokines and chemokines is summarised in **Table 4.1**. The principle of the assay involves biotinylated capture antibodies which are coupled to U-PLEX linkers and self-assemble onto unique spots on the U-PLEX plate. Analytes in the sample bind to the capture reagents and detection antibodies conjugated with electro-chemiluminescent labels (MSD Gold™ SULFO-TAG) bind to the analytes to complete the sandwich immunoassay (**Figure 4.1**).

Once the sandwich immunoassay is complete, the U-PLEX plate is loaded into an MSD instrument where a voltage is applied to the plate electrodes causing the captured labels to emit light. The reaction is catalysed by Tris(2,2'-bipyridyl)dichlororuthenium(II)

hexahydrate (Ru(bpy)₃) with the co-reactant, tripropylamine (TPA). The instrument measures intensity of emitted light (which is proportional to the amount of analyte present in the sample) and provides a quantitative measure. Assays were performed according to the manufacturer's instructions.

Table 4.1 Cytokines and chemokines measured for multiplex analysis and their functions

(Hughes and Nibbs, 2018)

Protein of interest	Function
IL-8	Chemoattractant specific for neutrophils, stimulates phagocytosis. Binds to CXCR1 and CXCR2.
CCL2	Chemoattractant specific for monocytes. Binds to CCR2 and CCR4.
CCL3	Chemoattractant for polymorphonuclear leukocyte. Binds to CCR1 and CCR5.
CCL4	Chemoattractant specific for monocytes and NK cells. Binds to CCR5.
CCL20	Strong chemoattractant for lymphocytes. Binds to CCR6.
CXCL10	Secreted in response to interferons, chemoattractant for monocytes, lymphocytes and NK cells. Binds to CXCR3.
TNFα	Inflammatory cytokine involved in systemic inflammation during acute phase.
IL-1β	Secreted following inflammasome activation. Mediator of cell proliferation, differentiation and apoptosis.
IL-10	Anti-inflammatory cytokine
IL-13	Mediator of allergic inflammation

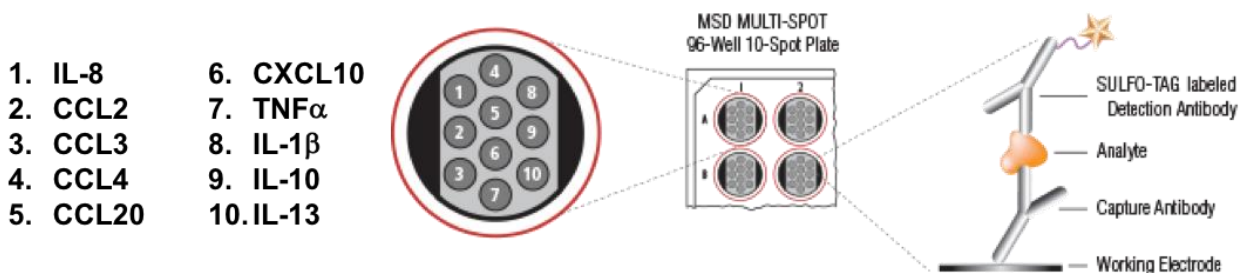


Figure 4.1 MSD multiplex method and set up

The MSD multiplex immunoassay employed involves adding a capture antibody to an MSD plate, adding samples and calibrators and washing away any unbound analyte. The SULFO-TAG-conjugated detection antibody is then added and incubated before adding read buffer and analysing with an MSD instrument. The MSD MULTI-SPOT panel allows the analysis of 10 different analytes using a single well. Image obtained and adapted from <https://www.mesoscale.com/en>

4.3.2.1 MSD Components

The components provided with the U-PLEX assay are listed in **Table 4.2**.

Table 4.2 Components of U-PLEX MSD assay

Reagent	Storage	Description
Diluent 43	<10°C	Diluent for samples and calibrators; contains serum, blockers and preservatives
Diluent 3	<10°C	Diluent for detection antibody; contains protein, blockers and preservatives
Stop solution	2-8 °C	Biotin-coating buffer to stop Linker-antibody coupling reaction
Read Buffer T (4X)	RT	Buffer to catalyse the electro-chemiluminescence reaction. Dilute to 2X before use

U-PLEX assays use MSD 96-well 10-spot plates. The spots correspond to 10 unique U-PLEX linkers, each linker has biotin-binding domain which couples to the biotinylated

capture antibody, as well as a domain which binds to its matching spot on the U-PLEX plate. The linkers are colour coded and numbered with the spot to which they attach to.

U-PLEX antibody sets were provided for the 10 proteins of interest. These sets contained the biotinylated capture antibody provided at a ready-to-use concentration and the SULFO-TAG conjugated detection antibody provided at a 100X concentration.

Calibrators 1 and 2 were provided for the analytes which were selected for this assay. Calibrators are multi-analyte blends, each containing multiple recombinant human proteins lyophilised in a buffered diluent.

4.3.2.2 Preparation of U-PLEX plate

All reagents were brought to room temperature before beginning the protocol. The preparation of the plate involved coating the plate with Linker-couple capture antibodies. A different linker must be used for each unique biotinylated antibody; 200µl of antibody was added to 300µl of the assigned linker and mixed by vortexing. The plate was then incubated at room temperature for 30 minutes. Following incubation, 600µl of each U-PLEX linker-coupled antibody solution (10X) was combined into a single tube, vortexed and 50µl of the multiplex coating solution mixture added to each well. The plate was then sealed and incubated with shaking at room temperature for 1 hour then washed three times with PBS-Tween (PBS plus 0.05% Tween-20).

4.3.2.3 Preparation of standards and samples

The calibrator vials were brought to room temperature and reconstituted by adding 250µl of Diluent 43 to the glass vials. This resulted in a 5X concentrated stock of each calibrator which is further diluted five-fold to generate the highest point in the standard curve. Diluent 43 was then used to dilute samples 1 in 15 for activated macrophage THP-1 cell supernatants based on results obtained from ELISAs for IL-8 and CCL3 (previously optimised data not shown). Once samples were added to the plate along with standards, the plate was sealed and incubated with shaking at room temperature for 1 hour then washed 3 times with PBS-Tween.

4.3.2.4 Preparation of detection antibody solution

The detection antibodies (stock 100X) were diluted to a 1X solution by combining 60µl of each 100X detection antibody and the addition of Diluent 3 to a final volume of 6ml. Following the previous wash step, 50µl of detection antibody solution was added to each well. The plate was then sealed and incubated with shaking at room temperature for 1 hour then washed 3 times with PBS-Tween. The Read Buffer T (stock 4X) was diluted to 2X by the addition of deionised water then 150µl added to each well. The plate was then immediately analysed on an MSD instrument.

4.3.3 Phagocytosis assay

The quantitative measurement of phagocytosis was assessed using pHrodo™ Red *E. coli* BioParticles® conjugates (ThermoFisher Scientific, UK). The phagocytic activity is based on acidification of the particles as they are ingested by the cells by conjugating the particles to pHrodo™ dye that increases in fluorescence as the pH of its surroundings become more acidic.

THP-1 cells were seeded in a 24 well plate (2×10^5 cells) and PMA treated to promote differentiation as described in **section 2.1.6**. Cells were then either; left untreated (used as a positive control as macrophages should have phagocytic capability) or stimulated with treatments of interest for 24 hours. For the final hour of stimulation, some cells were treated with a phagocytic inhibitor, Cytochalasin D (10µM) (ThermoFisher Scientific, UK) for 1 hour, as optimised in a previous study (Kapellos *et al.*, 2016).

Following 24 hours of stimulation, supernatant was removed, cells were washed with PBS then Accutase™ (Biologened, USA) added to detach adhered cells. Cells were transferred to fluorescence activated cell sorting (FACs) tubes and centrifuged at 300g for 5 minutes. Supernatant was removed and cells re-suspended in 100µl of incubation buffer (PBS + 500nM EDTA + 1% FBS). Different concentrations of pHrodo™ particles were added (5 to 25µg/ml) to each tube and incubated at 37°C for between 1 hour and 24 hours. Controls containing only pHrodo™ particles with no cells and cells without pHrodo™ particles were included. Tubes were then centrifuged at 300g for 5 minutes. For the analysis of PE-labelled pHrodo™ particles, the FACSCanto II was used,

utilising the FACSDiva Software (BD Biosciences, USA). Data were analysed using FlowJo 7.6 software (Treestar, USA)

4.4 Results

4.4.1 Effect of CoCr particles on cell viability

Cell viability for the MM6, THP-1 and J774 cell lines following treatment with CoCr particles was assessed using trypan blue staining to determine the percentage of healthy, viable cells and those with reduced viability. The proliferation rate of the THP-1 cell line was measured using the XTT assay.

4.4.1.1 Trypan blue staining

Cell lines were treated with a range of concentrations of CoCr particles (0.5 to 50 μm^3 per cell) as described previously (Germain *et al.*, 2003; Behl *et al.*, 2013; Papageorgiou *et al.*, 2014). Following exposure to CoCr particles for either 24 or 48 hours, cell viability was assessed using trypan blue exclusion as described in **section 2.5.1**. Viability was calculated as a percentage difference between untreated cells (100% viable) and treated cells. Across all cell lines, viability was not significantly affected across all concentrations of CoCr particles at 24 hours (MM6 cells $p=0.0898$, THP-1 cells $p=0.1847$ and J774 cells $p=0.1220$ for untreated versus 50 μm^3 CoCr particles per cell) (**Figure 4.2**). However, following 48 hours of exposure, cell viability was significantly decreased following stimulation with the highest concentration of CoCr particles (50 μm^3 per cell) in MM6 and THP1 cells ($p<0.0001$ and $p=0.0011$, respectively) whilst remaining unaffected in J774 cells ($p=0.1129$) (**Figure 4.3**).

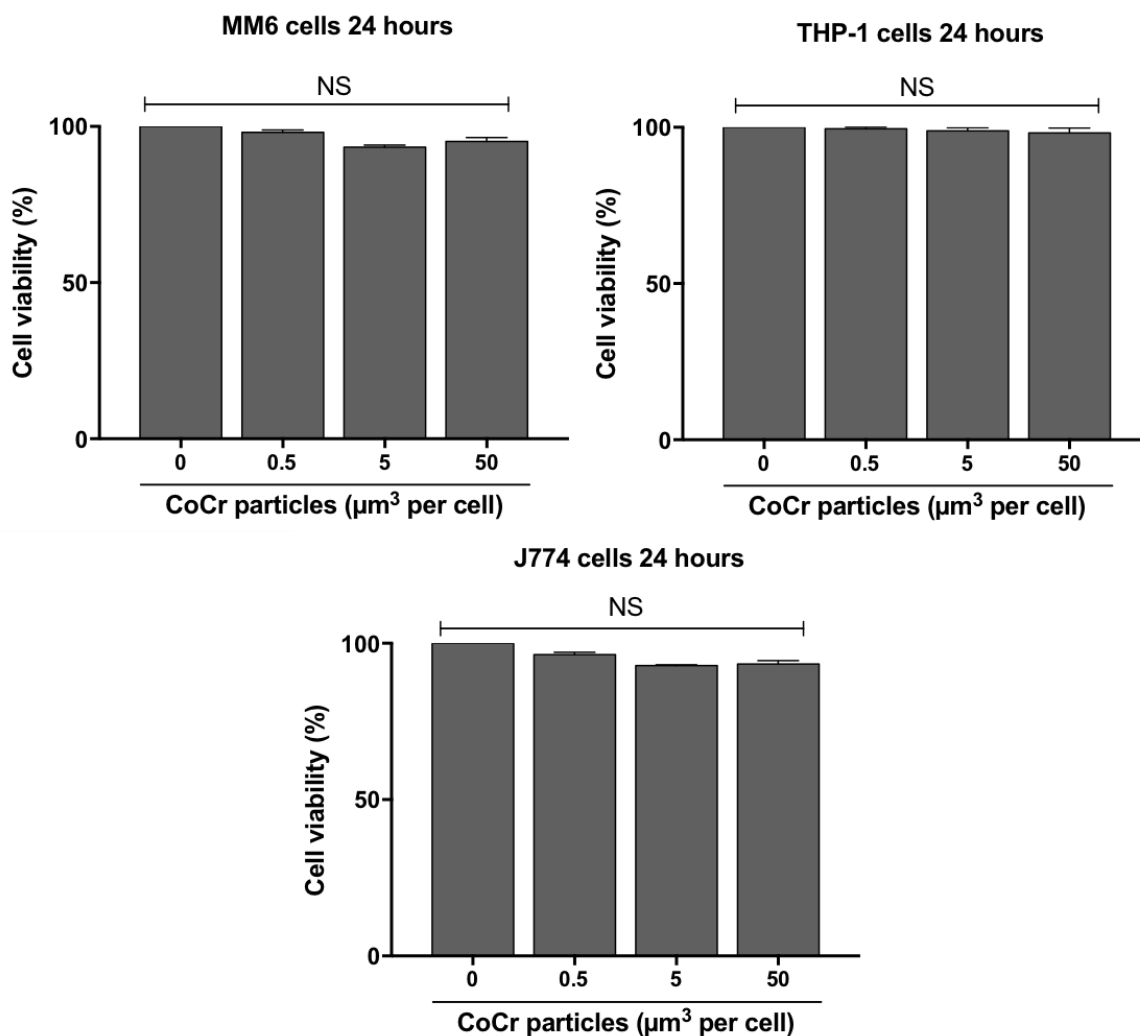


Figure 4.2 Cell line viability CoCr particle dose response at 24 hours determined by trypan blue staining

Cell lines were assessed for viability following stimulation with varying concentrations of CoCr particles (0.5 to 50 μm³ per cell) for 24 hours using trypan blue staining. Viability for all cell lines were not significantly affected across all concentrations of CoCr particles. Data was normalised to 100% viability in untreated cells. Graph is representative of 3 independent experiments. Statistical significance was calculated by one-way ANOVA with Dunnett's multiple comparisons test comparing treated samples to the untreated control.

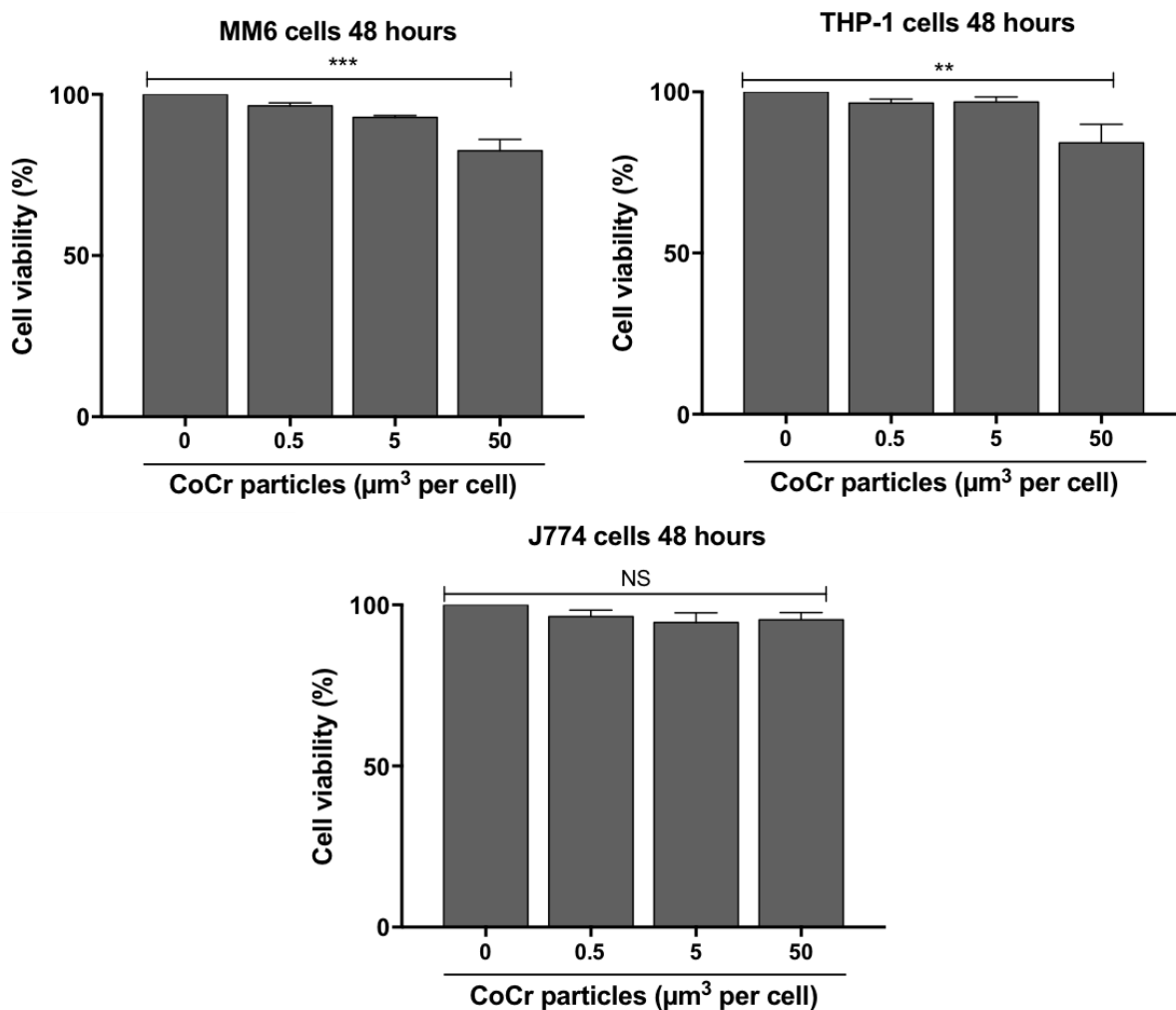


Figure 4.3 Cell line viability CoCr particle dose response at 48 hours determined by trypan blue staining

Cell lines were assessed for viability following stimulation with varying concentrations of CoCr particles (0.5 to 50 μm³ per cell) for 48 hours using trypan blue staining. Cell viability was significantly decreased in MM6 and THP1 cells following stimulation with the highest concentration of CoCr particles (50 μm³ per cell) whilst remaining unaffected in J774 cells. Graph is representative of 3 independent experiments. Statistical significance was calculated by one-way ANOVA with Dunnett's multiple comparisons test comparing treated samples to the untreated control.

4.4.1.2 XTT proliferation assay

Proliferation of differentiated THP-1 cells was evaluated using the XTT proliferation assay as described in **section 2.5.2**. Cells were treated with a range of concentrations of either LPS (10 to 1000 ng/ml), CoCl₂ (0.25 to 0.75 mM) or CoCr particles (0.5 to 50 μm³ per cell) for either 24 hours (**Figure 4.4**) or 48 hours (**Figure 4.5**) and

proliferation assessed 24 hours after the addition of the XTT reagent for 24 hour treatments and 6 hours for 48 hour treatments.

Following 24 hours of stimulation with LPS, there was no significant difference in proliferation of THP-1 cells across all concentrations (10ng/ml $p=0.0877$, 100ng/ml $p=0.2306$ and 1000ng/ml $p=0.4298$). However, CoCl_2 stimulation for 24 hours induced significant loss of proliferation in all concentrations (0.25mM $p=0.0003$ and 0.5mM and 0.75mM both $p<0.0001$). For CoCr particle treatments, lower concentrations of 0.5 and $5\mu\text{m}^3$ particles per cell did not significantly effect THP-1 proliferation ($p=0.9994$ and $p=0.1657$, respectively). However, at $50\mu\text{m}^3$ particles per cell there was a significant reduction in proliferation ($p=0.0015$).

THP-1 cells were then stimulated for 48 hours with the above treatments to assess proliferative changes. Following LPS stimulation, all concentrations significantly increased proliferation and this increase was most significant at the lowest concentration of 10ng/ml (10ng/ml $p=0.0013$, 100ng/ml $p=0.0021$ and 1000ng/ml $p=0.0166$). Conversely, CoCl_2 treatments again significantly reduced proliferation across all concentrations (all $p<0.0001$). Similarly to the 24 hour treatments, lower CoCr particle concentrations (0.5 and $5\mu\text{m}^3$ particles per cell) did not significantly effect THP-1 proliferation ($p=0.5151$ and $p=0.9642$, respectively). THP-1 cells treated with $50\mu\text{m}^3$ per cell of CoCr particles for 48 hours demonstrated significantly decreased proliferation ($p<0.0001$). However, this decrease in proliferation was far more significant after 48 hours of stimulation versus 24 hours ($p<0.0001$ versus $p=0.0015$, respectively). Therefore, in future experiments, stimulation with CoCr particles in cell treatments were for a maximum of 24 hours to avoid potential toxic effects.

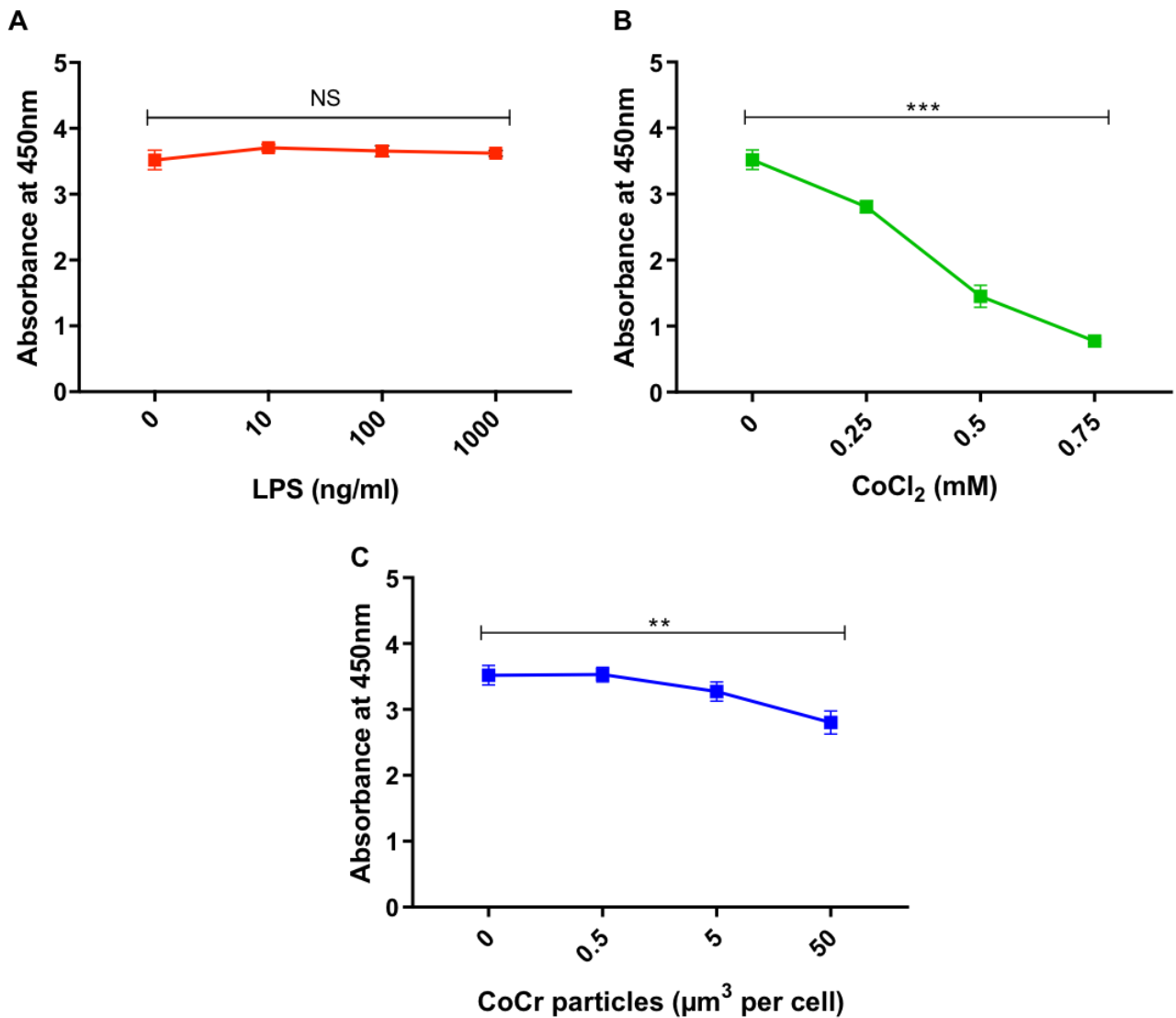


Figure 4.4 Proliferation of THP-1 cells following exposure to stimulants for 24 hours

THP-1 cells were stimulated for 24 hours with treatments prior to the addition of XTT reagent for a further 24 hours to assess proliferation. **(A)** LPS treatments across all concentrations did not significant effect the proliferation of THP-1 cells **(B)** CoCl₂ stimulation induced significant loss of proliferation in all concentrations **(C)** In CoCr particle treatments, the lower concentrations of 0.5 and 5μm³ per cell did not significantly effect THP-1 proliferation. However, at 50μm³ per cell there was a significant reduction in proliferation. Graph is representative of 3 independent experiments. Statistical significance was calculated by one-way ANOVA with Dunnett's multiple comparisons test comparing treated samples to the untreated control.

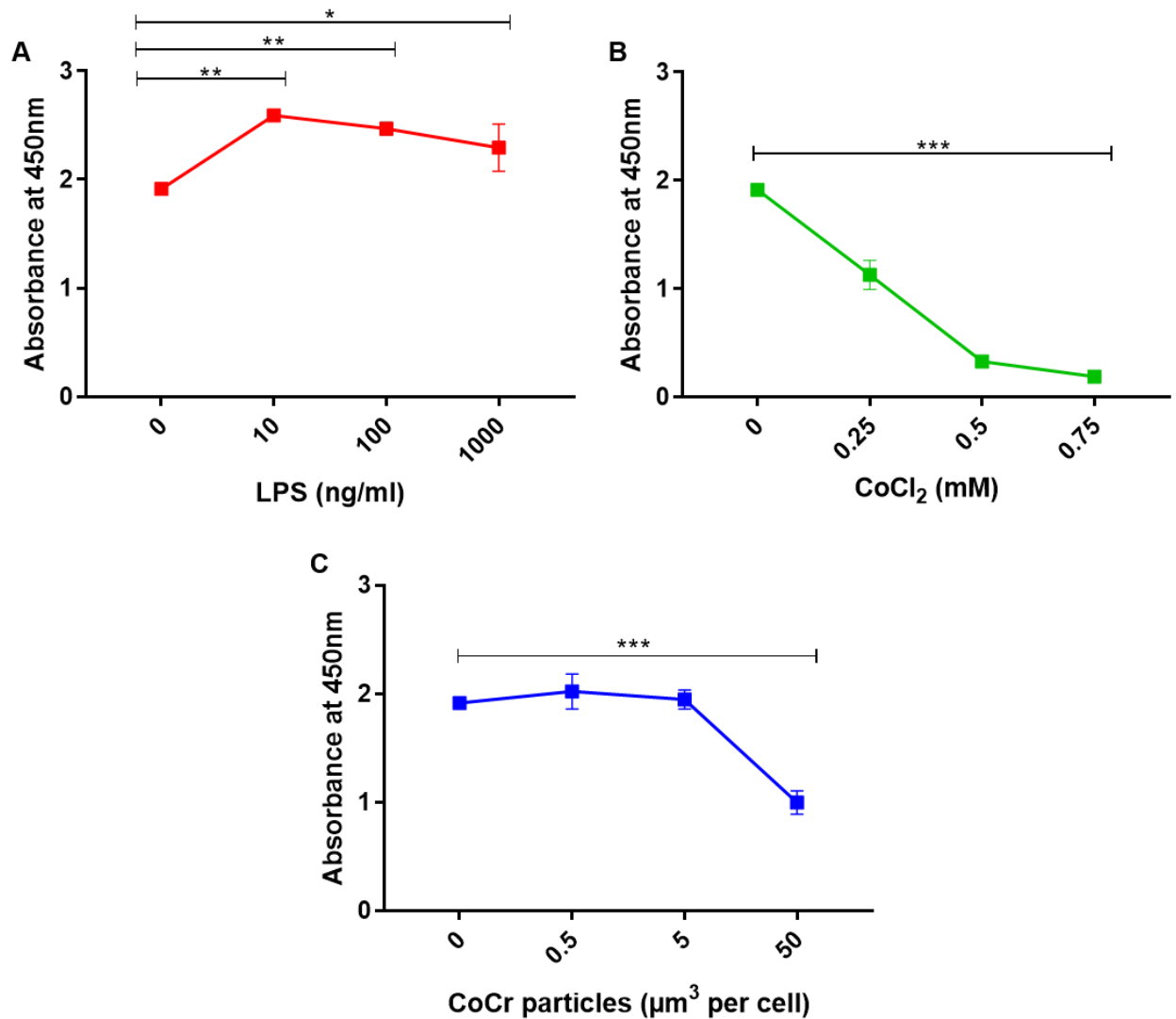


Figure 4.5 Proliferation of THP-1 cells following exposure to stimulants for 48 hours

THP-1 cells were stimulated for 48 hours with treatments prior to the addition of XTT reagent for a further 6 hours to assess proliferation. **(A)** Following LPS stimulation, all concentrations significantly increased proliferation and this increase was most significant at the lowest concentration of 10ng/ml **(B)** CoCl₂ treatments significantly reduced proliferation across all concentrations **(C)** Lower CoCr particle concentrations (0.5 and 5 μm^3 per cell) did not significantly effect THP-1 proliferation. THP-1 cells treated with 50 μm^3 per cell of CoCr particles demonstrated significantly decreased proliferation. Graph is representative of 3 independent experiments. Statistical significance was calculated by one-way ANOVA with Dunnett's multiple comparisons test comparing treated samples to the untreated control.

4.4.2 Internalisation of CoCr particles by THP-1 cells

Differentiated THP-1 cells i.e. in a macrophage-like state were treated with CoCr particles ($50\mu\text{m}^3$ per cell) for 24 hours and imaged using TEM as described in **section 2.6**. Untreated cells are shown in **Figure 4.6**. From these images, THP-1 cells have clearly become fully differentiated to macrophage-like cells as represented by their round, enlarged nuclei and enhanced granularity. Higher magnification images demonstrate the presence of fat droplets lying next to mitochondria. Most of the mitochondria are small and oval in shape with a few elongated.

Figure 4.7 to Figure 4.9 show THP-1 cells which have been stimulated with CoCr particles ($50\mu\text{m}^3$ per cell) for 24 hours. **Figure 4.7** shows whole cells which have increased nuclei irregularity, a slightly more irregular cell shape and the presence of pseudopodia. Interestingly the nuclei appear to have taken a more pronounced “bean-shape” which is more typical of a monocyte nucleus rather than the enlarged round shape shown in **Figure 4.6A and B**. Pseudopods are crucial to cellular movement and the sensing of potential pathogens. They are also involved in changes to the cell membrane to aid with phagocytosis (Rosales and Uribe-Querol, 2017). The TEM images confirmed the internalisation of CoCr particles by THP-1 macrophage-like cells. One of the most pronounced changes to CoCr treated THP-1 cells is the presence of aggregates and agglomerates of CoCr particles within phagosomes, lysosomes or endosomes; which appear to distinct to these vesicles and membrane bound. These phagosomes are shown more clearly in **Figure 4.8** and display particles being engulfed at the cell membrane (**Figure 4.8C**) before being contained within distinct vesicles. This suggests that internalisation of particles is an active process, for example, via endocytosis. There also appears to be an increase in the number of lysosomes (as shown by higher magnification in **Figure 4.9**) although the mitochondria appear to have not significantly changed compared to untreated cells. **Figure 4.10** demonstrates a high magnification (x100K) image of the CoCr particles individually and confirms the characterisation performed in **Chapter 3**; they are nanometre in size and mostly round in shape.

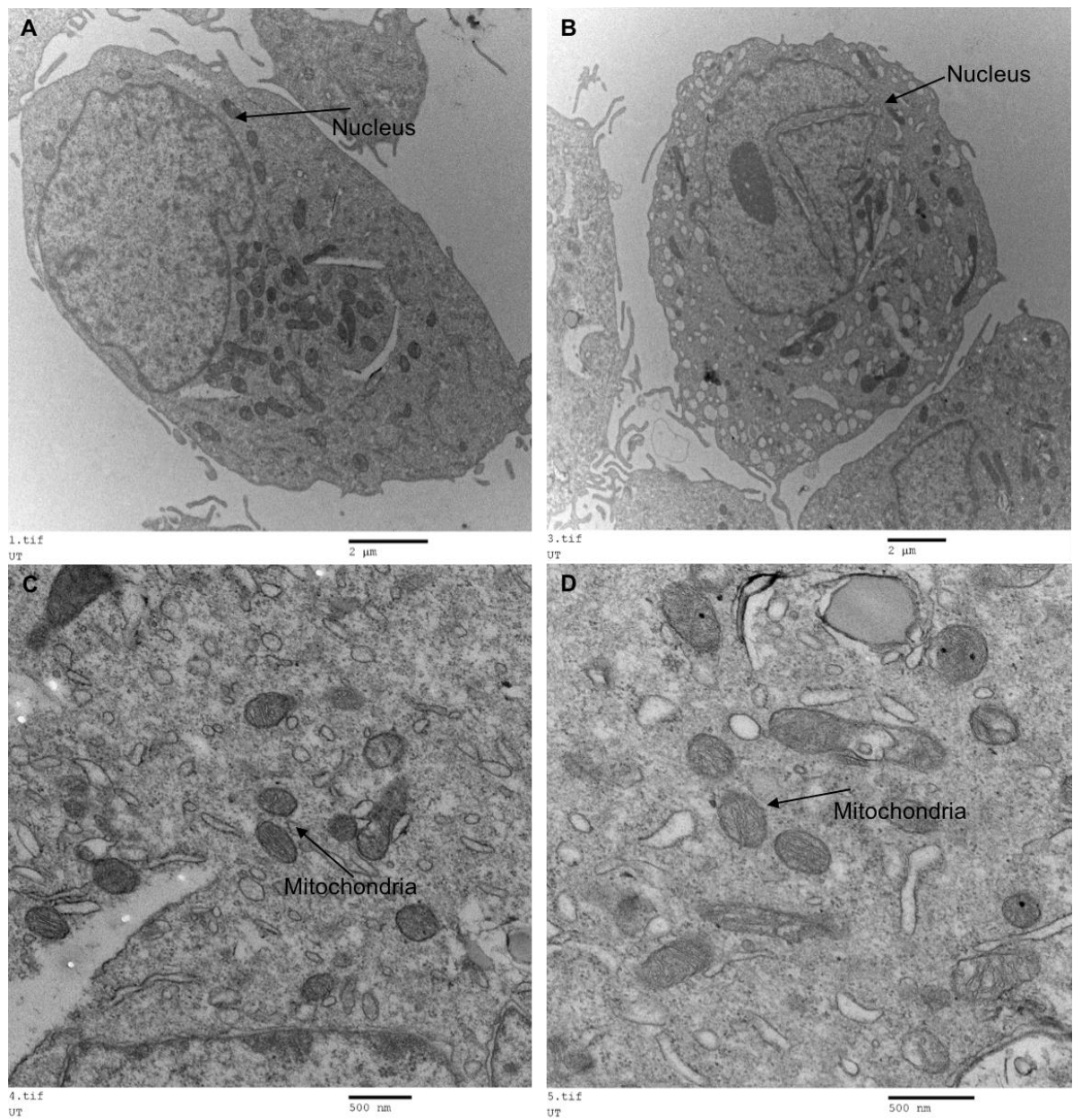


Figure 4.6 Transmission electron microscopy of untreated THP-1 cells

Representative TEM images of untreated THP-1 activated with 5ng/ml PMA. The nuclei in whole cell images is round and enlarged **(A)-(B)**. Scale bars represent either 2μm for whole cell images **(A)-(B)** or 500nm for cellular structures such as mitochondria **(C)-(D)**.

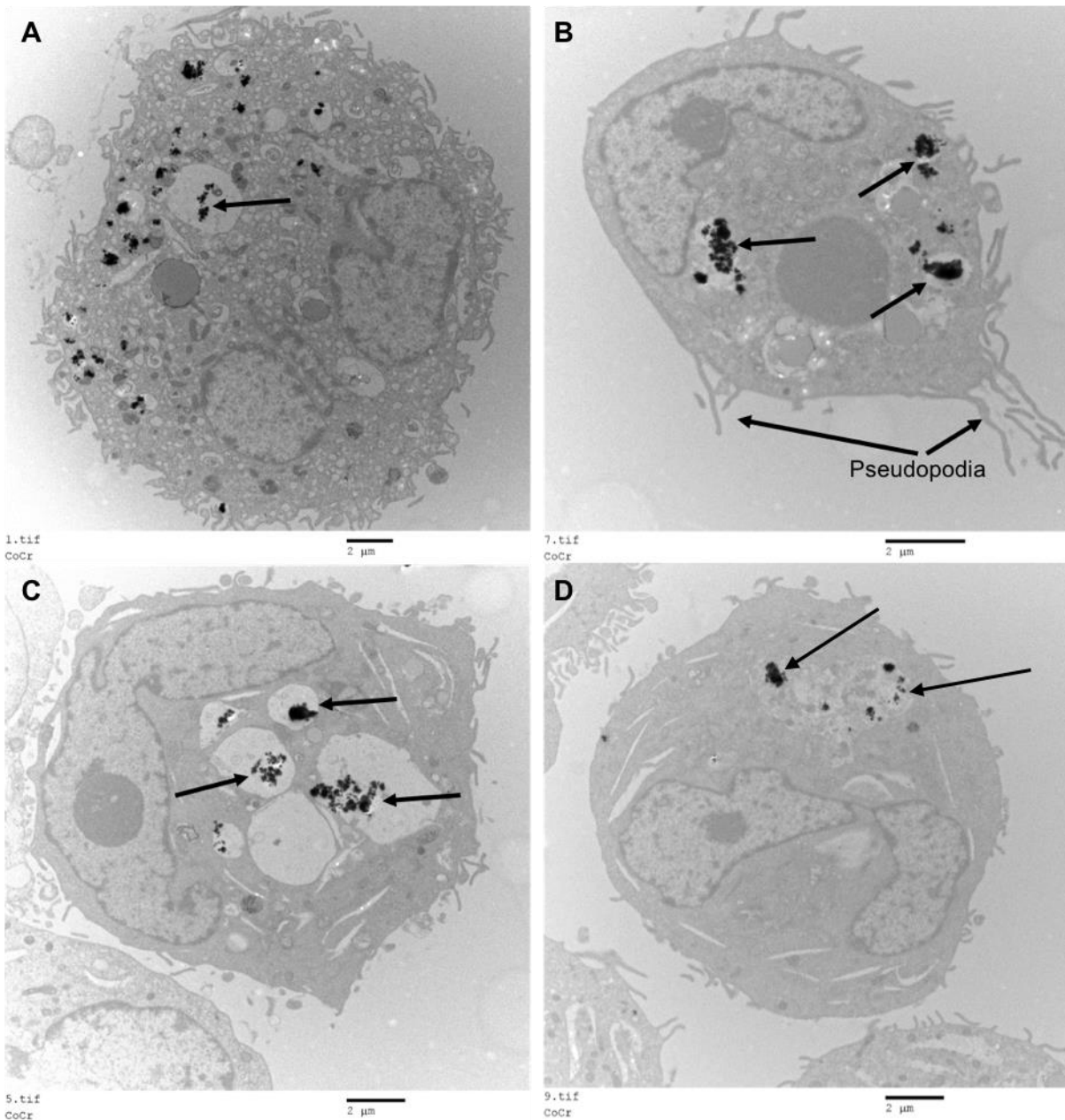


Figure 4.7 Transmission electron microscopy of THP-1 cells treated with CoCr particles

Representative TEM images of THP-1 cells activated with 5ng/ml PMA and treated with CoCr particles ($50\mu\text{m}^3$ per cell). **(B)** Arrows indicate the presence of pseudopodia. **(A)-(D)** Arrows point to examples of aggregates and agglomerates of CoCr particles within distinct membrane bound vacuoles. Scale bars represent $2\mu\text{m}$.

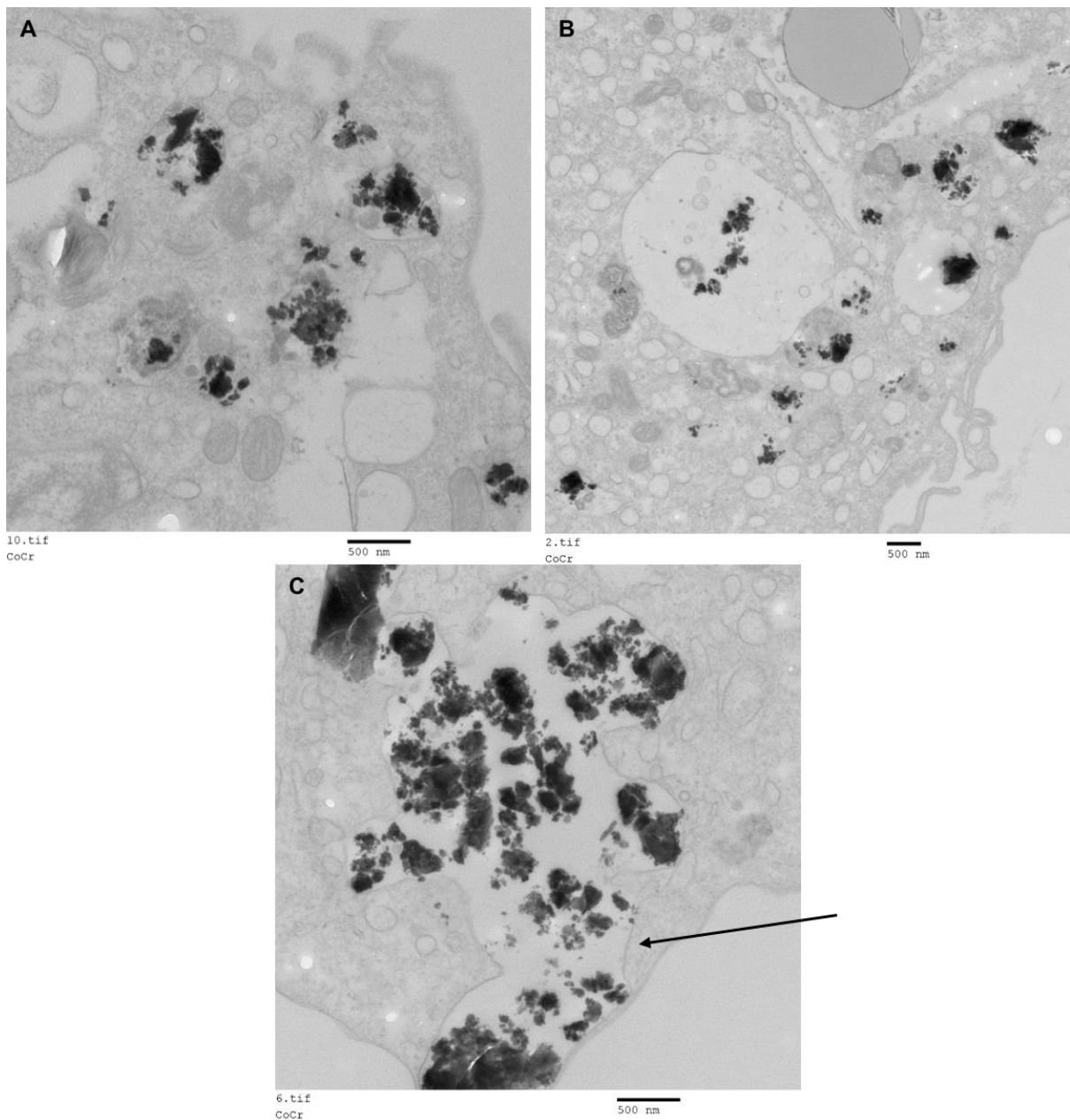


Figure 4.8 Transmission electron microscopy displaying aggregates of CoCr particles within phagosomes of THP-1 cells

Representative TEM images of THP-1 cells activated with 5ng/ml PMA and treated with CoCr particles ($50\mu\text{m}^3$ per cell). Images show CoCr particle aggregates located within distinct vacuoles **(A)-(C)** and arrow indicates the process of particles entering the cell, potentially through endocytosis **(C)**. Scale bars represent 500nm.

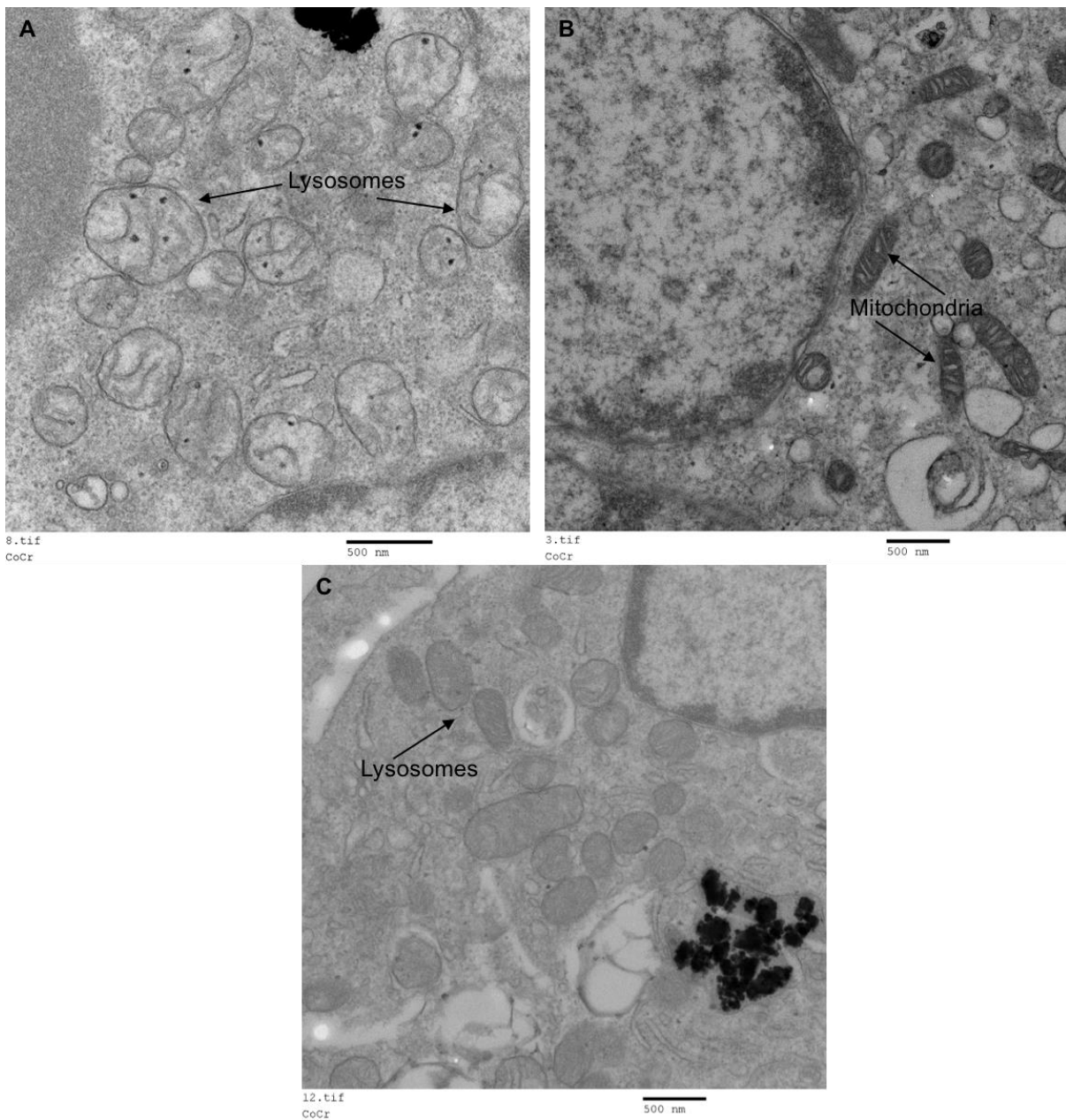


Figure 4.9 Transmission electron microscopy displaying THP-1 intracellular structures following CoCr particle treatment

Representative TEM images of THP-1 cells activated with 5ng/ml PMA and treated with CoCr particles ($50\mu\text{m}^3$ per cell). Images show the presence of numerous lysosomes **(A)** and **(C)** and mitochondria **(B)**. Scale bars represent 500nm.

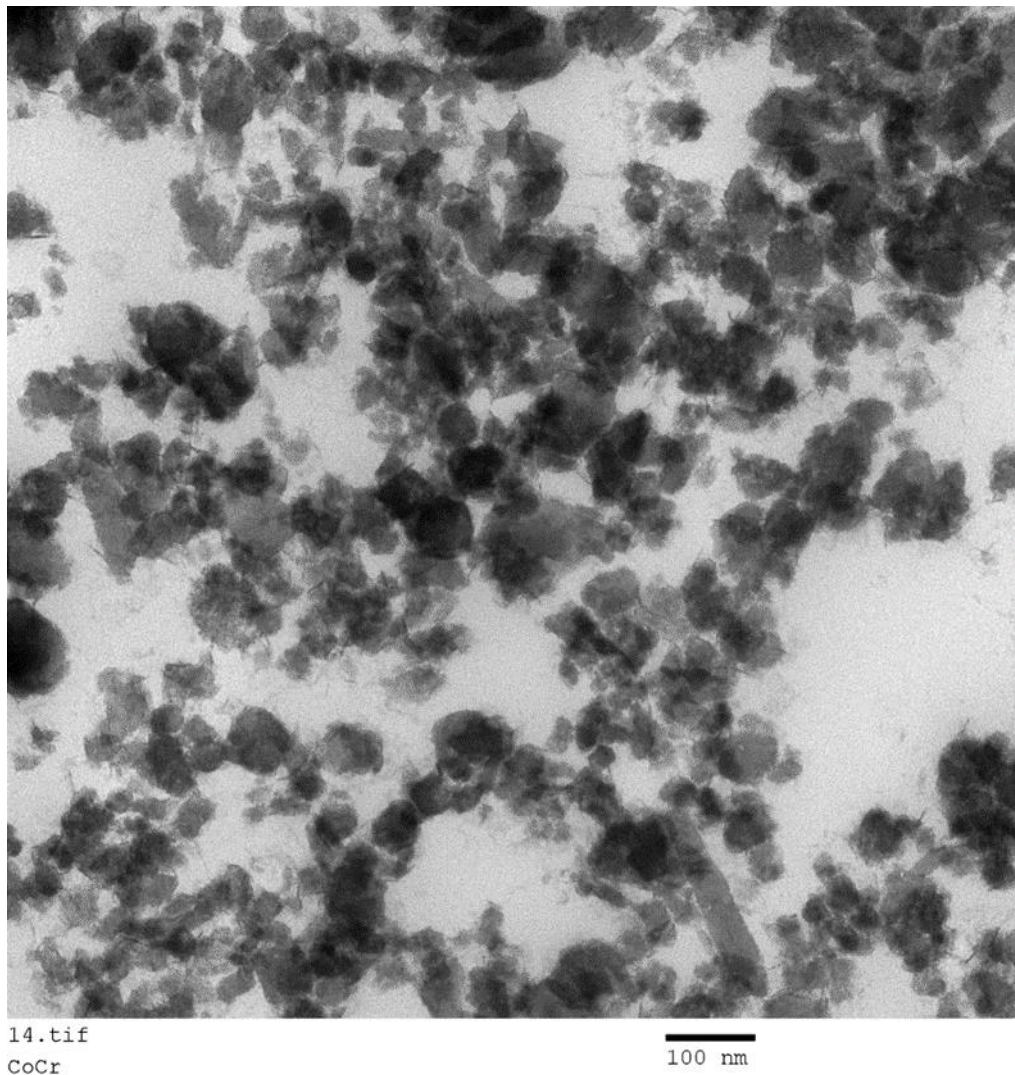


Figure 4.10 Transmission electron microscopy using high magnification to visualise and characterise individual CoCr particles

High magnification (x100K) image of CoCr particles within an intracellular phagosome of treated THP-1 cells. Individual particles are shown to be less than 100nm in size and mostly round with fewer irregular shaped particles. Scale bar represents 100nm

4.4.3 Phagocytic capability of THP-1 cells

A phagocytosis assay was undertaken, as described in **section 4.3.3**. Firstly, the optimal concentration of pHrodo™ particles was investigated using a dose response (5 to 25µg/ml) with untreated activated THP-1 macrophages. In this instance, cells were incubated with the pHrodo™ particles for 1 hour and uptake analysed by FACS (**Figure 4.11A**). Data are presented as percentage of cells expressing pHrodo™ particles from the population analysed.

Figure 4.11A demonstrates that cells which were treated with 25µg/ml pHrodo™ particles for 1 hour resulted in the greatest uptake of particles across the concentrations analysed. The percentage of cell expression was significantly higher than both 5 and 10µg/ml (both $p=0.0020$). However, overall cell expression was relatively low (reaching a maximum of approximately 7%). Therefore, a time course was completed treating activated THP-1 cells with 25µg/ml pHrodo™ particles for a longer period of between 6 and 24 hours (**Figure 4.11**). Furthermore, a negative control of cytochalasin D (10µM) was included to assess its ability to inhibit phagocytosis. As time increased, the percentage of cells expressing pHrodo™ particles also increased to a peak of 65% at 24 hours (**Figure 4.11E**). Cells which were pre-treated with cytochalasin D (10µM) for 1 hour expressed significantly less pHrodo™ particles at all time points investigated, therefore, cytochalasin D somewhat inhibited phagocytosis (at 6 hours; $p=0.0327$, 12 hours; $p=0.0203$ and 24 hours; $p=0.0079$) (**Figure 4.11B-D**). Therefore, the optimal conditions for this assay appeared to be treating THP-1 cells with 25µg/ml pHrodo™ particles for a minimum of 12 hours. Furthermore, cytochalasin D was confirmed as an effective negative control.

Due to time constraints, optimised conditions could not be completed for CoCr particle treatments to see how this effected the phagocytosis ability of THP-1 cells. However, it was hypothesised that phagocytosis of pHrodo™ particles would be compromised and therefore cell expression reduced.

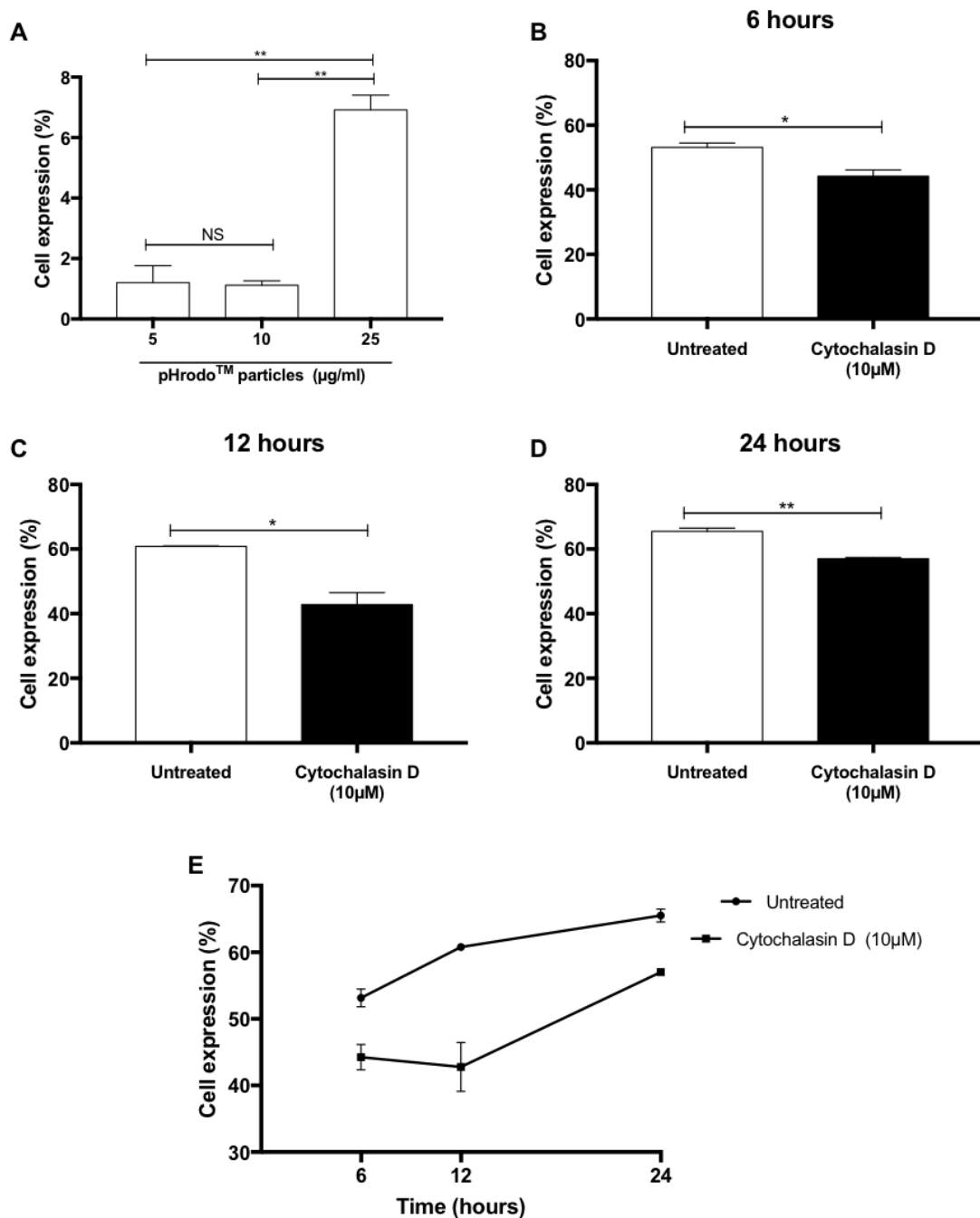


Figure 4.11 Optimisation of pHrodo™ Red E. coli BioParticles® phagocytosis assay, dose and time response in activated THP-1 cells

(A) Activated THP-1 cells were treated with pHrodo™ particles (5 to 5µg/ml) for 1 hour at 37°C and fluorescence emission measured using flow cytometry to give a percentage of expressing cells. Graph is representative of 3 independent experiments. Statistical significance was calculated by one-way ANOVA with Tukey's test for multiple comparisons comparing all samples to each other. **(B)-(E)** Activated THP-1 cells were pre-treated with cytochalasin D (10µM) for 1 hour prior to treatment with pHrodo™ particles (25µg/ml) for either 6, 12 or 24 hours at 37°C. Graph is representative of 3 independent experiments. Statistical significance was calculated by an unpaired Student's *t*-test comparing the treated sample to the untreated control.

4.4.4 Validation of cytokines and chemokines as a marker of inflammatory responses to CoCr particles

4.4.4.1 MSD assay

For the initial validation of a marker of CoCr-mediated inflammation, differentiated THP-1 cells were treated with a range of concentrations of CoCr particles (0.5 to 50 μm^3 per cell) for 24 hours and then the supernatant used for an MSD U-PLEX assay evaluating the targets described in **section 4.3.2**. LPS (10ng/ml) was used as a positive control as a known inducer of inflammation and subsequent enhanced cytokine/chemokine production. The results of this initial dose response are summarised in **Figure 4.12** and **Figure 4.13**.

Figure 4.12 demonstrates all proteins which were significantly increased following stimulation of THP-1 cells with CoCr particles. The most significantly increased inflammatory protein was the chemokine IL-8 reaching a peak of around 33,000pg/ml. All concentrations of CoCr particles significantly increased IL-8 secretion compared to untreated THP-1 cells (0.5 μm^3 per cell $p=0.0005$, 5 and 50 μm^3 per cell both $p<0.0001$).

Results show that the next most induced inflammatory proteins were CCL3 and CCL4, which reached maximal secretion of 1000pg/ml and 2800pg/ml, respectively when THP-1 cells were treated with 50 μm^3 CoCr particles per cell (both $p<0.0001$). For the lower CoCr particle concentrations, there was less of an increase in CCL3 but these increases were still significant (0.5 μm^3 per cell $p=0.0293$ and 5 μm^3 per cell $p=0.0023$). CCL4 saw more significant increases with lower CoCr particle concentrations (0.5 μm^3 per cell $p=0.0008$ and 5 μm^3 per cell $p=0.0009$).

Following the largest dose of CoCr particles, CCL2 secretion was significantly increased to around 350pg/ml ($p=0.0009$) although this is much less significant than the previous inflammatory markers discussed. The lowest concentration of CoCr particles did not increase CCL2 protein expression ($p=0.6854$) and there was only a slightly significant increase when THP-1 cells were treated with 5 μm^3 per cell ($p=0.0238$). These differences were less due to a relatively high concentration of CCL2 secretion in untreated THP-1 cells, approximately 220pg/ml.

CCL20 secretion reached a maximal peak of approximately 650pg/ml following treatment with 50 μm^3 CoCr particles per cell, significantly more than untreated THP-1

cells ($p=0.0007$). There were smaller but significant increases for lower CoCr particle concentrations ($0.5\mu\text{m}^3$ per cell $p=0.0111$ and $5\mu\text{m}^3$ per cell $p=0.0011$).

A similar pattern was observed for IL-1 β protein expression in which $50\mu\text{m}^3$ CoCr particles per cell increased secretion to 235pg/ml, which was particularly significant due to very little secretion from untreated cells (47pg/ml) ($p<0.0001$). Lower CoCr particle concentrations induced smaller but significant increases in IL-1 β expression ($0.5\mu\text{m}^3$ per cell $p=0.0498$ and $5\mu\text{m}^3$ per cell $p=0.00165$).

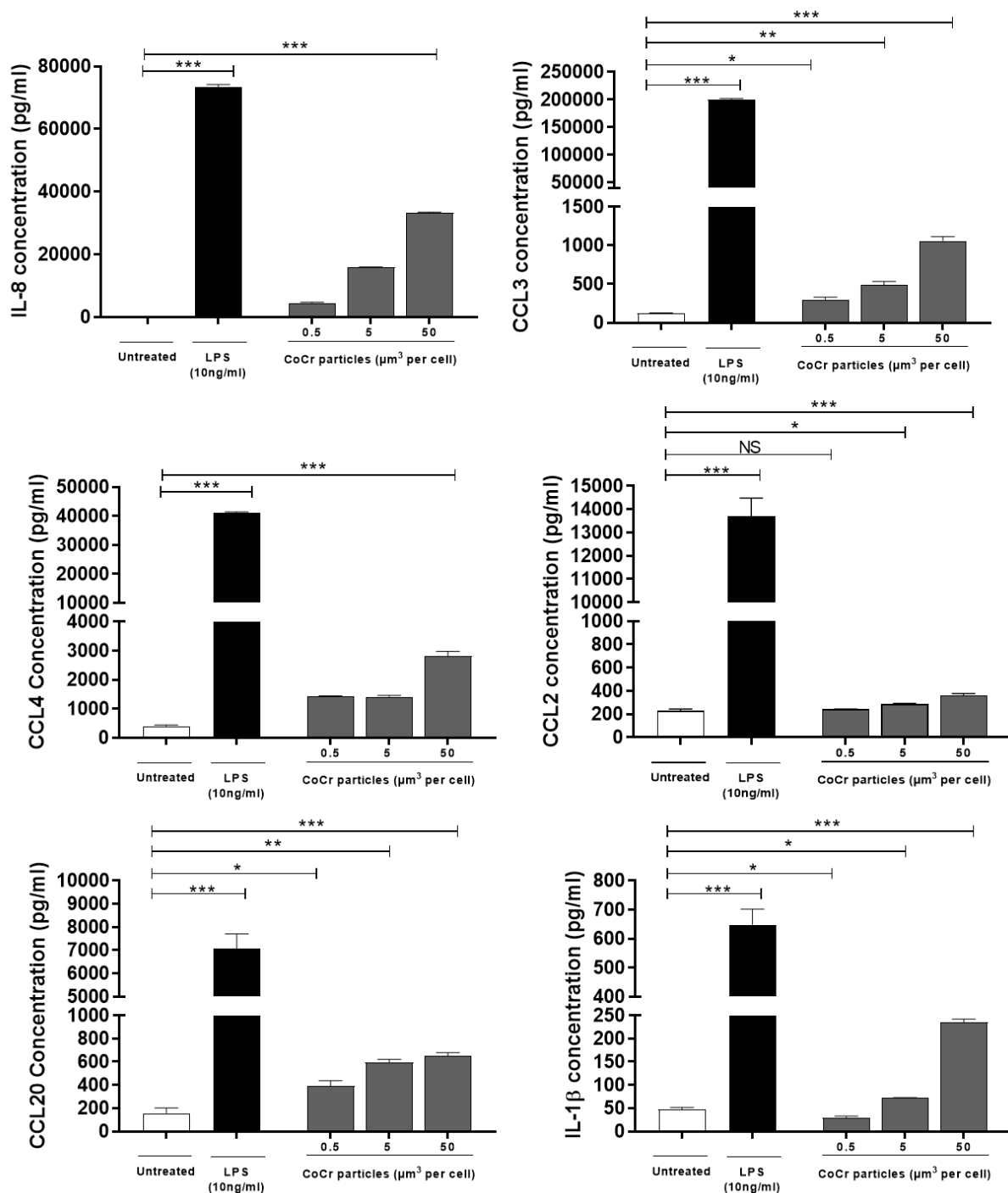


Figure 4.12 CoCr particle dose response in THP-1 cells, assessment of inflammatory proteins – significant changes

Activated THP-1 cells were treated with different doses of CoCr particles (0.5 to 50μm³ per cell) or LPS (10ng/ml) for 24 hours and changes to inflammatory protein expression assessed by MSD U-PLEX assay. The following markers were all significantly increased in response to 50μm³ CoCr particles per cell; IL-8, CCL3, CCL4, CCL2, CCL20 and IL-1β. Graph is representative of 3 independent experiments. Statistical significance was calculated by one-way ANOVA with Dunnett's multiple comparisons test comparing treated samples to the untreated control.

Some of the inflammatory markers investigated demonstrated no significant changes in response to CoCr particles which are summarised in **Figure 4.13**. Importantly, LPS (used as a positive control) significantly induced up-regulation of these markers. At the highest dose of CoCr particles ($50\mu\text{m}^3$ per cell), $\text{TNF}\alpha$ ($p=0.1871$), CXCL10 ($p=0.4221$), IL-10 ($p=0.9993$) and IL-13 ($p=0.5373$) were all non-significantly changed when compared to untreated THP-1 cells.

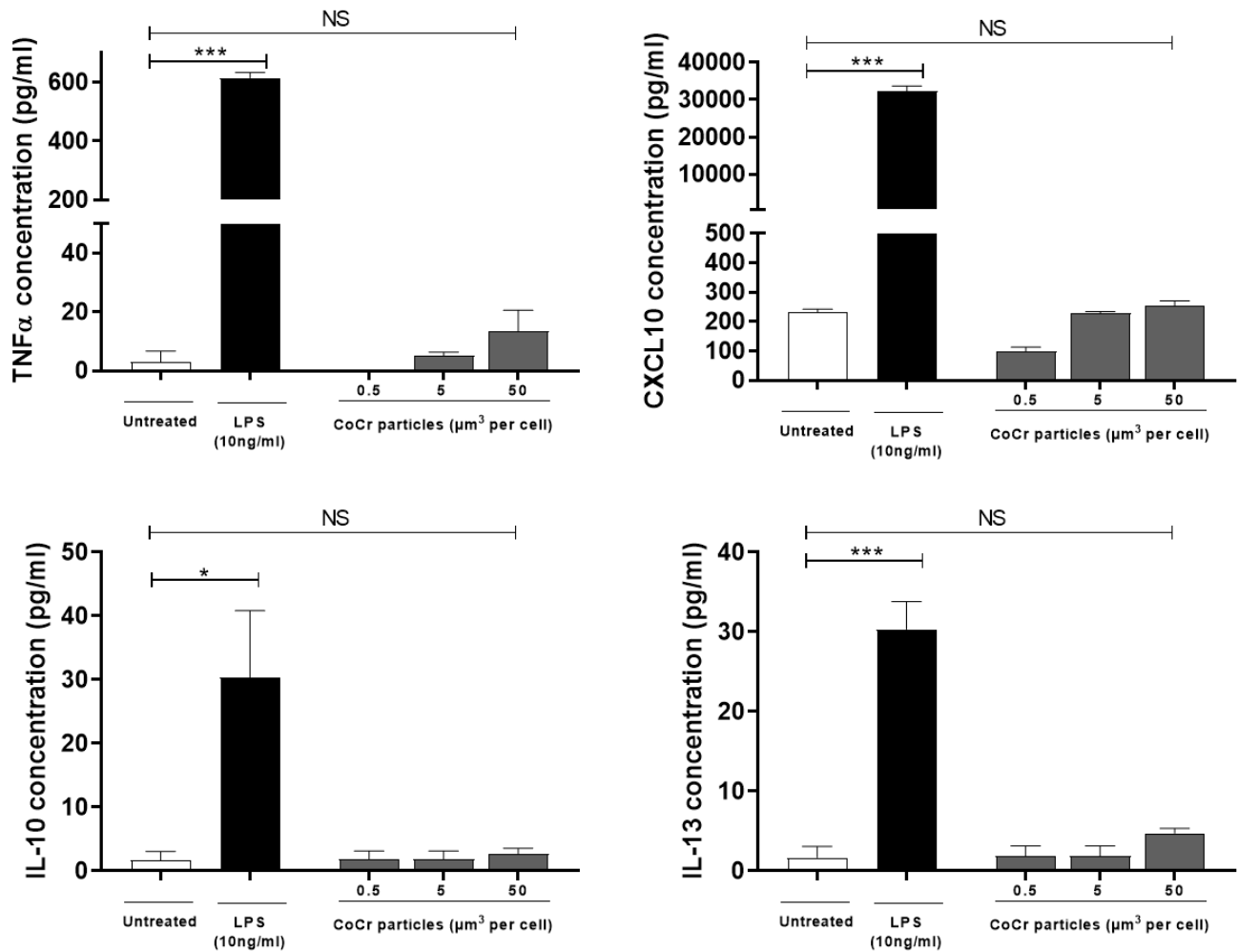


Figure 4.13 CoCr particle dose response in THP-1 cells, assessment of inflammatory proteins – non-significant changes

Activated THP-1 cells were treated with different doses of CoCr particles (0.5 to 50 μm^3 per cell) or LPS (10ng/ml) for 24 hours and changes to inflammatory protein expression assessed by MSD U-PLEX assay. At the highest dose of CoCr particles (50 μm^3 per cell), TNF α , CXCL10, IL-10 and IL-13 were all non-significantly changed when compared to untreated THP-1 cells. Graph is representative of 3 independent experiments. Statistical significance was calculated by one-way ANOVA with Dunnett's multiple comparisons test comparing treated samples to the untreated control.

4.4.4.2 Effect of CoCr particles on inflammatory gene expression

As IL-8 and CCL3 protein expression were both significantly up-regulated in response to CoCr particles, these were then used for qRT-PCR evaluation (as described in section 2.6).

Firstly, a dose response for *IL-8* gene expression was evaluated using the same CoCr particle concentrations described previously (0.5 to 50 μm^3 per cell) for a 24-hour

treatment with activated THP-1 cells to ensure the optimised dose from protein secretion was reflected for RT-PCR. **Figure 4.14** demonstrates that *IL-8* expression was significantly increased in response to the largest CoCr particle dose ($50\mu\text{m}^3$ per cell) ($p < 0.0001$). However, at the lower concentrations there was no significant increase of *IL-8* when compared to untreated THP-1 cells ($0.5\mu\text{m}^3$ per cell $p = 0.9990$, $5\mu\text{m}^3$ per cell $p = 0.8957$). Therefore, the previously optimised concentration of $50\mu\text{m}^3$ CoCr particles per cell was also deemed appropriate for evaluating gene expression.

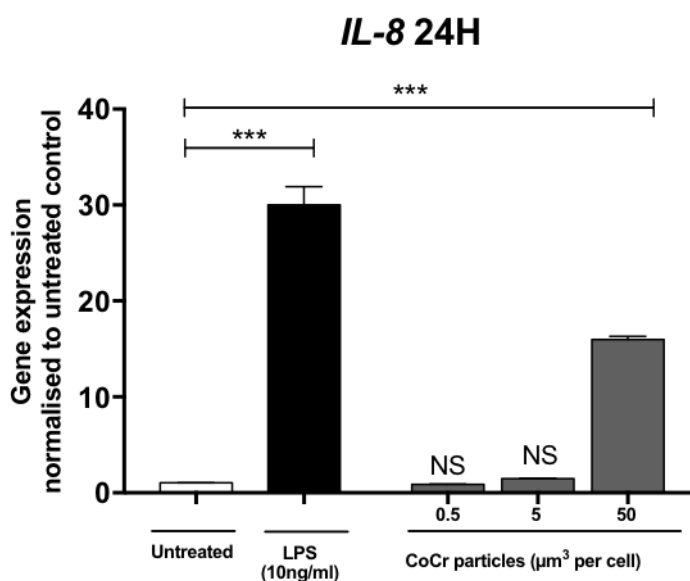


Figure 4.14 *IL-8* gene expression following CoCr particle dose response

IL-8 expression was significantly increased in response to the largest CoCr particle dose ($50\mu\text{m}^3$ per cell) in THP-1 cells following 24 hours of stimulation as measured by qRT-PCR. At lower concentrations, there was no significant increase of *IL-8* when compared to untreated THP-1 cells. Gene expression normalised to untreated control, set to 1. Graph is representative of 3 independent experiments. Statistical significance was calculated by one-way ANOVA with Dunnett's multiple comparisons test comparing treated samples to the untreated control.

A time course for this concentration of CoCr particles was then completed at 6, 12 and 24 hours to confirm at which point gene expression of inflammatory proteins reaches its maximal change. LPS (10ng/ml) was used as a positive control throughout and CoCl_2 was also used as a control to determine the effect that cobalt ions induce at the concentration obtained from the ICP-MS study shown in **Figure 3.21** (0.025mM). The results for the *IL-8* time course are shown in **Figure 4.15**. Following 6 hours of

stimulation with $50\mu\text{m}^3$ CoCr particles per cell, the gene expression of *IL-8* was approximately 6-fold when compared to untreated THP-1 cells ($p=0.0107$). CoCl_2 induced *IL-8* slightly more to 7-fold ($p=0.0022$). At the 12-hour time point, a similar pattern was observed in that CoCr particle treatment led to a 3-fold increase in *IL-8* and CoCl_2 was slightly higher at a 4-fold increase. However, these were both significant increases in comparison to untreated controls (both $p<0.0001$). At 24 hours, the largest fold-changes were observed for both treatments. Both CoCr particles and CoCl_2 increased *IL-8* by approximately 14-fold (both $p=0.0004$).

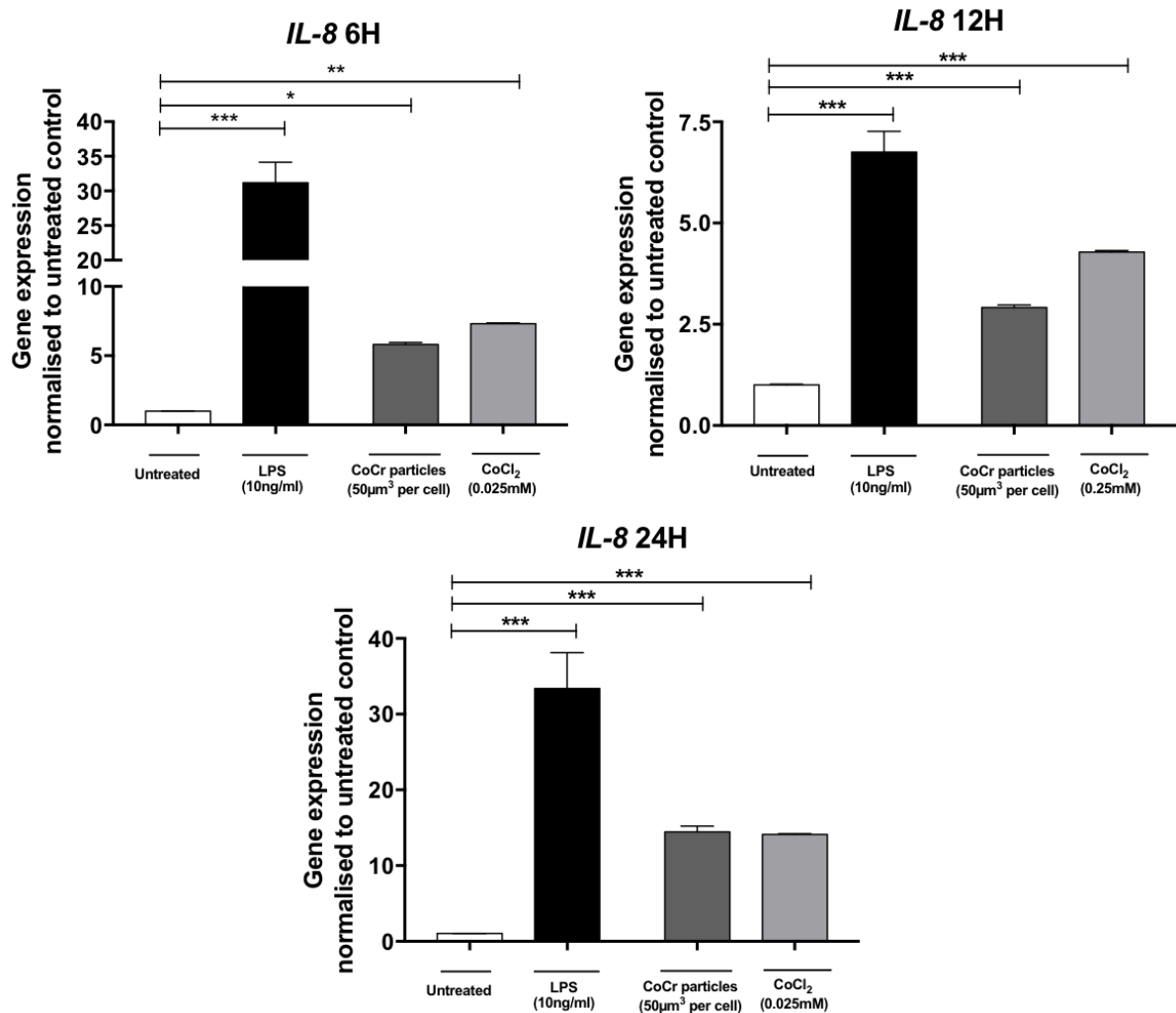


Figure 4.15 IL-8 gene expression following CoCr particle treatment time course

THP-1 cells were stimulated for either 6, 12 or 24 hours with either LPS (10ng/ml) CoCr particles (50µm³ per cell) or CoCl₂ (0.025mM) and gene expression of *IL-8* assessed by qRT-PCR. Gene expression normalised to untreated control, set to 1. Graph is representative of 3 independent experiments. Statistical significance was calculated by one-way ANOVA with Dunnett's multiple comparisons test comparing treated samples to the untreated control.

The same time course was repeated to analyse *CCL3* expression (**Figure 4.16**). Following 6 hours of stimulation with 50µm³ CoCr particles per cell, the gene expression of *CCL3* was approximately 3.5-fold when compared to untreated THP-1 cells ($p < 0.0001$). CoCl₂ induced *IL-8* almost twice as much to approximately 6-fold ($p < 0.0001$). Interestingly, at the 12-hour time point, both CoCr particle and CoCl₂ treatment did not significantly change *CCL3* expression compared to the untreated control ($p = 0.9999$ and $p = 0.9972$, respectively). Similarly to *IL-8*, the largest fold-change for *CCL3* was observed for CoCr particle treatment at 24 hours (11-fold,

$p < 0.0001$). Whilst CoCl_2 treatment for 24 hours increased *CCL3* expression 3-fold, this was not of significance ($p = 0.0547$).

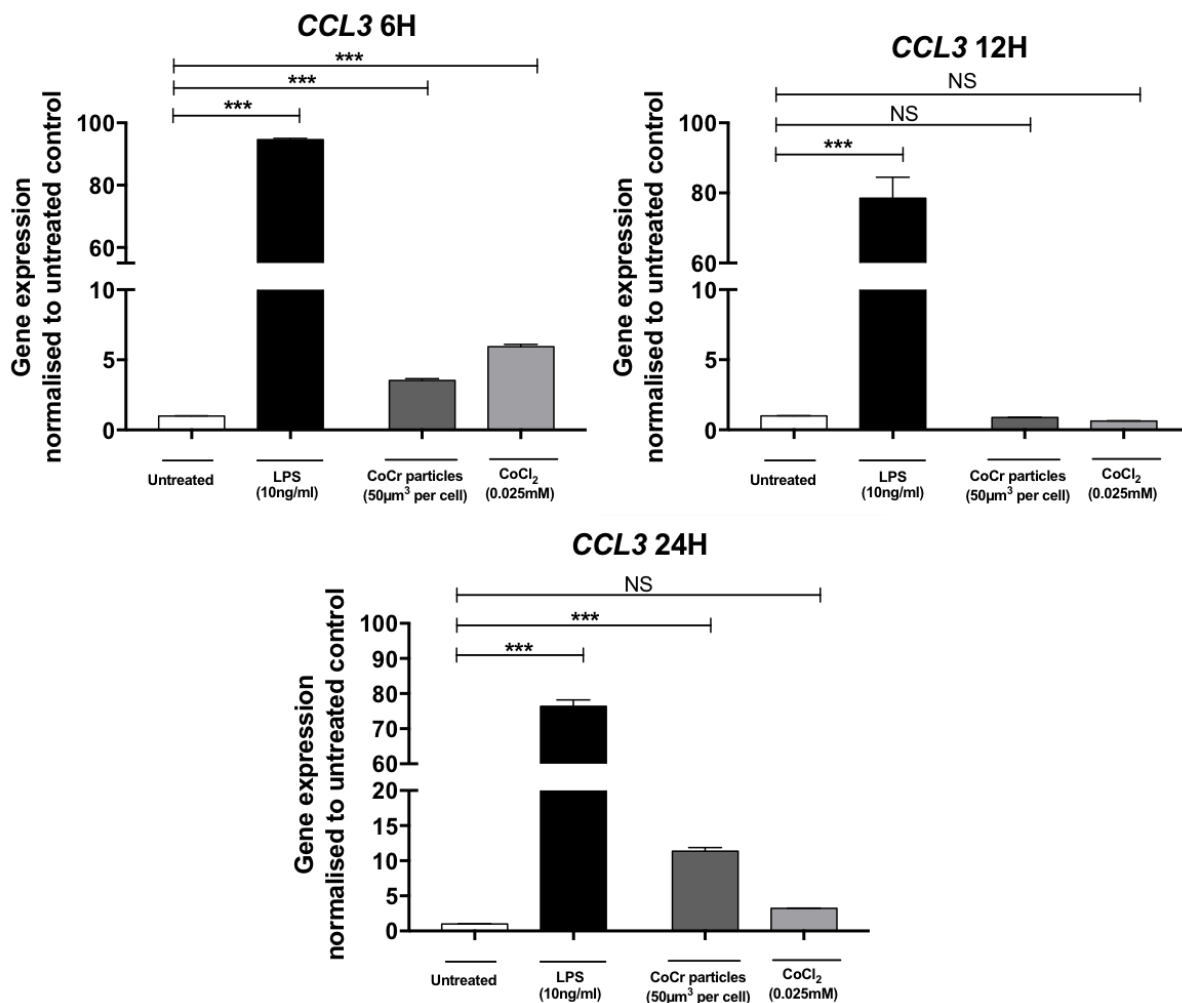


Figure 4.16 *CCL3* gene expression following CoCr particle treatment time course

THP-1 cells were stimulated for either 6, 12 or 24 hours with either LPS (10ng/ml) CoCr particles (50 μm^3 per cell) or CoCl_2 (0.025mM) and gene expression of *CCL3* assessed by qRT-PCR. Gene expression normalised to untreated control, set to 1. Graph is representative of 3 independent experiments. Statistical significance was calculated by one-way ANOVA with Dunnett's multiple comparisons test comparing treated samples to the untreated control.

4.4.5 Effect of TLR4 inhibition on CoCr-mediated cytokine release

The results from **section 4.4.4** demonstrate that CoCr particles can up-regulate both the protein and gene expression of inflammatory mediators (e.g. IL-8, *CCL3*, *CCL4*). This is indicative of an immune response and therefore, given what has been

established regarding metal ions such as cobalt and their ability to directly activate the immune pathway TLR4, was further investigated in the context of CoCr article-mediated inflammation. Activated THP-1 cells were pre-treated with CLI-095 (1µg/ml) (as described in **section 2.3.1**) for 6 hours prior to stimulation with either LPS (10ng/ml), CoCr particles (50µm³ per cell) or CoCl₂ (0.025mM) for 24 hours. Supernatant was collected from treatments and the MSD U-PLEX assay used to quantify protein expression. Using LPS as a positive control activator of TLR4; there was a highly significant decrease in protein expression in all markers of interest (**Figure 4.17 and Figure 4.18**) (all p<0.0001). Therefore, CLI-095 was established to be working effectively in blocking the TLR4 pathway.

Following CoCr particle treatment, IL-8 protein expression was reduced to approximately 9000pg/ml from 33,000pg/ml in the presence of CLI-095 (p<0.0001). Similarly, CoCl₂ treatment led to an increase of IL-8 to 15,000pg/ml which was significantly reduced to untreated levels of 5000pg/ml (p<0.0001) (**Figure 4.17**).

CCL3 expression followed a similar trend in that CoCr particles caused an increase of CCL3 to highs of 1000pg/ml which was significantly reduced to 180pg/ml with the addition of CLI-095 and CCL3 expression was reduced from 425pg/ml to 150pg/ml in CoCl₂ treated cells (p=0.0002 and p=0.0031, respectively) (**Figure 4.17**).

Other inflammatory markers assessed and the effect CLI-095 had on secretion in relation to CoCr particle and CoCl₂ treatments in THP-1 cells is summarised in **Table 4.3** and **Table 4.4**, respectively.

Table 4.3 Protein secretion of inflammatory markers of interest following CoCr particle treatment in THP-1 cells with and without the addition of TLR4 inhibitor (CLI-095)

Statistical significance was calculated by one-way ANOVA with Tukey's test for multiple comparisons comparing all samples to each other.

Protein of interest	Maximal secretion (pg/ml)	Secretion following addition of CLI-095 (pg/ml)	Significance (p number)
IL-8	33,323	9,042	<0.0001 ***
CCL3	1,059	184	0.0002 ***
CCL4	1,413	248	0.0001 ***
CCL2	363	146.50	0.0008 ***
CCL20	648.50	150.50	0.0012 **
IL-1 β	235	73.50	<0.0001 ***
TNF α	2	Not detectable	N/A
CXCL10	252.50	189	0.0277 *
IL-10	1	Not detectable	N/A
IL-13	Not detectable	Not detectable	N/A

Table 4.4 Protein secretion of inflammatory markers of interest following CoCl₂ treatment in THP-1 cells with and without the addition of TLR4 inhibitor (CLI-095)

Statistical significance was calculated by one-way ANOVA with Tukey's test for multiple comparisons comparing all samples to each other.

Protein of interest	Maximal secretion (pg/ml)	Secretion following addition of CLI-095 (pg/ml)	Significance (p number)
IL-8	15,501.50	4,987.50	<0.0001 ***
CCL3	428	152.50	0.0031 **
CCL4	2,030.5	288.50	<0.0001 ***
CCL2	286	142	0.0039 **
CCL20	437.50	146.50	0.0034 **
IL-1 β	115.50	41.50	<0.0001 ***
TNF α	Not detectable	Not detectable	N/A
CXCL10	295.50	132.50	0.0004 ***
IL-10	Not detectable	Not detectable	N/A
IL-13	Not detectable	Not detectable	N/A

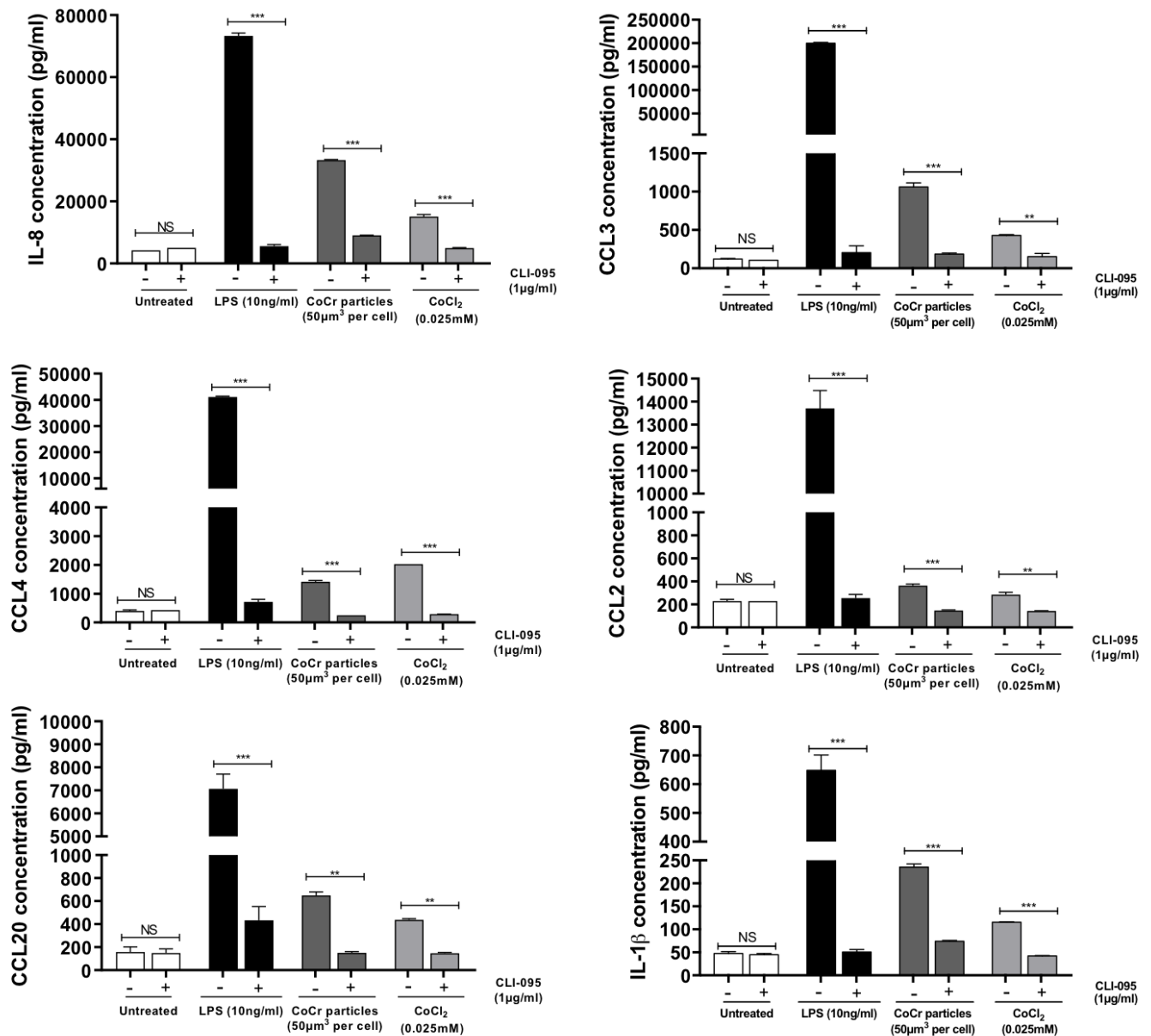


Figure 4.17 Effect of TLR4 inhibition in CoCr particle treated THP-1 cells, assessment of inflammatory proteins - significant changes

Activated THP-1 cells were pre-treated with CLI-095 (1μg/ml) for 6 hours then stimulated with either LPS (10ng/ml) CoCr particles (50μm³ per cell) or CoCl₂ (0.025mM) for 24 hours. Changes to inflammatory protein expression were assessed by the MSD U-PLEX assay. Graph is representative of 3 independent experiments. Statistical significance was calculated by one-way ANOVA with Tukey's test for multiple comparisons comparing all samples to each other.

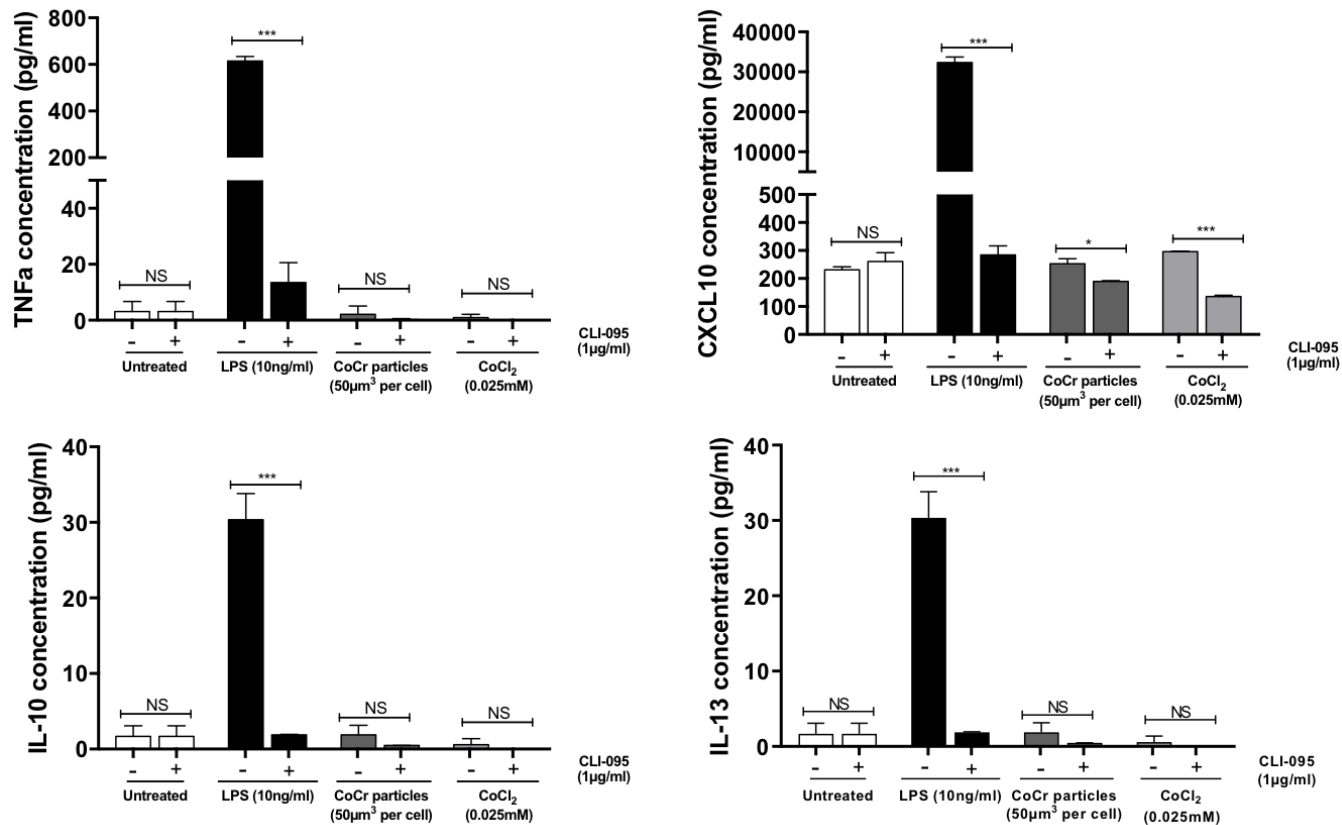


Figure 4.18 Effect of TLR4 inhibition in CoCr particle treated THP-1 cells, assessment of inflammatory proteins - non-significant changes

Activated THP-1 cells were treated with CLI-095 (1 μg/ml) for 6 hours then stimulated with either LPS (10ng/ml) CoCr particles (50 μm³ per cell) or CoCl₂ (0.025mM) for 24 hours. Changes to inflammatory protein expression were assessed by the MSD U-PLEX assay. Graph is representative of 3 independent experiments. Statistical significance was calculated by one-way ANOVA with Tukey's test for multiple comparisons comparing all samples to each other.

4.4.6 Effect of TLR4 inhibition on CoCr-mediated inflammatory gene expression

The findings from **section 4.4.5** demonstrate that CoCr particle-mediated inflammation may be due to activation of the TLR4 pathway as inflammatory protein expression is significantly reduced when using the TLR4 inhibitor, CLI-095. Therefore, qRT-PCR was performed to assess whether there was a similar change in gene expression of *IL-8* when TLR4 is inhibited (**Figure 4.19**). Firstly, LPS used as a positive control demonstrated a significant reduction in *IL-8* expression when THP-1 cells were firstly pre-treated with CLI-095, validating its effectiveness as a TLR4-specific inhibitor (21-fold increase vs 0.5-fold) (p<0.0001). *IL-8* expression was increased 6-fold in response to CoCr particles (50 μm³ per cell) which was reduced to 2.75-fold with the addition of

CLI-095 ($p < 0.0001$). This was similar to CoCl_2 -mediated *IL-8* expression which was increased to 8-fold in comparison to untreated THP-1 cells and significantly down-regulated to 2-fold in the presence of CLI-095 ($p < 0.0001$).

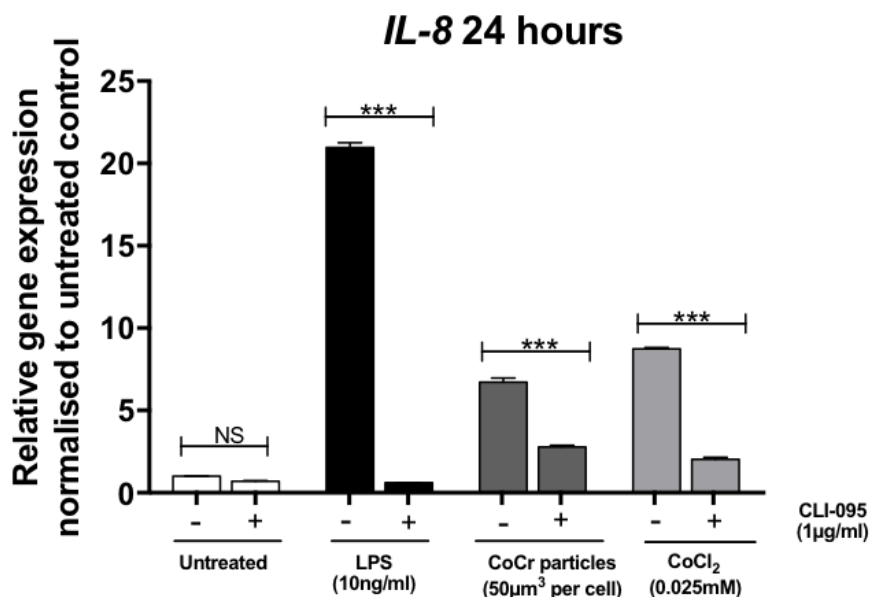


Figure 4.19 Effect of TLR4 inhibition in CoCr particle treated THP-1 cells, assessment of *IL-8* gene expression

Activated THP-1 cells were pre-treated with CLI-095 (1µg/ml) for 6 hours then stimulated with either LPS (10ng/ml) CoCr particles (50µm³ per cell) or CoCl₂ (0.025mM) for 24 hours. *IL-8* expression was measured using qRT-PCR. Gene expression normalised to untreated control, set to 1. Graph is representative of 3 independent experiments. Statistical significance was calculated by one-way ANOVA with Tukey's test for multiple comparisons comparing all samples to each other

4.4.7 Effect of anti-TLR4 neutralising antibody on the inflammatory response to CoCr particles

The data presented so far demonstrate a potential role of TLR4 signalling in regulating CoCr particle-mediated inflammation and up-regulated expression of specific chemokines (e.g. *IL-8*, *CCL2*, *CCL3*, *CCL4* and *CCL20*). This has been shown using CLI-095, a small molecule antagonist which specifically targets the intracellular region of TLR4. However, if a TLR4 antagonist was to be considered as a potential therapeutic option for treating ARMD, CLI-095 would not be suitable as this would prevent the immune response required against gram-negative bacteria containing LPS. Therefore,

a more attractive option could be the use of TLR4-specific antibodies, particularly monoclonal antibodies which are used as therapeutics in other diseases and conditions. This could allow specific inhibition of CoCr particle-mediated TLR4 activation whilst preserving the LPS response.

For this study, MAb-tlr4 was selected for investigation (as described in **section 2.3.2**). However, according to the manufacturer, the exact concentration of MAb-tlr4 required for TLR4 inhibition is dependent on cell type used and the TLR4 agonist and its concentration. Therefore, MAb-tlr4 concentration was firstly optimised in untreated cells to assess any toxic effects and then using LPS as a positive control for TLR4 activation to determine required concentration to effectively inhibit TLR4.

4.4.7.1 Optimisation of MAb-tlr4

The ability of MAb-tlr4 to inhibit LPS-induced *IL-8* expression and protein secretion was investigated to determine the optimal concentration to be used in further assays involving CoCr particles and CoCl₂. Activated THP-1 cells were firstly treated with 0.5-10µg/ml MAb-tlr4 for 1 hour prior to stimulation with 10ng/ml LPS for 24 hours. Untreated cells were also treated with the largest concentration of MAb-tlr4 (10µg/ml) and with an IgG isotype antibody (10µg/ml) (**Figure 4.20**). Following LPS stimulation, expression and secretion of IL-8 was significantly increased (both $p < 0.0001$). When pre-incubated with MAb-tlr4, all concentrations significantly reduced LPS-induced *IL-8* gene expression in a dose dependent manner (0.5µg/ml $p = 0.0006$, 1µg/ml $p = 0.0003$, 5µg/ml $p = 0.0002$ and 10µg/ml $p < 0.0001$). This was similarly reflected in IL-8 protein secretion which was significantly reduced in the presence of all concentrations of MAb-tlr4 (all $p < 0.0001$). There was no significant difference in the response of untreated cells in the presence or absence of MAb-tlr4 (10µg/ml) or the IgG isotype control antibody (all $p < 0.9999$). Therefore, it was concluded that 10µg/ml MAb-tlr4 was the optimal concentration for maximal TLR4 inhibition in LPS-treated cells.

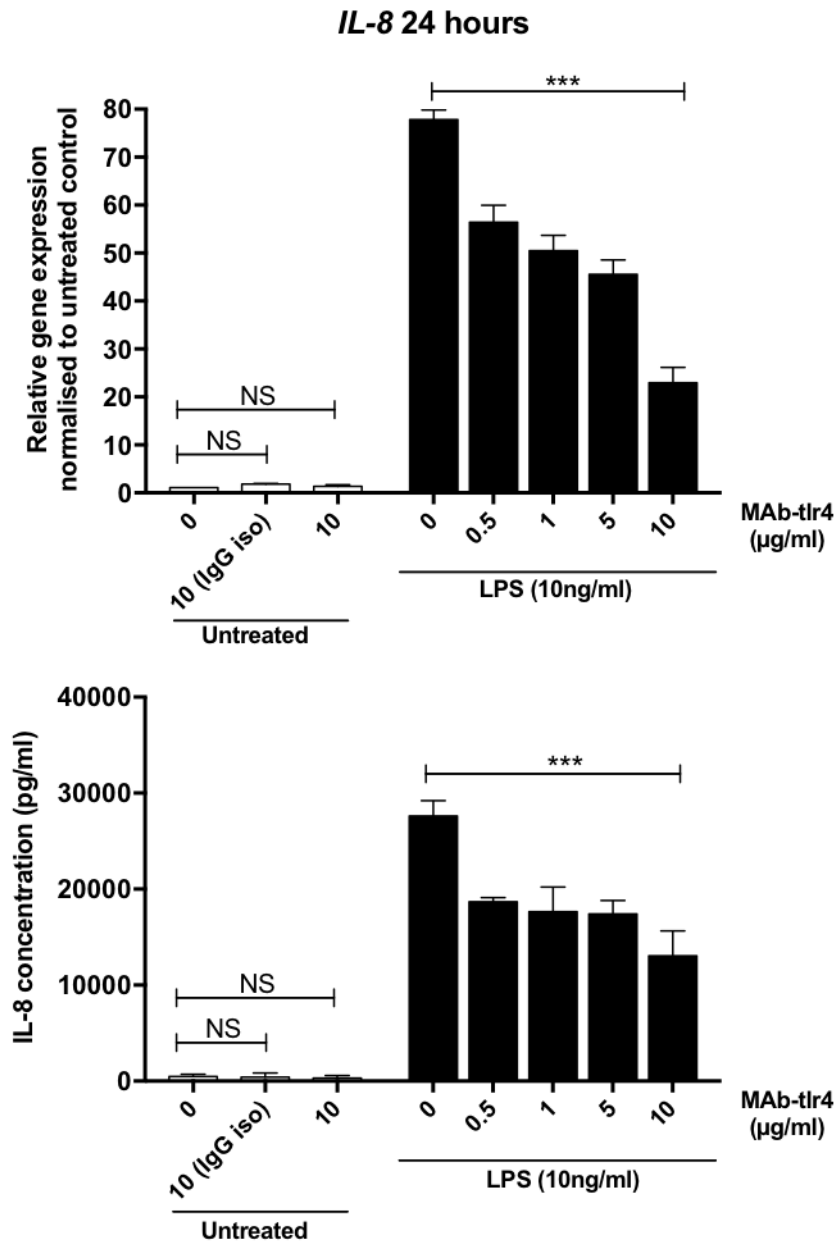


Figure 4.20 Optimisation of MAb-tlr4 in LPS-stimulated THP-1 cells

Activated THP-1 cells were pre-treated with 0.5, 1, 5 or 10µg/ml MAb-tlr4 for 1 hour prior to stimulation with 10ng/ml LPS for 24 hours. An untreated control was included, in the presence and absence of the highest concentration of antibody as well as with an IgG isotype control antibody. *IL-8* gene expression was assessed by qRT-PCR and protein secretion by ELISA. Gene expression normalised to untreated control, set to 1. Graph is representative of 3 independent experiments. Statistical significance was calculated by one-way ANOVA with Tukey's test for multiple comparisons comparing all samples to each other.

4.4.8 Mouse macrophage inflammatory response to CoCr particles

4.4.8.1 CCL3 Dose response

As discussed in **section 1.5.2**, previous research demonstrated that cobalt ions can activate human TLR4, and it is a human-specific response. Therefore, to determine whether CoCr particles could activate murine macrophages, J774 cells were stimulated for 24 hours with either a range of CoCr particle concentrations (0.5 μ m to 50 μ m³ per cell), 10ng/ml LPS or 0.75mM CoCl₂ (**Figure 4.21**). This higher dose of CoCl₂ was selected as it has previously been shown to give maximal activation in other macrophage cell lines (Tyson-Capper *et al.*, 2013). CCL3 was chosen as the inflammatory marker of interest as mice do not express IL-8. CCL3 concentration was measured using ELISA from the supernatants of stimulated cells. Following treatment with LPS, CCL3 protein secretion was significantly increased to approximately 10,000pg/ml (p<0.0001) whereas stimulation with CoCl₂ did not change significantly compared to untreated cells (p=0.9966). The two higher doses of CoCr particles (5 and 50 μ m³ per cell) both significantly increased CCL3 secretion to a peak of 6000pg/ml (vs 4000pg/ml in untreated cells) (p=0.0225 and p=0.0147, respectively).

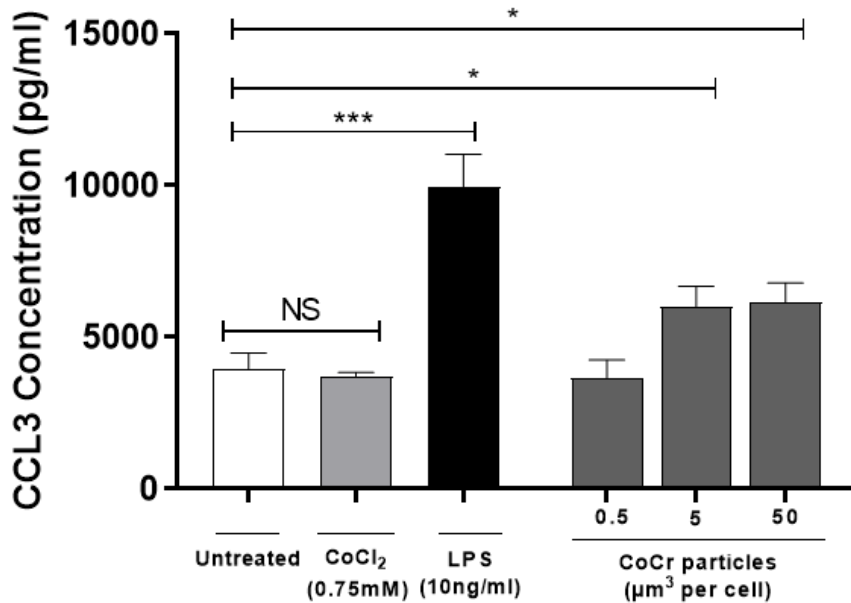


Figure 4.21 CoCr particle dose response in mouse J774 cells - assessment of CCL3 protein expression

J774 macrophage cells were treated with either; LPS (10ng/ml), CoCl₂ (0.75mM) or different doses of CoCr particles (0.5 to 50μm³ per cell) for 24 hours and changes to CCL3 protein expression assessed by ELISA. Graph is representative of 3 independent experiments. Statistical significance was calculated by one-way ANOVA with Dunnett's multiple comparisons test comparing treated samples to the untreated control.

4.4.8.2 Effect of TLR4 inhibition on CCL3 protein secretion

To determine whether the observed small yet significant increase in CCL3 secretion following CoCr particle stimulation was TLR4 dependent, the small molecule TLR4 antagonist, CLI-095 was used in further J774 cell treatments (**Figure 4.22**). The same treatment method was employed described in **section 4.4.8.1**, however, prior to the addition of stimulants for 24 hours, some cells were pre-treated with 1μg/ml CLI-095 for 6 hours. CCL3 secretion was then quantified by ELISA. In LPS stimulated cells, there was a significant decrease in CCL3 protein expression with the addition of CLI-095, roughly halving secretion from 25,000pg/ml to 13,000pg/ml (p<0.0001). However, this was not reflected in the CoCr particle treatments which demonstrated no significant difference in CCL3 secretion in the presence of CLI-095 (p>0.9999). Once more, CoCl₂ stimulation did not induce an up-regulation in CCL3 expression and was unaffected by CLI-095 (p=0.9977).

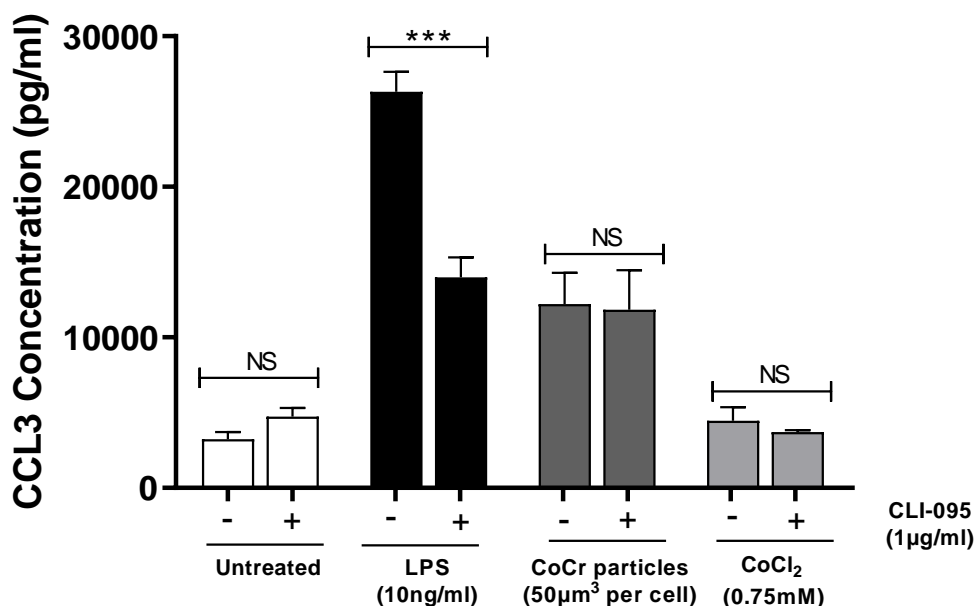


Figure 4.22 Effect of TLR4 inhibition in CoCr particle treated J774 cells, assessment of CCL3 protein expression

J774 macrophage cells were pre-treated with CLI-095 (1 µg/ml) for 6 hours then stimulated with either LPS (10ng/ml) CoCr particles (50 µm³ per cell) or CoCl₂ (0.75mM) for 24 hours. CCL3 protein expression assessed by ELISA. Graph is representative of 3 independent experiments. Statistical significance was calculated by one-way ANOVA with Tukey's test for multiple comparisons comparing all samples to each other.

4.4.9 Monocyte inflammatory response to CoCr particles

4.4.9.1 Naïve THP-1 cells

The response of naïve THP-1 cells i.e. in their monocyte-like state to CoCr particles was also investigated. The same dose response as described in **section 4.4.4** was used for the treatment of inactivated THP-1 cells with a range of CoCr particle concentrations (0.5 to 50 µm³ per cell) for 24 hours before supernatant was collected for protein expression quantification by ELISA. Two doses of LPS were used as positive controls (10 and 100ng/ml). The higher concentration of 100ng/ml LPS was used in addition to previous treatments as monocytes can require larger stimuli to induce an inflammatory response in comparison to macrophage cells. Both IL-8 and CCL3 secretion were assessed and the results shown in **Figure 4.23**. LPS at both concentrations significantly up-regulated IL-8 and CCL3 protein expression (all

$p < 0.0001$) so therefore going forward 10ng/ml LPS was deemed an effective positive control. For IL-8 expression, only the highest concentration of CoCr particles ($50\mu\text{m}^3$ per cell) led to a significant increase compared to untreated cells, reaching a peak secretion of 250pg/ml ($p = 0.0402$) (**Figure 4.23A**). There was a small but non-significant increase in CCL3 secretion following CoCr particle concentration again at the highest concentration, 40pg/ml vs 7pg/ml for untreated cells ($p = 0.2868$) (**Figure 4.23B**). Therefore, $50\mu\text{m}^3$ CoCr particles per cell was the optimised concentration to be used in future treatments.

The TLR4-specific inhibitor, CLI-095 was used to investigate whether the observed effects were TLR4 dependent as seen previously for activated THP-1 cells (**Figure 4.24**). CoCl_2 (0.025mM) was also included to determine its effect on naïve THP-1 cells. There was a significant down-regulation of both IL-8 and CCL3 protein secretion with the addition of CLI-095 in CoCr particle treated naïve THP-1 cells ($p = 0.0056$ and $p < 0.0001$, respectively). This was also reflected in CoCl_2 treatments, both proteins demonstrating significant reductions when cells were pre-treated with CLI-095 ($p < 0.0001$ and $p = 0.0210$, respectively).

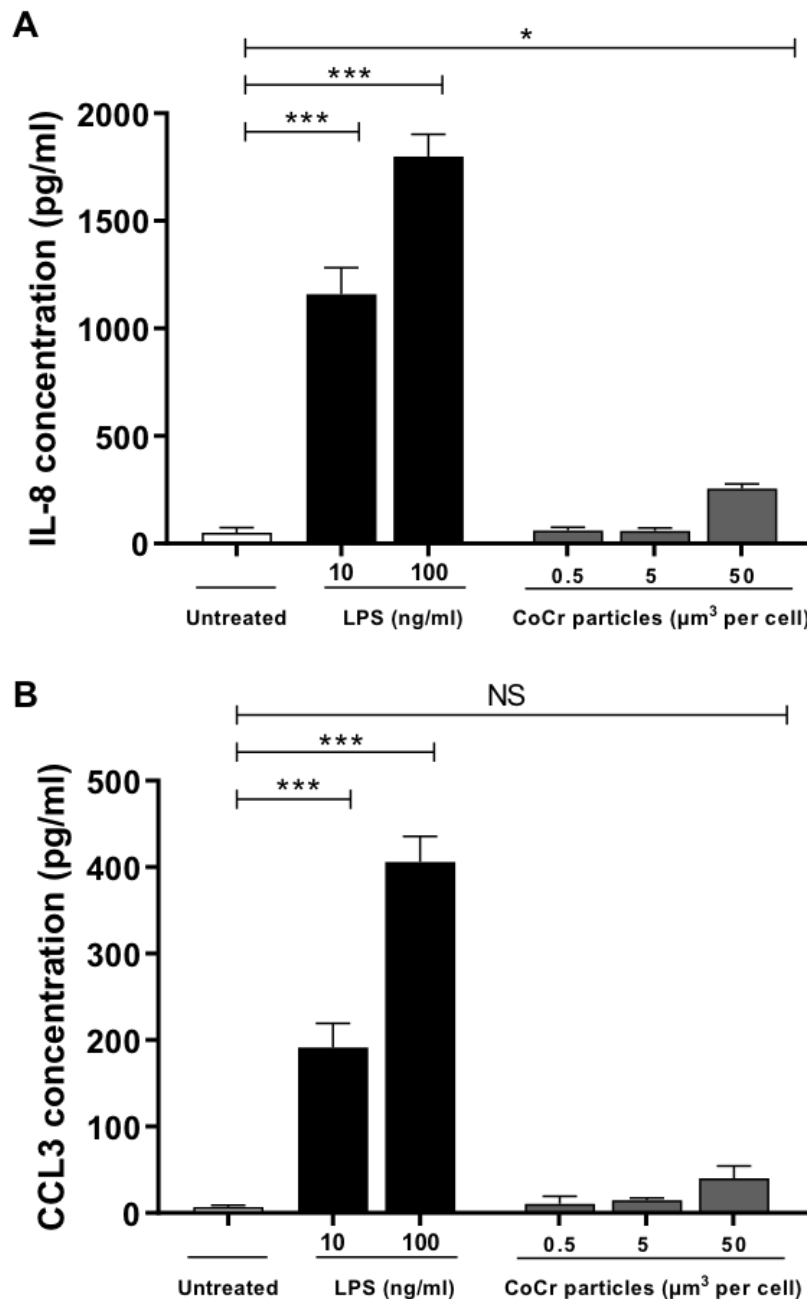


Figure 4.23 CoCr particle dose response in naive THP-1 monocytic cells - assessment of IL-8 and CCL3 protein expression

Inactivated naïve THP-1 cells were treated with either; LPS (10ng/ml or 100ng/ml), or different doses of CoCr particles (0.5 to 50 μm^3 per cell) for 24 hours and changes to **(A)** IL-8 and **(B)** CCL3 protein expression assessed by ELISA. Graph is representative of 3 independent experiments. Statistical significance was calculated by one-way ANOVA with Dunnett's multiple comparisons test comparing treated samples to the untreated control.

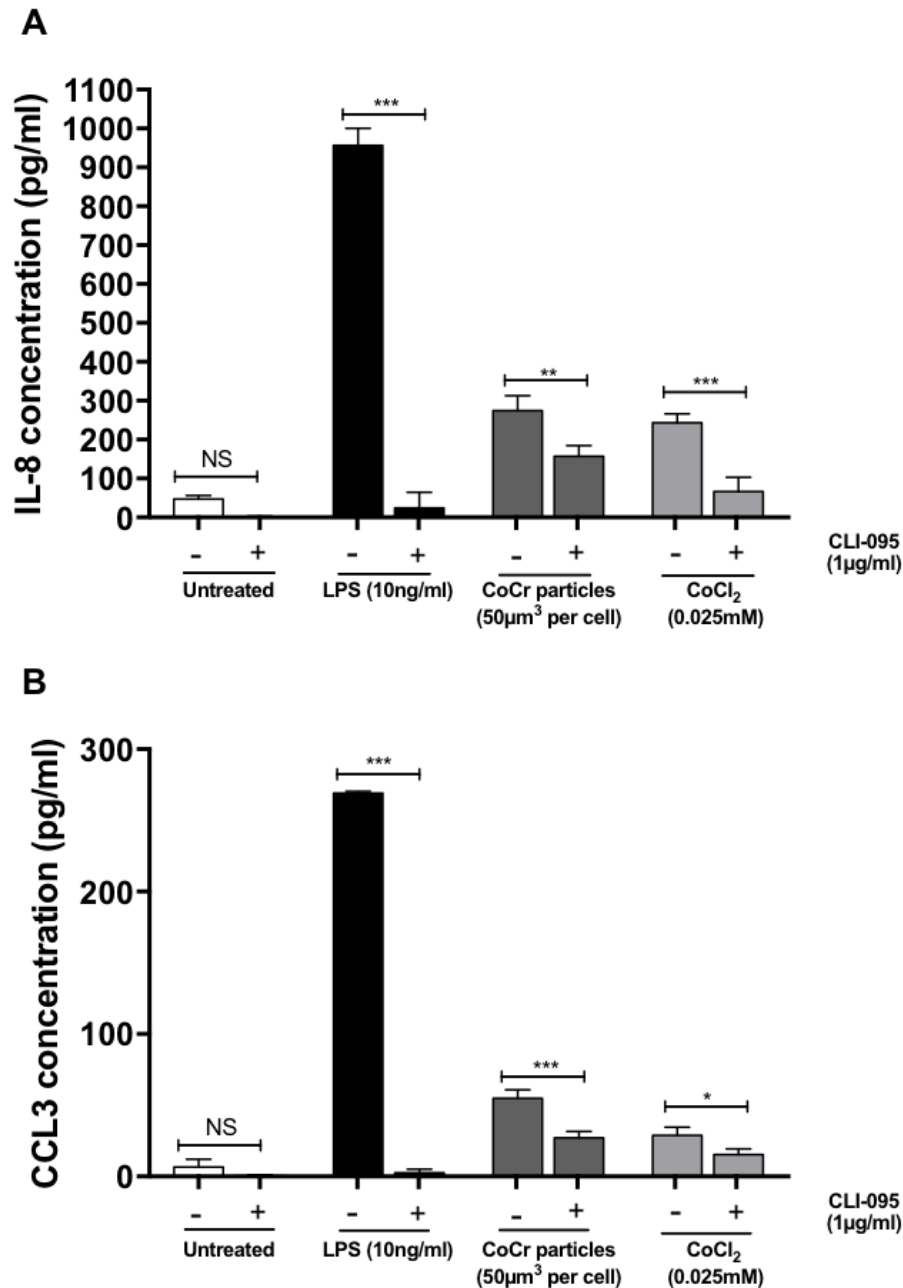


Figure 4.24 Effect of TLR4 inhibition in CoCr particle treated naïve THP-1 monocytic cells, assessment of IL-8 and CCL3 protein expression

Inactivated naïve THP-1 cells were pre-treated with CLI-095 (1µg/ml) for 6 hours then stimulated with either LPS (10ng/ml) CoCr particles (50µm³ per cell) or CoCl₂ (0.025mM) for 24 hours. **(A)** IL-8 and **(B)** CCL3 protein expression assessed by ELISA. Graph is representative of 3 independent experiments. Statistical significance was calculated by one-way ANOVA with Tukey's test for multiple comparisons comparing all samples to each other.

4.4.10 Effect of CoCr particles on the inflammasome

As discussed in **section 1.7** some research groups have suggested that metal wear debris-mediated inflammation is a result of inflammasome activation (i.e. acting as a DAMP inducer) rather than a direct activator of PAMP pathways such as TLR4. As IL-1 β is a marker of inflammasome activation, its protein and gene expression was investigated further using a model of NLRP3 activation, which is the most well studied of the inflammasomes (Lopez-Castejon and Brough, 2011). The NLRP3 specific inhibitor, MCC950, has been shown to significantly reduce IL-1 β secretion in an inflammatory model (Perera *et al.*, 2018). CoCr particles were either substituted as the first 'priming' PAMP signal in place of LPS followed by treatment with ATP to allow full NLRP3 activation. Or, LPS was used as the priming signal followed by stimulation with CoCr particles; thereby acting as a DAMP inducer. IL-1 β protein secretion was assessed by ELISA from the supernatants of treated THP-1 cells and qRT-PCR was used to analyse IL-1 β gene expression.

4.4.10.1 Protein and gene expression of IL-1 β

Firstly, activated THP-1 cells were treated with either LPS (10ng/ml) or CoCr particles (50 μm^3 per cell) for 23 hours to replicate the initial 'priming' signal of NLRP3 activation. The second activation signal was then induced by the addition of ATP (5mM) for 1 hour. Following this stimulation, the expression of IL-1 β was quantified using ELISA and qRT-PCR (**Figure 4.25**). The model of NLRP3 activation was confirmed by treating THP-1 cells with LPS either alone or with the addition of ATP, which should increase up-regulation of IL-1 β . For gene expression, LPS treatment alone increased IL-1 β approximately 13-fold in comparison to cells treated only with ATP which was increased to 27-fold when LPS-stimulated cells were then treated with ATP. There was a similar trend for protein secretion which was 25pg/ml in LPS-only cells and increased to 145pg/ml with the addition of the second signal of ATP. Therefore, there was a significant increase in IL-1 β gene and protein expression when THP-1 cells were treated with LPS for 23 hours followed by ATP for 1 hour (both $p < 0.0001$).

The treatment was repeated but LPS was replaced with CoCr particles to act as the initial 'priming' signal which did not lead to any significant changes to gene or protein expression of IL-1 β ($p = 0.9961$ and $p = 0.6504$, respectively). The addition of the second

activation signal of ATP for 1 hour, also had no significant effect on IL-1 β expression (p=0.9999 and p=0.1516, respectively).

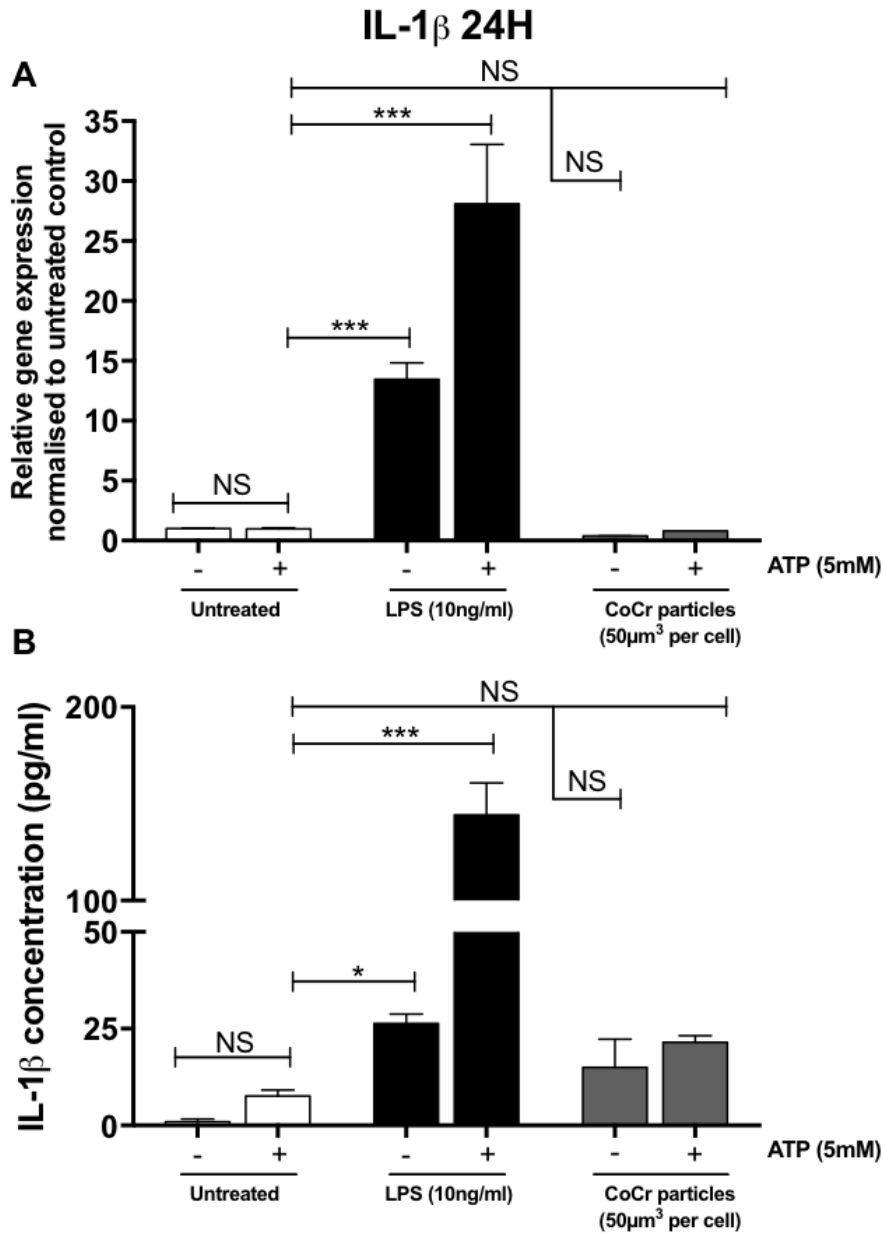


Figure 4.25 IL-1 β gene and protein expression following CoCr particle and ATP treatment in THP-1 cells

Activated THP-1 cells were either left untreated or stimulated with LPS (10ng/ml) or CoCr particles (50 μ m³ per cell) for 23 hours. Cells were then treated with ATP (5mM) for 1 hour before IL-1 β gene expression was analysed by qRT-PCR (**A**) or IL-1 β protein expression assessed by ELISA (**B**). Gene expression normalised to untreated control, set to 1. Graph is representative of 3 independent experiments. Statistical significance was calculated by one-way ANOVA with Dunnett's multiple comparisons test comparing treated samples to the untreated control with ATP and Tukey's test for multiple comparisons comparing all samples to each other.

To establish whether CoCr particles stimulate THP-1 cells as a DAMP inducer rather than a PAMP stimulus, LPS-treated cells were treated with a 1 hour stimulation of either CoCr particles or CoCl₂ (i.e. to be used in place of ATP). Therefore, THP-1 cells were treated with 10ng/ml LPS for 23 hours and then stimulated for 1 hour either with; ATP (5mM), CoCr particles (50µm³ per cell) or CoCl₂ (0.025mM) (**Figure 4.26**). Similarly to results shown in **Figure 4.25**, LPS treatment followed by ATP stimulation led to the largest increases in IL-1β gene and protein expression. When THP-1 cells were firstly treated with LPS and then with either CoCr particles or CoCl₂ there was no significant difference in IL-1β gene expression for either treatments when compared to LPS alone (p=0.9631 and p=0.9982, respectively). This was also reflected in IL-1β protein expression with no significant increases following the addition of either CoCr particles or CoCl₂ for 1 hour after 24 hours of LPS stimulation (p=0.2018 and p=0.5773, respectively).

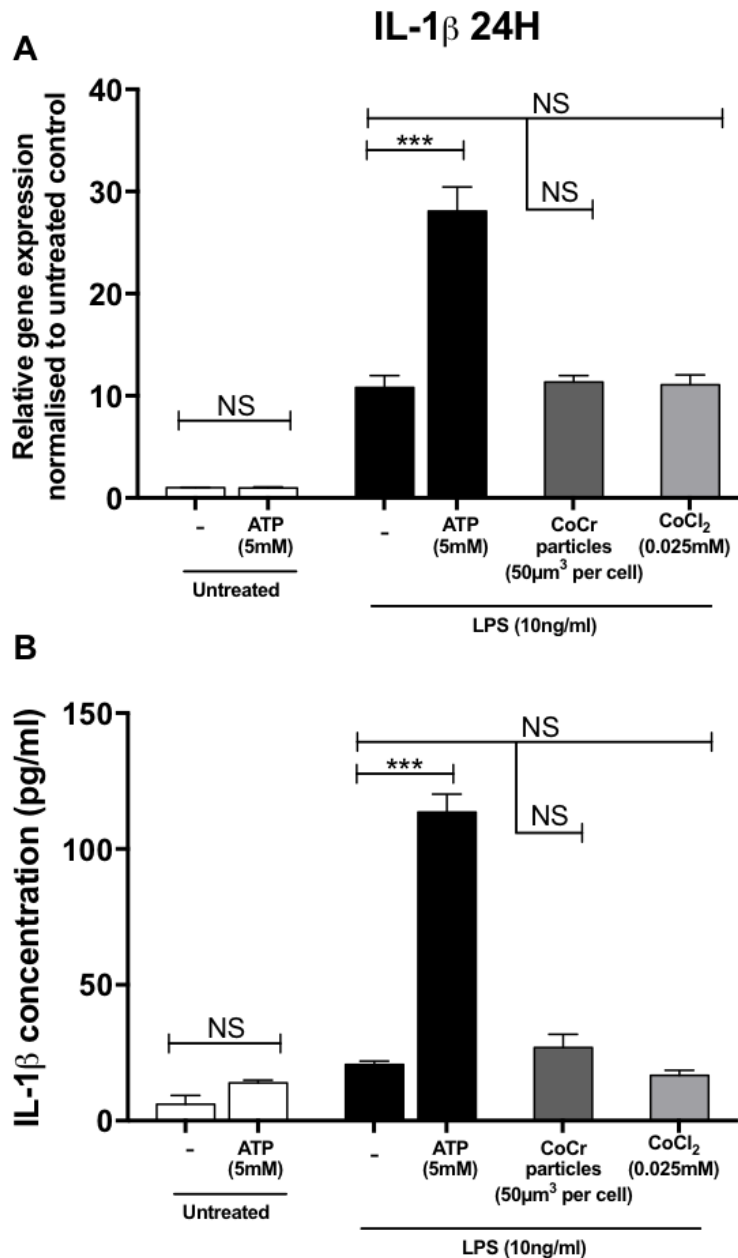


Figure 4.26 IL-1 β gene and protein expression following LPS treatment and CoCr particle stimulation in THP-1 cells

Activated THP-1 cells were either left untreated or stimulated with LPS (10ng/ml) for 23 hours. Cells were then treated with either; ATP (5mM), CoCr particles (50µm³ per cell) or CoCl₂ (0.025mM) for 1 hour before IL-1 β gene expression was analysed by qRT-PCR (A) or IL-1 β protein expression assessed by ELISA (B). Gene expression normalised to untreated control, set to 1. Graph is representative of 3 independent experiments. Statistical significance was calculated by one-way ANOVA with Dunnett's multiple comparisons test comparing treated samples to LPS-stimulated only cells and Tukey's test for multiple comparisons comparing all samples to each other.

4.5 Discussion

Selection of CoCr particle concentration

Previous studies have investigated the biological effects of CoCr particles in various cell lines and the results and outcomes vary significantly in deciding what is the optimal dose to use and the method used to calculate 'doses'. For example, some studies will employ a 'particle: cell ratio' method or $\text{mg}\cdot\text{ml}^{-1}$ (Potnis *et al.*, 2013; Samelko *et al.*, 2017; Klinder *et al.*, 2018). However, the issue with 'particle: cell ratio' is that it does not take into consideration the size of each individual particle which can vary greatly in any given sample, especially when generated on simulators (as opposed to commercially available particles which tend to be more uniform). As previously discussed, the size of CoCr particles can have an impact on the effects observed in cell treatments and the reactivity is thought to be greater for nanoparticles versus microparticles (Papageorgiou *et al.*, 2007). Therefore, using μm^3 per cell, allows for the size of the particles to be taken into consideration and has been previously used frequently in other similar studies (Germain *et al.*, 2003; Papageorgiou *et al.*, 2007; Behl *et al.*, 2013). These studies also used a concentration range of 0.5 to $50\mu\text{m}^3$ per cell and found, for example, the viability of dural eplithelial cells were reduced in a dose-dependent manner but not fibroblasts, demonstrating the clear difference of sensitivity between cell types used (Behl *et al.*, 2013).

The results presented in **Chapter 3** regarding cobalt ion release from particles in cell culture media, measured by ICP-MS, demonstrated that 0.5 to $50\mu\text{m}^3$ CoCr particles per cell released a relatively low concentration of CoCl_2 (with a maximum of approximately 0.025mM or $1500\mu\text{g/L}$). Previous studies in the group have used concentrations ranging from 0.25mM-1mM CoCl_2 (Lawrence *et al.*, 2016a; Lawrence *et al.*, 2016b), however, this is significantly higher than reports investigating serum cobalt concentrations in patients with MoM implants, therefore, this lower concentration is perhaps a more 'clinically-relevant' representation (Kwon *et al.*, 2011) (**see section 1.3.2**). However, it is particularly difficult to select and define a concentration range deemed to be 'clinically-relevant' as the concentrations observed vary significantly. For example, either between individual patients or whether the synovial fluid or serum is used for concentration measurements, the latter typically being much lower.

Cytotoxicity of CoCr particles

Cobalt ions and CoCr particles are known to cause cytotoxicity at high concentrations, with some cell lines more sensitive than others (Laumonier *et al.*, 2020). For example, Behl *et al.* found that dural epithelial cells were more sensitive than fibroblasts (Behl *et al.*, 2013). All concentrations of CoCr particles investigated in this study did not significantly affect cell viability following 24 hours of treatment in MM6, THP-1 and J774 cells. However, when treated for 48 hours, there was a significant decrease in viability at the highest concentration of $50\mu\text{m}^3$ CoCr particles per cell in both MM6 and THP-1 cells. It is interesting that J774 mouse macrophages remained unaffected at 48 hours. This may be because previous studies have shown that only human and primate species perpetuate a TLR4-mediated inflammatory response to cobalt ions, suggesting it is in fact the ions which are most toxic to cells (Raghavan *et al.*, 2012; Tyson-Capper *et al.*, 2013). Despite MM6 cells having previously been used most frequently by this group when investigating responses to CoCl_2 , THP-1 cells were selected as the most appropriate cell line for this study as they can be activated to a mature macrophage phenotype and therefore are more responsive to stimuli when compared to MM6 cells. Furthermore, macrophages are one of the most common cell types located within the peri-implant tissue of inflammatory pseudotumours (Perino *et al.*, 2014).

The proliferative capacity of activated THP-1 cells treated with CoCr particles over 48 hours was also investigated using an XTT assay. There was a small but significant decrease in proliferation only at the highest concentration of $50\mu\text{m}^3$ CoCr particles per cell following 24 hours of treatment. At 48 hours, this reduction of proliferation for the same treatment was far more significant. It is hypothesised that dose-dependent cytotoxicity from metal ions is due to interference with DNA replication and DNA repair mechanisms which ultimately results in cell necrosis (Kwon *et al.*, 2009). Furthermore, production of ROS is likely to contribute to these cytotoxic effects by initiating oxidative cell stress as cobalt ions have been shown to induce ROS leading to cell damage and death (Petit *et al.*, 2005).

It is important that cytotoxicity is avoided where possible so that subsequent assays assessing inflammatory effects are not influenced by this factor. As toxic effects appeared to be minimal at $50\mu\text{m}^3$ CoCr particles per cell following 24 hours of treatment, and provided an approximate 'clinically-relevant' concentration, this range of concentrations were selected for future investigations.

Phagocytosis of CoCr particles

Phagocytosis of CoCr particles was confirmed by TEM images of activated THP-1 cells which had been treated for 24 hours with 50µm³ CoCr particles per cell. This finding is consistent with other studies which have shown that CoCr particles can be phagocytosed by other cells such as osteoblasts (Lohmann *et al.*, 2000). However, from reviewing the literature, this appears to be the first study to demonstrate the phagocytosis of CoCr particles in THP-1 macrophage cells. CoCr particle aggregates were surrounded by distinct membranes suggesting similarities to phagosomes or lysosomes when engulfing pathogens. The suggestion internalisation of particles is due to an active endocytosis process was highlighted by images of THP-1 cells engulfing CoCr particles at the cell membrane which would require ATP energy. It could be that ATP stores become depleted over time through continual exposure to CoCr particles. By phagocytosing CoCr particles into distinct phagosomes, it can be assumed that this could cause cellular stress and therefore activate an immune inflammatory response. Therefore, in a clinical setting, this indicates that CoCr aggregates are present in peri-implant tissue containing macrophages, causing inflammation within the tissue, which could be attributed to the formation of pseudotumours and ARMD.

Although the phagocytosis assay using pHrodo™ particles could not be completed for CoCr particle treatments in THP-1 cells, it was hypothesised phagocytosis would be compromised. A study has investigated 'endotoxin tolerance' and how this can affect *E. coli* phagocytosis when macrophages are pre-treated with LPS and hypothesised this as the reason M1 macrophages have decreased phagocytic capacity (Kapellos *et al.*, 2016). The authors found with increasing concentrations of LPS, phagocytosis was inhibited, suggesting tolerance to M1 stimuli. Therefore, similar effects may have been observed for THP-1 cells pre-treated with CoCr particles. It is important to be aware of limitations with these type of assays, the use of commercially available 'dead' pathogens do not accurately reflect *in vivo* situations.

Cytokine and chemokine expression; potential roles in ARMD

An MSD U-PLEX assay was utilised to determine the protein secretion of 10 selected inflammatory cytokine/chemokines across a dose response of CoCr particles. Out of the ten markers investigated, six were increased in a dose dependent manner in response to CoCr particles; IL-8, CCL2, CCL3, CCL4, CCL20 and IL-1β. Whereas four

markers were not significantly affected compared to untreated control cells; TNF- α , IL-10, CXCL10 and IL-13.

In agreement with previous studies within the group which have investigated the effect of CoCl₂ on IL-8 expression, CoCr-mediated IL-8 secretion showed the largest increase of expression. IL-8 is a pro-inflammatory chemokine which mainly attracts neutrophils to sites of inflammation via activation of CXCR1 and CXCR2 receptors. Several studies have shown the presence of IL-8 in periprosthetic tissues in cases of aseptic loosening and IL-8 has been suggested to be a potential biomarker of osteolysis (Lassus *et al.*, 2000; Koulouvaris *et al.*, 2008). One study has also demonstrated a correlation between increased IL-8 expression and earlier time to revision surgeries (Jamsen *et al.*, 2017). Furthermore, IL-8 appears to play an important role in the formation of osteoclasts and subsequent bone resorption. For example, in metastatic bone disease, IL-8 can stimulate osteoclast differentiation leading to enhanced bone destruction (Bendre *et al.*, 2003). RANKL stimulation of osteoclasts can lead to increased secretion of IL-8 which in turn enhances osteoclastogenesis. This effect can be blocked by using IL-8 antibodies or CXCR1/CXCR2 inhibitors *in vitro* (Kopesky *et al.*, 2014). Therefore, in the context of ARMD, if patients with a CoCr-containing implant have increased secretion of IL-8 in response to wear debris particles then this could potentially cause IL-8-mediated osteoclastogenesis and therefore aseptic loosening of the implant.

CCL2 potently chemoattracts monocytes but also macrophages, NK cells and T cells through activation of the CCR2 and CCR4 receptors. A study used a rodent air-pouch model to assess the inflammatory response to CoCr wear debris to demonstrate vast monocyte/macrophage cellular infiltration and attributed this to increased expression of CCL2 (Akbar *et al.*, 2012). However, CCL2 is also involved in the formation of osteoclasts and can therefore promote bone resorption and osteolysis. For example, CCL2 knockouts in bone marrow cells caused significant reduction in osteoclast formation when compared to wild-types (Khan *et al.*, 2016). The role of CCL2 in the context of failed UHMWPE implants is well studied, for example, blocking CCR2 and its interaction with CCL2 in a murine implant model reduced macrophage recruitment to the site of the implant (Gibon *et al.*, 2012). Furthermore, recently, a group investigated the use of a mutant form of CCL2; 7ND (functioning as a competitive inhibitor) (Long *et al.*, 2020). They found that osteoclast differentiation of PBMCs was significantly inhibited and in an LPS-induced bone erosion animal model, the protein

attenuated bone resorption, concluding that competitively inhibiting CCL2 could be a potential approach in treating inflammatory osteolysis (Long *et al.*, 2020).

CCL3 and CCL4 are secreted mostly by macrophages, NK cells and fibroblasts. Both chemokines can bind to the chemokine receptor, CCR5 and CCL3 has a strong affinity to CCR1. Both CCL3 and CCL4 are strong chemoattractants for monocytes and CCL3 has been shown to induce the differentiation of monocytes to osteoclasts (Dapunt *et al.*, 2014b). Increased expressions of CCL3 are found in osteolytic lesions around implants (Dapunt *et al.*, 2014b). Similarly to CCL2, the differentiation of osteoclasts by CCL3 is believed to be RANK/RANKL dependent as mice deficient in RANK which are injected with CCL3 do not increase osteoclast numbers when compared with wildtype (Oyajobi *et al.*, 2003). In comparison to CCL3, CCL4 does not appear to play as major a role in osteoclast differentiation with one study indicating that CCL4 is not directly involved in the osteoclastogenetic process (Lee *et al.*, 2018). However, the same study suggested that CCL4 is involved in the early osteoclast differentiation process by recruiting viable preosteoclast cells (Lee *et al.*, 2018). However, there are few investigations involving the expression of CCL3 and CCL4 in response to wear debris or metal ions.

CCL20 is strongly chemotactic for lymphocytes and less so for neutrophils and acts via the CCR6 receptor, which is highly expressed by lymphocytes. As previously discussed, a hallmark of ARMD is ALVAL which describes the infiltration of immune cells, particularly T lymphocytes to peri-implant tissues. Previously, CCL20 has been shown to increase its expression by MM6 cells in response to cobalt ions in our research group (Lawrence *et al.*, 2016a). Therefore, if monocytes or macrophages secrete CCL20 in the peri-implant tissues, this may contribute to the infiltration of lymphocytes observed in ARMD.

The cytokine, IL-1 β and its mode of expression following NLRP3 activation is described in detail in **section 1.7**. The increase in concentration of IL-1 β was not as high (albeit significant) compared to previously discussed markers in response to CoCr particles. It may be that increases in IL-1 β may promote further activation of immune responses and lead to inflammatory processes such as osteolysis, particularly due to its interaction with TNF α . For example, IL-1 β upregulates the production of RANKL and therefore stimulates osteoclastogenesis. Reports have suggested that blocking both IL-1 β and TNF α can completely abrogate bone resorption (Amarasekara *et al.*, 2018).

Interestingly, in this study, TNF α secretion was not increased in response to CoCr particles, despite being a cytokine which is involved in many inflammatory processes. However, this is in agreement with other studies which have demonstrated increased expression of IL-1 β but not TNF α by THP-1 macrophages treated with CoCr particles (Samelko *et al.*, 2016).

IL-10 is an anti-inflammatory cytokine that plays an important role in limiting inflammation and is up-regulated in response to LPS-mediated TLR4 activation (Den Haan *et al.*, 2007). Therefore, if CoCr particles mediate a pro-inflammatory cytokine and chemokine response then increased concentrations of IL-10 would also be expected. However, IL-10 levels were undetectable in the supernatants of THP-1 cells treated with CoCr particles. This could be due to the secretion of IL-10 believed to primarily be a T cell response *in vivo* (Kubo and Motomura, 2012).

Although CXCL10 concentrations were increased slightly following CoCr particle stimulation, this did not reach statistical significance. CXCL10 is secreted by cells such as monocytes and endothelial cells in response to IFN γ and binds to the chemokine receptor CXCR3. CXCL10 can also stimulate osteoclast formation by inducing RANKL expression in osteoblasts (Lee *et al.*, 2012). Patients with ARMD have elevated concentrations of CXCL10 protein expression in the synovial fluid and to a lesser extent, serum (Kolatat *et al.*, 2015). MM6 cell treatment with cobalt ions have also shown increased expression of CXCL10 (Lawrence *et al.*, 2014).

IL-13 was also undetectable in the supernatants of THP-1 cells treated with CoCr particles. Perhaps this is unsurprising given IL-13 is mostly secreted by T cells, mast cells, basophils and eosinophils rather than monocytes/macrophages (Junttila, 2018). However, studies have investigated its role in particle-induced inflammation alongside IL-4. In a mouse air pouch model with polyethylene particles, injection with both IL-13 and IL-4 reduced both bone collagen loss and osteoclast function, therefore offering a protective, anti-inflammatory role (Wang *et al.*, 2013). It is likely this is due to the link between both IL-4 and IL-13 stimulating the production of OPG and inhibiting RANKL which is discussed in more detail in **section 1.3.3** (Stein *et al.*, 2008).

The role of TLR4 in CoCr particle-mediated increases in cytokine and chemokine expression

The results discussed so far demonstrate that THP-1 macrophages treated with CoCr particles can induce the secretion of some cytokines and chemokines. One of the aims of this study was to elucidate the role of TLR4 in this response, given its importance of activation in relation to metal ions such as cobalt. Previous research within the group have utilised the small molecule TLR4 inhibitor, CLI-095 under similar conditions when investigating CoCl₂ stimulation so was therefore previously optimised. For all the protein markers discussed previously which were up-regulated in response to CoCr particles, this increase was significantly abrogated with the addition of CLI-095 – indicating that these increases are TLR4-mediated. A similar pattern was observed for CoCr-mediated *IL-8* gene expression which was also significantly decreased when THP-1 cells were pre-treated with CLI-095. In all cases, cytokine and chemokine expression was reduced to that of untreated THP-1 cells, indicating that TLR4 plays a major role in these responses. It was important to note that the inclusion of untreated control cells with the addition of CLI-095 demonstrated no significant changes in protein expression for all markers investigated.

The equivalent concentration of CoCl₂ (0.025mM) released from 50µm³ CoCr particles per cell over 24 hours was also included in this set of experiments. The reason for its inclusion was to determine whether increases in cytokine and chemokine expression by CoCr particles were mostly due to the presence of CoCl₂ released from the particles or whether the particles themselves have an additive effect to the observed response. CoCl₂ solutions were also tested for any endotoxin contamination (using the LAL assay described in **section 3.4.5**) to ensure responses observed were not due to LPS activation of TLR4.

In nearly all inflammatory markers investigated (with the exception of CCL4), there was a larger increase in secretion from CoCr particle treatments compared to CoCl₂. Therefore, it could be assumed that although much of the increases in expression from CoCr particle treatments may be due to CoCl₂ released from particles, the particles enhance this increase. This could be due to a more generalised stress response as the THP-1 cells attempt to phagocytose the particles (as demonstrated by TEM) or also due to the presence of chromium. Chromium ions have been shown to be less toxic than cobalt in human myoblasts and do not increase expression of ICAM-1 or inflammatory cytokines (Jonitz-Heincke *et al.*, 2019; Laumonier *et al.*, 2019). This finding is consistent with another study which demonstrated that chromium ions were

unable to induce ROS production, inflammasome activation and cytotoxicity (Adam *et al.*, 2017). Furthermore, chromium ions are thought to play a lesser role in bone homeostasis than cobalt ions with no effect on TGF- β or RANKL expression (Drynda *et al.*, 2018b). Therefore, it is likely that any effects due to the presence of chromium in CoCr particles are negligible.

Inhibiting TLR4 in CoCr particle treated cells reduced protein expression to that of untreated cells suggesting that cobalt ions (known to activate TLR4) may be the major source initiating these observed increases. It is difficult to accurately measure the concentration of cobalt ions released from particles for each individual treatment which could explain the observed differences between CoCr particle and CoCl₂ treatments. Despite the fact that concentrations were measured by ICP-MS in **Chapter 3** it may be that there are slight inaccuracies when dosing cells (potentially due to aggregation of particles) which account for the larger increases in concentration in this instance.

Interestingly, with *IL-8* gene expression, CoCl₂ treatment over 24 hours increased expression more than CoCr particle treatment. In both treatments, *IL-8* expression was significantly reduced with the addition of CLI-095. The difference may be the time point investigated (at 24 hours) as the time course for either treatment may differ from each other (as shown in previous time course experiments for *IL-8* and *CCL3*). For example, in CoCl₂ treatments, the cells are exposed to the concentration of ions for the entire treatment time whereas with CoCr particle treatments, the ions are gradually released. Additionally, this may also come down to inaccuracies in dosing of CoCr particles for them to release the exact concentration of cobalt ions calculated by ICP-MS.

CLI-095 is effective at inhibiting downstream signalling of TLR4 by binding to Cys747 in the intracellular domain of TLR4 and thus preventing the recruitment of all adaptor proteins involved in TLR4 activation (Matsunaga *et al.*, 2011). As all adaptor proteins are prevented from recruitment this means that both the MyD88 and TRIF (MyD88 independent) pathways are inhibited. These signalling pathways ultimately result in activation of different transcription factors (e.g. NF κ B or IRF3) which are responsible for the regulation and production of different inflammatory cytokines and chemokines which are investigated in this study. For example, *IL-8* is known to be regulated by the MyD88-dependent pathway via activation of NF κ B whereas *CXCL10* production is mostly associated with the TRIF-dependent pathway (Weighardt *et al.*, 2004; He *et al.*, 2013). Both pathways have been shown to be involved in the response to metal ions

(Oblak *et al.*, 2015). However, in this study, most markers investigated are involved in MyD88-dependent responses (CXCL10 expression increases were minimal in comparison to other chemokines). Therefore, to reach firmer conclusions as to which arms of the TLR4 pathway play a more dominant role in CoCr-mediated inflammatory responses, inhibitors targeting specific adapter molecules e.g. MyD88 or TRIF could be utilised.

Anti-TLR4 neutralising antibodies have previously been tested to inhibit CoCl₂-mediated inflammatory responses with the monoclonal antibody (MAb2-Htlr4) inhibiting cobalt-mediated IL-8 and CCL20 expression (Lawrence *et al.*, 2016b). However, a polyclonal neutralising antibody (PAb-hTLR4), did not inhibit IL-8 secretion and did not significantly reduce *IL-8* gene expression in CoCl₂ treated MM6 cells (Lawrence *et al.*, 2016b). It was concluded that the differences in effective inhibition were likely due to the antibodies different binding sites. Furthermore, the fact the antibodies effectively reduced LPS-mediated activation of TLR4 supports the hypothesis that metal ions and LPS bind to different regions of TLR4.

In this study, a different monoclonal neutralising antibody (MAb-tlr4), was used to investigate its effectiveness in reducing chemokine expression in THP-1 cells treated with CoCr particles (due to antibodies previously used having discontinued). Firstly, the antibody concentration was optimised using LPS as the TLR4 ligand and IL-8 as a marker of TLR4 activation. Both IL-8 gene expression and protein secretion were significantly reduced in a dose-dependent manner with the addition of increasing concentrations of MAb-tlr4. Due to the circumstances of time constraints, experiments with CoCr particles could not be completed but we would have done so using the concentration optimised.

TLR4 is the most studied TLR as a target in clinical trials for the treatment of many different diseases and conditions such as rheumatoid arthritis, sepsis and other inflammatory diseases (Fox *et al.*, 2018; Monnet *et al.*, 2020). However, clinical success is minimal, for example, two phase III clinical trials using CLI-095 and eritoran (a TLR4 antagonist) as a treatment for sepsis were suspended (Rice *et al.*, 2010; Opal *et al.*, 2013). In the context of ARMD, the results from this study have shown a potential role of TLR4 in the inflammatory response to CoCr particles and/or cobalt ions. However, for TLR4 to be considered as a therapeutic option, careful consideration would be required in the design of a potential antagonist. For example, if TLR4 was to

be inhibited, it is crucial that the natural response to LPS and Gram negative bacteria is preserved so that an immune response can be initiated to clear infection. It is possible that this could be achieved as it is known that cobalt ions and LPS do not share the same TLR4 binding sites. By designing an antibody which specifically targets the histidine pocket which cobalt ions are believed to bind to; initiating TLR4 activation, this could prevent this response whilst conserving the LPS activation of TLR4.

Monocyte response

The response of monocytic (i.e. inactivated THP-1) cells to CoCr particles was evaluated to confirm whether this cell type was also able to mount similar inflammatory effects observed by THP-1 macrophages. Monocytes are more typically found circulating in the blood compared to tissue resident macrophages. It has been shown that cobalt ions can be detected in relatively high concentrations in the serum of patients with implants containing CoCr, therefore, monocytes are likely to be one of the first cell types to encounter these ions.

IL-8 and CCL3 protein expression were investigated firstly using the dose response of CoCr particles discussed previously (0.5 to 50 μm^3 per cell). There was a small but significant increase of IL-8 expression at the highest concentration of CoCr particles. CCL3 expression was increased compared to untreated THP-1 monocytes but did not reach significance. It is perhaps unsurprising that the concentrations observed were relatively low compared to the activated THP-1 macrophage response as monocytes are generally much less inflammatory. Furthermore, CD14 expression is much lower in THP-1 monocytes compared to primary monocytes. As a result, THP-1 monocytes are less responsive to TLR4 stimuli such as LPS and metal ions (Bosshart and Heinzelmann, 2016).

CLI-095 was then utilised to see whether this response was also TLR4-mediated. Similarly to the activated THP-1 results, both IL-8 and CCL3 secretion were significantly reduced when cells were pre-treated with CLI-095. Furthermore, there was a slight increase in response to CoCr particles when compared to CoCl₂ (at the concentration of ions expected to be released from particles). Again, this strengthens the hypothesis previously discussed that perhaps the particles have an additive effect compared to ions alone.

Mouse macrophage response

As discussed previously, cobalt ions can only activate human and primate TLR4 as other species do not express the conserved histidine residues required for the ions to bind to and allow activation. Therefore, it was interesting to investigate a mouse macrophage cell line (J774) to see whether CoCr particles could elicit an inflammatory response. If inflammatory chemokine expression increased this would suggest that CoCr particles are initiating the immune response independently of TLR4. The muroid lineage do not express IL-8 so CCL3 was used instead as a marker of inflammation (Modi and Yoshimura, 1999). A study has also shown that mice carrying a TLR4 mutation have diminished CCL3 expression in monocytes (Song *et al.*, 2011).

In this study, CoCl₂ treatments (at a relatively high concentration known to activate human macrophages) were included as an additional negative control. As expected, CoCl₂ failed to increase CCL3 secretion in comparison to untreated J774 cells. This provided confirmation that cobalt ions are unable to elicit an inflammatory response in mice via TLR4 activation. Interestingly, CoCr particle treatments caused a small but significant increase in CCL3 secretion at both 5 and 50µm³ per cell. This small increase in CCL3 suggests CoCr particles are activating the immune response via an alternative pathway to TLR4, again perhaps through a more generalised stress response. These findings were confirmed using CLI-095 as previously described, which worked effectively at inhibiting LPS-mediated CCL3 secretion. However, there was no significant difference in CCL3 secretion between CoCr particle-treated J774 cells with and without the addition of CLI-095. Therefore, any increases in CCL3 secretion following CoCr particle stimulation were not due to TLR4 activation. This further supports the hypothesis that CoCr particles may cause inflammatory effects in addition to TLR4 activation from released cobalt ions in human cells.

The fact CoCr particles could induce CCL3 secretion in mouse J774 macrophages demonstrates the particles ability to induce inflammation through alternative pathways to TLR4. Inflammatory responses caused by CoCr particles could be due to the phagocytosis of particles by macrophages (as shown by TEM imaging) which can then potentially be presented to T cells in conjunction with immunogenic haptens, activating the adaptive immune response. Although it is clear cobalt ions can directly activate TLR4, the role CoCr particles play in activating either the innate or adaptive immune response and specific pathways, is less certain.

The role of the NLRP3 inflammasome in CoCr particle-mediated inflammatory responses

The role of the NLRP3 inflammasome in CoCr particle-mediated inflammation was investigated to evaluate whether its activation was responsible for the added effects observed from CoCr particles when compared to cobalt ions alone. The activation of NLRP3, caspase-1 and subsequent release of IL-1 β is described in greater detail in **section 1.7**. Several studies have hypothesised that both CoCr particles and metal ions can lead to NLRP3 activation *in vitro* (Li and Zhong, 2014; Samelko *et al.*, 2016; Ferko and Catelas, 2018). The inflammasome pathway requires sensing of DAMPs such as ATP or lysosomal destabilisation following stimulation from an initial PAMP (e.g. LPS). Therefore, CoCr particles were investigated to see whether they primarily act as a PAMP primary stimulus or as a DAMP 'danger signal' inducer of NLRP3 activation.

Firstly, THP-1 macrophages were primed with CoCr particles for 23 hours followed by stimulation with the DAMP inducer, ATP for 1 hour. IL-1 β expression was used as a marker of NLRP3 activation. However, IL-1 β expression and secretion were not significantly increased under these conditions. These findings were interesting, as MSD protein secretion analysis had shown CoCr particle-treated THP-1 macrophages demonstrated increased IL-1 β expression even without further ATP stimulation. This highlights potential differences between using different techniques for measuring protein concentrations i.e. MSD versus ELISA. It cannot be ruled out that under the artificial conditions of cell culture (e.g. the differentiation of cells using PMA), this provides sufficient 'PAMP stimulus' to increase IL-1 β expression when THP-1 macrophages are then dosed with CoCr particles. It has been shown PMA can play the priming role in THP-1 cells as demonstrated by increased expression of pro-IL-1 β (Song *et al.*, 2017). It may be plausible during the 'rest period' of THP-1 cell activation when PMA is removed, the reversal of over-activation differs each time so cells are in altered states of activation prior to stimulation.

To determine whether CoCr particles play a role in the second NLRP3 activation step (i.e. act as a DAMP inducer), THP-1 macrophages were primed with LPS for 23 hours followed by 1 hour of stimulation with CoCr particles. CoCl₂ was also included in the experimental set up to compare responses. There was no significant difference between IL-1 β expression between cells treated with LPS alone and those further

stimulated with either CoCr particles or CoCl₂. This would suggest CoCr particles and cobalt ions do not act as a DAMP inducer following PAMP stimulation. This contrasts with findings by Samelko *et al.* who hypothesised that CoCr particles induce lysosomal damage, subsequent cathepsin B release and therefore activate NLRP3 (Samelko *et al.*, 2016).

However, for any conclusions to be made, this work requires much further investigation. For example, the expression of cytosolic pro-IL-1 β expression by western blotting would be beneficial to determine whether stimulants are providing the initial 'priming' signal. Furthermore, assessing IL-18 (and pro-IL-18) as an additional marker of NLRP3 activation would also confirm findings shown by IL-1 β . Assessment of caspase-1 activation could also provide further insight into the activation of the NLRP3 inflammasome pathway.

4.5.1 Future work

One important factor to consider was the CoCr particles used in this part of the study. For all experiments, particles generated in sterile water in the six-station pin-on-plate wear simulator were used for dosing cells. As **Chapter 3** demonstrated, although these do not differ morphologically from those generated in the sterile single-station pin-on-plate wear simulator, they are not generated in the mostly 'clinically-relevant' lubricant which would be containing FBS. Furthermore, ions released from particles during their generation are lost when sterilising prior to cell treatments. It would be important to repeat all investigations using particles generated in the single-station wear simulator to provide further clinical relevance.

This work has also focussed on one cell line, THP-1, which although is a good model for *in vitro* investigations into cell responses to CoCr particles, further cell lines (e.g. osteoblasts) and primary cells would need to be assessed to make firmer conclusions. Primary cells (such as PBMCs) offer better *in vivo* representation and physiological relevance when compared to cell lines. Cell lines, particularly at higher passages, can have a varied phenotype and genotype meaning results obtained can be difficult to fully translate to humans. Therefore, the use of primary cells in future experiments is of great importance to determine whether similar effects can be replicated. However, as it is known some patients appear to be more sensitive to ARMD than others, the

use of primary cells such as PBMCs may prove difficult to draw conclusions from as it is likely results would be variable. Therefore, for preliminary results presented here, cell lines were a suitable model to obtain consistent findings which should be repeated using human primary cells to replicate key findings.

The small molecule antagonist, CLI-095 was the only TLR4 inhibitor which was fully investigated regarding CoCr particle-mediated inflammation. Therefore, the use of other TLR4 inhibitors such as neutralising antibodies would provide additional confirmation that TLR4 plays a central role in the upregulation of pro-inflammatory chemokines and cytokines in response to CoCr particles. By investigating several TLR4 inhibitors this would give an improved overview of the efficacy of each antagonist and which exact part of TLR4 should be targeted for targeting CoCr particle-mediated responses.

To further understand the role of the NLRP3 inflammasome in CoCr particle-mediated responses, much more detailed investigations are required into each stage of NLRP3 activation. As previously discussed, this would involve assessing the expression of cytosolic pro-IL-1 β and pro-IL-18 as well as the cleavage of caspase-1 and its activity.

4.5.2 Conclusion

The primary aim of this chapter was to determine which inflammatory cytokines and chemokines are upregulated in response to CoCr particle-mediated inflammation and which pathways are potentially involved in initiating this response.

Overall, results suggest it is unlikely that inflammatory effects elicited by CoCr particles and metal ions are limited to the activation of one specific pathway. The results demonstrated in this part of the study suggest a central role for the TLR4 pathway, particularly cellular effects from cobalt ions *in vitro*. In contrast, preliminary studies regarding the NLRP3 inflammasome, CoCr particles did not appear to directly influence its activation as measured by IL-1 β expression. However, it is probable other pathways are involved and CoCr particles may well act as both a PAMP and a DAMP rather than exclusively one or the other. For example, cobalt ions released from CoCr particles appear to primarily act through TLR4 activation to initiate an immune response whereas the particles themselves may initiate a more general stress response by enhancing ROS production and causing lysosomal destabilisation.

Chapter 5 : Functional Effects of CoCr particles *in vitro* and Translation to Patient Tissue Following Hip and Knee Revision Surgery

5.1 Introduction

The data presented in **Chapter 4** demonstrate CoCr particles can alter the expression and secretion of various chemokines and cytokines in THP-1 macrophages which in turn regulate a number of different immune functions. For example, as discussed in **section 1.6.3**, the process of immune cell migration and infiltration into tissues is initiated by inflammatory cytokines and chemokines, causing leukocyte recruitment. Furthermore, TLR4 activation increases expression of adhesion molecules such as ICAM-1 and VCAM-1 which bind to integrins (LFA-1 and VLA-4) on the cell surface of the recruited leukocytes resulting in transendothelial migration of immune cells into local tissues (Sawa *et al.*, 2008).

Inflammatory pseudotumours observed in patients who have received MoM implants are histologically associated with increased inflammatory cell infiltration, particularly macrophages as well as lymphocytes (i.e. ALVAL) and a small population of granulocytes (e.g. neutrophils) (Pandit *et al.*, 2008; Campbell *et al.*, 2010; Paukkeri *et al.*, 2016). For example, in a study which examined the histology of periprosthetic hip tissues from revised MoM implants for aseptic loosening, 88% of patients displayed macrophage infiltration whereas only 30% had moderate to high ALVAL scores (Phillips *et al.*, 2014). In this study, a collection of soft tissue was collected from patients undergoing both hip and knee revision surgery for various reasons. Therefore, histological analysis was performed to determine inflammatory infiltrate for the presence of both macrophages and T cells.

The expression of ICAM-1 and VCAM-1 are crucial for promoting the interactions required between endothelial and leukocytes to elicit an effective immune response, particularly leukocyte extravasation and immune cell infiltration. Their expression is usually tightly regulated to prevent unwanted stimulation of the inflammatory response. However, in response to pathogens, their expression is increased to promote this process. Previous work has shown the effect of CoCl₂ on HMEC-1 endothelial cells, which resulted in significantly increased expression of ICAM-1 (Anjum *et al.*, 2016). Furthermore, studies have demonstrated increased ICAM-1 and VCAM-1 expression

in primary endothelial cell lines treated with cobalt ions and CoCr nanoparticles (Ninomiya *et al.*, 2013; Alinovi *et al.*, 2015). The expression of ICAM-1 and VCAM-1 in HMEC-1 cells following treatment with CoCr particles generated in **Chapter 3** was assessed. Furthermore, a chemotaxis assay using a transwell insert system was set up to determine endothelial activation with CoCr particle treatment and whether this enhanced neutrophil migration towards a chemokine gradient.

It was also hypothesised CoCr particles and subsequent up-regulated cytokine and chemokine expression can influence bone homeostasis (i.e. the balance of osteoclastogenesis and osteoblast formation) and cell migration of the cell types involved in these processes. Therefore, the osteoblast-like cell line, MG63, was stimulated with CoCr particles and used in a migration wound healing assay to analyse migration properties.

5.2 Aims and Objectives

The aim of this chapter was to assess the effect of CoCr particles on an endothelial cell line, HMEC-1, including adhesion molecule expression and activation to enhance transendothelial migration of neutrophils. The migratory properties of MG63 cells were used as a model of bone homeostasis, proliferation and metabolic activity. Finally, a small collection of soft tissue from patients undergoing revision hip and knee surgery was analysed by haematoxylin and eosin (H&E) staining for the presence of immune cell infiltration and the phenotype of infiltrate determined by IHC.

5.2.1 Objectives

- To investigate the effect of CoCr particles on HMEC-1 cells, including cell viability, proliferation and internalisation of particles
- To establish the effect of CoCr particles on adhesion molecule expression in HMEC-1 cells
- To investigate the effect of CoCr particles on neutrophil chemotaxis
- To investigate the histology of patient derived soft tissue using immunohistochemistry to determine inflammatory cell phenotype

- To analyse the migration properties of MG63 cells following CoCr particle treatment

5.3 Specific Methods

5.3.1 Chemotaxis assay

Chemotaxis of neutrophils was evaluated using a transwell system in a protocol optimised by Dr Georgie Wilkins, Newcastle University, UK (**Figure 5.1**). Transwells with 3µm pores (Sigma Aldrich, USA) were coated with HMEC-1 cells to replicate the endothelial barrier. Approximately 250,000 HMEC-1 cells were seeded per transwell and allowed to grow to confluency for 48 hours. The HMEC-1 cells were then stimulated for 24 hours with either 100ng/ml LPS or CoCr particles (50µm³ per cell). The lower chamber was then blocked with 2% BSA in PBS then replaced with 30nM IL-8 (R&D Systems, USA) diluted in serum free media. A chemokinesis control, in which 30nM IL-8 was also added to the upper chamber, was included to determine direction of chemotaxis. Neutrophils were isolated from healthy human blood and kindly provided by Mr Jonathan Scott, Newcastle University, UK. Following a 1 hour rest period in serum free medium (RPMI-1640 medium containing 0.1% BSA), approximately 200,000 neutrophils were added to the upper chamber and allowed to migrate for 2 hours at 37°C. Any neutrophils which had adhered to the lower chamber were firstly washed with PBS, detached with Accutase™ (Biolegend, USA) then counted using Absolute Countbright beads™ (ThermoFisher Scientific, UK) by flow cytometry on the FACS Canto II (**Figure 5.2**). The chemotactic index was calculated as described in **Figure 5.2E** by normalising the number of migratory neutrophils in treatments (i.e. LPS and CoCr particles) to untreated controls relative to the total number of cells added to the upper chamber.

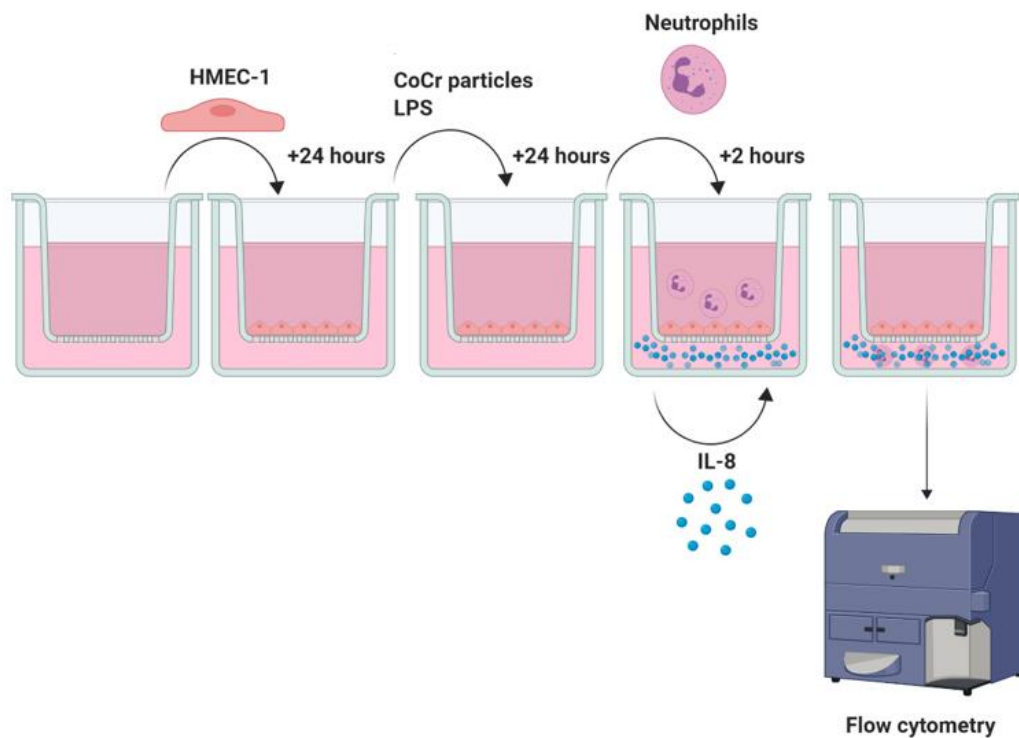
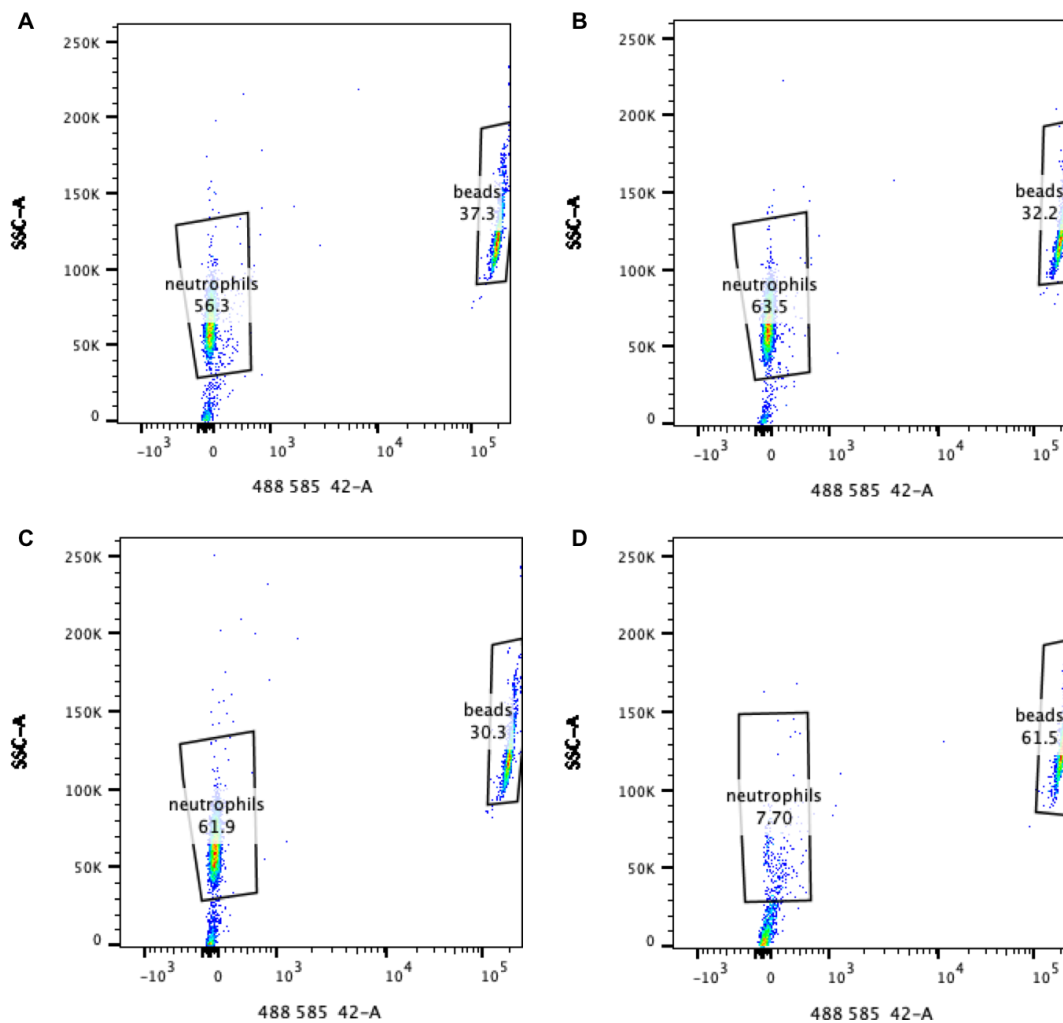


Figure 5.1 Neutrophil chemotaxis protocol

Approximately 250,000 HMEC-1 cells were seeded into a 3 μ m transwell and grown to confluency over 48 hours. The cells were then either treated with CoCr particles (50 μ m³ per cell) or LPS (10ng/ml) for 24 hours or left untreated. The lower chamber was blocked with 2% BSA in PBS then replaced with 30nM IL-8. Approximately 200,000 neutrophils were then added to the upper chamber and allowed to migrate for 2 hours. Neutrophils which had migrated to the lower chamber could then be detached and counted using absolute count bright beads on the FACs Canto II. Image created using Biorender.



E

$$\text{Number of migratory neutrophils} = (\text{number of cell events/number of bead events})^* (\text{number of beads added/volume of sample } (\mu\text{l}))$$

Figure 5.2 Migratory neutrophil counting using absolute count bright beads by flow cytometry

For counting of migratory neutrophils, cells were detached from the lower chamber of the transwell, pelleted and re-suspended in 200µl FACS buffer. To the cell suspension, 30µl Absolute Countbright beads™ were added. The suspension was then counted by flow cytometry. **(A)-(D)** Gating strategy to identify counting beads and neutrophil population. **(A)** Untreated **(B)** LPS **(C)** CoCr particles **(D)** Chemokinesis control. **(E)** Equation to calculate total number of migratory neutrophils based on total counting bead events. Graphs are representative of 2 independent experiments.

5.3.2 Haematoxylin and eosin (H&E) staining

Human soft tissue was collected from patients undergoing hip and knee revision surgery at the Freeman Hospital, Newcastle. This collection was approved by the Newcastle Academic Health Partners Bioresource (REC 12/NE/0395). All patients gave their informed consent for collection of the tissue. The tissue was retrieved fresh, as soon as possible following surgery, and kept on ice. All sections were formalin fixed, processed and paraffin embedded using standard procedures.

Sections were stained to assess cellular infiltration using haematoxylin (Sigma Aldrich, USA) for 60 seconds then washed thoroughly in tap water. Slides were then blued in Scott's tap water for 20 seconds to blue the nuclei and again washed in tap water. Sections were then stained with Eosin (Sigma Aldrich, USA) for 30 seconds and then washed in tap water. Slides were then dehydrated through graded alcohols (70%, 95% and 99% ethanol), mounted using Dibutylphthalate Polystyrene Xylene (DPX) and left to dry at room temperature overnight.

5.3.3 Immunohistochemistry

IHC is a staining technique used to visualise protein distribution (antigens) in cells of tissues. Tissues can be fixed, stained with specific antibodies and visualised by microscopy.

For this study, IHC was performed on formalin-fixed paraffin-embedded (FFPE) human soft tissue retrieved from patients undergoing hip and knee revision surgery as described in **section 5.3.2**. FFPE tissue sections were cut to a thickness of 3µm onto a glass slide coated with 3-aminopropylthriethoxysilane (APES) to help tissue adhere to the slides. Slides were then incubated at 37°C for 24 hours to further help sections adhere to slides due to the high content of fat in the tissue used.

Slides were de-waxed in xylene for 5 minutes then rehydrated through graded alcohols (99%, 95% and 70% ethanol) and washed in tap water. Slides were then blocked with 1.5% hydrogen peroxide for 10 minutes, prior to antigen retrieval. Both primary antibodies used in this study had been previously optimised by Mrs Barbara Innes, Newcastle University, UK for both concentration and antigen retrieval method (**Table 5.1**). Antigen retrieval was performed using citrate buffer (pH 6) in a pressure cooker.

Once at boiling point, slides were placed inside the cooker and were incubated for 2 minutes once the cooker had reached pressure, before rapidly cooling in water.

Slides were next blocked for 10 minutes in normal horse blocking serum (Vector Laboratories) to block endogenous peroxidase and alkaline phosphatase activity. Diluted primary antibodies were then added to all appropriate sections for 1 hour. A negative control section with no primary antibody (tris buffered saline (TBS) only) was also included. Staining was continued using the ImPRESS™ HRP Universal Antibody Polymer Detection Kit (Vector Laboratories, USA) according to the manufacturer's protocol. Specifically, the secondary antibody was added to each section for 30 minutes. All kit components and antibodies were prepared and diluted in TBS. In between all steps, slides were washed 3 times for 5 minutes in TBS.

The Vector® 3, 3'-diaminobenzidine (DAB) peroxidase substrate kit (Vector Laboratories, USA) was then used as a substrate, to develop colour, according to the manufacturer's protocol. Once colour was developed, slides were washed thoroughly in tap water, counterstained in haematoxylin for 60 seconds and blued in in alkaline solution for 20 seconds. Slides were then dehydrated through graded alcohols (70%, 95% and 99% ethanol) and finally placed in xylene. Slides were mounted using DPX and left to dry at room temperature overnight. In all cases, tonsil tissue was used as a positive control for immune cell markers.

Table 5.1 Primary antibodies used in immunohistochemistry

Primary antibodies were diluted in tris-buffered saline (TBS) (pH 7.6)

Target Protein	Dilution	Description	Clone	Antigen Retrieval	Source
CD3	1:20	Monoclonal mouse anti-human	PS1	Citrate	Leica Biosystems, USA
CD68	1:100	Monoclonal mouse anti-human	KP1	Citrate	Dako, USA
Ki67	1:300	Polyclonal rabbit anti-human	Polyclonal	Citrate	Novus Biological, USA

5.3.3.1 Dual colour immunohistochemistry

To determine whether cells stained positive for CD3 were in fact proliferating, dual coloured IHC was employed to visualise both CD3 and Ki67 (nuclear proliferation marker) staining in the same tissue section. As both antibodies require the same optimal antigen retrieval step (using citrate buffer), dual coloured IHC was possible for CD3 and Ki67.

Sections were stained using the ImpRESS™ HRP Universal Antibody Polymer Detection Kit as described in **section 5.3.3** for the first primary antibody according to the manufacturer's protocol and developed using the Vector® 3, 3'-diaminobenzidine (DAB) peroxidase substrate kit. Slides were then washed with TBS before staining could continue for the second primary antibody. Avidin-Biotin block was then used and followed by with the ImmPRESS™-AP Alkaline Phosphatase Polymer Detection Kit (Vector Laboratories, USA) according to the manufacturer's instructions. An AP system was used in conjunction with the peroxidase kit to prevent enzyme cross-reactivity and prevent false labelling. Stains were developed using the Vector® Blue Substrate Alkaline Phosphatase Kit (Vector Laboratories, USA) following the manufacturer's instructions. To prevent confusion between colours, the haematoxylin step was

omitted. Sections were aqueous mounted using Faramount aqueous mounting medium (Dako, USA). Single-stained slide controls for each antibody were included to demonstrate a lack of epitope masking as well as no primary antibody controls.

5.3.4 Cell migration assay

Cell migration was assessed by using a wound healing scratch assay with MG63 cells in which 100,000 cells were seeded and grown to approximately 80-90% confluency for 72 hours to create a monolayer. A scratch of approximately 600 μ m was created in each well by scratching down the middle of the monolayer of cells with a pipette tip, visible under light microscope. Cells were then washed with PBS and media replaced containing either 100ng/ml LPS, 0.25mM CoCl₂ or 50 μ m³ per cell of CoCr particles. The closure of the gap was then analysed over 48-hours. Images were analysed using ImageJ analysis software. Cell migration was expressed as a percentage of the initial wound area measured at 0 hours to give a percentage of closure at a given time point (24 or 48 hours).

5.4 Results

5.4.1 Effect of CoCr particles on human microvascular endothelial cells

5.4.1.1 Cell viability

HMEC-1 cells were treated with varying concentrations of CoCr particles (0.5 to 50 μm^3 per cell) for either 24 or 48 hours (**Figure 5.3**). Cell viability was assessed using trypan blue exclusion as described in **section 2.5.1**. Viability was calculated as a percentage difference between untreated cells (100% viable) and treated cells. Following 24 hours of stimulation, viability was not significantly affected at the lowest concentration of 0.5 μm^3 particles per cell ($p=0.2050$) but was significantly decreased at both 5 and 50 μm^3 particles per cell (both $p<0.0001$) (**Figure 5.3A**). However, following 48 hours of exposure, all concentrations of CoCr particles significantly decreased HMEC-1 cell viability (0.5 μm^3 particles per cell; $p=0.0023$, 5 and 50 μm^3 particles per cell; both $p<0.0001$) (**Figure 5.3B**).

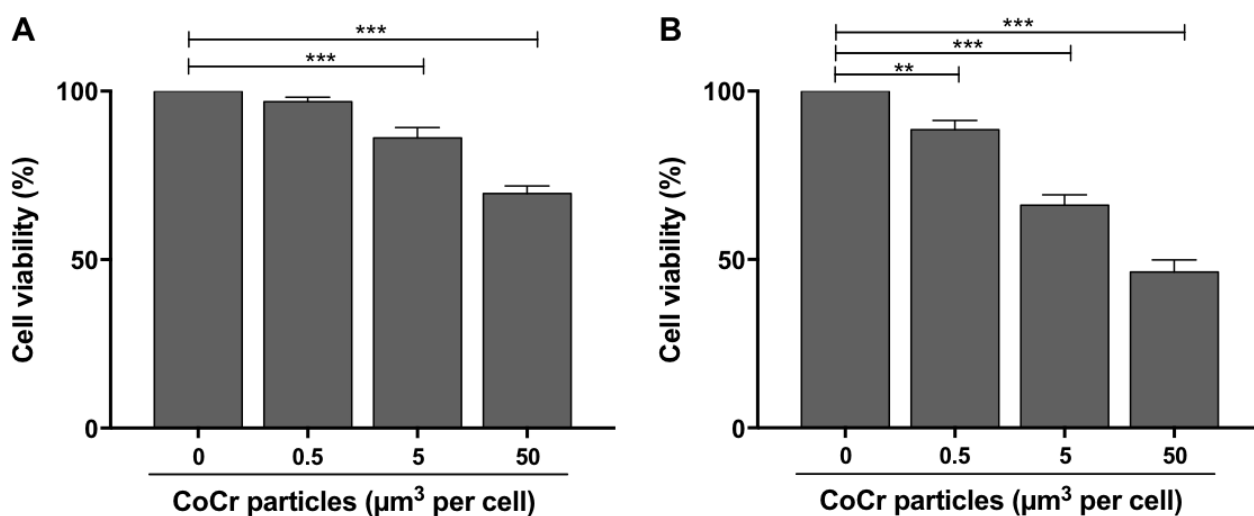


Figure 5.3 HMEC-1 cell viability following CoCr particle treatment determined by trypan blue staining

HMEC-1 cells were assessed for viability following stimulation with varying concentrations of CoCr particles (0.5 to 50 μm^3 per cell) for **(A)** 24 hours and **(B)** 48 hours using trypan blue staining. Data was normalised to 100% viability in untreated cells. Graph is representative of 3 independent experiments. Statistical significance was calculated by one-way ANOVA with Dunnett's multiple comparisons test comparing treated samples to the untreated control.

5.4.1.2 XTT proliferation assay

The effect of CoCr particles on HMEC-1 proliferative capacity was assessed using the XTT assay as described in **section 2.5.2**. Cells were treated with varying concentrations of CoCr particles (0.5 to 50 μm^3 per cell) for either 24 hours or 48 hours and proliferation assessed 6 hours after the addition of the XTT reagent (**Figure 5.4**).

Following 24 hours of stimulation with CoCr particles, there was no significant difference in proliferation of HMEC-1 cells at both 0.5 and 50 μm^3 particles per cell ($p=0.2109$ and $p=0.3598$, respectively). However, treatment with 5 μm^3 particles per cell resulted in a significant increase in proliferation ($p=0.0339$) (**Figure 5.4A**).

HMEC-1 cells which were treated for 48 hours with CoCr particles displayed a dose dependent loss of proliferation (**Figure 5.4B**). Although there was no significant difference in cell proliferation at either 0.5 or 5 μm^3 particles per cell ($p=0.9991$ and $p=0.1215$, respectively), stimulation with 50 μm^3 particles per cell significantly decreased proliferation of HMEC-1 cells ($p=0.0015$).

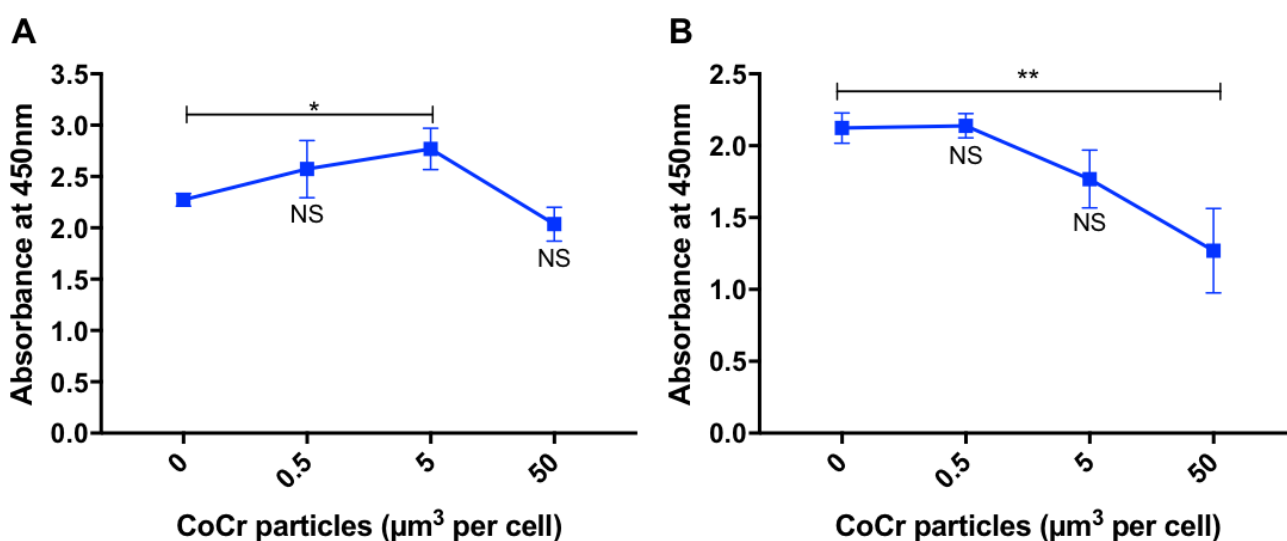


Figure 5.4 Proliferation of HMEC-1 cells following exposure to CoCr particles

HMEC-1 cells were stimulated for either **(A)** 24 hours or **(B)** 48 hours with CoCr particles prior to the addition of XTT reagent for a further 6 hours to assess proliferation. Graph is representative of 3 independent experiments. Statistical significance was calculated by one-way ANOVA with Dunnett's multiple comparisons test comparing treated samples to the untreated control.

5.4.1.3 Internalisation of CoCr particles

HMEC-1 cells were imaged using TEM as described in **section 2.6** to assess whether an endothelial cell line could also internalise CoCr particles as shown previously by THP-1 cells. Untreated cells are shown in **Figure 5.5**. **Figure 5.5A** shows numerous cells forming a monolayer using a relatively low magnification (1200X). Individual cells can be observed which have classic endothelial cell structure with little presence of vacuoles or lysosomes and a large nucleus.

Following 24 hours' stimulation with CoCr particles ($50\mu\text{m}^3$ per cell), **Figure 5.6** clearly shows the internalisation of CoCr particles within phagocytic vacuoles. **Figure 5.6C** shows a particularly large vacuole containing CoCr particles which has potentially formed due to the fusion of several phagosomes, encompassing much of the single cell cytoplasmic volume. However, in comparison to the THP-1 cells, the number of phagocytic vacuoles appears to be fewer (**see Figure 4.7**).

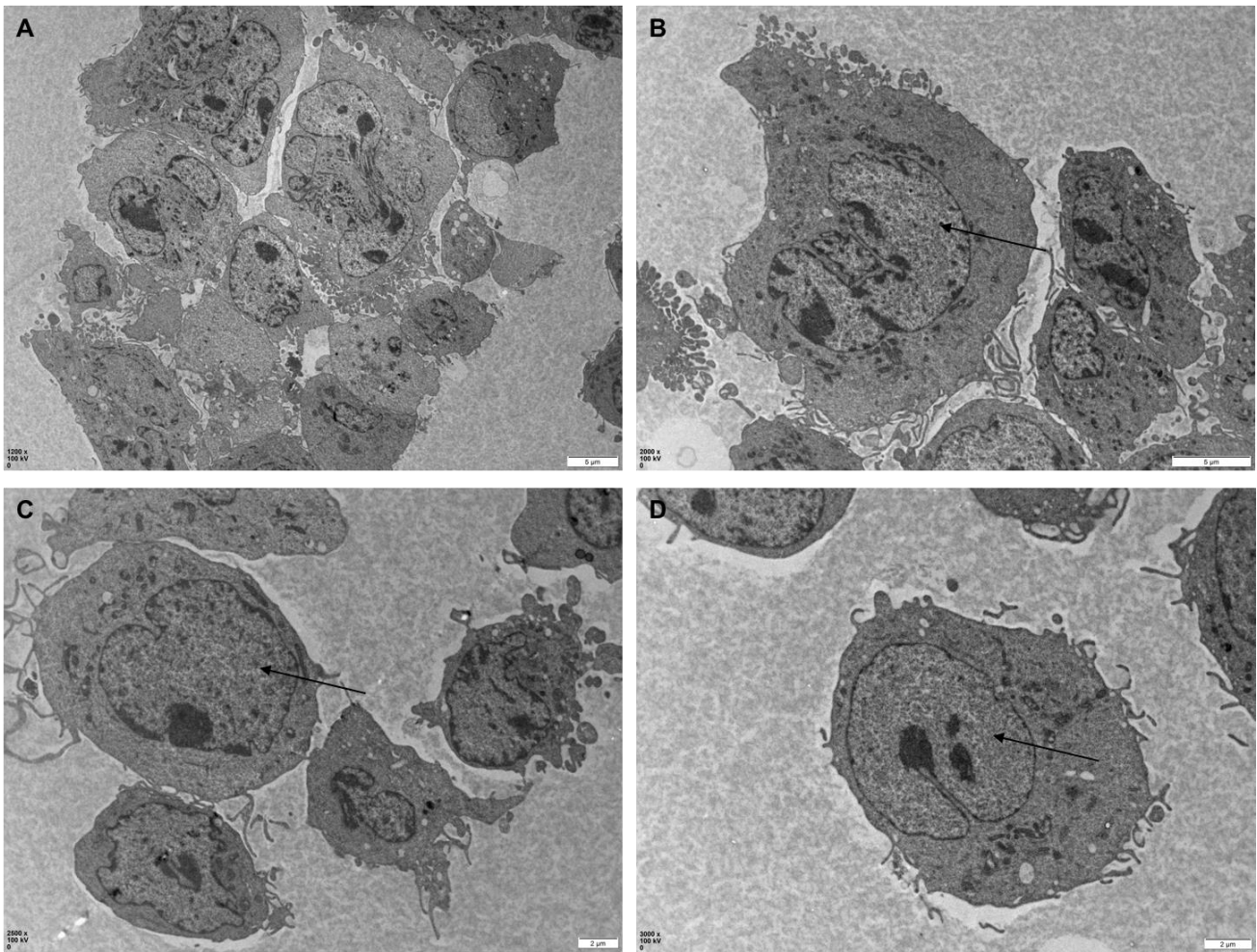


Figure 5.5 Transmission electron microscopy of untreated HMEC-1 cells

Representative TEM images of untreated HMEC-1 cells. Images show classic HMEC-1 individual endothelial cell structure as well as the formation of monolayers and interaction between cells **(A)**. Arrows indicate HMEC-1 cell nuclei. Scale bars represent either 5 μ m for **(A)-(B)** or 2 μ m **(C)-(D)**.

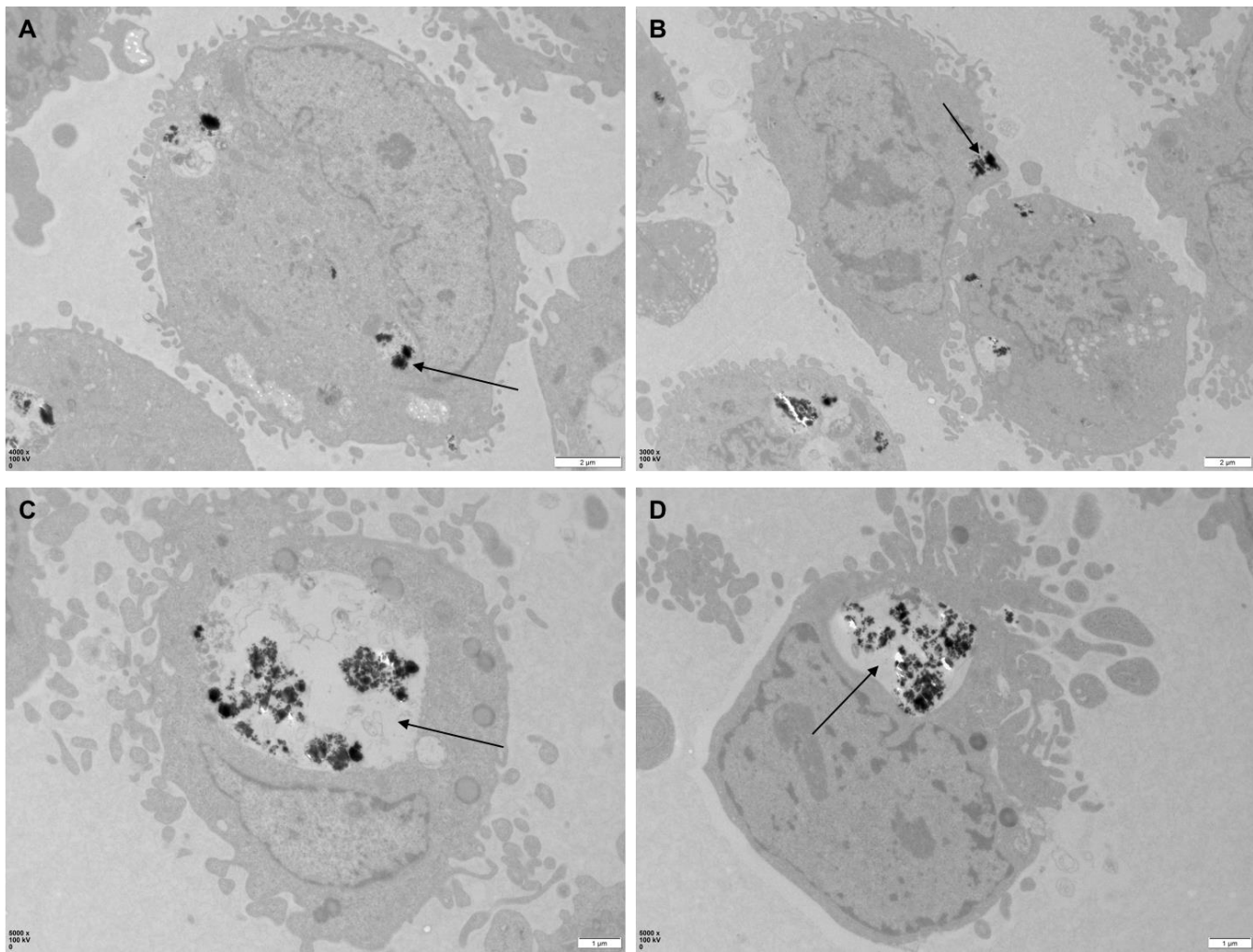


Figure 5.6 Transmission electron microscopy of CoCr particle treated HMEC-1 cells

Representative TEM images of HMEC-1 cells treated with CoCr particles ($50\mu\text{m}^3$ per cell). **(A)-(D)** Arrows point to examples of aggregates and agglomerates of CoCr particles within distinct membrane bound vacuoles. Scale bars represent either $2\mu\text{m}$ **(A)-(B)** or $1\mu\text{m}$ **(C)-(D)**.

5.4.2 Effect of CoCr particles on adhesion molecule expression

The effect of CoCr particles on expression of adhesion molecule expression in HMEC-1 cells was investigated as ICAM-1 and VCAM-1 expression in response to stimuli are frequently studied in endothelial cell lines (Munoz-Vega *et al.*, 2018).

HMEC-1 cells were treated with $50\mu\text{m}^3$ CoCr particles per cell despite the results from the cell viability and proliferative XTT assay having shown potentially cytotoxic effects and a reduction in cell proliferation. This was to keep challenges consistent with previous investigations using THP-1 macrophages in **Chapter 4**. Following 24 hours' stimulation with CoCr particles, HMEC-1 cells were analysed for *ICAM1* and *VCAM1*

expression by qRT-PCR (**Figure 5.7**). Treatment with CoCr particles significantly increased the expression of both *ICAM1* ($p=0.0004$) and *VCAM1* ($p=0.0009$) compared to untreated control HMEC-1 cells.

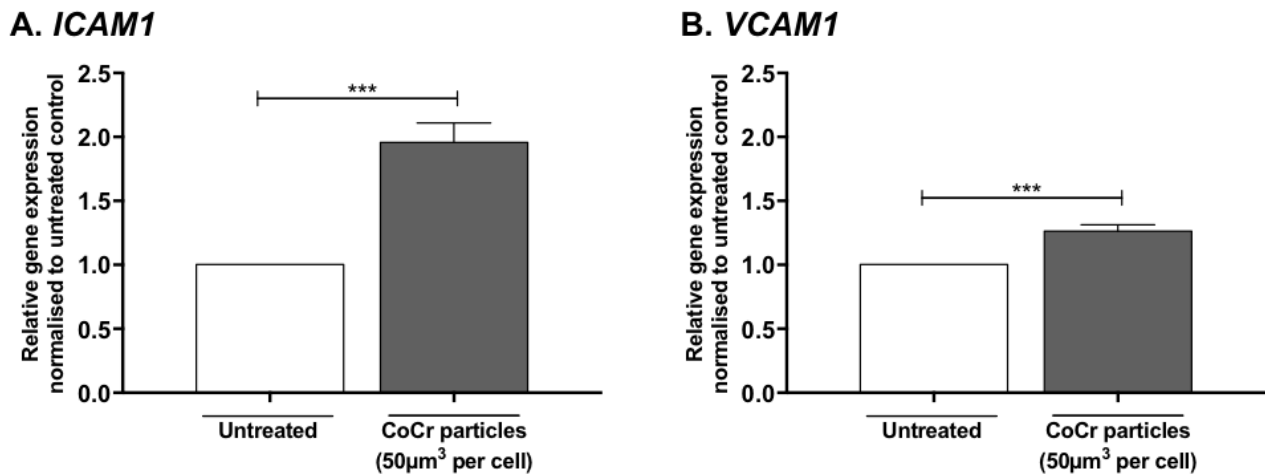


Figure 5.7 Effect of CoCr particles on ICAM1 and VCAM1 expression

HMEC-1 cells were stimulated with 50µm³ CoCr particles per cell for 24 hours then **(A)** *ICAM1* and **(B)** *VCAM1* expression analysed by qRT-PCR. Gene expression normalised to untreated control, set to 1. Graphs are representative of three independent experiments. Statistical significance was calculated by an unpaired Student's *t*-test comparing the treated sample to the untreated control.

5.4.3 CoCr particle-mediated neutrophil migration

The results shown in **section 5.4.2** demonstrate increased expression of *ICAM1* and *VCAM1* in response to CoCr particles. It has been previously shown that cobalt ions can up-regulate the expression of the adhesion markers ICAM-1 and VCAM-1 (Anjum *et al.*, 2016). Furthermore, cobalt ions can also increase the recruitment of inflammatory cells *in vitro* (Lawrence *et al.*, 2016a). Therefore, for this part of the study, the effect of CoCr particles on the endothelium and subsequent chemotaxis of neutrophils was investigated as described in **section 5.3.1**. LPS was used a positive control and a chemokinesis control was also included. HMEC-1 cells seeded onto transwell inserts were stimulated with either CoCr particles (50µm³ per cell) or LPS (10ng/ml) for 24 hours. Neutrophils were then added to the upper chamber of the transwell and 30nM IL-8 to the lower chamber (and also the upper chamber of the chemokinesis control) and incubated for 2 hours at 37°C. Migratory neutrophils were

counted by flow cytometry using Absolute Countbright beads™ and chemotactic index calculated (**Figure 5.8**). Treatment with both LPS and CoCr particles resulted in a significant increase in neutrophil chemotaxis compared with untreated control cells (p=0.0198 and p=0.0259, respectively).

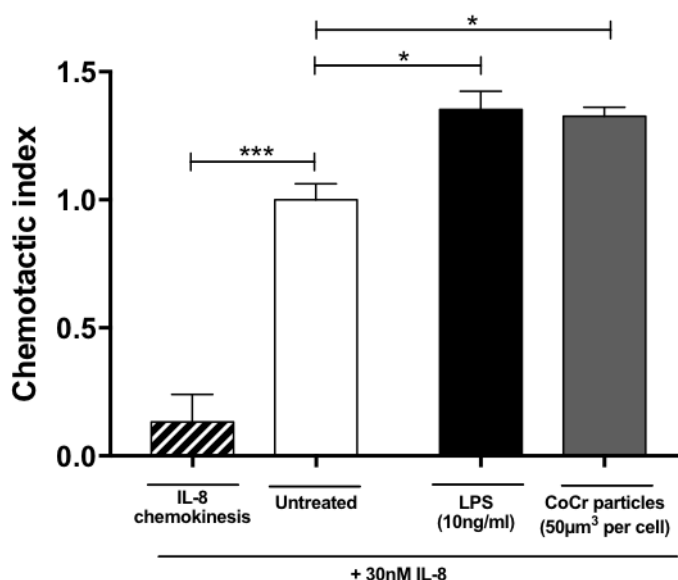


Figure 5.8 Trans-endothelial chemotaxis of neutrophils towards IL-8 following stimulation of HMEC-1 with CoCr particles

HMEC-1 cells were seeded onto 3µm transwells for 48 hours then stimulated with either LPS (10ng/ml) or CoCr particles (50µm³ per cell) for 24 hours. Neutrophils were then added to the upper chamber of the transwell and 30nM IL-8 added to the lower chamber (and the upper of the chemokinesis control) and incubated for 2 hours at 37°C. Migratory neutrophils were counted using Absolute Countbright Beads™ and analysed by flow cytometry. Graphs are representative of 2 independent experiments. Statistical significance was calculated by one-way ANOVA with Dunnett's multiple comparisons test comparing treated samples to the untreated control.

5.4.4 Periprosthetic soft tissue analysis from patients undergoing hip and knee revision surgeries

Soft tissue samples from regions adjacent to implanted total hip or knee replacements were collected during revision surgery as part of a collection described in **section 5.3.2**.

5.4.4.1 Patient clinical information

Of the soft tissue collected from patients undergoing hip and knee revision surgeries, 11 in total were analysed for inflammatory cell infiltrate by H&E staining and phenotyping of the infiltrate by IHC. The clinical characteristics of the patient cohort are summarised in **Table 5.2**. All primary operations were performed for treatment of osteoarthritis.

Of the samples analysed, seven were taken from total hip revision surgeries (63.66%) and four from total knee revisions (36.36%). Eight of the eleven patients were male (72.73%) and 27.27% were female. The average age of patients was 66 (range: 43-87), and the mean duration of implant survival was 97 months (approximately 8 years) (range: 27 to 240 months). The reasons for revision were varied, the most common being aseptic loosening (4/11) followed by other isolated reasons such as recurrent dislocation (2/11), infection (1/11), pain (1/11), initial surgery error (1/11), chondral degeneration (1/11) and hip avulsion fracture (1/11). Of the hip revisions, two were MoM implants (including one resurfacing) (2/6) and four were MoP (4/6). The knee implants used for primary surgery were either the DePuy Press Fit Condylar® (2/5) or the Stryker Triathlon® (3/5), both of which contain cobalt-chrome components. There was limited clinical information available. Two patients had recorded cobalt and chromium serum tests, both of which were below the acceptable range dictated by the MHRA (119 nmol/L cobalt or 134 nmol/L chromium). Both patients had MoM implants for their primary surgery.

Table 5.2 Summary of patient clinical information

Patient ID	Hip/Knee Revision	Implant Type	Gender	Age of Patient	Implant <i>in-situ</i> time (months)	Cobalt/Chromium Test (nmol/L)	Reason for revision
1	Right Hip	MoM (resurfacing)	Male	51	96	48.2/31.8	Aseptic loosening
2	Left Hip	MoM	Male	80	240	12.3/12.3	Aseptic loosening
3	Left Hip	MoP	Female	63	30	N/A	Recurrent dislocation
4	Right Hip	MoP	Male	83	180	N/A	Aseptic loosening
5	Left Knee	Press fit condylar	Male	76	120	N/A	Aseptic Loosening
6	Right Knee	Triathlon	Female	62	102	N/A	Infection
7	Left Knee	Triathlon	Male	61	35	N/A	Pain following re-surfacing of the patella
8	Left Knee	Press fit condylar	Male	43	27	N/A	Initial surgery unsuccessful – not securely implanted
9	Right Knee	Triathlon	Male	44	98	N/A	Chondral degeneration in the tibiofemoral
10	Left Hip	MoP	Female	74	38	N/A	Post-traumatic avulsion of hip
11	Left Hip	MoP	Male	87	108	N/A	Recurrent dislocation

5.4.4.2 Histological findings of periprosthetic soft tissue following revision surgery, H&E staining

To visualise immune cell infiltrate in the periprosthetic soft tissue, H&E staining was performed on FFPE sections as described in **section 5.3.2**. Representative images of staining are shown in **Figure 5.9 to Figure 5.12**. Most cases studied, seven out of eleven (63.64%), demonstrated large areas of immune cell infiltration (patients #1, 2, 3, 5, 6, 8 and 10). However, in three of the eleven samples analysed (36.36%), few immune cells were observed in the soft tissue, as shown in representative images in **Figure 5.12** (patients #4, 7, 9 and 11). Generally, there was considerable variability in the number and arrangement of inflammatory cells between samples.

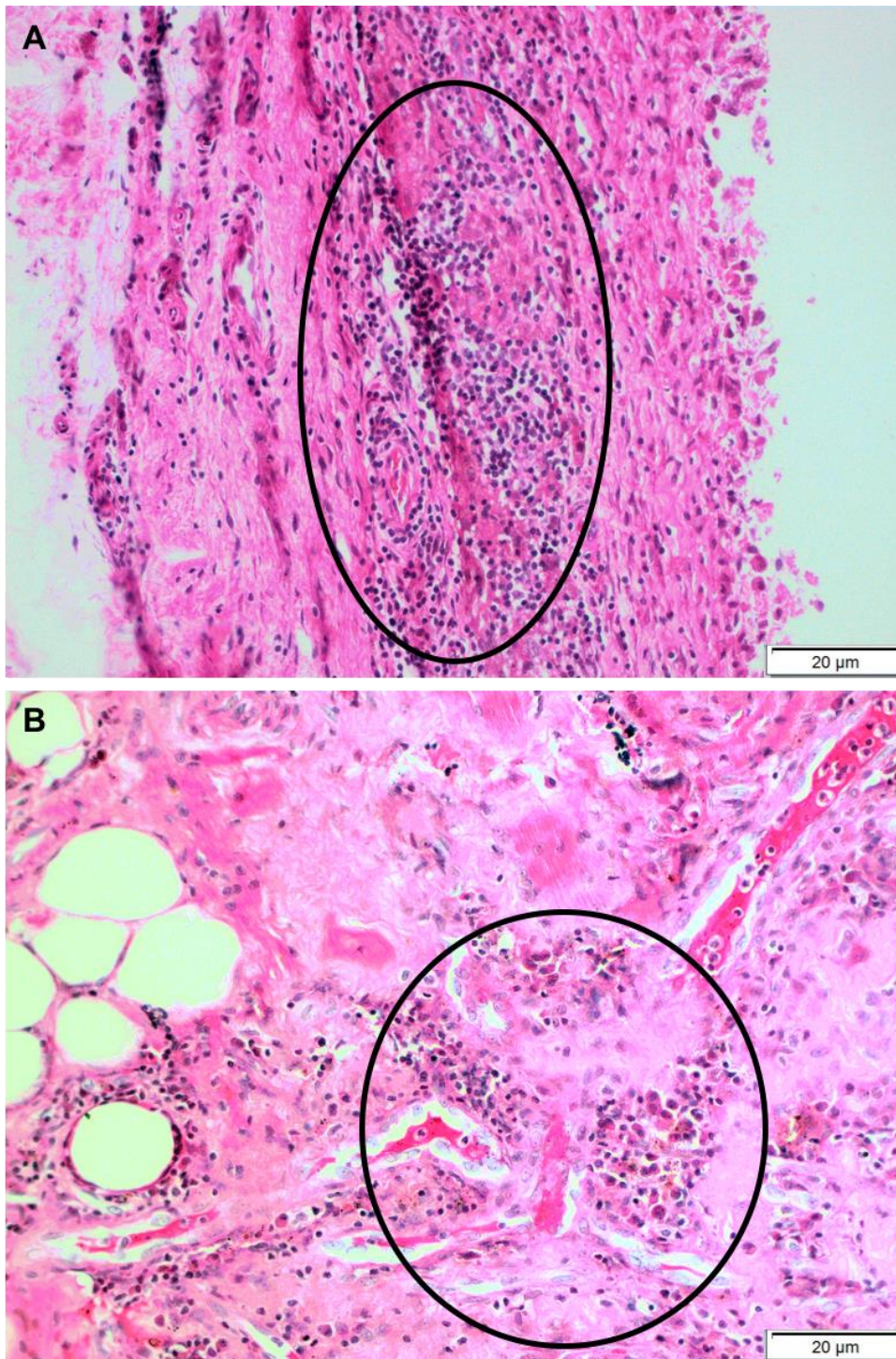


Figure 5.9 Representative H&E images illustrating inflammatory infiltration I

Representative H&E staining in FFPE patient tissues showing medium to high immune cell infiltrate **(A)** (x100) **(B)** (x200). Highlighted areas indicate presence of immune cells.

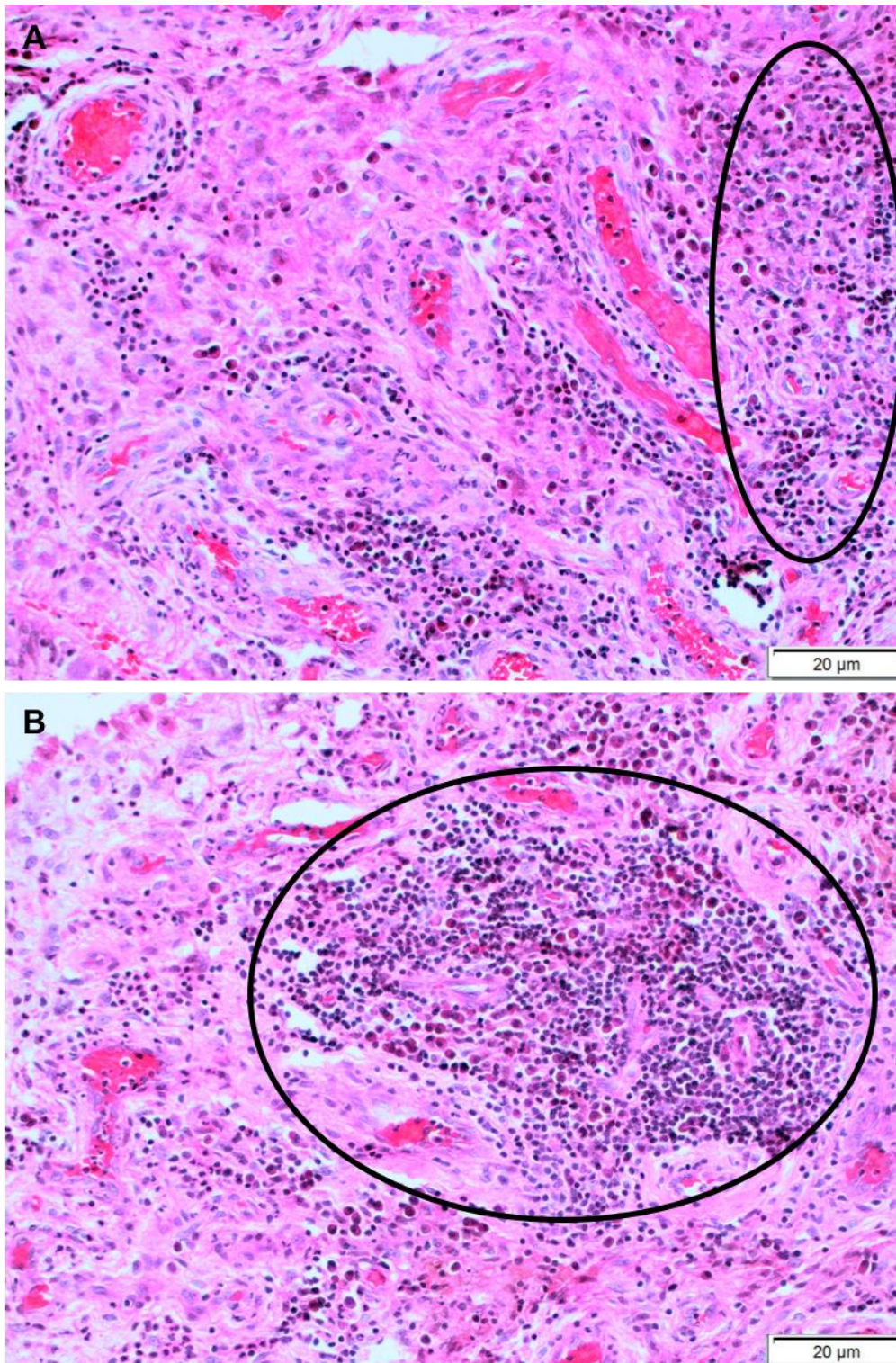


Figure 5.10 Representative H&E images illustrating inflammatory infiltration II

Representative H&E staining in FFPE patient tissues showing high immune cell infiltrate (x200). **(A)** and **(B)** represent different tissue samples. Highlighted areas indicate presence of immune cells.

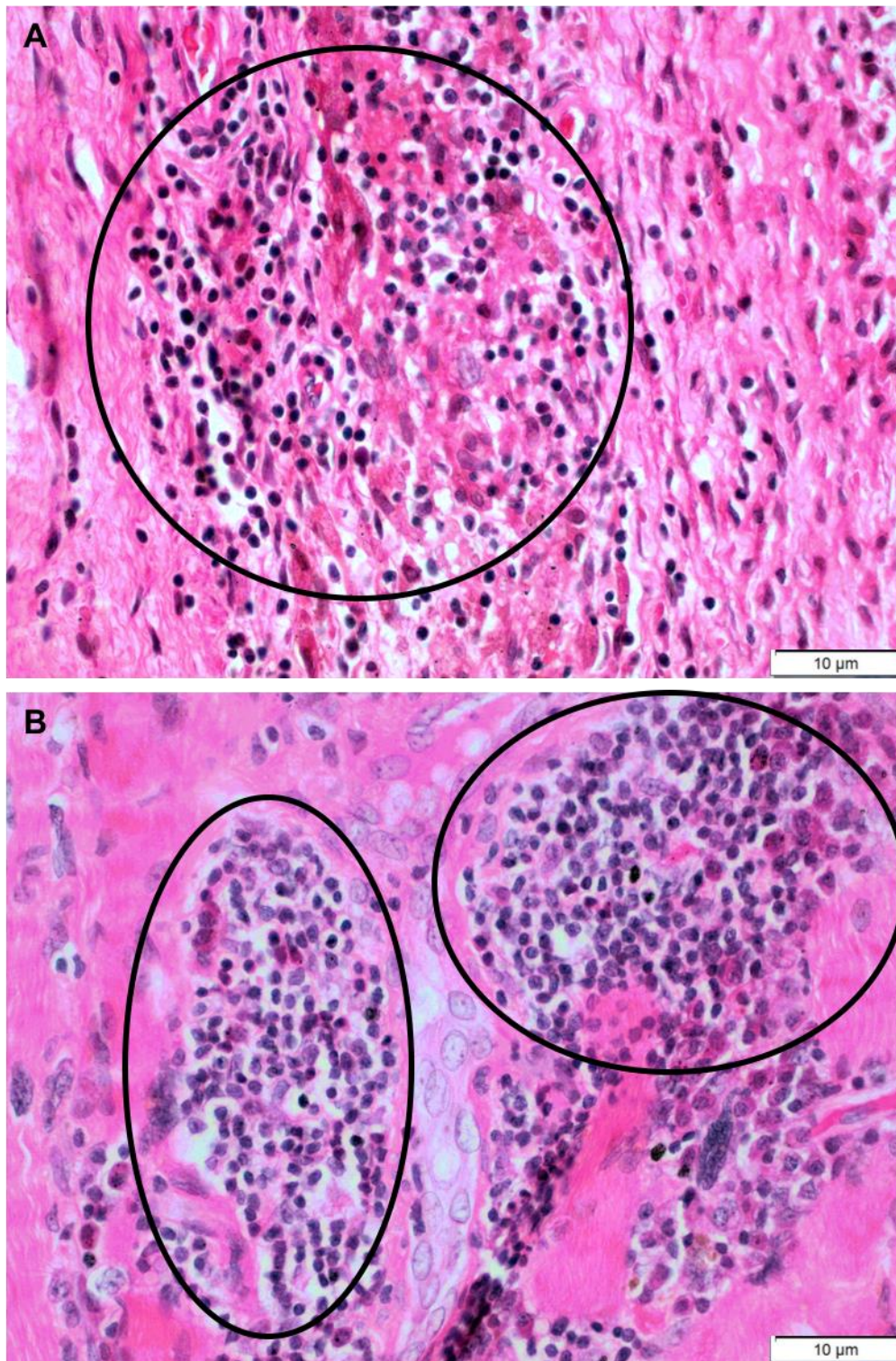


Figure 5.11 Representative H&E images illustrating inflammatory infiltration III

Representative H&E staining in FFPE patient tissues showing high immune cell infiltrate (x400). **(A)** and **(B)** represent different tissue samples. Highlighted areas indicate presence of immune cells.

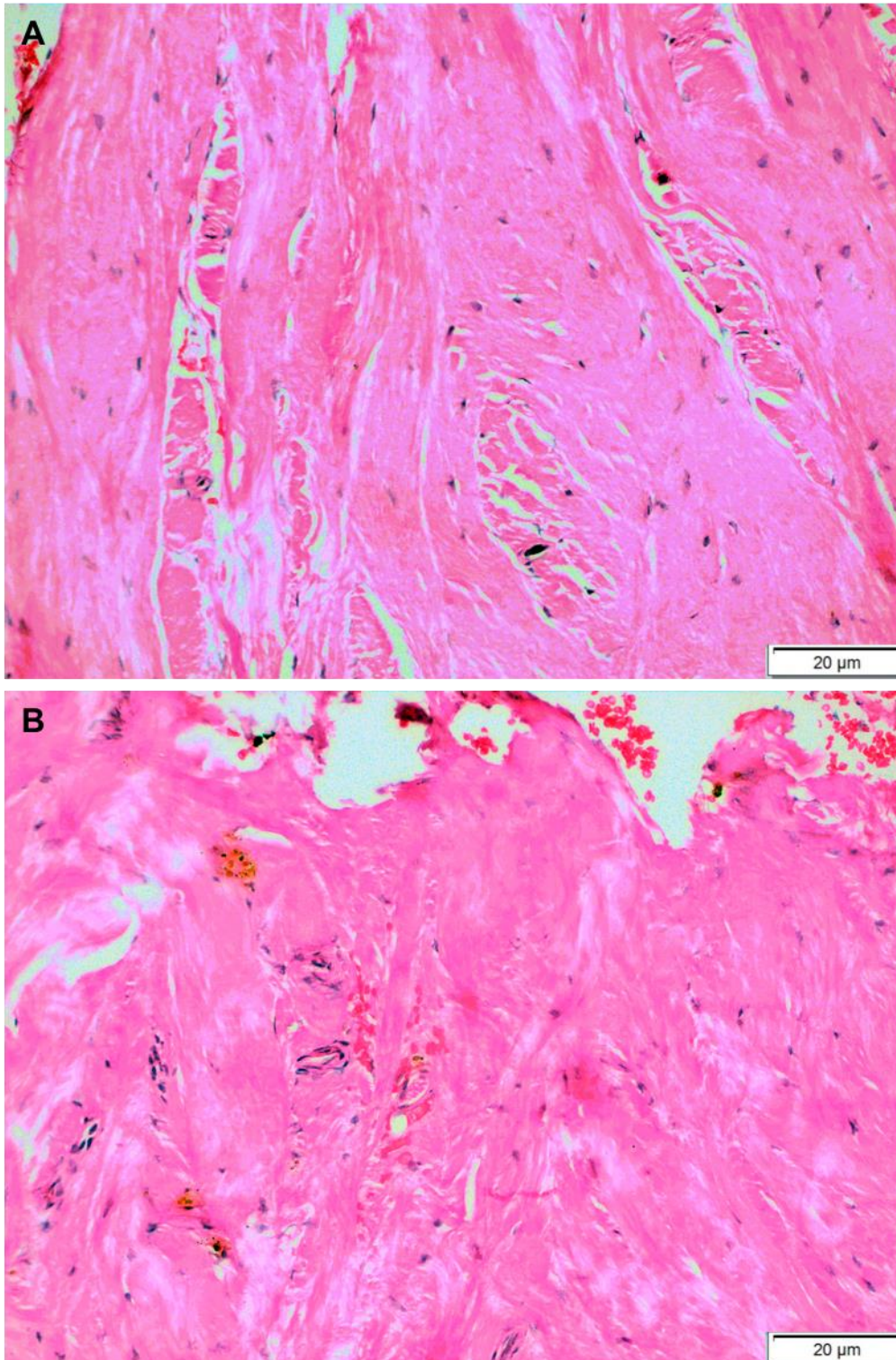


Figure 5.12 Representative H&E images illustrating inflammatory infiltration IV

Representative H&E staining in FFPE patient tissues showing very low immune cell infiltrate (x200). **(A)** and **(B)** represent different tissue samples.

5.4.4.3 Histological findings of periprosthetic soft tissue following revision surgery, IHC staining

To determine whether the inflammatory infiltrate observed in **section 5.4.4.2** was more lymphocyte- or macrophage-dominant, IHC was performed on the same soft tissue samples using antibodies to T lymphocytes (CD3) and macrophages (CD68) as described in **section 5.3.3**. Controls for both CD3 and CD68 were performed on tonsil tissue (**shown in Appendix B**). Overall, the inflammatory infiltrate was primarily a combination of both lymphocytes and macrophages.

Figure 5.13 and Figure 5.14 shows areas of tissue which were positive for T lymphocytes. There were seven soft tissue patient samples which had particularly high inflammatory cell infiltrate and of these seven, three were lymphocyte-dominant (patients #2, 5 and 10) (42.86%). A further two of these seven (28.57%) (patients #1 and 8) were observed to be macrophage-dominant (representative images shown in **Figure 5.15 and Figure 5.16**). Therefore, the remaining two patient's tissues were of a mixed population of both lymphocytes and macrophages (28.57%) (patients #3 and 6).

Of the cases which had relatively low cell infiltrate, two patients stained negatively for both cell types (patients #4 and 11) and two others stained weakly for macrophages and negative for lymphocytes (patients #7 and 9).

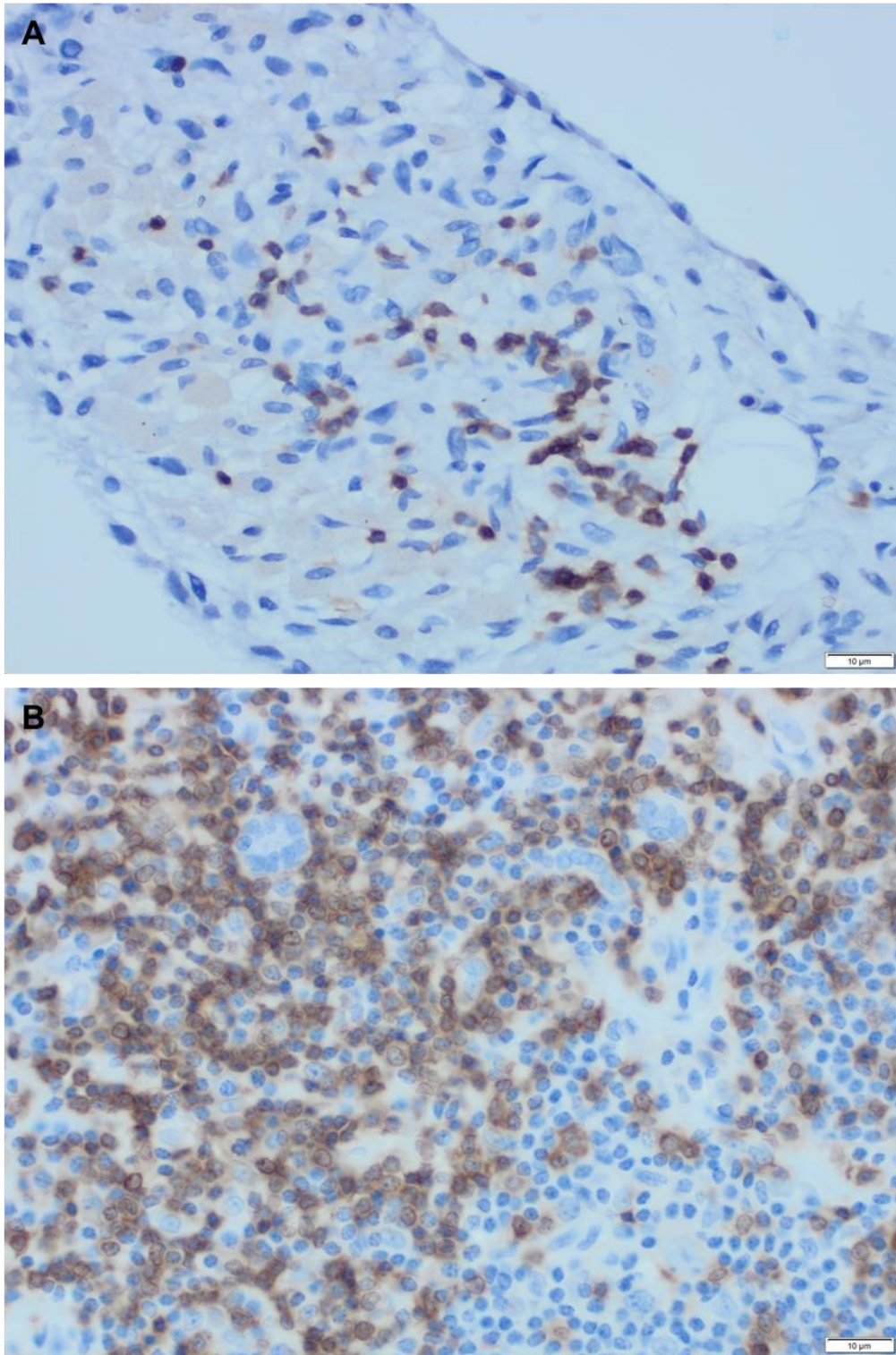


Figure 5.13 Representative IHC images illustrating T lymphocyte population I

Representative IHC staining for CD3 in FFPE patient tissues (x400) **(A)** lower number of CD3 positive cells as indicated by brown staining of cell cytoplasm **(B)** higher number of CD3 positive cells as indicated by brown staining of cell cytoplasm.

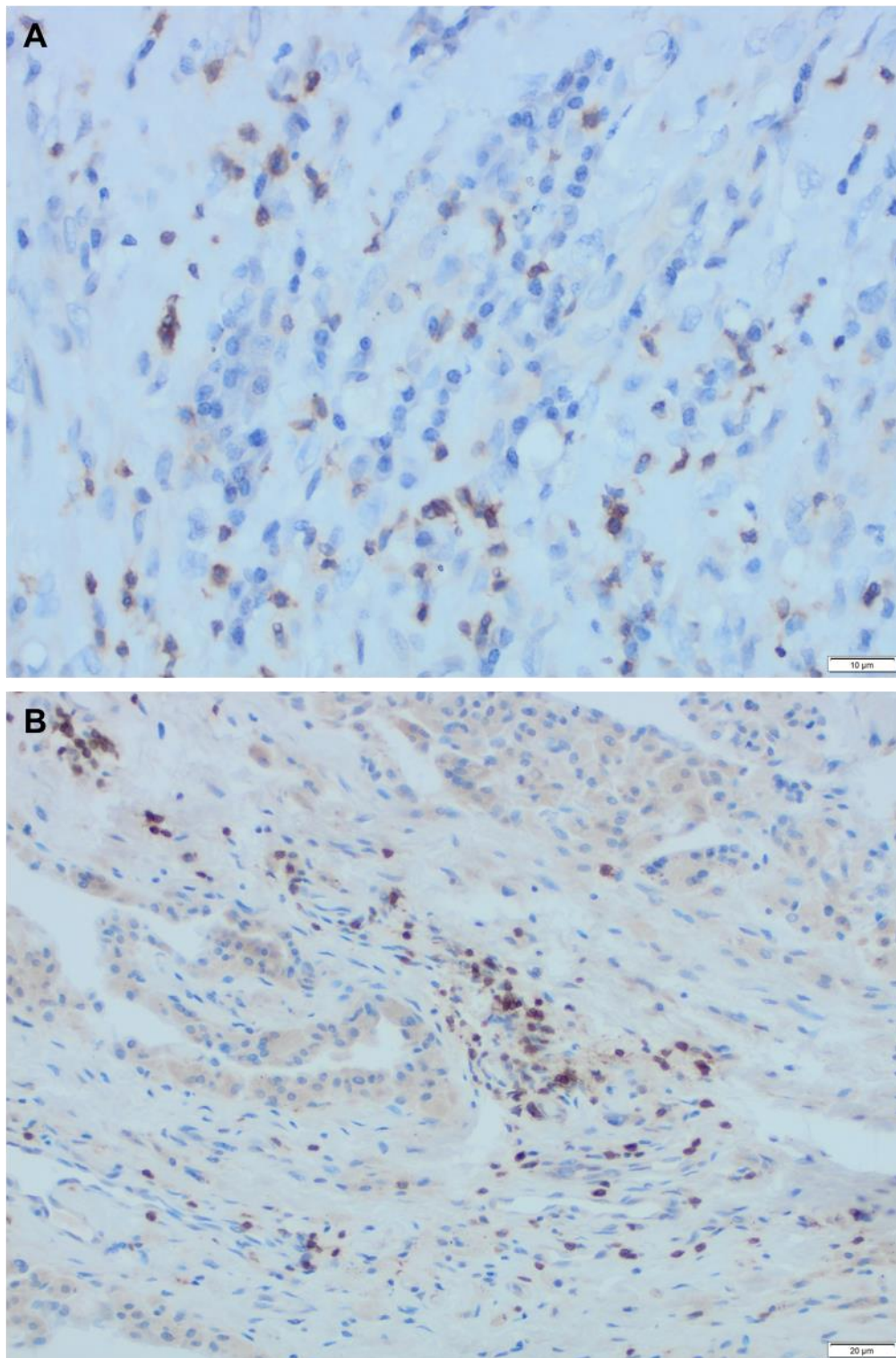


Figure 5.14 Representative IHC images illustrating T lymphocyte population II

Representative IHC staining for CD3 in FFPE patient tissues **(A)** (x400) medium number of CD3 positive cells as indicated by brown staining of cell cytoplasm **(B)** (x200) medium number of CD3 positive cells

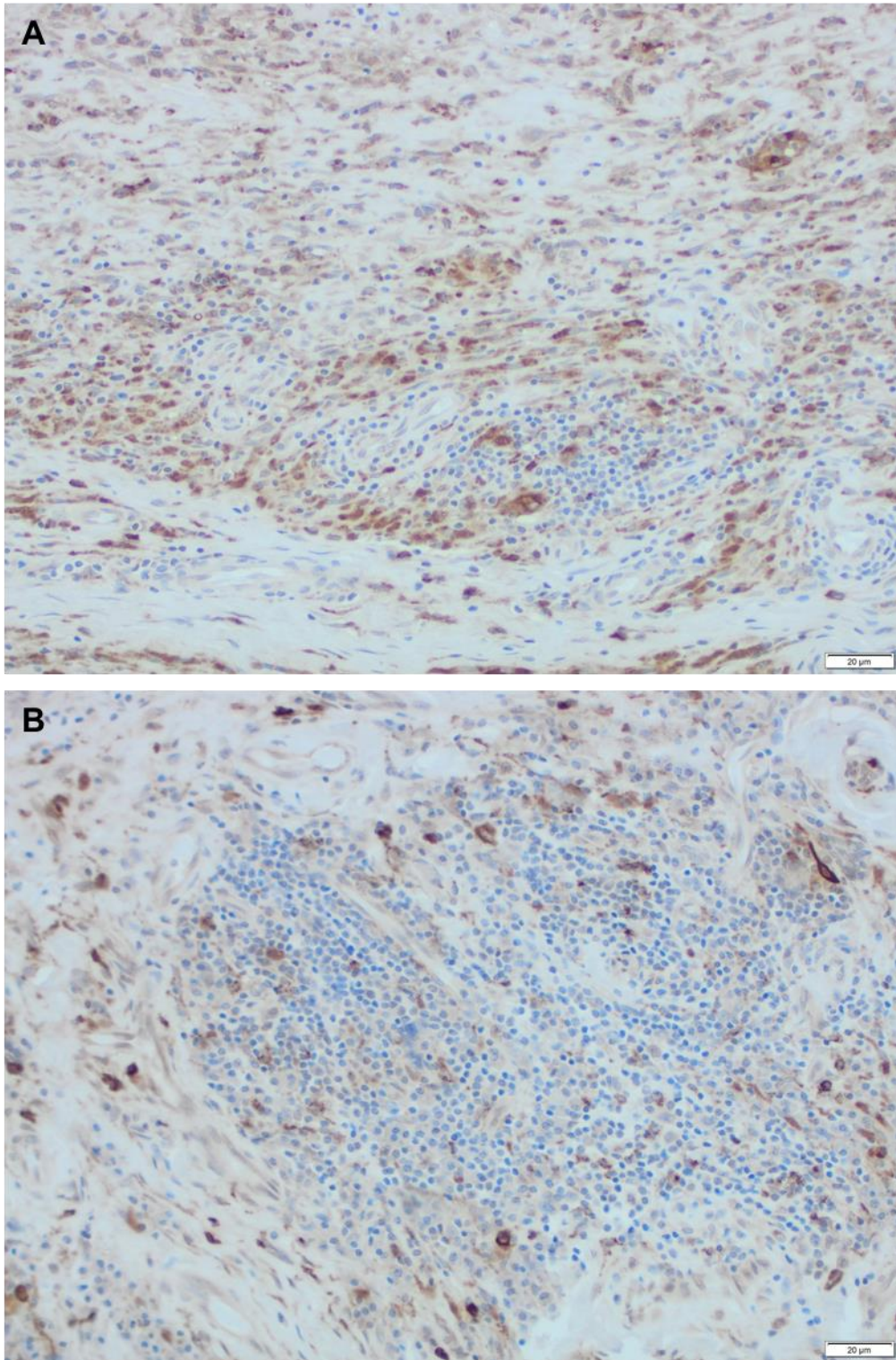


Figure 5.15 Representative IHC images illustrating macrophage population I

Representative IHC staining for CD68 in FFPE patient tissues (x400) **(A)** high number of CD68 positive cells as indicated by brown staining of cell cytoplasm **(B)** mid-high number of CD68 positive cells

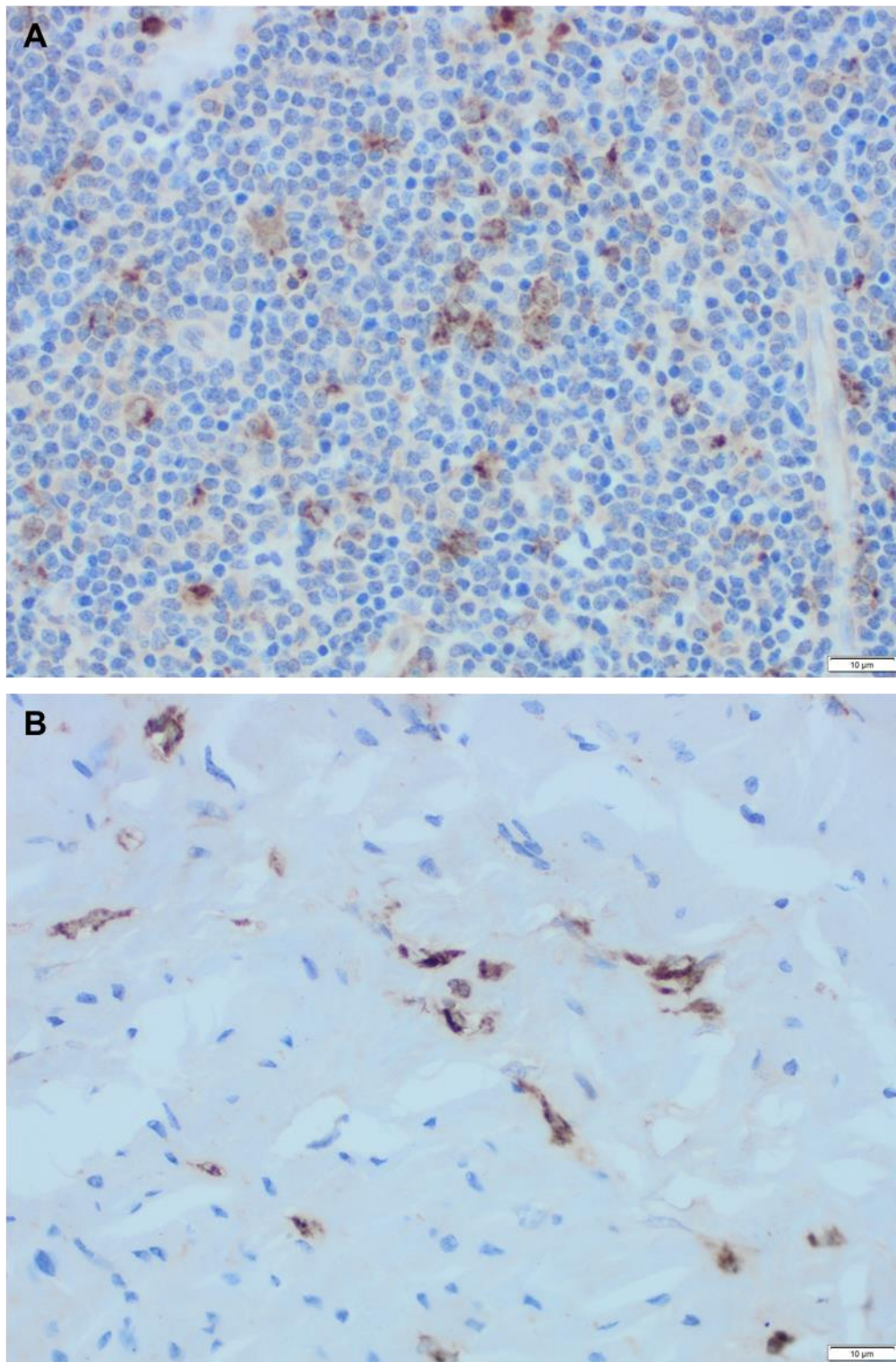


Figure 5.16 Representative IHC images illustrating macrophage population II

Representative IHC staining for CD68 in FFPE patient tissues (x400) **(A)** mid-high number of CD68 positive cells as indicated by brown staining of cell cytoplasm **(B)** lower number of CD68 positive cells.

5.4.4.4 Are T cells present in periprosthetic tissues proliferative?

To assess whether the CD3 positive T cells observed in the periprosthetic tissues were proliferative or in a resting state, dual coloured IHC was performed using Ki67 as a nuclear marker of proliferation. Unfortunately, positive control images for dual staining were unavailable. This part of the study was undertaken in a small number of samples (patients #2, 5 and 6) which stained positive for CD3 and were either deemed to be lymphocyte-dominant or mixed. **Figure 5.17A and Figure 5.17B** shows representative staining for both CD3 and Ki67 positive cells but across all tissues analysed there did not appear to be any clear co-localisation of both. Some cells, in close proximity, appear to be potentially dual-coloured, however these are not clear (**Figure 5.17B**). These findings suggest that T cells resident in these patient tissues are resting rather than proliferative.

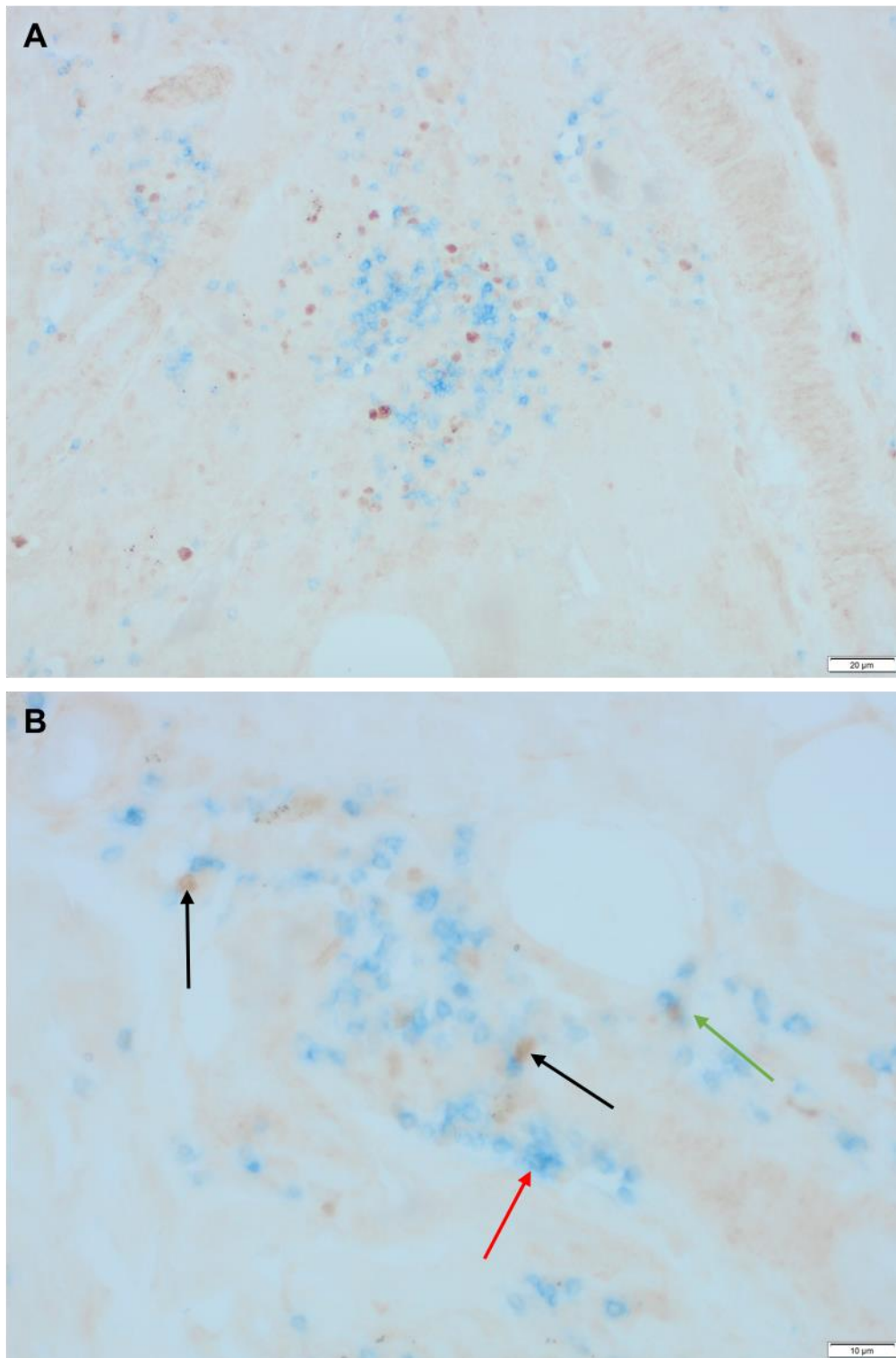


Figure 5.17 Representative images of CD3 and Ki67 dual coloured IHC staining

Representative dual coloured IHC staining for CD3 (blue) and Ki67 (brown) in FFPE patient tissues **(A)** (x200) **(B)** (x400) Black arrows indicate Ki67 positive cells, red arrow indicates CD3 positive cells, green arrow indicates potential dual-positive cell population.

5.4.5 CoCr particles effect on cell migration of MG63 cells

The effect of CoCr particles and CoCl₂ on the migration of MG63 cells was assessed using a wound healing scratch assay as described in **section 5.3.4**. In untreated cells, the gap was reduced by an average of $27.34 \pm 4.37\%$ after 24 hours and $82.23 \pm 3.22\%$ following 48 hours (**Figure 5.18 and Figure 5.19**). LPS treatment (100ng/ml) significantly accelerated cell migration when cells were observed after 48 hours (100%), although there was no significant difference at 24 hours, $32 \pm 2.06\%$ ($p=0.0033$ and $p=0.8533$, respectively). **Figure 5.18** clearly shows how confluent LPS treated cells were after 48 hours, with monolayers growing on top of each other when compared with untreated cells.

CoCr particle treatment ($50\mu\text{m}^3$ per cell) did not significantly affect the process of cell migration in comparison to unstimulated control cells at both time points; $15.28 \pm 3.30\%$ at 24 hours and $82.70 \pm 9.16\%$ at 48 hours ($p=0.0584$ and $p=>0.9999$, respectively). However, after 24 hours, CoCl₂ (0.25mM) resulted in a significant deceleration of this process ($p=0.0005$). Following 48 hours, CoCl₂ treated cells had completely lost their monolayer formation and adherence to the cell culture plate, suggesting cell death due to toxicity.

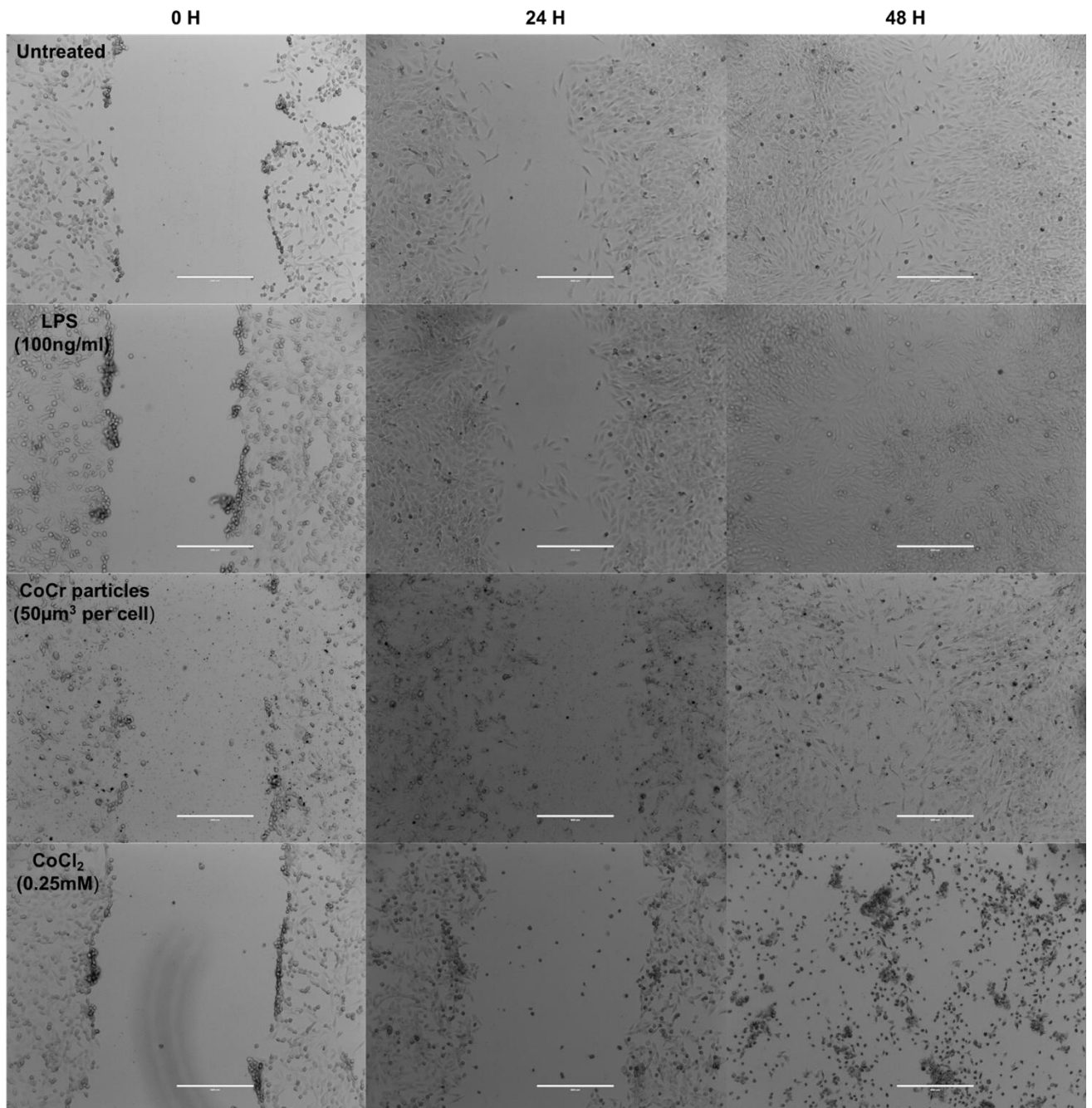


Figure 5.18 Effect of treatment with CoCr particles and CoCl₂ on wound closure and migration in MG63 cells I

Representative images of MG63 cells stimulated with either; LPS (100ng/ml), CoCr particles (50µm³ per cell) or CoCl₂ (0.25mM). Effect on relative cell migration over 48 hours using a scratch wound healing assay. Images are representative of 3 independent experiments. Scale bars represent 400µm.

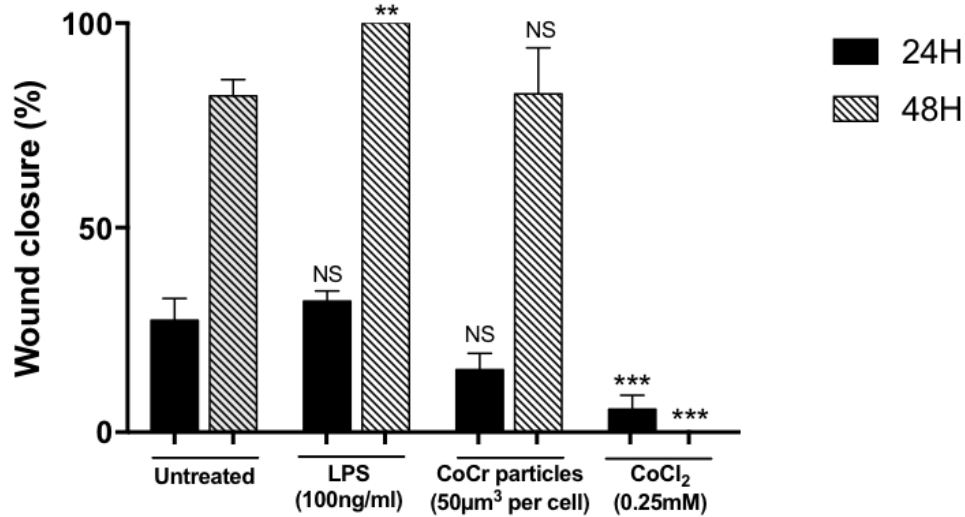


Figure 5.19 Effect of treatment with CoCr particles and CoCl₂ on wound closure and migration in MG63 cells II

MG63 cells were stimulated with either; LPS (100ng/ml), CoCr particles (50µm³ per cell) or CoCl₂ (0.25mM). Effect on relative cell migration over 48 hours using a scratch wound healing assay. Graph is representative of 3 independent experiments. Statistical significance was calculated by one-way ANOVA with Tukey's test for multiple comparisons comparing all samples to each other.

5.5 Discussion

The aim of this chapter was to investigate the effect of CoCr particles on the immune response in endothelial cells, specifically the HMEC-1 cell line. Following on from these findings the second aim was to establish how this translates *in vivo* by histologically phenotyping soft tissue from patients who have received both hip and knee implants containing cobalt-chromium. An additional aim was to see how CoCr particles effect the migratory properties of an osteoblast-like cell line.

Effect of CoCr particles on HMEC-1 cells and neutrophil chemotaxis

Transendothelial migration of immune cells into tissues following cell adhesion is of importance in the context of this study, as it is known that pseudotumours formed due to ARMD display high immune cell infiltrate. Furthermore, results described in **Chapter 4** demonstrate increased expression of IL-8 (along with other chemokines) in response to CoCr particles which will increase the chemotaxis of neutrophils and other immune cells. Furthermore, cobalt ion- and CoCr particle-mediated chemokine and cytokine secretion has been hypothesised to increase adhesion molecule expression *in vitro* (ICAM-1 and VCAM-1) (Alinovi *et al.*, 2015; Anjum *et al.*, 2016). HMEC-1 cells were selected for this part of the study to model the endothelium which potentially becomes activated by CoCr particles, thus increasing neutrophil chemotaxis into peri-implant tissue via increased expression of adhesion molecules. HMEC-1 cells have been previously used by the group for similar studies involving CoCl₂ and were readily available (Anjum *et al.*, 2016; Lawrence *et al.*, 2016a).

Firstly, cell viability of HMEC-1 cells treated with a range of CoCr particles was assessed over 48 hours. Cell viability was significantly affected at both 24 and 48 hours at the two highest concentrations of CoCr particles (5 and 50µm³ per cell) but only following 48 hours of stimulation with the lowest concentration (0.5µm³ per cell) was viability significantly reduced. This reiterates reports of varied susceptibility of different cell types to the effects of CoCr particles, as for example, a dose of 50µm³ per cell was better tolerated in THP-1, MM6 and J774 macrophage cell lines in the previous chapter (Behl *et al.*, 2013).

The proliferative capacity of HMEC-1 cells following CoCr particle treatment was then assessed using the XTT assay. Interestingly, following 24 hours of stimulation, there was a significant increase in proliferation at 5µm³ CoCr particles per cell before a

decrease at $50\mu\text{m}^3$ per cell. This would suggest the cells are becoming somewhat activated by CoCr particles up until a certain concentration where cytotoxicity may then occur. HMEC-1 cells treated for 48 hours with CoCr particles confirmed this hypothesis as there was a dose-dependent downward trend of proliferation resulting in a significant decrease at $50\mu\text{m}^3$ particles per cell. This therefore reflects the results from assessment of cell viability. However, it was decided to continue with a concentration of $50\mu\text{m}^3$ CoCr particles per cell so maximal activation could be investigated as endothelial cells were likely to be less inflammatory than previously studied macrophage cells. This also meant treatments could be kept consistent throughout the study to draw comparisons.

There is no evidence in the literature in respect to the uptake or internalisation of either wear debris or CoCr particles by endothelial cells by TEM. However, Alinovi *et al.* confirmed uptake of cobalt and titanium nanoparticles by flow cytometry (Alinovi *et al.*, 2015). Although not classically known to be phagocytic, endothelial cells have shown phagocytosis-like uptake of particles and bacteria (Serda *et al.*, 2009; Rengarajan *et al.*, 2016). Furthermore, it is hypothesised that phagocytosis by endothelial cells may also recruit immune cells to the vasculature, potentially by increased expression of pro-inflammatory cytokines and chemokines such as IL-8 (Opitz *et al.*, 2006). The TEM images from this study indicated that HMEC-1 cells could internalise CoCr particles following 24 hours of stimulation. The particles appeared to be similar to those phagocytosed by THP-1 macrophages; dense clusters within membrane bound vacuoles. Therefore, it is likely that CoCr particles will be inducing inflammatory or stress effects on endothelial cells as well as monocytes/macrophages *in vivo*.

As discussed previously, interaction between leukocytes and endothelial cells is crucial to the process of leukocyte binding and migration into inflamed tissues. Importantly, one of the first steps of leukocyte adhesion to the endothelium requires the expression of ICAM-1 and VCAM-1. Therefore, HMEC-1 cells treated with CoCr particles were assessed for the expression of these adhesion molecules. The results demonstrated significantly increased expression of both *ICAM-1* and *VCAM-1*, suggesting increased activation of endothelial cells following CoCr particle exposure. These findings are consistent with a recent study which showed increased *ICAM-1* expression after monocyte exposure to cobalt ions (Laumonier *et al.*, 2020). However, this does not necessarily translate to increased vascular permeability and immune cell chemotaxis.

Therefore, a neutrophil chemotaxis assay was used to determine whether endothelial activation by CoCr particles led to increased leukocyte migration.

Neutrophil chemotaxis was selected for this study as results discussed previously in **Chapter 4** indicate that IL-8 expression and secretion, which is particularly chemotactic for neutrophils, is significantly increased in response to CoCr particles. Neutrophil migration was significantly increased when HMEC-1 cells were treated with CoCr particles, indicating the activated endothelium did in fact lead to increased permeability and enhanced transendothelial migration. The results were comparable to those cells treated with the positive control, LPS. This data, however, was taken from only two independent experiments (two separate neutrophil donors). Therefore, caution must be taken when inferring significance from results and be repeated further to reach more meaningful conclusions. Previous investigations within the group have found conditioned supernatant from CoCl₂-treated MM6 cells can significantly increase the chemotaxis of both neutrophils and monocytes (Lawrence *et al.*, 2016a). However, this is the first study to show the physiological relevance of this by recreating the endothelium and determining how CoCr particles can affect this cell barrier.

Histological findings of periprosthetic soft tissue following revision surgery

The findings discussed so far suggest a role for possible endothelial activation as a result of CoCr particle stimulation which then increases expression of adhesion molecules and promote the migration of leukocytes such as neutrophils. Therefore, it would be expected that patients' periprosthetic soft tissue would contain these types of immune cells.

The purpose of analysing a small cohort of patients' periprosthetic soft tissue was to compare the histology as part of a preliminary study to be further continued using a much larger cohort. Therefore, it is important to accept there are several limitations when attempting to draw meaningful conclusions from the findings represented, particularly due to the small sample size.

Firstly, the patient clinical information was too variable for a cohort of its size. For example, inconsistencies with type of implant (hip or knee), material/manufacturer used and more important reason for revision. For this type of study, the reason for revision should be ideally aseptic loosening or signs of ARMD e.g. pseudotumour formation rather than infection, surgical error at primary surgery or fractures. However,

the histological methods employed in this study, H&E and IHC staining, were shown to be useful for identifying both immune cell infiltration and phenotyping of these cells. Therefore, as a pilot study, for both retrieval of tissue and subsequent analysis, proof-of-concept was successfully achieved and could be continued to create a larger patient cohort in the future. Once a larger cohort of patient tissue is collected and stained perhaps a more quantitative measure of cell counting could be employed as opposed to the qualitative analysis used in this study. Semi-quantitative analysis could be employed using a 'grading system' in which H&E immune infiltrates as well as CD3 and CD68 positive cells could be added together to give an overall score to determine the inflammatory status of each patient. This data could then be used to compare different patient groups and whether this is a link to increased inflammation, for example, gender, type of implant or reason for revision.

There was one particular case of interest (patient #1) involving a 51-year-old male who had received a unilateral (right side) Birmingham Hip Resurfacing (BHR) MoM implant in primary surgery 9 years previously. The implant was revised due to aseptic loosening despite a relatively short duration, however, there is no information regarding activity levels of the patient. Cobalt and chromium ions levels in the serum were recorded on the day of revision surgery at 48.2 nmol/L and 31.8 nmol/L, respectively. These were considerably below the acceptable range dictated by the MHRA (119 nmol/L cobalt or 134 nmol/L chromium). The tissue from this patient had significant areas of positive staining for both T cells and particularly macrophages, indicating a potential immune response.

The majority of patients' tissues (7 out of 11) had prominent immune cell infiltrate. However, even in cases of low cell infiltrate, two of these patients had a small number of macrophages staining positive. Overall, the findings were similar to other studies investigating similar patient cases, with a fairly even mixture of lymphocytes and macrophages between the cohort with most patients either being predominantly lymphocyte-dominant or macrophage-dominant (Campbell *et al.*, 2010; Phillips *et al.*, 2014; Paukkeri *et al.*, 2016). It has been hypothesised that general wear leading to aseptic loosening has a significantly lower population of lymphocytes compared to those patients suspected to have ARMD, and particularly ALVAL (Campbell *et al.*, 2010).

The dual coloured IHC to determine whether CD3 positive T cells were proliferating suggested that the cells were in a resting state. However, this was analysed in only three samples in this instance. The method employed did prove to be potentially useful for expansion as this could help gain further insight into the pathology of ALVAL reactions. For example, if T cells are activated and proliferating this would suggest contact hypersensitivity (delayed type IV reaction) plays a central role and metal ions or particles are working as haptens presented by antigen presenting cells. However, a study which treated isolated human lymphocytes with CoCr particles hypothesised the potential for T cell anergy, which describes a state of reduced function due to a tolerance mechanism following antigen encounter and therefore inhibition of proliferation (Posada *et al.*, 2015). The authors found a decrease in proliferation, IL-2 secretion and reduction in pro-inflammatory cytokines from lymphocytes in the presence of CoCr particles (Posada *et al.*, 2015).

The role of T cells in these responses could be further elucidated by staining specifically for CD4-positive T helper cells, which are specific for antigens presented by major histocompatibility complex II molecules (MHC II) or for CD8-positive cytotoxic T cells which function through major histocompatibility complex I molecules (MHC I), endogenously. Previous studies have shown an increased proportion of CD8-positive T cells and decreased ratio of CD4 to CD8 in patients with worn implants as well as a correlation between serum cobalt and chromium concentrations and percentage of CD8-positive cells (Case *et al.*, 2000; Hailer *et al.*, 2011). This is in agreement with a more recent study which incubated CoCr particles with blood samples from 25 donors and assessed T-cell phenotypes by IHC and flow cytometry (Du *et al.*, 2018). Furthermore, CoCr particles injected into murine knee joints displayed a largely CD8-positive T cell driven immune response rather than CD4-positive (Du *et al.*, 2018). It could be that the cytotoxic effects caused by CoCr particles and cobalt ions activate MHC I molecules which increases CD8-positive T cell responses.

Other studies have shown a link between cobalt and chromium ions from MoM resurfacing implants and a decreased lymphocyte population, particularly CD8-positive T cells (Hart *et al.*, 2009). It has been hypothesised that cobalt ion-mediated cytotoxicity of T cells inhibits further T cell proliferation, thus lowering overall numbers (Akbar *et al.*, 2011). It could be that although the overall population of CD8-positive T cells is decreased in comparison to healthy controls, it remains the most dominant T

cell response in the presence of CoCr particles and cobalt ions. Therefore, these findings make it clear further studies are required to elucidate the specific mechanisms of lymphocyte-mediated osteolytic responses.

It would be interesting to also stain for other granulocytes such as neutrophils and eosinophils (e.g. CD15 and CD16) due to results from chemokine analysis (i.e. high expression of IL-8) as well as the enhanced neutrophil migration observed in the chemotaxis assay. Furthermore, RNA isolation from cells within the tissue would allow for the analysis of inflammatory markers of interest and how these are expressed. Unfortunately, there remains difficulties with obtaining appropriate control tissue to draw comparisons to healthy tissue. The most suitable control would be to obtain soft tissue in patients undergoing primary surgeries verses revision.

Migratory capacity of osteoblast-like cells treated with CoCr particles

The migratory capacity of MG63 cells was assessed by using a wound healing assay. Although the cell images appeared to show the migratory capacity of cells was reduced following CoCr particle treatment after 24 hours particularly, this did not reach statistical significance. However, the enhanced proliferative effect shown by treatment with LPS was not mirrored. Interestingly, treatment with CoCl₂ almost completely abrogated migration of the cells and following 48 hours, the cells appeared to have suffered from cytotoxicity and were no longer adhered to the cell culture plate. This may have been due to the larger concentration of CoCl₂ used for treatments in this series of experiments (0.25mM). However, this concentration has been tolerated by different cell lines previously such as MM6 and HMEC-1 (Lawrence *et al.*, 2016a; Lawrence *et al.*, 2016b), suggesting osteoblast-like cells are especially sensitive to CoCl₂.

The findings presented here are similar to those published by Drynda *et al.* who demonstrated the deceleration of migratory MG63 cells following CoCl₂ treatment but this was not reflected with CoCr particle treatment (Drynda *et al.*, 2018a). Furthermore, a study investigated the migrating ability of smooth muscle cells treated with CoCl₂ and also found that migration was slowed as a result despite only a slight reduction in cell proliferation (Li and Wang, 2014). It would therefore be of interest to see how CoCr particles effect other pathways which are potentially involved such as TGF- β /Smad3 which regulates the secretion of collagens (Lin *et al.*, 2017). The extracellular matrix, which includes molecules such as collagens, is known to influence cell migration

(Painter, 2009). A recent study found that collagen 1 synthesis was reduced after treatment with CoCl₂ in human primary osteoblasts (Jonitz-Heincke *et al.*, 2019).

5.5.1 Future work

The expression of ICAM-1 and VCAM-1 was increased by CoCr particles at gene level, however, the expression at protein level was not explored in this study. Therefore, it would be interesting to assess these changes either by flow cytometry or Western blotting. Furthermore, soluble ICAM-1 (sICAM-1) is a secreted form of the membranous adhesion molecule and could be measured by ELISA. Investigation by the group have previously shown CoCl₂-mediated sICAM-1 expression is TLR4 dependent (Anjum *et al.*, 2016). sICAM-1 is thought to be a marker of endothelial activation as well as infection and inflammatory responses (Videm and Albrigtsen, 2008; De Pablo *et al.*, 2013). The expression of integrins LFA-1 and VLA-4 in leukocytes and how CoCr particles may affect their expression would also provide further insight into the processes of transendothelial migration.

The chemotaxis assay data presented from this study indicated that CoCr particles could activate HMEC-1 cells to promote the migration of neutrophils. It would also be interesting for these experiments to be repeated using PBMCs to analyse the migration of monocytes/macrophages. Particularly, as these types of cells are found in such high numbers in the tissue of pseudotumours from patients with ARMD. The use of primary cells such as PBMCs and neutrophils adds complexity to these assays as there will be variability between donor cells meaning some may be more migratory than others. Therefore, the number of repeated independent experiments would likely have to be higher to account for this. Furthermore, it would be of interest to analyse the expression of specific chemokine receptors e.g. CXCR2 to determine whether there is a correlation between expression and migratory potential. It would also be interesting to use the TLR4 inhibitor, CLI-095 in the chemotaxis assay to see whether the CoCr particle-mediated endothelial activation is in fact TLR4 dependent. Furthermore, the inclusion of CoCl₂ controls would provide further insight into whether the effect is due to cobalt ion release from the particles or direct.

As discussed, the importance of generating a larger cohort of patient tissue to be analysed will strengthen the findings presented here. Once a larger cohort has been

analysed for immune cell infiltrate and the presence of both T cells and macrophages, this data can be semi-quantified to produce more meaningful conclusions as to whether certain implants or reasons for revision surgery are more closely associated with inflammatory responses. Future work should also focus on the potential of adding primary surgery patients to the tissue collection cohort as this could provide suitable control tissue to draw further comparisons.

The migratory potential of MG63 cells demonstrated that CoCr particles did not significantly affect the closure of the scratch wound in comparison to untreated cells. However, it would be useful to study these osteoblast-like cells further to determine how the process of bone resorption is affected by CoCr particles and could be linked to increased osteolysis in cases of ARMD. For example, gene expression analysis of genes involved in osteogenesis such as TGF- β , and other members of its superfamily such as bone morphogenetic proteins 4 and 5 (BMP4/5) could be investigated. For example, Zijlstra *et al.* also examined RNA levels of OPG and RANKL using qRT-PCR in cells treated with cobalt ions which would provide insight into this balance of bone resorption and formation (Zijlstra *et al.*, 2012).

5.5.2 Conclusion

In summary, the data presented in this chapter shows that CoCr particles can activate the endothelium which can then lead to increased migration of leukocytes. Firstly, HMEC-1 cells treated with CoCr particles significantly increased expression of the adhesion molecules, ICAM-1 and VCAM-1. In a chemotaxis assay, an endothelial monolayer stimulated with CoCr particles lead to increased migration of neutrophils towards an IL-8 chemotactic gradient. These results suggest CoCr particles increase transendothelial migration of leukocytes into periprosthetic tissues by activating the endothelium, increasing adhesion molecule expression which results in leukocyte arrest and migration. It is likely that this response is also driven by inflammatory chemokine and cytokine secretion which has been shown to be increased following CoCr particle stimulation in the previous chapter. Ultimately, in the clinical context of ARMD, this process could contribute to the inflammatory cell infiltrate observed in the tissues of patients with pseudotumours.

Chapter 6 : Investigating the Biological Effects of Ceramic Oxides

6.1 Introduction

It is clear from the findings in previous chapters that CoCr particles and cobalt ions can activate the immune system through stimulation of receptors such as TLR4 which in turn promotes the secretion of pro-inflammatory cytokines and chemokines by both monocytes/macrophages. This leads to activation of the endothelium, promoting the migration of leukocytes from the circulation into inflamed tissues. These processes can therefore potentially explain some of the adverse reactions observed in patients who have received joint implants containing CoCr.

As discussed in **Chapter 1**, these adverse reactions are not unique to CoCr-containing MoM implants and inflammatory pseudotumours have been shown to develop in patients who have received both CoP and CoC implants (Malem *et al.*, 2013; Campbell *et al.*, 2017; Serrano *et al.*, 2018). Due to their increasing popularity, it is important to investigate the inflammatory potential of materials such as ZTA, which is used in ceramic implants. Furthermore, because ceramics are known to be very low-wearing in comparison to their MoP and MoM counterparts, it has been suggested that these materials are 'bio-inert'. However, reports have shown ceramic wear debris in tissue of patients who have received ceramic implants suggesting that these implants may still produce significant wear debris accumulations over time (Bertrand *et al.*, 2018; Rony *et al.*, 2018). Bertrand *et al.* also looked at the effects of fibroblasts and PBMCs cultured on either alumina-toughened zirconia (ATZ) or ZTA ceramic surfaces and demonstrated increased expression of cytokines, particularly for ATZ ceramics when compared with ZTA (Bertrand *et al.*, 2018).

J774 mouse cells have been shown to increase their secretion of TNF- α in response to alumina particles (Rodrigo *et al.*, 2006). Furthermore, other mouse macrophage cell lines (e.g. RAW 264.7) have been shown to increase IL-6, ROS, NF- κ B as well as TNF- α when stimulated with aluminium nanoparticles (Olivier *et al.*, 2003; Nishanth *et al.*, 2011). Therefore, J774 cells were used as a mouse macrophage cell model to determine whether ceramic oxides can up-regulate the inflammatory chemokine, CCL3 in this species.

So far, very few studies of the biological effects of zirconium or alumina have been published. In the few that have, the results are usually dwarfed by comparisons made with CoCr or UHMWPE particles (Petit *et al.*, 2002; Germain *et al.*, 2003). Therefore, the techniques demonstrated in **Chapter 4** were applied to investigate the biological response to both aluminium oxide (Al₂O₃) and zirconium oxide (ZrO₂) nanopowders.

6.2 Aims and Objectives

The aim of this chapter was to establish the effects of ceramic oxides in the THP-1 macrophage cell line by assessing toxicity and expression of pro-inflammatory chemokines. The TLR4 and NLRP3 inflammasome signalling pathways were investigated to determine their potential role in these responses.

6.2.1 Objectives

- To investigate the effect of ceramic oxides on THP-1 macrophage cell viability and proliferation
- To establish whether THP-1 and HMEC-1 cells can phagocytose ceramic oxides
- To establish which chemokines are significantly up-regulated in response to ceramic oxides in THP-1 cells
- To investigate whether the use of a TLR4-specific inhibitor can prevent the inflammatory response mediated by ceramic oxides
- To investigate whether ceramic oxides can activate the NLRP3 inflammasome complex

6.3 Specific Materials

6.3.1 Ceramic oxides

Both aluminium oxide (Al_2O_3) and zirconium(IV) oxide (ZrO_2) (both Sigma Aldrich, USA) were tested for any endotoxin contamination (using the LAL assay described in **section 3.4.5**) to ensure responses observed were not due to LPS activation of TLR4.

6.3.1.1 Aluminium oxide

Al_2O_3 was used to replicate wear debris released from joint implants containing ceramics, specifically ZTA. The particles which make up the nanopowder are stated to be less than 50nm in size by the manufacturer. Cells were cultured with Al_2O_3 particles at volumes of $0.5\mu\text{m}^3$, $5\mu\text{m}^3$ and $50\mu\text{m}^3$ per cell using the calculation specified in **Appendix A**.

6.3.1.2 Zirconium(IV) oxide

ZrO_2 was used to replicate wear debris released from joint implants containing ceramics, specifically ZTA. The particles which make up the nanopowder are stated to be less than 100nm in size by the manufacturer. Cells were cultured with ZrO_2 particles at volumes of $0.5\mu\text{m}^3$, $5\mu\text{m}^3$ and $50\mu\text{m}^3$ per cell using the calculation specified in **Appendix A**.

6.4 Results

6.4.1 TEM images of ceramic oxide nanopowders

High magnification TEM was used (x100K) to characterise both the Al₂O₃ and ZrO₂ nanopowders purchased for *in vitro* cell treatments (**Figure 6.1** and **Figure 6.2**). **Figure 6.1** demonstrates individual aluminium oxide particles, which are mostly 'shard like' rather than spherical in morphology and form agglomerations and aggregates of particles. It is possible to identify single particles which are less than 50nm from the scale bar which confirms the manufacturer's specifications and suitability for the study in which nanoparticles are preferred.

Zirconium oxide particles were imaged as shown in **Figure 6.2** and demonstrate a very different morphology to that of aluminium. The particles appear to be much denser in appearance with globular/round morphology. The particles are uniform in their morphology and size which again appear to be under 50nm for individual particles as demonstrated by the scale bar. Therefore, being nanoscale in their size, these particles were also deemed appropriate for the study.

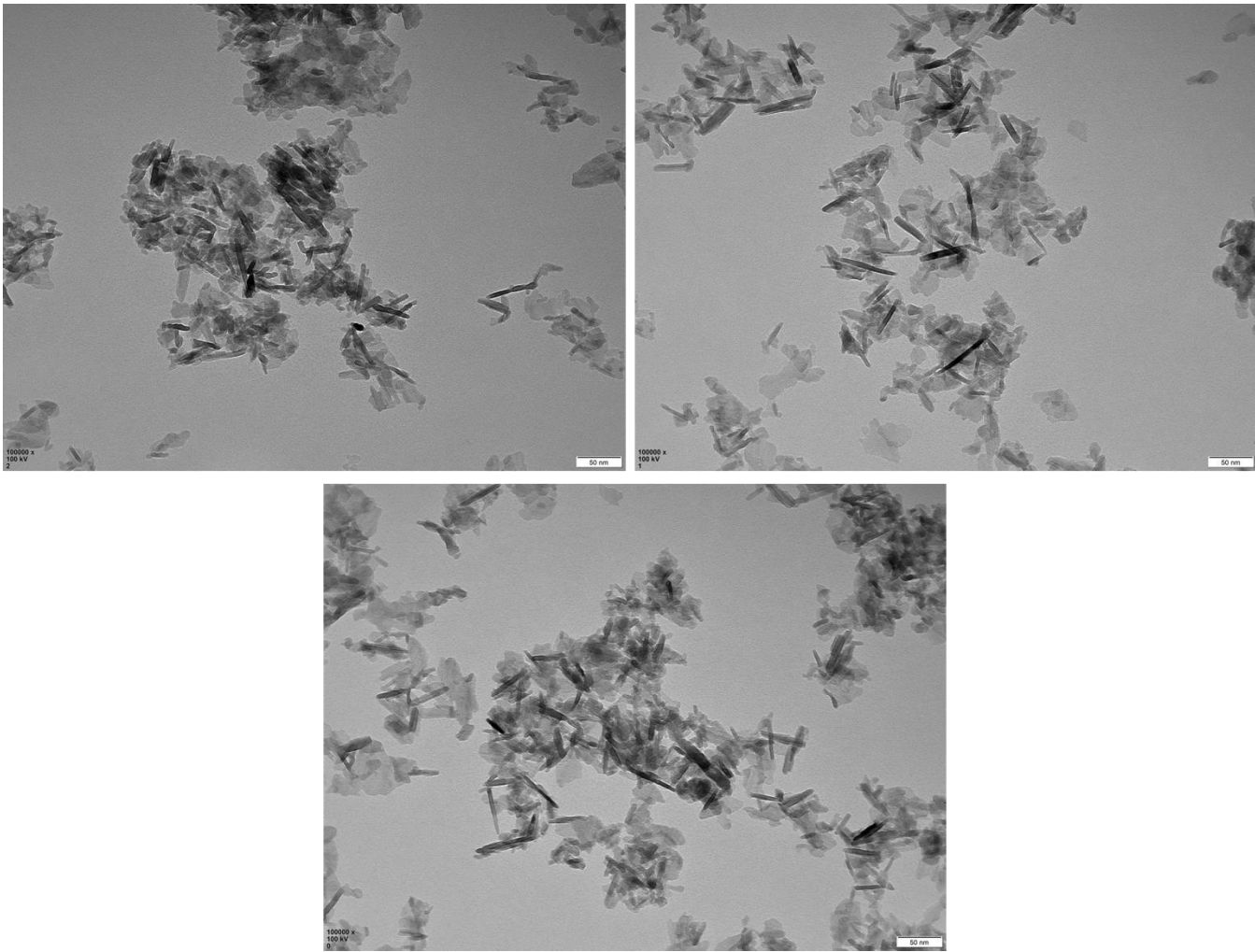


Figure 6.1 Transmission electron microscopy using high magnification to visualise and characterise individual aluminium oxide particles

Representative images of aluminium oxide particles (x100K). Scale bars represent 50nm.

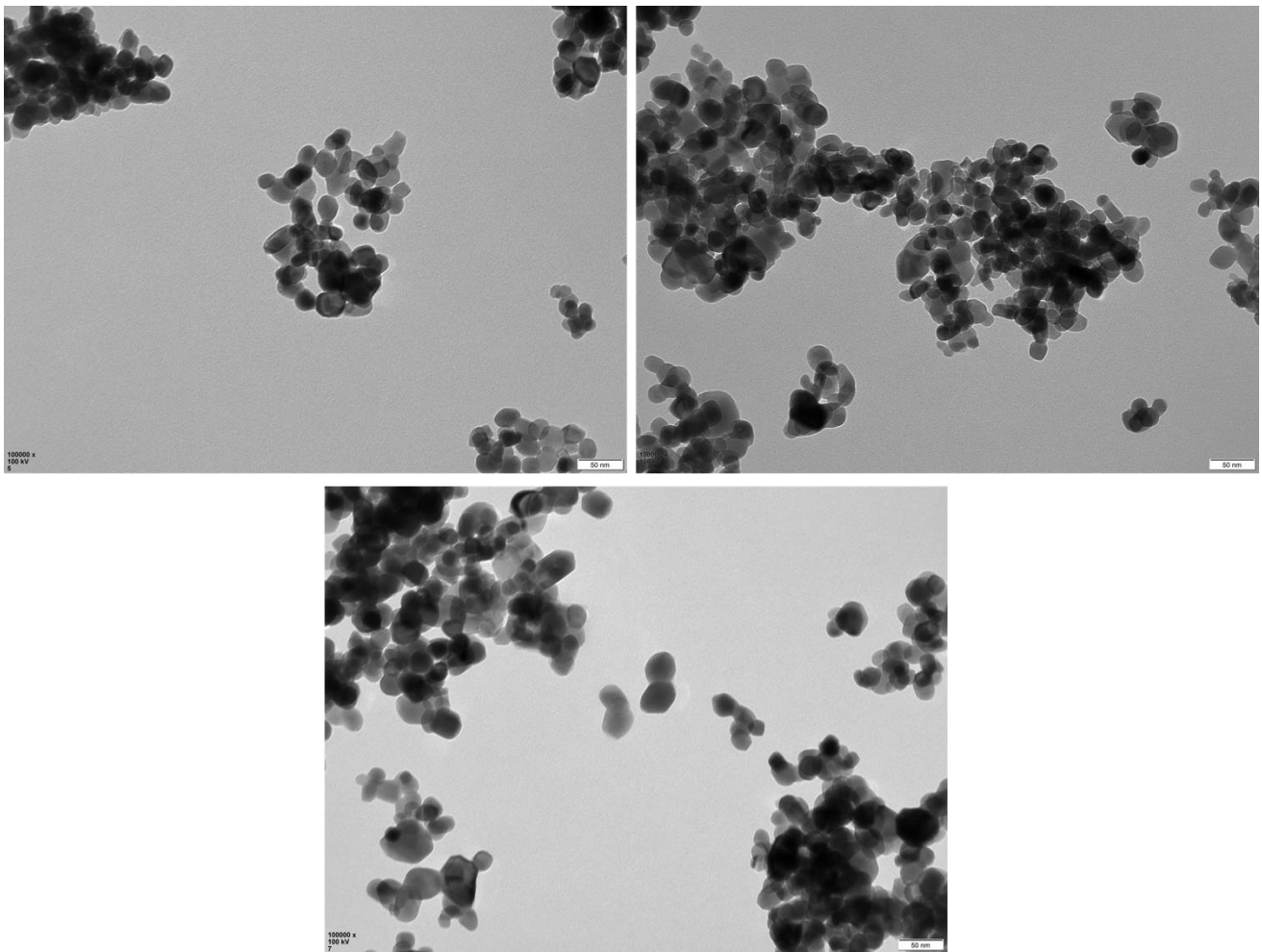


Figure 6.2 Transmission electron microscopy using high magnification to visualise and characterise individual zirconium oxide particles

Representative images of zirconium oxide particles (x100K). Scale bars represent 50nm.

6.4.2 Effect of ceramic oxides on THP-1 cell viability

The viability of THP-1 cells treated with ceramic oxides was assessed by trypan blue staining and an XTT proliferation assay.

6.4.2.1 Trypan blue staining

Activated THP-1 cells were treated for 24 hours with varying concentrations of either Al_2O_3 or ZrO_2 (0.5 to $50\mu\text{m}^3$ particles per cell) and assessed for viability using trypan blue exclusion as described in **section 2.5.1**. There was no significant differences in cell viability following treatment for both Al_2O_3 or ZrO_2 across all concentrations (**Figure 6.3**). At the highest concentration of $50\mu\text{m}^3$ particles per cell, Al_2O_3 treated cells had a viability of approximately 92% ($p=0.5984$) and in ZrO_2 treated cells, 87% ($p=0.1142$).

Given that previous CoCr treatments were optimised for 24 hours and there was no significant effect on cell viability, the same treatments and time point were investigated for cellular proliferation by XTT assay.

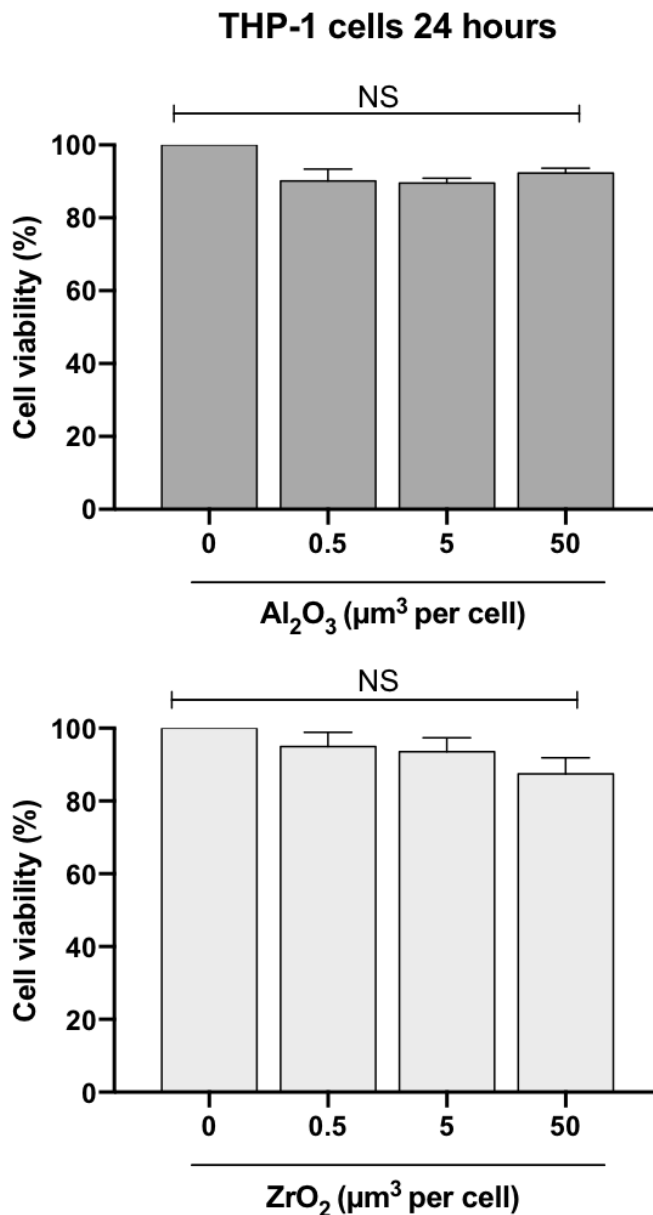


Figure 6.3 THP-1 cell viability Al₂O₃ and ZrO₂ dose response at 24 hours determined by trypan blue staining

Activated THP-1 cells were assessed for viability following stimulation with varying concentrations of Al₂O₃ or ZrO₂ (0.5 to 50 μm³ particles per cell) for 24 hours using trypan blue staining. Viability was not significantly affected across all concentrations of Al₂O₃ and ZrO₂. Data were normalised to 100% viability in untreated cells. Graph is representative of 3 independent experiments. Statistical significance was calculated by one-way ANOVA with Dunnett's multiple comparisons test comparing treated samples to the untreated control. These experiments were conducted in collaboration with MRes student Shannon Jamieson, who worked under my guidance.

6.4.2.2 XTT proliferation assay

The proliferation of activated THP-1 cells was evaluated using the XTT proliferation assay as described in **section 2.5.2**. Cells were treated with varying concentrations of either Al₂O₃ or ZrO₂ (0.5 to 50µm³ particles per cell) for 24 hours and proliferation assessed 24 hours after the addition of the XTT reagent (**Figure 6.4**).

Following 24 hours of stimulation with Al₂O₃, there was a significant increase in proliferation of THP-1 cells across all concentrations (0.5µm³ particles per cell p=0.0006, 5µm³ per cell p=0.0002 and 50µm³ per cell p=0.0021). Similarly, for ZrO₂ treatments, all concentrations significantly increased proliferation of THP-1 cells (0.5µm³ particles per cell p=0.0083, 5µm³ per cell p=0.0015 and 50µm³ per cell p=0.0041).

The results from **Figure 6.3 and Figure 6.4** indicate that similarly to CoCr particle treatments, the 24-hour treatment time and a dose of 50µm³ particles per cell did not affect the viability of THP-1 cells and we could therefore use these conditions in subsequent investigations.

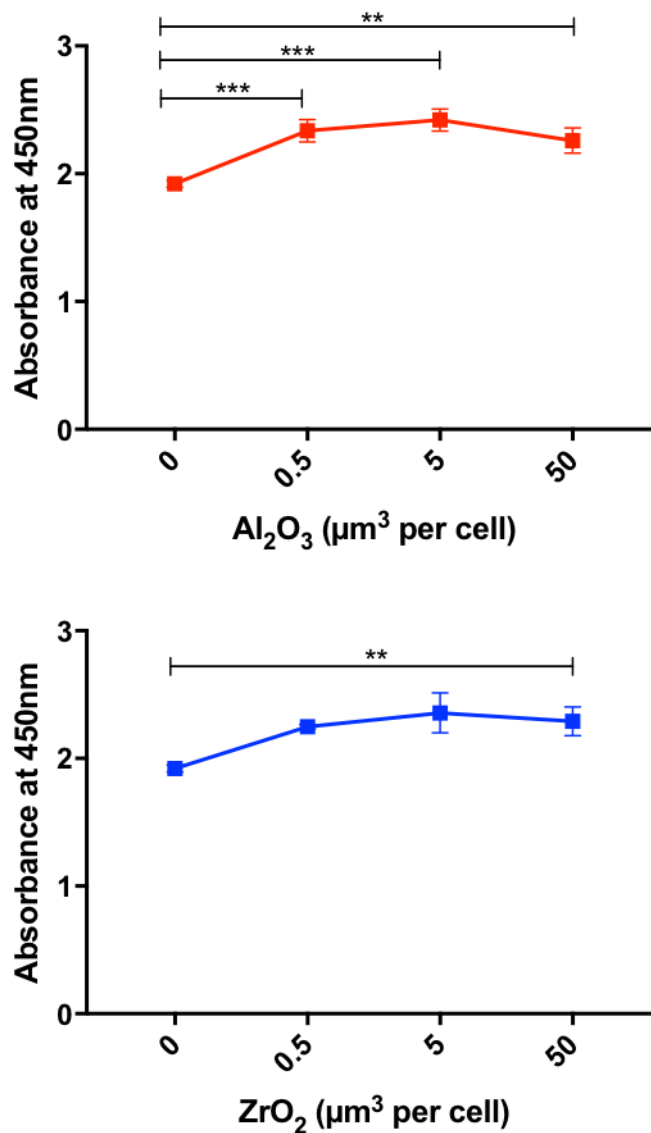


Figure 6.4 Proliferation of THP-1 cells following exposure to Al₂O₃ and ZrO₂ for 24 hours

THP-1 cells were stimulated for 24 hours with treatments prior to the addition of XTT reagent for a further 24 hours to assess proliferation. Graph is representative of 3 independent experiments. Statistical significance was calculated by one-way ANOVA with Dunnett's multiple comparisons test comparing treated samples to the untreated control. These experiments were conducted in collaboration with MRes student Shannon Jamieson, who worked under my guidance.

6.4.3 Uptake of ceramic oxides by macrophage and endothelial cells

Cells (either THP-1 macrophages or HMEC-1 endothelial cells) were treated with Al₂O₃ or ZrO₂ (50µm³ particles per cell) for 24 hours and imaged using TEM as described in **section 2.6**.

6.4.3.1 THP-1 cells

The images shown in **Figure 6.5 to Figure 6.8** clearly show differentiated THP-1 cells in a macrophage-state can phagocytose both Al₂O₃ and ZrO₂. Similarly, to results found with CoCr particle treatment, aggregates of both Al₂O₃ and ZrO₂ were observed in distinct membrane bound vacuoles (as shown in **Figure 6.6 and Figure 6.8**, respectively). It is likely these vacuoles are phagosomes, endosomes and eventually fused with lysosomes in an attempt to break down the phagocytosed particles. There is also evidence of pseudopodia, indicating the THP-1 macrophages are in an activated inflammatory state.

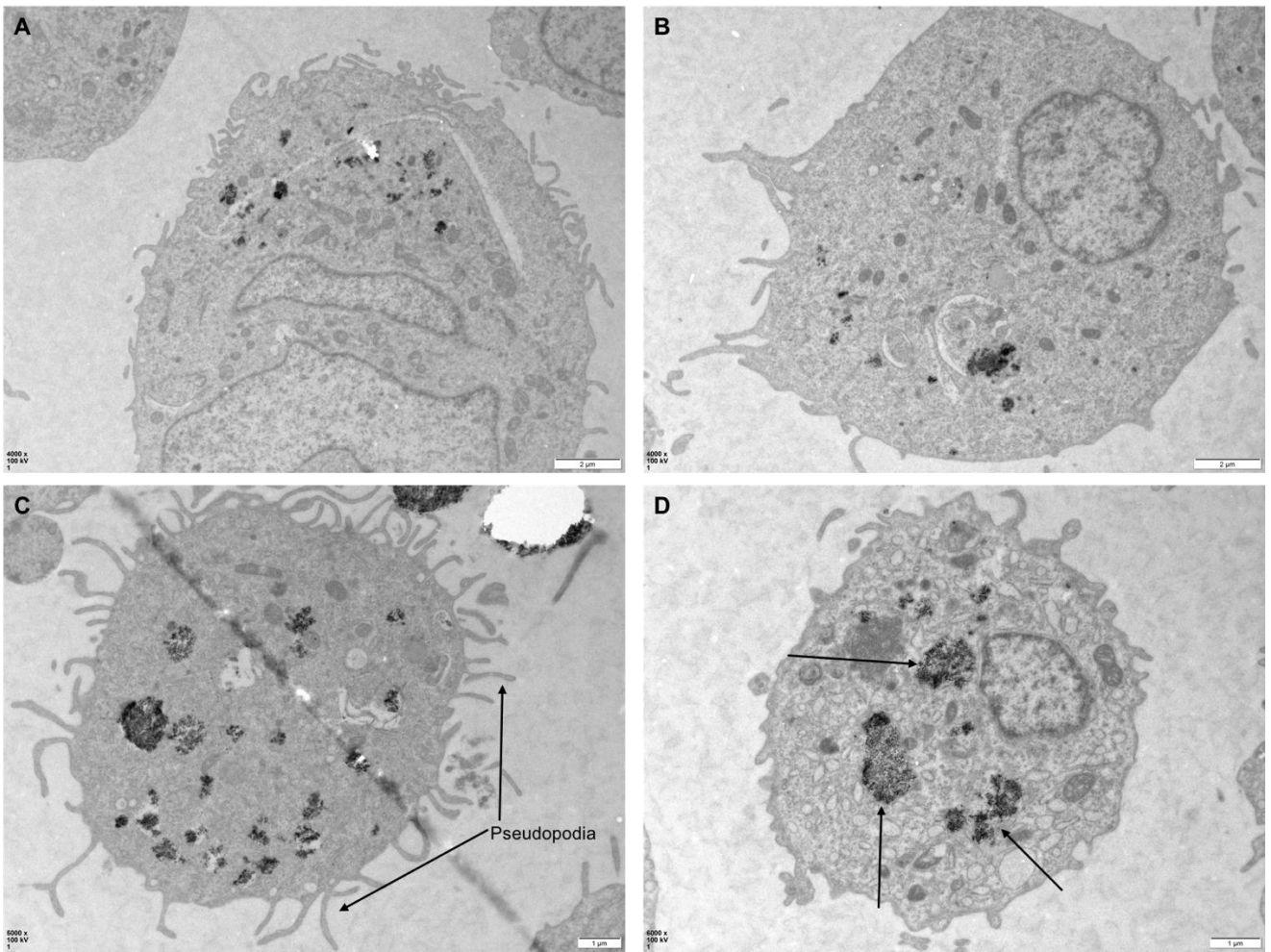


Figure 6.5 Transmission electron microscopy of THP-1 cells treated with Al_2O_3

Representative TEM images of THP-1 cells activated with 5ng/ml PMA and treated with Al_2O_3 ($50\mu m^3$ particles per cell). **(C)** Arrows indicate the presence of pseudopodia. **(D)** Arrows point to examples of aggregates and agglomerates of aluminium oxide particles within distinct membrane bound vacuoles. Scale bars represent either $2\mu m$ **(A)-(B)** or $1\mu m$ **(C)-(D)**.

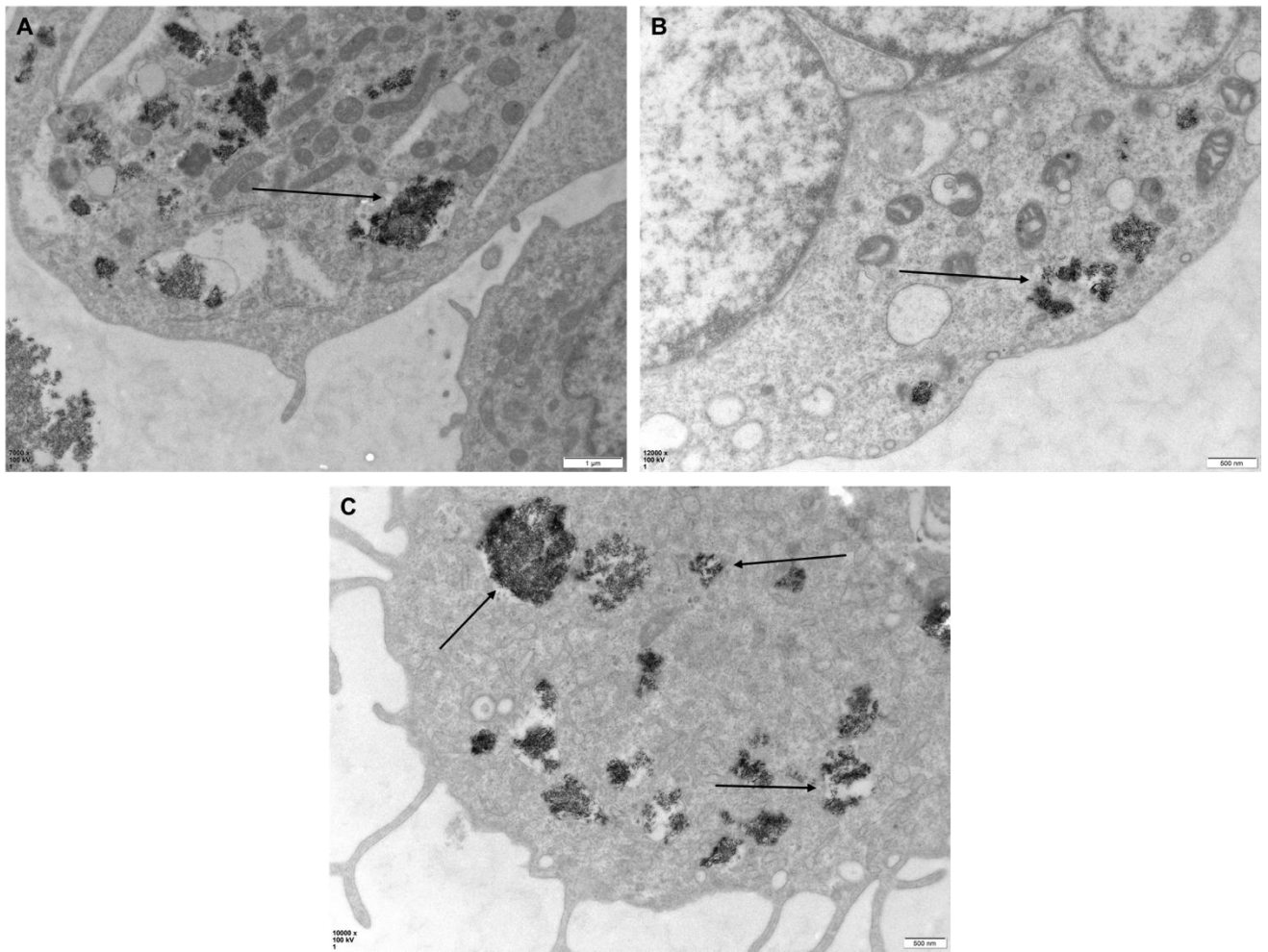


Figure 6.6 Transmission electron microscopy displaying aggregates of Al_2O_3 within vacuoles of THP-1 cells

Representative TEM images of THP-1 cells activated with 5ng/ml PMA and treated with Al_2O_3 ($50\mu m^3$ particles per cell). Arrows point to examples of aggregates and agglomerates of aluminium oxide particles within distinct membrane bound vacuoles. Scale bars represent either $1\mu m$ (A) or 500nm (B)-(C).

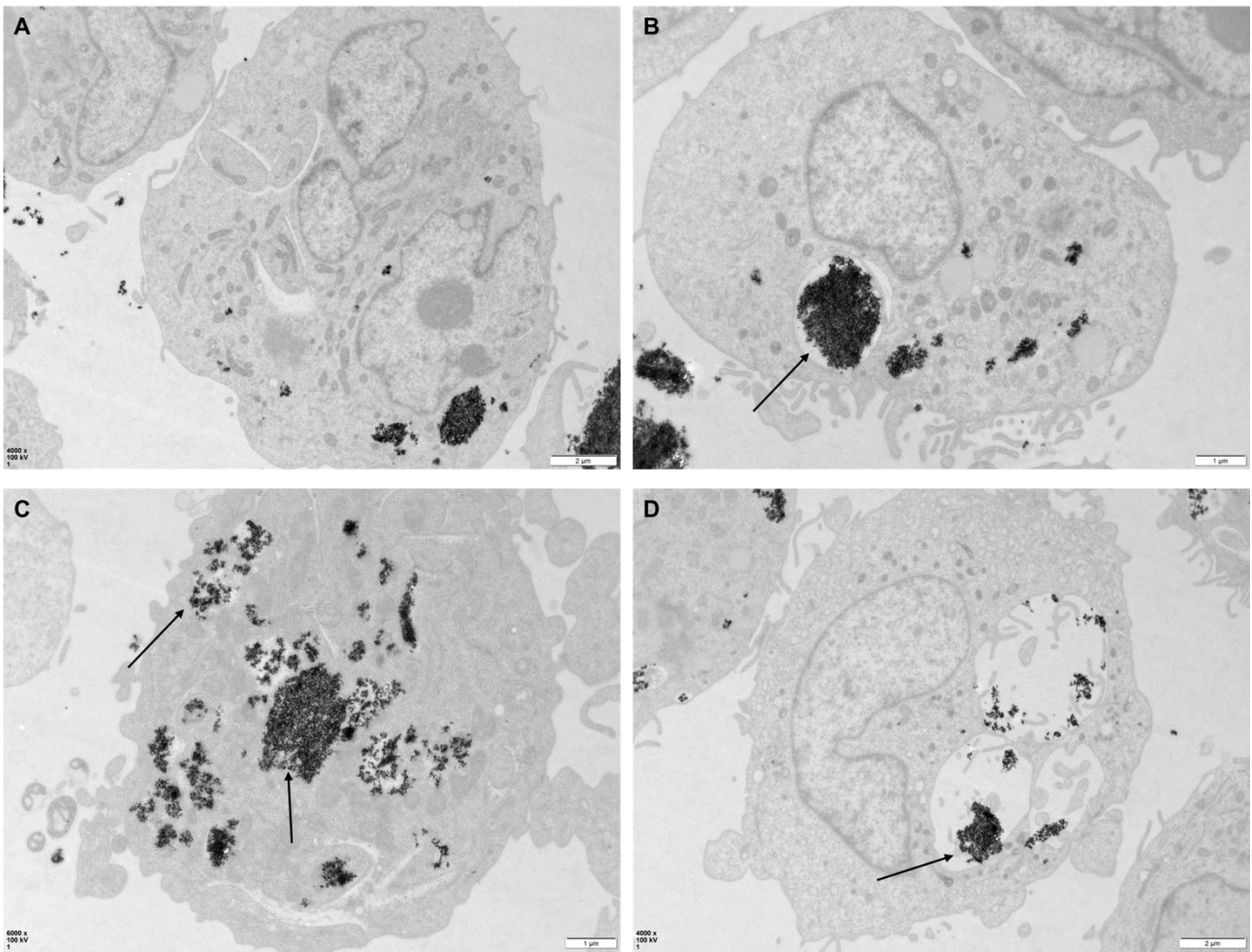


Figure 6.7 Transmission electron microscopy of THP-1 cells treated with ZrO₂

Representative TEM images of THP-1 cells activated with 5ng/ml PMA and treated with ZrO₂ (50μm³ particles per cell). Arrows point to examples of aggregates and agglomerates of zirconium oxide particles within distinct membrane bound vacuoles. Scale bars represent either 2μm (**A**) and (**D**) or 1μm (**B**) and (**C**).

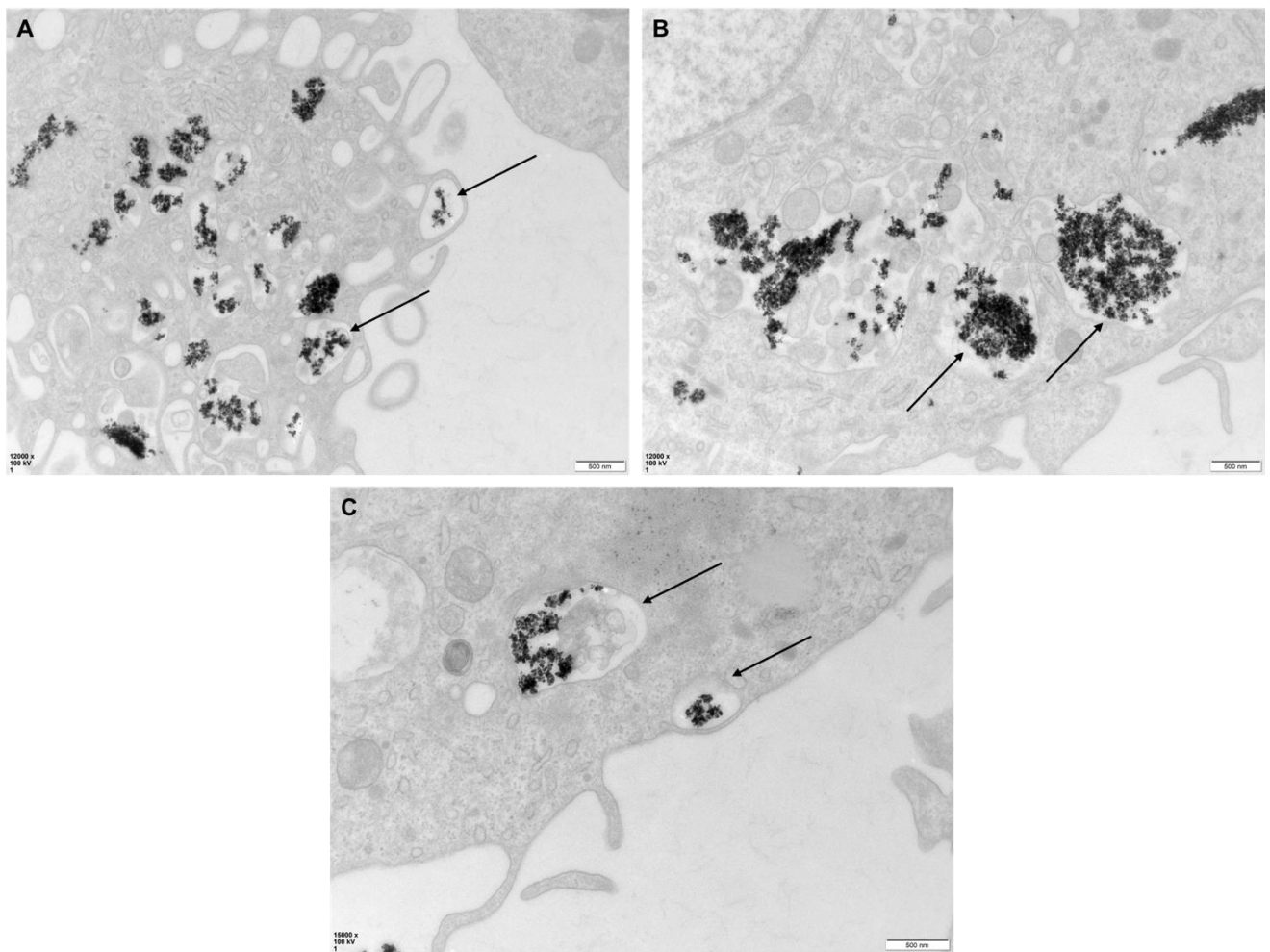


Figure 6.8 Transmission electron microscopy displaying aggregates of ZrO_2 within phagosomes of THP-1 cells

Representative TEM images of THP-1 cells activated with 5ng/ml PMA and treated with ZrO_2 ($50\mu m^3$ particles per cell). Arrows point to examples of aggregates and agglomerates of zirconium oxide particles within distinct membrane bound vacuoles. Scale bars represent 500nm (A)-(D)

6.4.3.2 HMEC-1 cells

Figure 6.9 and **Figure 6.10** represent TEM images of HMEC-1 cells treated with either Al_2O_3 or ZrO_2 ($50\mu m^3$ particles per cell) for 24 hours, respectively. Again, there was evidence that HMEC-1 cells can phagocytose ceramic oxides, as shown by aggregates within distinct vacuoles. However, these vacuoles were generally in fewer numbers compared to THP-1 cells treated with ceramic oxides, particularly for Al_2O_3 treatments.

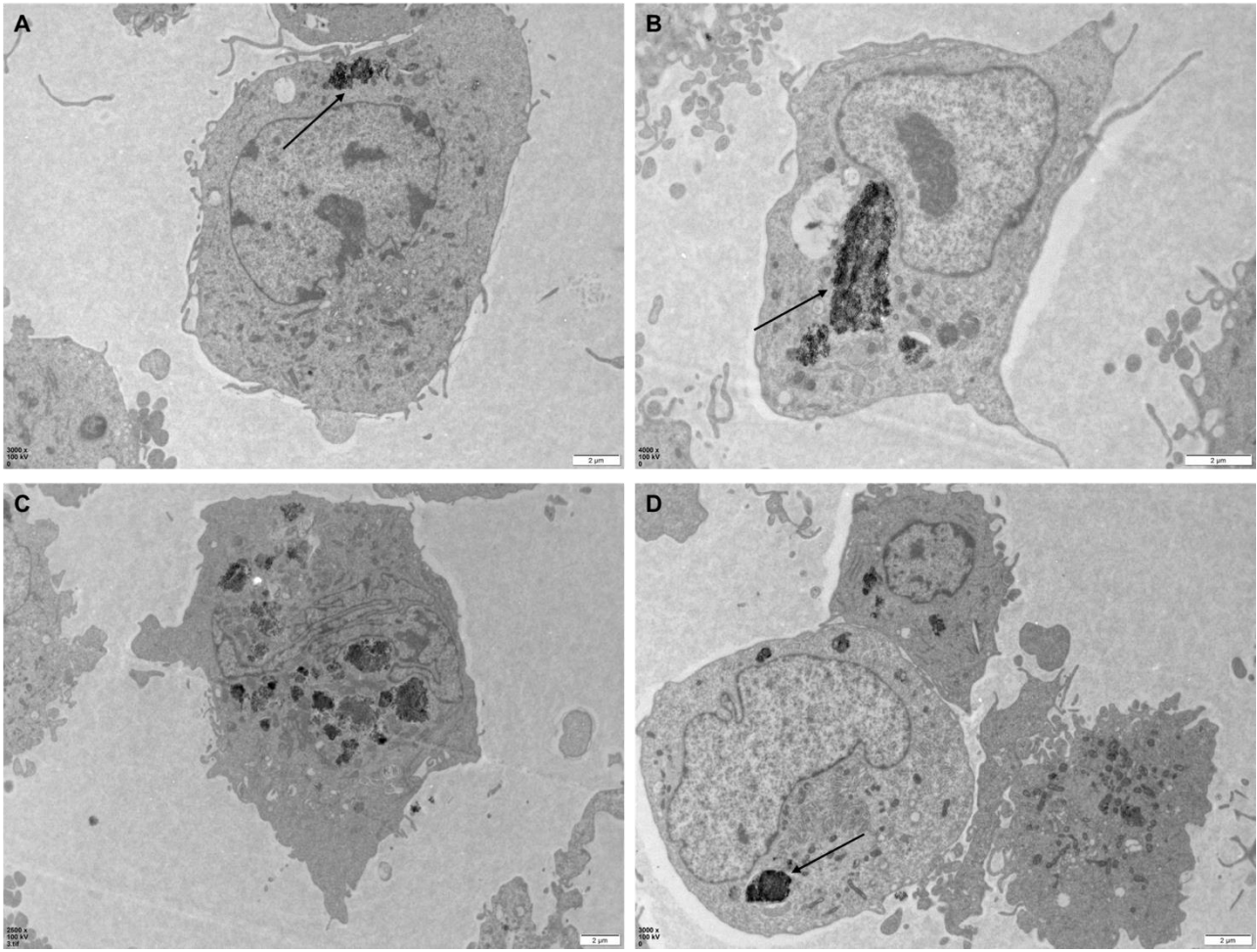


Figure 6.9 Transmission electron microscopy of HMEC-1 cells treated with Al_2O_3

Representative TEM images of HMEC-1 cells treated with Al_2O_3 ($50\mu m^3$ particles per cell). Arrows point to examples of aggregates and agglomerates of aluminium oxide particles within distinct membrane bound vacuoles. Scale bars represent $2\mu m$ (A)-(D).

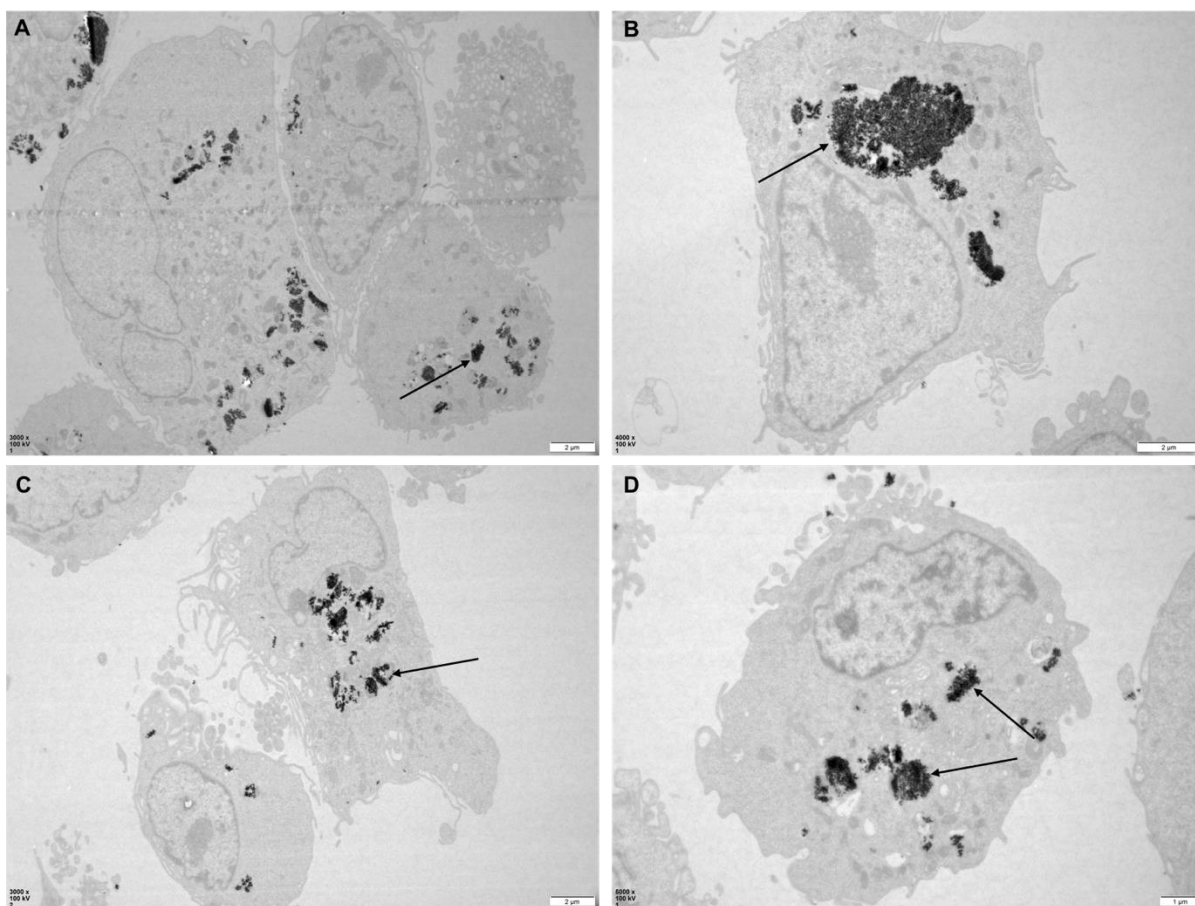


Figure 6.10 Transmission electron microscopy of HMEC-1 cells treated with ZrO_2

Representative TEM images of HMEC-1 cells treated with ZrO_2 ($50\mu m^3$ particles per cell). Arrows point to examples of aggregates and agglomerates of zirconium oxide particles within distinct membrane bound vacuoles. Scale bars represent either $2\mu m$ (A)-(C) or $1\mu m$ (D).

6.4.4 Effect of ceramic oxides on THP-1 cells

THP-1 macrophages were shown to phagocytose ceramic oxides without any significant effect to cell viability or proliferation at a concentration of $50\mu m^3$ particles per cell. Therefore, the effect of ceramic oxides on the protein and gene expression of inflammatory chemokines and cytokines was assessed in THP-1 cells.

6.4.4.1 Inflammatory and chemotactic protein secretion

Differentiated THP-1 cells were treated with varying concentrations of either Al_2O_3 or ZrO_2 (0.5 to $50\mu m^3$ particles per cell) for 24 hours and then the supernatant analysed by ELISA for IL-8, CCL2, CCL3 and CCL4 protein secretion as described in **section**

2.8.1 (Figure 6.11). Stimulation for a duration of 24 hours was optimised by MRes student Shannon Jamieson (data not shown). LPS (10ng/ml) was used as a positive control throughout all experiments.

Similarly, to results from CoCr particle treatments, IL-8 was the most significantly increased chemokine following treatment with both Al₂O₃ and ZrO₂, reaching a maximal concentration of approximately 5000pg/ml for both treatments at 50µm³ particles per cell. This was significant in comparison to untreated THP-1 cells (both p<0.0001).

CCL2 secretion reached a maximal concentration of approximately 850pg/ml following stimulation with ZrO₂ (p<0.0001) and approximately 500pg/ml with Al₂O₃ treatment (p=0.0141) (both 50µm³ particles per cell). CCL3 secretion was also significantly up-regulated in response to both Al₂O₃ and ZrO₂ at the largest concentration of particles investigated (50µm³ per cell) (both p<0.0001). Interestingly for CCL4, the middle concentration of ZrO₂ (5µm³ particles per cell) also significantly increased secretion (p=0.0057) as well as at 50µm³ particles per cell (p<0.0001). Treatment with Al₂O₃ (50µm³ per cell) increased CCL4 secretion to approximately 1300pg/ml which was almost double untreated THP-1 cell concentrations (750pg/ml) (p<0.0001).

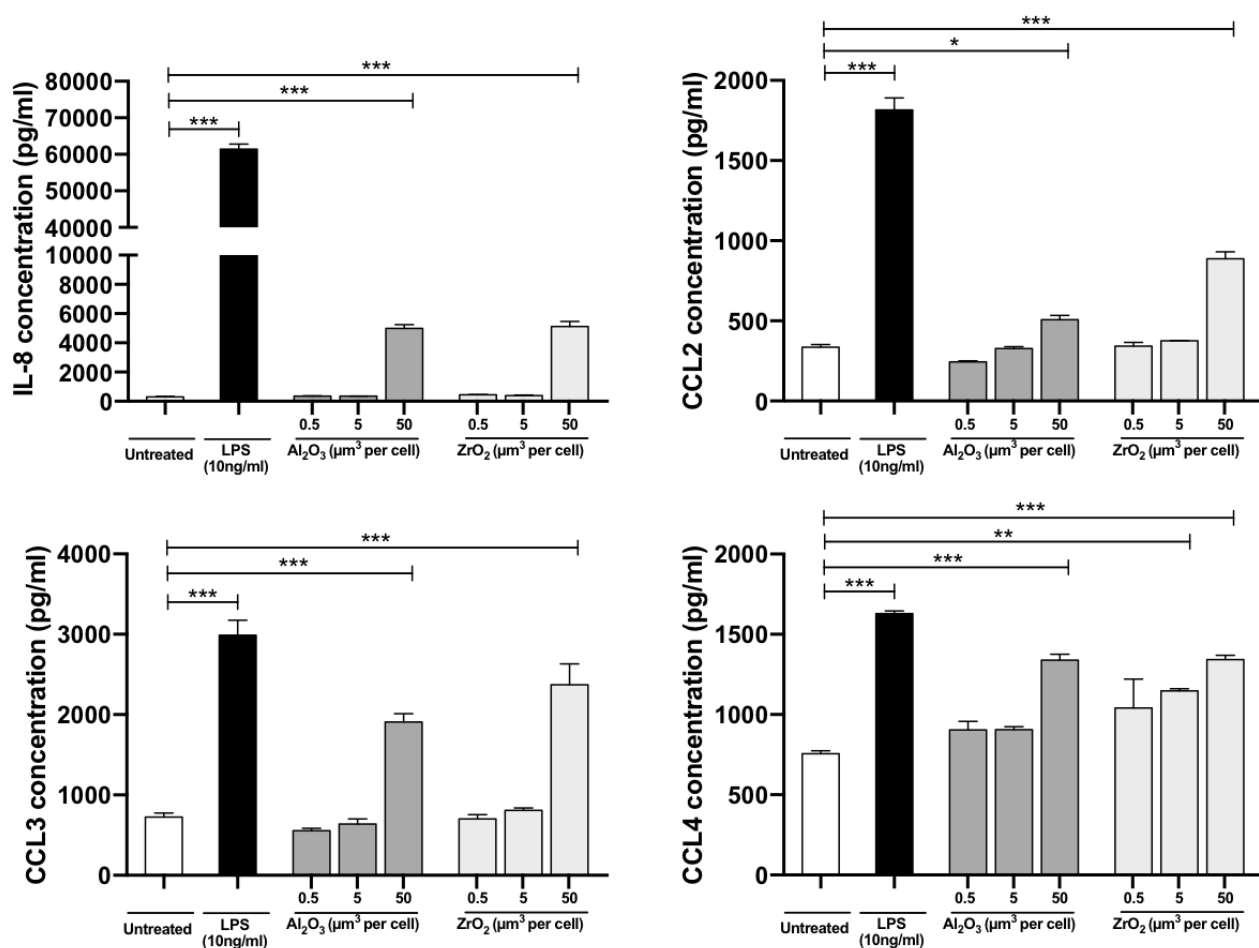


Figure 6.11 Al_2O_3 and ZrO_2 particle dose response in THP-1 cells, assessment of inflammatory proteins

Activated THP-1 cells were treated with different doses of either Al_2O_3 or ZrO_2 (0.5 to $50\mu\text{m}^3$ particles per cell) or LPS (10ng/ml) for 24 hours and changes to inflammatory protein expression assessed by ELISA. Graph is representative of 3 independent experiments. Statistical significance was calculated by one-way ANOVA with Dunnett's multiple comparisons test comparing treated samples to the untreated control. These experiments were conducted in collaboration with MRes student Shannon Jamieson, who worked under my guidance.

6.4.4.2 Inflammatory and chemotactic gene expression

THP-1 cells were also assessed for changes to gene expression following treatment with either Al_2O_3 or ZrO_2 (0.5 to $50\mu\text{m}^3$ particles per cell) for 24 hours (this time point was optimised by MRes student Shannon Jamieson, data not shown). After stimulation, RNA was extracted from cells, cDNA synthesised and qRT-PCR used to analyse relative gene expression as described in **section 2.7**.

Figure 6.12 summarises the changes observed to the gene expression of *IL-8*, *CCL2*, *CCL3* and *CCL4*. Following treatment with both Al_2O_3 and ZrO_2 (both $50\mu\text{m}^3$ particles per cell) there was a significant increase in *IL-8* expression with a 5-fold increase for Al_2O_3 and 10-fold increase for ZrO_2 when compared to untreated control THP-1 macrophages (both $p < 0.0001$).

Interestingly, *CCL2* was the gene with the highest fold-change following THP-1 cell treatments, 24-fold for Al_2O_3 and 36-fold for ZrO_2 (both $50\mu\text{m}^3$ particles per cell and $p < 0.0001$). In fact, there was a significant increase in *CCL2* expression across all concentrations of ZrO_2 ($0.5\mu\text{m}^3$ particles per cell, $p = 0.0025$ and $5\mu\text{m}^3$ particles per cell, $p < 0.0001$).

For *CCL3* expression, only the highest concentration of ZrO_2 ($50\mu\text{m}^3$ particles per cell) elicited a significant increase, reaching an 11-fold increase compared to untreated THP-1 macrophages ($p = 0.0020$). Although there was a 6-fold increase in *CCL3* expression following Al_2O_3 stimulation, this did not reach statistical significance ($p = 0.2068$).

CCL4 expression was significantly up-regulated following treatment with both Al_2O_3 and ZrO_2 (both $50\mu\text{m}^3$ particles per cell). There was a 3-fold increase for Al_2O_3 ($p = 0.0005$) and a 7-fold increase for ZrO_2 treatment in comparison to untreated THP-1 macrophages ($p < 0.0001$).

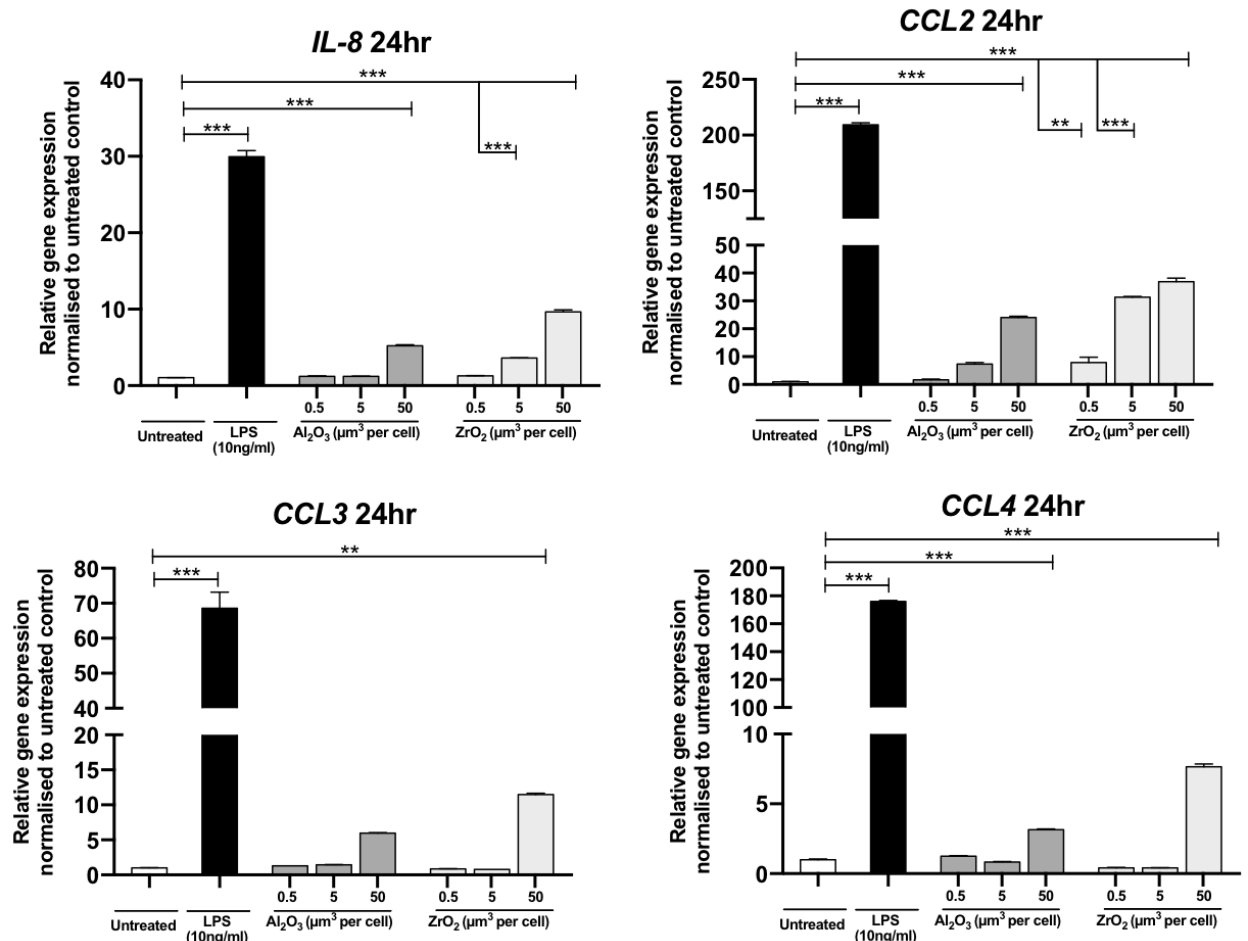


Figure 6.12 Al₂O₃ and ZrO₂ particle dose response in THP-1 cells, assessment of inflammatory gene expression

Activated THP-1 cells were treated with different doses of either Al₂O₃ or ZrO₂ (0.5 to 50 μm³ particles per cell) or LPS (10ng/ml) for 24 hours and changes to inflammatory gene expression assessed by qRT-PCR. Gene expression normalised to untreated control, set to 1. Graph is representative of 3 independent experiments. Statistical significance was calculated by one-way ANOVA with Dunnett's multiple comparisons test comparing treated samples to the untreated control. These experiments were conducted in collaboration with MRes student Shannon Jamieson, who worked under my guidance.

6.4.5 The role of TLR4 in ceramic oxide-mediated inflammation

Due to the findings presented in **Chapter 4** regarding the role of the TLR4 pathway in CoCr particle-mediated inflammation, it was of interest to see whether the observed increases in chemokine expression following ceramic oxide stimulation in THP-1 macrophages was also TLR4 dependent.

Activated THP-1 cells were pre-treated with the TLR4 small molecule antagonist, CLI-095 (1µg/ml) for 6 hours prior to stimulation with either Al₂O₃ or ZrO₂ (50µm³ particles per cell) for 24 hours and expression of *IL-8* analysed by both qRT-PCR and ELISA (**Figure 6.13**). Treatment with LPS (10ng/ml) was again used as a positive control throughout which demonstrated a significant decrease in *IL-8* expression and secretion in cells which were pre-treated with CLI-095 (both p<0.0001). There was also no significant change in untreated cells treated with and without CLI-095 (both p>0.9999).

For THP-1 macrophages stimulated with Al₂O₃ and ZrO₂, there was also significant decreases in *IL-8* gene expression when cells were pre-treated with CLI-095 (p=0.0070 and p=0.0065, respectively) (**Figure 6.13A**). These findings were reflected when analysing IL-8 protein secretion which was also significantly reduced when THP-1 cells were pre-treated with CLI-095 then received stimulation with both Al₂O₃ and ZrO₂ (both p<0.0001) (**Figure 6.13B**). Secretion in this instance dropped to concentrations observed in untreated THP-1 macrophages (approximately 1000pg/ml).

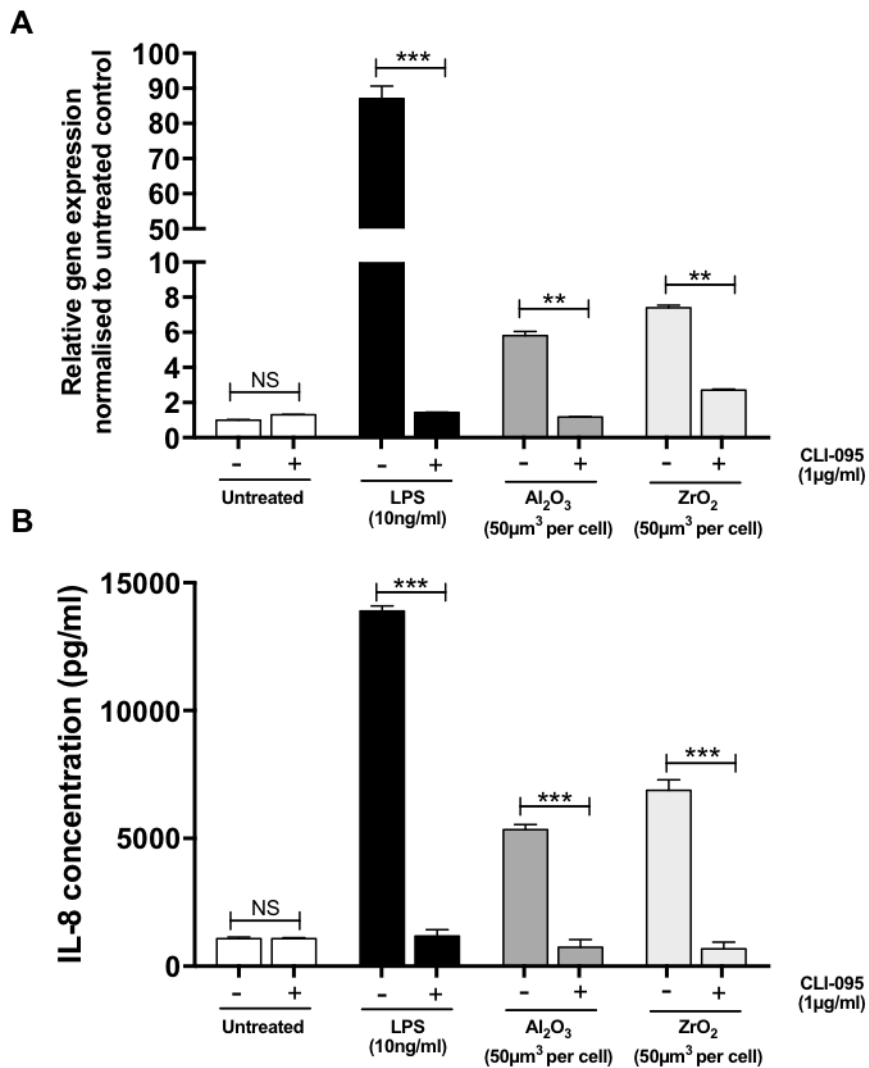


Figure 6.13 Effect of TLR4 inhibition in Al₂O₃ and ZrO₂ treated THP-1 cells, assessment of IL-8 gene and protein expression

Activated THP-1 cells were pre-treated with CLI-095 (1µg/ml) for 6 hours then stimulated with either LPS (10ng/ml), Al₂O₃ or ZrO₂ (both 50µm³ particles per cell) for 24 hours. **(A)** IL-8 expression was measured using qRT-PCR. **(B)** Changes to IL-8 protein expression was assessed by ELISA. Gene expression normalised to untreated control, set to 1. Graph is representative of 3 independent experiments. Statistical significance was calculated by one-way ANOVA with Tukey's test for multiple comparisons comparing all samples to each other. These experiments were conducted in collaboration with MRes student Shannon Jamieson, who worked under my guidance.

6.4.6 Mouse macrophage inflammatory response to CoCr particles

6.4.6.1 CCL3 dose response

Results from **Chapter 4** indicated that CoCr particles could cause a small but significant increase in CCL3 secretion from J774 mouse macrophages whereas CoCl₂ could not. Therefore, it was of interest to determine whether Al₂O₃ and ZrO₂ could also activate murine macrophages.

J774 cells were stimulated for 24 hours with either; a range of Al₂O₃ and ZrO₂ particle concentrations (0.5µm to 50µm³ per cell) or 10ng/ml LPS. CCL3 concentration was measured by ELISA using supernatants from stimulated cells (**Figure 6.14**). Following treatment with LPS, CCL3 protein secretion was significantly increased to approximately 10,000pg/ml (p<0.0001). The highest dose of Al₂O₃ (50µm³ particles per cell) significantly increased CCL3 secretion to a similar concentration observed in LPS-treated cells (p<0.0001). There were significant increases in CCL3 secretion in all ZrO₂-concentrations used for treatments, up to a maximum of 11,000pg/ml at 50µm³ particles per cell (p<0.0001).

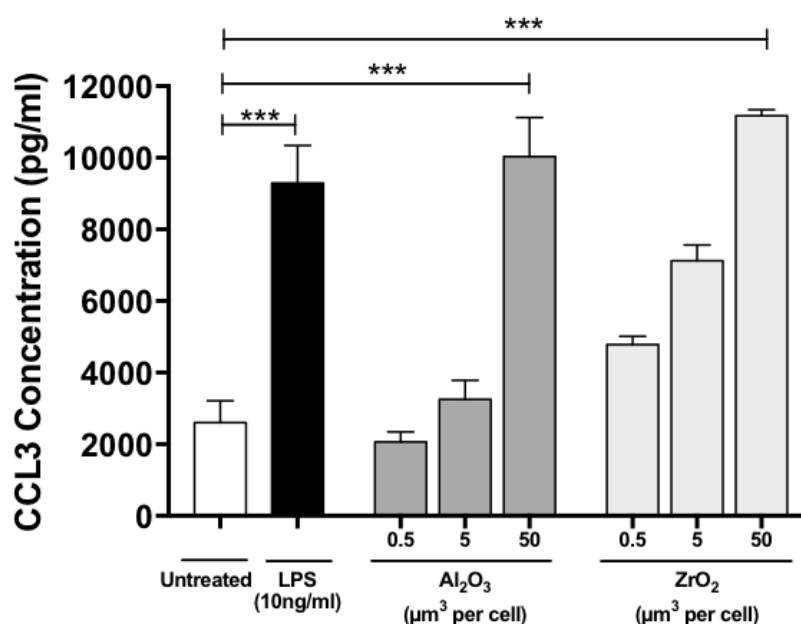


Figure 6.14 Al₂O₃ and ZrO₂ dose response in mouse J774 cells - assessment of CCL3 protein expression

J774 macrophage cells were treated with either; LPS (10ng/ml), or different doses of Al₂O₃ or ZrO₂ (0.5 to 50μm³ particles per cell) for 24 hours and changes to CCL3 protein expression assessed by ELISA. Graph is representative of 3 independent experiments. Statistical significance was calculated by one-way ANOVA with Dunnett's multiple comparisons test comparing treated samples to the untreated control.

6.4.6.2 Effect of TLR4 inhibition on CCL3 protein secretion

To determine whether the observed significant increase in CCL3 secretion following Al₂O₃ and ZrO₂ stimulation was TLR4 dependent, the small molecule TLR4 antagonist, CLI-095 was used in further J774 cell treatments. The same protocol is described in **section 6.4.6.1**, however, prior to the addition of stimulants for 24 hours, some cells were pre-treated with 1μg/ml CLI-095 for 6 hours. CCL3 protein secretion was then quantified by ELISA (**Figure 6.15**).

In LPS stimulated cells, there was a significant decrease in CCL3 protein expression with the addition of CLI-095 (p<0.0001). There were also significant decreases in CCL3 secretion in both Al₂O₃ and ZrO₂ treatments in the presence of CLI-095 (p=0.0014 and p=0.0113, respectively).

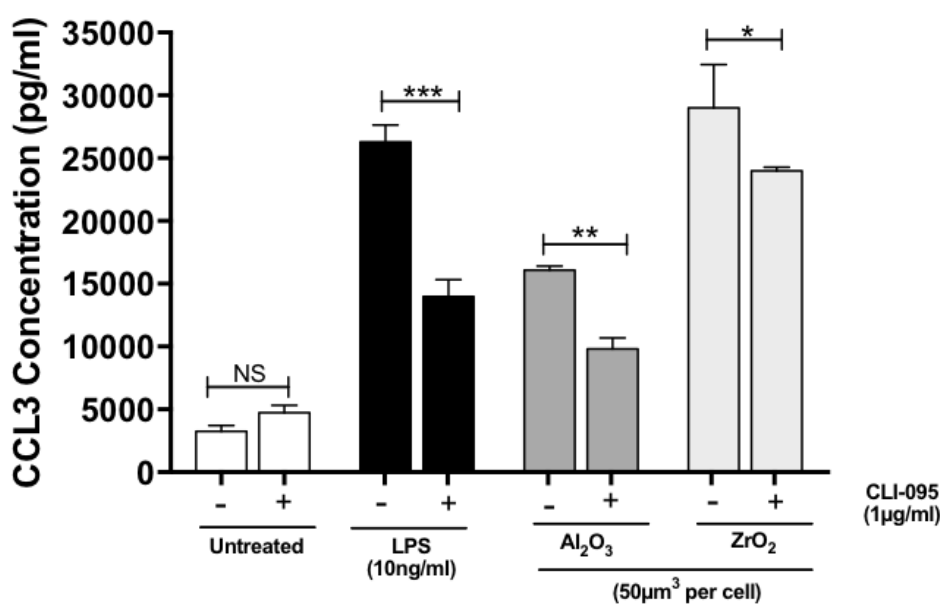


Figure 6.15 Effect of TLR4 inhibition in Al₂O₃ and ZrO₂ treated J774 cells, assessment of CCL3 protein expression

J774 macrophage cells were pre-treated with CLI-095 (1µg/ml) for 6 hours then stimulated with either LPS (10ng/ml), Al₂O₃ or ZrO₂ (both 50µm³ particles per cell) for 24 hours. CCL3 protein expression assessed by ELISA. Graph is representative of 3 independent experiments. Statistical significance was calculated by one-way ANOVA with Tukey's test for multiple comparisons comparing all samples to each other.

6.4.7 The role of the inflammasome in ceramic oxide-mediated inflammation

Supernatant from Al₂O₃ and ZrO₂-treated THP-1 macrophages was analysed on the MSD U-PLEX assay for the expression of chemokine and cytokine targets described in **section 4.3.2** (data not shown). As there was a significant increase in IL-1β secretion, the activation of the NLRP3 inflammasome was assessed as discussed in **section 4.4.10**. Briefly, Al₂O₃ or ZrO₂ were either substituted as the first 'priming' PAMP signal in place of LPS followed by treatment with ATP to allow full NLRP3 activation. Or, LPS was used as the priming signal followed by stimulation with Al₂O₃ or ZrO₂ particles; thereby acting as a DAMP inducer. IL-1β protein secretion was assessed by ELISA from the supernatants of treated THP-1 cells and qRT-PCR was used to analyse IL-1β gene expression.

Firstly, activated THP-1 cells were treated with either LPS (10ng/ml), Al₂O₃ or ZrO₂ (both 50µm³ particles per cell) for 23 hours to replicate the initial 'priming' signal of NLRP3 activation. The second activation signal was then induced by the addition of

ATP (5mM) for 1 hour. Following this stimulation, the expression of IL-1 β was quantified using ELISA and qRT-PCR (**Figure 6.16**).

For *IL-1 β* expression, THP-1 macrophages stimulated with Al₂O₃ or ZrO₂ only, did not demonstrate any significant increase, remaining at untreated cell levels (p=0.1823 and p=0.1291, respectively) (**Figure 6.16A**). However, with the addition of ATP, *IL-1 β* expression was significantly increased approximately 4-fold for Al₂O₃ treated cells (p=0.0002) and 4.5-fold for ZrO₂ treatments (p<0.0001) in comparison to cells treated with ATP only. There was no significant difference in *IL-1 β* expression between untreated cells with and without ATP (p=0.0642).

IL-1 β protein secretion, as measured by ELISA, demonstrated a similar trend to gene expression (**Figure 6.16B**). However, there was a small but significant increase in THP-1 macrophages which received ATP treatment only (p=0.0202). Again, THP-1 macrophages stimulated with Al₂O₃ or ZrO₂ only, did not demonstrate any significant increase, remaining at untreated cell levels (p=0.1657 and p=0.4786, respectively). IL-1 β protein secretion reached a maximal peak of approximately 100pg/ml for both Al₂O₃ and ZrO₂ treatments which were then stimulated with ATP. This was a significant increase in comparison to untreated cells with the addition of ATP for 1 hour (both p<0.0001).

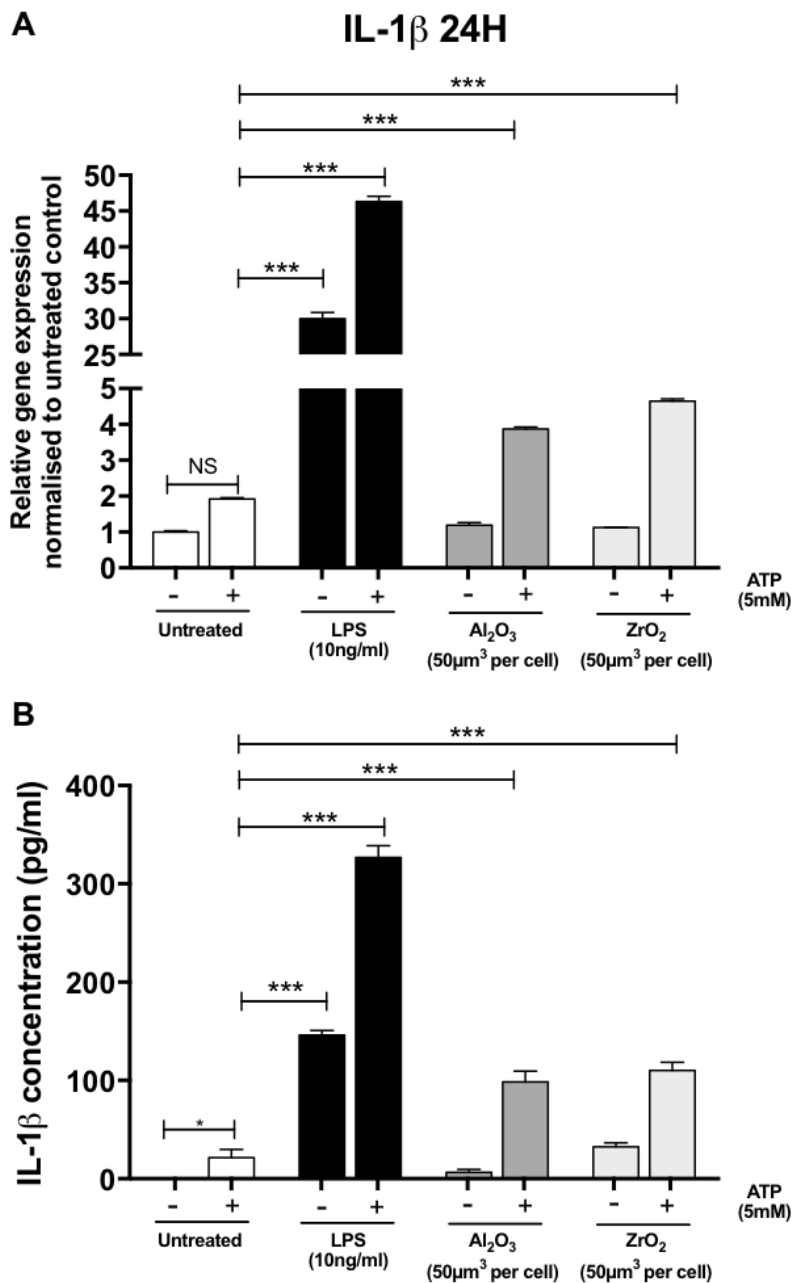


Figure 6.16 IL-1 β gene and protein expression following Al₂O₃ or ZrO₂ stimulation and ATP treatment in THP-1 cells

Activated THP-1 cells were either left untreated or stimulated with either LPS (10ng/ml), Al₂O₃ or ZrO₂ (both 50µm³ particles per cell) for 23 hours. Cells were then treated with ATP (5mM) for 1 hour before IL-1 β gene expression was analysed by qRT-PCR (**A**) or IL-1 β protein expression assessed by ELISA (**B**). Gene expression normalised to untreated control, set to 1. Graph is representative of 3 independent experiments. Statistical significance was calculated by one-way ANOVA with Dunnett's multiple comparisons test comparing treated samples to the untreated control with ATP and Tukey's test for multiple comparisons comparing all samples to each other. These experiments were conducted in collaboration with MRes student Shannon Jamieson, who worked under my guidance.

To establish whether Al₂O₃ and ZrO₂ were stimulating THP-1 cells as a DAMP-inducer rather than a PAMP-stimulus, LPS-treated cells were followed by a 1 hour stimulation with either Al₂O₃ or ZrO₂ (i.e. to be used in place of ATP). Therefore, THP-1 cells were treated with 10ng/ml LPS for 23 hours and then stimulated for 1 hour either with ATP (5mM), Al₂O₃ or ZrO₂ (both 50µm³ particles per cell) (**Figure 6.17**). LPS treatment followed by ATP stimulation led to the largest increases in IL-1β gene and protein expression. When THP-1 cells were firstly treated with LPS and then with Al₂O₃ there was no significant difference in IL-1β gene expression or protein secretion when compared to LPS alone (p=0.1367 and p=0.2975, respectively). However, there were significant increases in both IL-1β gene and protein expression following the addition of ZrO₂ for 1 hour after 24 hours of LPS stimulation (p<0.0001 and p=0.0018, respectively).

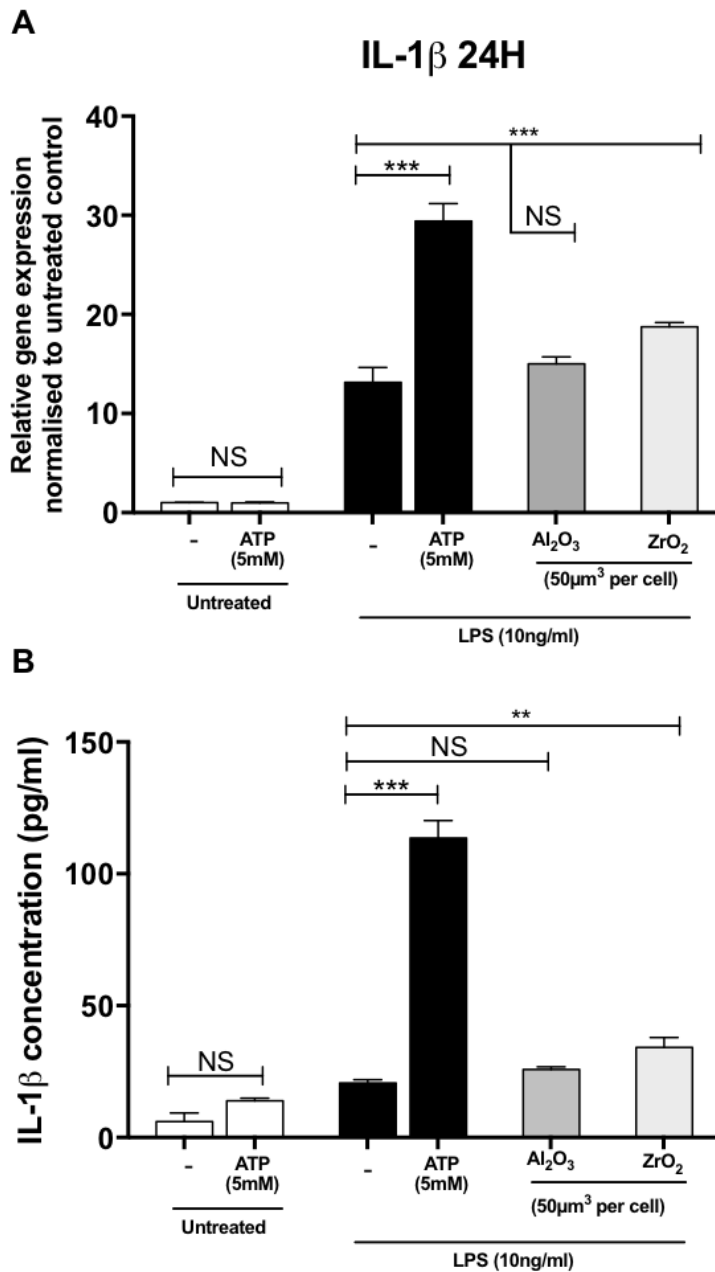


Figure 6.17 IL-1 β gene and protein expression following LPS treatment and Al₂O₃ or ZrO₂ stimulation in THP-1 cells

Activated THP-1 cells were either left untreated or stimulated with LPS (10ng/ml) for 23 hours. Cells were then treated with either; ATP (5mM), Al₂O₃ or ZrO₂ (both 50 μ m³ particles per cell) for 1 hour before IL-1 β gene expression was analysed by qRT-PCR (**A**) or IL-1 β protein expression assessed by ELISA (**B**). Gene expression normalised to untreated control, set to 1. Graph is representative of 3 independent experiments. Statistical significance was calculated by one-way ANOVA with Dunnett's multiple comparisons test comparing treated samples to LPS-stimulated only cells and Tukey's test for multiple comparisons comparing all samples to each other.

6.5 Discussion

Characterisation of ceramic oxide nanoparticles

The ceramic oxides used for this part of the study, Al₂O₃ and ZrO₂, were characterised using TEM to determine their size and shape. As expected, the images revealed particles were all nanometre in size. However, Al₂O₃ nanoparticles were shard-like in appearance and ZrO₂ nanoparticles displayed a round morphology. Interestingly, it is believed that clinically-relevant alumina wear particles have a bimodal size distribution, with some nanometre sized (5-90nm) particles and some larger particles (0.2-10µm) observed by SEM and TEM (Tipper *et al.*, 2002). A study compared responses from PBMCs challenged with either clinically-relevant alumina wear particles as described above or with alumina nanopowder, with uniform morphology and nanometre in size (similar to the one used in this study) (Hatton *et al.*, 2003). Significantly higher volumes of the clinically-relevant particles than the alumina powder were required to stimulate TNF-α secretion (Hatton *et al.*, 2003). The authors hypothesised this was due to the clinically-relevant particles having fewer particles in the size range most likely to be phagocytosed by cells (0.1-1µm) (Green *et al.*, 2000).

Therefore, the ceramic oxide nanopowders used in this study offer an *in vitro* model for ceramic wear debris particles but cannot be classified as accurately clinically-relevant. However, the size range observed by TEM means they are within the critical size range required for macrophage activation.

Cytotoxicity of ceramic oxides

A previous study has shown that ceramic particles do not reduce viability of fibroblasts and only at a high concentration of 50µm³ particles per cell was viability reduced in a macrophage cell line following 48 hours of stimulation (Germain *et al.*, 2003). In this study, both Al₂O₃ and ZrO₂ did not affect THP-1 macrophage cell viability when treated for 24 hours. Therefore, it would be interesting to treat the THP-1 cells for a longer period (e.g. 48 hours) to determine whether this would cause cytotoxicity. Similarly to the findings presented here, Radziun *et al.* found that 24 hours of cell exposure to Al₂O₃ did not decrease cell viability (Radziun *et al.*, 2011).

Alumina particles have consistently demonstrated increased cytotoxicity for macrophages than fibroblasts in previous studies (Olivier *et al.*, 2003; Tsaousi *et al.*, 2010). It is likely that macrophages such as THP-1 cells are more susceptible to the

effects of Al₂O₃ and ZrO₂ as they more actively phagocytic in comparison to other cell types such as fibroblasts. This was emphasised by TEM images of both THP-1 and HMEC-1 cells treated with Al₂O₃ and ZrO₂ as it appeared the THP-1 cells had phagocytosed a greater volume of particles compared to the HMEC-1 cells. Assessment of HMEC-1 cytotoxicity following ceramic oxide treatment would provide further insight into this hypothesis.

Studies have demonstrated the potential for primary fibroblasts and J774 macrophages to engulf both aluminium and zirconium nanoparticles in endocytosis vesicles (Hashimoto and Imazato, 2015; Faye *et al.*, 2017). A study comparing internalisation of different sized Al₂O₃ particles indicated that with decreasing particle diameter more particles were internalised, particularly those less than 100nm (the size of particles used in this study) (Bohme *et al.*, 2014). These findings are supported by the fact ceramic wear debris have been observed in the peri-prosthetic tissues of patients with CoC implants and appear to be engulfed by macrophages (Rony *et al.*, 2018).

Interestingly, the proliferation of THP-1 cells, assessed by XTT assay, appeared to significantly increase when treated with both Al₂O₃ and ZrO₂. Roualdes *et al.* also found that Al₂O₃ and ZrO₂ particle slightly increased fibroblast proliferation using a similar assay used here (Roualdes *et al.*, 2010). Furthermore, another study showed increase in proliferation of monocytes treated with ZrO₂ at low concentrations (Dalal *et al.*, 2012). However, the duration of cell treatments in these studies were 3 and 48 hours, respectively, and in this study for 24 hours. Whereas, a study which treated an epithelial cell line with Al₂O₃ found that proliferation reduced by day 5 of exposure (Wei *et al.*, 2014). Therefore, investigating the proliferative capacity of THP-1 cells over a longer time could also be useful.

Ceramic oxide-mediated chemokine expression

In this study, THP-1 macrophages stimulated with both Al₂O₃ and ZrO₂ demonstrated significant increases in chemokine gene expression and protein secretion (IL-8, CCL2, CCL3 and CCL4). This finding is consistent with a previous study which observed increased IL-8 and CCL2 secretion from primary human macrophages treated with alumina particles (Kaufman *et al.*, 2008). Interestingly, Klinder *et al.* demonstrated a greater induction of IL-8 expression from ceramic particles compared to CoCr particles in human osteoblasts (Klinder *et al.*, 2018). Furthermore, CCL2 concentrations in the

synovial fluid of patients are found to be significantly higher in patients with CoC implants compared to controls (Montesi *et al.*, 2012). This highlights the importance of investigating the biological effects of ceramics used in CoP and CoC implants as their popularity increases. The notion that these materials are considered highly biocompatible can be brought into question given the results presented here and from others.

However, it is important to note that wear from CoP and CoC implants is significantly lower than their MoP and MoM counterparts so any adverse effects from wear debris may take considerably longer to come to fruition. For example, in a patient cohort study, only 18% of patients with a CoC implant had elevated levels of serum aluminium, emphasising the low corrosion level (Savarino *et al.*, 2006). For that reason, the concentrations used in this study ($50\mu\text{m}^3$ particles per cell) for *in vitro* cell treatments may be considerably higher than what is experienced *in vivo*. Nevertheless, despite the general low wear rates from CoP and CoC implants, these prostheses have reported cases of osteolysis and pseudotumour formation (Campbell *et al.*, 2017; Serrano *et al.*, 2018). Therefore, understanding the biological effects of ceramics at high concentrations may be beneficial in understanding these more extreme cases.

The increased expression of the chemokine IL-8 following Al_2O_3 and ZrO_2 stimulation was found to be largely TLR4-dependent as inhibiting TLR4 signalling significantly reduced these observed increases. The role of TLR4 in biological responses to ceramics has not been investigated extensively by other groups. Zirconium particles have been reported to increase TLR4, MyD88, TRIF and NF- κ B gene expression in isolated mouse macrophages (Obando-Pereda *et al.*, 2014). The authors also found increased expression of TNF- α , IL-1 β and IL-6. Therefore, this is the first study to demonstrate that TLR4 plays a central role in ceramic oxide-mediated chemokine expression in a human macrophage cell line.

Results from this study also indicated that both Al_2O_3 and ZrO_2 could perpetuate an inflammatory response in J774 mouse macrophages, as measured by CCL3 secretion. This is perhaps unsurprising given that many other studies investigating the biological effects of ceramics have used this cell line and other similar (e.g. RAW 264.7 cells) as an *in vitro* model (Petit *et al.*, 2002; Rodrigo *et al.*, 2006; Nishanth *et al.*, 2011). For example, studies have reported an increase in TNF- α secretion when J774 cells were incubated with alumina particles (Petit *et al.*, 2002; Rodrigo *et al.*, 2006). As both Al_2O_3

and ZrO₂ could significantly increase CCL3 secretion in J774 mouse macrophages, this highlights the differing mechanisms of TLR4 activation when compared to cobalt ions which bind to conserved histidine residues which are not expressed by murine TLR4. The results presented here demonstrate that Al₂O₃ and ZrO₂ must use an alternative mechanism of TLR4 activation which are yet to be fully elucidated.

It was interesting that although CCL3 secretion was significantly reduced when J774 cells were pre-treated with the TLR4 inhibitor (CLI-095), this decrease was not as prominent as observed in THP-1 macrophages. This could be due to the particularly large increases in CCL3 secretion following ceramic oxide treatment (specifically ZrO₂). Therefore, the efficacy of CLI-095 to inhibit these observed high concentrations may be reduced. This was emphasised by the fact CCL3 expression in J774 cells stimulated with LPS in the presence of CLI-095 did not reduce to untreated control cell levels, despite eliciting its response exclusively through TLR4 signalling.

The role of the NLRP3 inflammasome in ceramic oxide-mediated inflammatory responses

As discussed in **Chapter 4** for CoCr particles, the role of the NLRP3 inflammasome in ceramic oxide-mediated inflammatory responses was initially investigated by using IL-1 β secretion as a marker of NLRP3 activation. Previous studies have focused on the potential role of NLRP3 activation in CoCr particles or CoCl₂ mediated inflammatory osteolysis (Caicedo *et al.*, 2009; Samelko *et al.*, 2016). Therefore, it was of interest to investigate this model of NLRP3 activation in ceramic oxide inflammatory responses.

The results from this part of the study were in contrast to the findings from CoCr particles in that both Al₂O₃ and ZrO₂ appeared to effectively 'prime' THP-1 macrophages as IL-1 β expression was significantly increased following treatment with the ceramic oxides and then stimulation with ATP. These observed effects were not reflected when THP-1 cells were solely treated with Al₂O₃ and ZrO₂. These findings suggest that ceramic oxides activate the NLRP3 inflammasome as a PAMP priming inducer, similar to LPS (Mariathasan *et al.*, 2006). Moreover, this highlights the results discussed previously regarding the central role for TLR4 in ceramic oxide inflammatory responses.

Aluminium salts (sometimes referred to as alum) are commonly used in vaccine adjuvants and have been shown to induce NLRP3-dependent induction of IL-1 β and

IL-18 (Hornung *et al.*, 2008). Importantly, it has been shown alum achieves this by lysosomal destabilisation and therefore works through the second activation signal of the NLRP3 activation pathway (Hornung *et al.*, 2008). Although alum has a different composition (alum hydroxide) to the Al_2O_3 used in this study, its potential to act as a DAMP inducer in place of ATP was investigated further. THP-1 macrophages were firstly primed with LPS for 23 hours and then stimulated with either Al_2O_3 or ZrO_2 for 1 hour. Interestingly, there was no significant increase in IL-1 β expression between cells treated with LPS alone and those further stimulated with Al_2O_3 . However, there was a significant increase in IL-1 β expression when LPS pre-treated cells were then stimulated with ZrO_2 . The observed differences between the ceramic oxides could be because ZrO_2 has been proven to be a more potent inflammatory inducer in terms of chemokine expression compared to Al_2O_3 .

Another possible explanation for these findings could be the possibility of induced 'lysosomal mediated necrosis'. Lima *et al.* performed a set of experiments comparing the effect of either lysosome-disrupting agents (such as alum) with ATP on mouse macrophages (Lima *et al.*, 2013). When ATP was used as the second NLRP3 activation signal, caspase-1 became activated resulting in caspase-1 induced pyroptosis and secretion of IL-1 β . However, alum, which is known to cause lysosomal destabilisation, induced caspase-1 independent cell death with minimal release of IL-1 β . The investigators therefore demonstrated the potential for alum to cause complete lysosomal rupture, release of cathepsins, which can then degrade inflammatory proteins such as caspase-1, preventing NLRP3 activation and resulting in necrotic cell death (Lima *et al.*, 2013). Therefore, in the set of experiments presented in this study, both Al_2O_3 and ZrO_2 may have potentially caused lysosomal mediated necrosis following previous priming with LPS, preventing significant increases in IL-1 β secretion. The findings presented in **Chapter 4** when CoCr particles were used as a potential NLRP3 inducer and failed to induce IL-1 β secretion may also be due to lysosomal rupture caused by the phagocytosis of particles as presented in TEM images.

Conclusions made from these set of experiments should be taken with caution as further optimisation and markers of NLRP3 activation are required. For example, a time course in which perhaps a shorter LPS 'priming' period followed by a longer stimulation with Al_2O_3 or ZrO_2 would be useful. For example, a recent study investigating

responses to titanium particles primed macrophages with LPS for 1 hour and then stimulated with titanium for 8 hours (versus 23 hours and 1 hour used in this study, respectively) (Jamsen *et al.*, 2020). Furthermore, the use of NLRP3 or caspase-1 inhibitors would confirm the specificity of this response. To fully elucidate whether Al₂O₃ and ZrO₂ predominantly influence the first 'priming' step or second activation step of NLRP3 activation, western blot analysis of pro-IL-1-β, IL-1β, NLRP3 and activation of caspase-1 could be investigated in future work.

6.5.1 Future work

It is important to emphasise that this study focussed on the use of ceramic oxide nanopowders and not wear debris or particles generated from materials used in ceramic implants. The use of commercially-obtained ceramic wear particles is very common in previous *in vitro* investigations and is probably due to the difficulties in generating high volumes of clinically-relevant particles due to the extremely low wear rates from ceramics. This means wear simulators must be run for extended periods of time to generate the number of particles required for studies. The issue with commercially available particles is that their size, morphology and composition may not be clinically-relevant nor accurate when determining biological responses *in vitro* when modelling the wear debris generated *in vivo*.

Additionally, cell treatments in this study were with Al₂O₃ and ZrO₂ independently of each other. However, the materials used in CoP and CoC implants are usually composed from ZTA and therefore wear debris particles will contain both Al₂O₃ and ZrO₂. Therefore, future work could focus on the use of clinically-relevant ZTA particles which would provide more accurate and meaningful conclusions.

Furthermore, the effect ceramic oxides have on the endothelium as discussed in **Chapter 5** would be of interest to determine whether this could enhance the migration of immune cells. This could be investigated by studying the response of HMEC-1 cells to ceramics in both adhesion molecule expression and as part of a chemotaxis assay.

6.5.2 Conclusion

The results from this chapter present a potential inflammatory profile of THP-1 macrophage cell model following treatment with both Al₂O₃ and ZrO₂. Significant increases in IL-8, CCL2, CCL3 and CCL4 chemokine expression was comparable with results presented in **Chapter 4** from THP-1 cells treated with CoCr particles. These increases in chemokine expression were found to be largely TLR4-dependent which helps establish a possible role for ceramic oxides in activating immune signalling pathways. This was further emphasised by the ability of Al₂O₃ and ZrO₂ 'prime' THP-1 macrophages through a PAMP-like mechanism to up-regulate IL-1 β expression when stimulated with ATP. These findings provide a sound basis for further research into ZTA-mediated inflammatory effects and how these are regulated. Given the increasing popularity of joint implants containing ceramics it is important that these effects are fully understood if patients do experience ceramic-mediated inflammation in the future more commonly.

Chapter 7 : Concluding Discussion

7.1 Aims and Outcomes

The hypothesis of this study was that metal wear debris from joint implants can activate human TLR4 and, subsequently the inflammasome, resulting in inflammatory responses accounting for the development of ARMD in patients with failed joint implants.

The main aims and outcomes of this study are summarised below:

A. To generate and characterise clinically relevant CoCr wear particles suitable for cell culture

Nanoscale particles were generated using a six-station pin-on-plate wear simulator using the material which is used in MoM implants, CoCrMo. Particles were characterised using SEM and found to be of the correct size, morphology and composition to be classified as 'clinically-relevant' according to the literature. Generated CoCr particles from the six-station pin-on-plate wear simulator were successfully sterilised to be used in cell culture treatments. ICP-MS confirmed the concentration of cobalt ions released from particles so concurrent treatments could be investigated with cobalt ions alone or alongside CoCr particles.

B. To determine the role of TLR4 and the inflammasome in the inflammatory response to CoCr particles

THP-1 macrophages stimulated with CoCr particles were clearly shown to phagocytose and internalise particles in membrane bound vacuoles, as shown by TEM. An MSD U-PLEX cytokine/chemokine assay was conducted to investigate potential markers of CoCr-mediated inflammation secreted by THP-1 macrophages. CoCr particles significantly up-regulated the secretion of several chemokines and cytokines, including IL-8, CCL2, CCL3, CCL4, CCL20 and IL-1 β . The small molecule TLR4 inhibitor, CLI-095, demonstrated that observed increases were largely TLR4-dependent. Using *IL-8* as a marker of activation, these results were also confirmed by analysis of gene expression using qRT-PCR. The inflammasome response to CoCr

particles was also investigated by evaluating IL-1 β expression and secretion which showed no significant increases in either models of activation (either using CoCr particles as a PAMP- or DAMP-inducer).

C. Investigate the functional effects of CoCr particles *in vitro* and the translation to patient tissue following hip and knee revision surgery

HMEC-1 endothelial cells stimulated with CoCr particles could also internalise particles in a similar manner to THP-1 cells. Both *ICAM-1* and *VCAM-1* adhesion molecule expression was significantly up-regulated in response to CoCr particles. The migration of neutrophils was investigated using a transwell chemotaxis assay which showed an increase in migration when the HMEC-1 endothelial barrier was activated by CoCr particles. Soft tissue was collected from 11 patients undergoing revision TJR and stained by H&E which demonstrated increased immune cell infiltration in the majority of cases. Out of these cases, there was a mixture of lymphocyte- and macrophage-dominant inflammation as determined by IHC staining. The findings from this cohort require expansion so semi-quantitative analysis can be used to determine whether there are links between either the age, gender, type of implant or reason for revision and the number of infiltrating immune cells and their phenotype.

D. To investigate the biological effect of ceramic oxide nanopowders

THP-1 macrophages treated with the ceramic oxide nanopowders, Al₂O₃ and ZrO₂, displayed significantly increased chemokine gene expression and secretion of IL-8, CCL2, CCL3 and CCL4. These observed increases were found to be largely TLR4-dependent when pre-treating cells with CLI-095. Using a model of inflammasome activation both Al₂O₃ and ZrO₂ were shown to potentially act as a PAMP 'priming' signal since IL-1 β expression increased upon stimulation with ceramic oxides followed by ATP. Furthermore, ZrO₂ also increased IL-1 β expression in THP-1 macrophages following pre-treatment with LPS, indicating a potential role as a DAMP inducer, acting in place of ATP. Both Al₂O₃ and ZrO₂ may have induced lysosomal mediated necrosis which would prevent full activation of NLRP3 and subsequent IL-1 β secretion.

7.2 Overall Conclusions

The data presented in this study demonstrate that both clinically-relevant CoCr particles and ceramic oxides can increase the expression of inflammatory cytokines and chemokines in THP-1 macrophages. This inflammatory response appears to be largely regulated through TLR4 signalling as a TLR4 inhibitor proved effective at reducing the expression of both CoCr particle- and ceramic oxide-mediated cytokine and chemokine expression. Both THP-1 macrophages and HMEC-1 endothelial cells can also internalise these particles, possibly through a phagocytic process in which particles are found as dense agglomerates within membrane-bound vacuoles. In a model of NLRP3 inflammasome activation, CoCr particle treated macrophages which were then stimulated with ATP failed to increase expression of IL-1 β . This suggested that at least with the concentrations used in this instance, CoCr particles were unable to effectively 'prime' macrophages in the same way LPS could or had possibly caused lysosomal mediated necrosis. Therefore, further investigation is required to fully elucidate the role of NLRP3 in these responses. Contrastingly, both Al₂O₃ and ZrO₂ treatments resulted in significant increases in IL-1 β expression with the addition of ATP.

Further analysis of adhesion molecule expression and neutrophil cell migration suggested a role for CoCr-mediated endothelial activation. Both *ICAM-1* and *VCAM-1* expression were significantly up-regulated in HMEC-1 cells treated with CoCr particles. Furthermore, in a model of neutrophil migration, HMEC-1 cells replicating the endothelial cell barrier were activated when treated with CoCr particles which subsequently enhanced neutrophil migration.

In summary, metals commonly used in joint implants such as CoCr, Al₂O₃ and ZrO₂ can all mediate an inflammatory response by activation of TLR4, increasing inflammatory cytokine and chemokine expression, which in turn may activate the NLRP3 inflammasome and IL-1 β production. These effects can not only increase the migration of immune cells into the peri-implant tissues, forming inflammatory pseudotumours but also enhance osteolytic processes leading to failure of joint implants. Therefore, both the TLR4 and NLRP3 signalling pathways should be targets for further investigation into ARMD as well as a role in potential therapeutics.

7.3 Final Discussion

The failure of MoM implants in some patients has been associated with ARMD, formation of inflammatory pseudotumours and osteolysis. Ultimately, this leads to swelling, discomfort or aseptic loosening of the implant and the need for complicated revision surgery. Furthermore, these observed effects do not appear to be unique to MoM implants, with reported cases of pseudotumours developing from both MoP and CoC or CoP prostheses (Matharu *et al.*, 2016). The exact underlying immune mechanisms remain to be fully elucidated. However, previous *in vitro* studies appear to indicate a role for a pro-inflammatory response to metal wear debris and ions, characterised by increases to cytokines and chemokines. Many of these studies have modelled the *in vivo* environment using either metal ions or commercially available wear debris particles which lack accurate size, morphology and composition (Dalal *et al.*, 2012). Therefore, the present study shows the potential for clinically-relevant CoCr particles to mediate inflammation through activation of the TLR4 signalling pathway in THP-1 macrophages. Moreover, it appears that the cellular responses observed were mostly driven by cobalt ions released from CoCr particles.

The THP-1 macrophage cell line was used throughout the study as macrophages are found in the periprosthetic tissues and inflammation associated with ARMD is associated with both macrophage infiltration and activation (Nich *et al.*, 2016). This was further confirmed in this study in which patient soft tissue stained positive for macrophages using IHC. The THP-1 cell line has also been commonly used by other groups when investigating cellular responses to metal wear debris and ions (Caicedo *et al.*, 2013; Potnis *et al.*, 2013; Samelko *et al.*, 2016). THP-1 cells were selected instead of using PBMCs from human donors to reduce inter-donor variability which would make it particularly difficult to compare responses. Results demonstrated increased TLR4-dependent inflammatory chemokine and cytokine expression when THP-1 cells were stimulated with CoCr particles. This suggests that macrophages present in periprosthetic tissues may become activated in response to wear debris from implants which would account for the elevated chemokine levels found in osteolytic lesions around implants (Dapunt *et al.*, 2014b; Jansen *et al.*, 2017).

The role of the NLRP3 inflammasome in CoCr-mediated inflammation requires further investigation. In this study, although IL-1 β secretion was significantly increased in CoCr particle treated THP-1 macrophages when measured by an MSD U-PLEX assay this

increase was not reflected using ELISA, despite the addition of ATP as a further activation signal. To gain further insight, IL-18 expression and caspase-1 activation could be investigated as these are also markers of NLRP3 activation. Numerous studies have focussed on this signalling pathway as NLRP3 mediates the activation of IL-1 β which is known to promote osteoclast function and believed to be a key inflammatory cytokine associated with aseptic loosening (Caicedo *et al.*, 2013; Jamsen *et al.*, 2020). For full NLRP3 activation to occur, both a 'priming' and activation signal are required (Bauernfeind *et al.*, 2009). It remains to be fully understood whether CoCr particles alone can provide both or either of these signals.

The results presented throughout the study aimed to provide comparative cellular responses between CoCr particles and cobalt ions (using a concentration of ions similar to the concentration expected to be released from particles). Generally, chemokine and cytokine expression was comparable for both treatments. This suggests that CoCr-mediated inflammation is likely caused by cobalt ions which are released from the particles. However, CCL3 secretion was increased in J774 mouse macrophages following CoCr particle stimulation. This indicates that CoCr particles may activate other pathways or cause general inflammation in addition to cobalt ions since ions cannot activate murine TLR4 (Tyson-Capper *et al.*, 2013). Moreover, murine models of CoCr particle-induced osteolysis have been used by groups indicating observed inflammatory effects *in vivo* are not unique to humans and primates (Samelko *et al.*, 2016; Paulus *et al.*, 2019). This is reflected in findings presented by Paulus *et al.* who observed increased numbers of adherent and rolling leukocytes in mice injected with CoCr particles but not with metal ions (Paulus *et al.*, 2019). Additionally, despite high cobalt ion treatment, no pseudotumour-like tissue could be induced in the mice whereas it was observed frequently in CoCr particle-stimulated mice (Paulus *et al.*, 2019).

HMEC-1 endothelial cells were also selected as an endothelium model, representing the barrier between the circulation and tissues surrounding the joint. Adhesion molecule expression of both *ICAM-1* and *VCAM-1* was significantly increased when HMEC-1 cells were challenged with CoCr particles, suggesting their ability to activate the endothelium. HMEC-1 cells have previously shown increased chemokine expression (e.g. IL-8) in response to cobalt ions which is also TLR4-dependent (Anjum *et al.*, 2016). Therefore, it could be the case that CoCr-mediated chemokine secretion

causes this observed up-regulation in adhesion molecule expression. Both TNF- α and IFN- γ have been shown to increase the expression of *ICAM-1* and *VCAM-1* (Hosokawa et al., 2006). Evidence of CoCr particle-mediated endothelial activation was further confirmed as neutrophil migration was enhanced using a transwell chemotaxis assay, suggesting increased leukocyte extravasation, adhesion and subsequent migration.

An additional aim of this study was to investigate the biological effects of ceramic oxides which are commonly used in both CoP and CoC implants, specifically ZTA. Therefore, the techniques and assays optimised with CoCr particle treatments were applied to Al₂O₃ and ZrO₂ stimulation of THP-1 macrophages. Although wear from these type of implants is considerably less than MoM or MoP prostheses it remains important to understand any potential biological and inflammatory effects from ceramics as reports of excessive wear, inflammatory pseudotumours and aseptic loosening are uncommon but not unheard of (Malem et al., 2013; Campbell et al., 2017).

Results indicated that both Al₂O₃ and ZrO₂ increased chemokine expression in THP-1 macrophages in a TLR4-dependent manner. Moreover, IL-1 β expression was significantly increased when Al₂O₃ and ZrO₂ 'primed' THP-1 macrophages prior to challenge with ATP, suggesting a role as a PAMP inducer. This is interesting as ceramics are generally believed to be 'bio-inert' particularly in comparison to other biomaterials such as CoCr and UHMWPE. However, it is important when considering these findings, whether the ceramic oxide nanopowders used in this study were of clinical-relevance. This limitation is not uncommon given the difficulties in generating high volumes of ceramic wear particles, with many other groups using similar nanopowders in previous investigations (Tsaousi et al., 2010; Faye et al., 2017). Moreover, given the low wear rate of CoC bearings it is unlikely the higher concentrations used in this study would be reached in an *in vivo* setting in most well working prostheses.

A working model summarising the findings from this study is shown in **Figure 7.1**.

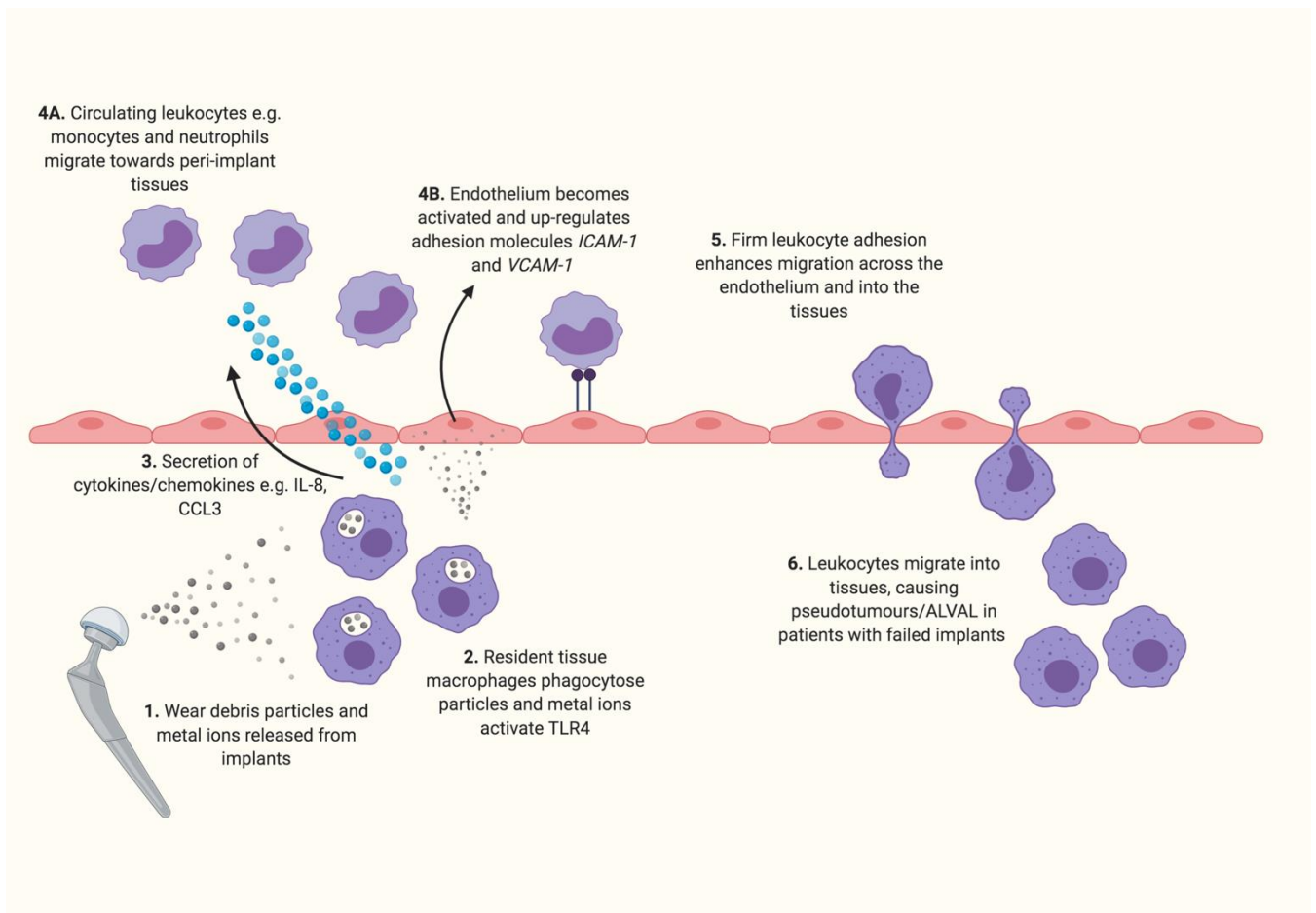


Figure 7.1 Working model

1. Wear debris particles and metal ions (CoCl_2 , Al_2O_3 , ZrO_2) are released from joint implants as the prostheses wear over time and enter the peri-implant tissues. **2.** Resident tissue macrophages phagocytose particles whilst metal ions directly activate TLR4. **3.** This immune activation results in increased cytokine and chemokine expression and secretion e.g. IL-8 and CCL3. **4A.** Chemokines attract leukocytes such as monocytes and neutrophils to the site of inflammation. **4B.** Secreted cytokines as well as wear debris particles directly activate the endothelium, up-regulating adhesion molecule expression e.g. *ICAM-1* and *VCAM-1*. **5.** This enhances firm adhesion of leukocytes, inducing increased leukocyte migration across the endothelium and into the tissues. **6.** Leukocytes infiltrate the peri-implant tissues, causing pseudotumour formation and ALVAL in patients with failed implants. Image created using Biorender.

7.4 Study Limitations

The selection of cell lines throughout this study (e.g. THP-1 and HMEC-1) were used as they are used widely in the literature and maintain consistency in cellular responses which would be more difficult with primary cells such as PBMCs which would cause inter-donor variability. However, it is important to acknowledge that these cell lines are not fully representative of primary cells which would respond to stimuli *in vivo*. For

example, THP-1 cells were activated to a macrophage-like phenotype using PMA which may influence the effect of treatments on cells since it has been reported that PMA can increase secretion of cytokines and chemokines such as IL-1 β , CCL2, CCL3 and IL-8 (Schutte *et al.*, 2009). These unwanted effects were negated to a degree by resting the cells for 24 hours following PMA stimulation and using negative control, untreated cells throughout as a comparative baseline. In the future, it would be useful to use PBMCs for CoCr particle treatments, as this could offer further insight into the variability of patient-specific responses to stimuli.

Furthermore, the use of *in vitro* assays is not truly representative of the *in vivo* environment in which there are numerous tissue layers containing different cell types which are able to interact with one another. Therefore, although useful for preliminary investigations, *in vitro* cell culture cannot reproduce this specific three-dimensional environment and interactions to replicate CoCr particle-induced inflammation *in vivo*. Originally, animal *in vivo* models had been previously ruled out due to the specificity of cobalt ions binding to only human and primate TLR4. However, the findings presented here and in the literature, offer a case for further investigation into mouse *in vivo* models, specifically osteolytic effects and histological analysis. However, it is important to emphasise that the human response to cobalt ions released from particles would be lost in this model.

The study is further limited by concentrations used for CoCr particle treatments. It is particularly difficult to select 'clinically-relevant' concentrations given the discrepancies in the literature regarding concentrations observed in patients with failed implants. Importantly, the largest inflammatory effects were only observed using the highest concentration of CoCr particles which is potentially at the higher end of concentrations previously reported in patients' synovial fluid (Kwon *et al.*, 2011). However, the concentrations selected have been used extensively by other groups when investigating CoCr particle-mediated inflammation *in vitro* (Behl *et al.*, 2013). *In vitro* studies usually require larger concentrations as the *in vivo* environment is far more sophisticated, for example with concentration gradients, which are impossible to reproduce using a simple cell culture system. Additionally, exposure of wear debris particles and metal ions *in vivo* will occur perhaps at lower concentration but over a prolonged period of up to years which is not feasible using *in vitro* systems.

Unfortunately, the CoCr particles which were generated on the single-station pin-on-plate wear simulator could not be used for cell culture studies due to possible endotoxin contamination. However, in future studies, these particles would be important to include and could enhance clinical relevance since the lubricant used contained serum rather than water which is a better representation of the *in vivo* joint fluid environment. To avoid possible contamination in the future, extra care must be taken when transferring lubricants between containers and the endotoxin quantitation kit should be completed in a microbiological safety cabinet.

7.5 Clinical Implications

The clinical implications from the findings in this study are far reaching given the number of patients worldwide who either have MoM or ceramic joint implants as well as other medical devices containing CoCr such as dental implants and spinal rods. Currently, the use of MoM hip implants is negligible since the emergence of ARMD and increased revision rates for these prostheses. However, as previously discussed, ARMD does not appear to be unique to MoM implants, therefore investigating cellular responses to both CoCr (which is still used in MoP implants and in the trunnions of ceramic implants) provides further understanding of potentially involved immunological mechanisms. This could lead to therapeutic prevention in cases of ARMD from these types of implants or possible biomarkers for diagnosis.

It is clear from the results presented in this study that TLR4 plays a central role in CoCr particle- and ceramic-mediated inflammation. Therefore, the prospect of a therapy which specifically targets TLR4 to prevent this unwanted activation and subsequent immune response is an attractive option. The fact that J774 mouse macrophages appeared to be activated by CoCr particles suggests that TLR4 is not the sole mode of inflammatory activation in this response. Although it is worth acknowledging these investigations have only been demonstrated in THP-1 macrophages, the use of CLI-095 significantly reduced chemokine secretion to similar concentrations observed in untreated control cells, suggesting in this case the response is completely TLR4-dependent. Targeting TLR4 in this way is possible as metal ions (specifically cobalt) are known to have a separate binding site to TLR4's natural ligand LPS. Therefore, the response to bacterial LPS could be preserved whilst preventing cobalt ion-mediated TLR4 activation and inflammation. Therefore, it is possible that future therapeutics for

patients with ARMD could be designed to specifically target the histidine residues, the known binding site for cobalt ions in their activation of TLR4. Furthermore, if future investigations confirm the role of the NLRP3 inflammasome in the inflammatory response to both CoCr and ceramic particles, this could also be exploited in potential therapeutics by targeting proteins involved in the pathway.

7.6 Future Directions

The data presented in this study have helped to provide insight into the mechanisms of CoCr particle- and ceramic-mediated inflammation. However, as discussed in specific chapters, the questions arisen from this study allow for further investigation. Therefore, a number of different avenues would be useful to further investigate the potential inflammatory effects of both CoCr and ceramic particles.

The role of both CoCr and ceramic particles in activating the NLRP3 inflammasome requires further work. Particularly, the potential for both materials to cause lysosomal mediated necrosis, which has been shown when macrophages are treated with alum in previous studies. Further investigations could involve the use of both caspase-1 and cathepsin inhibitors to establish whether cell death is dependent on either of these mechanisms. If cathepsin inhibitors could prevent cell death when cells are pre-treated with LPS followed by the addition of CoCr or ceramic particles, this would suggest that particles which are phagocytosed by cells cause lysosomal degradation and release of cathepsins. Therefore, this set of events would prevent full activation of NLRP3 and secretion of IL-1 β .

An important factor to continue to pursue from this study is the inflammatory effects observed by ceramic oxides. The use of CoP implants especially are increasing year-on-year due to their attractive wear properties and perceived biocompatibility. However, although this study demonstrated the potential for ceramic oxides to activate TLR4 and increase chemokine expression, the use of clinically-relevant ZTA ceramic wear particles would enhance these findings by providing an improved *in vitro* model. With these particles, assays could be repeated to determine whether these effects are replicated. This is particularly important due to the lack of studies in the literature which use both clinically-relevant ceramic particles at relevant concentrations.

It would also be useful to assess the expression of cytokines and chemokines from HMEC-1 cells treated with CoCr particles. This has been previously investigated using cobalt ions, however, it would be of interest to determine whether clinically-relevant CoCr particles demonstrate a similar expression profile in this cell type. Moreover, this would offer further explanation for the mechanisms behind endothelial activation observed in this study if inflammatory chemokines and cytokines were up-regulated.

Further functional studies would provide further insight into the effect increased expression of chemokines and cytokines have on different cell types. For example, the neutrophil chemotaxis assay used in this study could be further expanded to include both PBMCs as well as inhibiting TLR4 in HMEC-1 cells which provide the endothelial barrier. This would help determine whether the observed increase in leukocyte migration was in fact TLR4-dependent. Cell adhesion can also be analysed using a Cellix platform which better replicates shear stress along blood vessels.

It would also be of interest to further establish the osteolytic processes which are potentially effected by CoCr particles and ceramics. MG63 osteoblast-like cells were used briefly in this study for a cell migration, wound healing assay. However, this cell type could be investigated further, for example, assessing the expression of osteogenic markers such as different collagens and members of the TGF- β superfamily. Assessment of RANKL and OPG expression by either ELISA, qRT-PCR or western blotting would also be useful given the importance of these proteins for osteoclastogenesis balance. Furthermore, mouse models which were discussed previously can also demonstrate bone loss following treatments with wear particles.

Further analysis of tissue samples from patients undergoing hip and knee revision surgeries would also strengthen the clinical translation of this work. In this study only 11 samples were collected and analysed, however, a larger patient cohort would be hugely beneficial in providing links between histological analysis and patient information such as types of implant used, duration of implant and reasons for revision. A larger cohort of patient tissue would allow for semi-quantitative analysis by counting the number of cell types present (e.g. T cells or macrophages) and whether these correlate with either the implant material, age, gender or reason for revision. Additionally, quantification of cytokines and chemokines in synovial fluid could be assessed as well as their expression in the tissue by isolating RNA.

To conclude, this study demonstrates that CoCr particles and ceramic oxides from prosthetic joint implants can activate the innate immune receptor TLR4, leading to increased expression and secretion of inflammatory cytokines and chemokines. Additionally, CoCr particles can also up-regulate adhesion molecule expression by activating the endothelium which enhances neutrophil migration. Therefore, wear debris particles released from these implants have the potential to promote a pro-inflammatory environment which can induce immune cell infiltration, pseudotumours, osteolysis and eventual failure of the implant. A greater understanding of the pathways which are involved in this response gives opportunity to potential novel therapeutics in the future which could prevent CoCr particle- and ceramic-mediated inflammation in symptomatic patients allowing for their safe use as a biomaterial.

Appendix A

Calculating particle volumes for generated **cobalt chromium particles**:

Density of CoCr = 7.7g/cm^3

7.7g in 1cm^3

$7.7 \times 10^{-12}\text{g}$ in $1\mu\text{m}^3$

$3.85 \times 10^{-10}\text{g}$ in $50\mu\text{m}^3$

$3.85 \times 10^{-4}\text{g}$ in $50\mu\text{m}^3$ per cell

192.5 μg particles required per well for 500,000 THP-1 cells

115.5 μg particles required per well for 300,000 HMEC-1 cells

Calculating particle volumes for generated **aluminium oxide particles**:

Density of Al_2O_3 = 3.85g/cm^3

3.85g in 1cm^3

$3.85 \times 10^{-12}\text{g}$ in $1\mu\text{m}^3$

$1.925 \times 10^{-10}\text{g}$ in $50\mu\text{m}^3$

$1.925 \times 10^{-4}\text{g}$ in $50\mu\text{m}^3$ per cell

96.25 μg particles required per well for 500,000 THP-1 cells

57.75 μg particles required per well for 300,000 HMEC-1 cells

Calculating particle volumes for generated **zirconium oxide particles**:

Density of ZrO_2 = 5.89g/cm^3

5.89g in 1cm^3

$5.89 \times 10^{-12}\text{g}$ in $1\mu\text{m}^3$

$2.945 \times 10^{-10}\text{g}$ in $50\mu\text{m}^3$

$2.945 \times 10^{-4}\text{g}$ in $50\mu\text{m}^3$ per cell

147.25 μ g particles required per well for 500,000 THP-1 cells

88.35 μ g particles required per well for 300,000 HMEC-1 cells

Appendix B

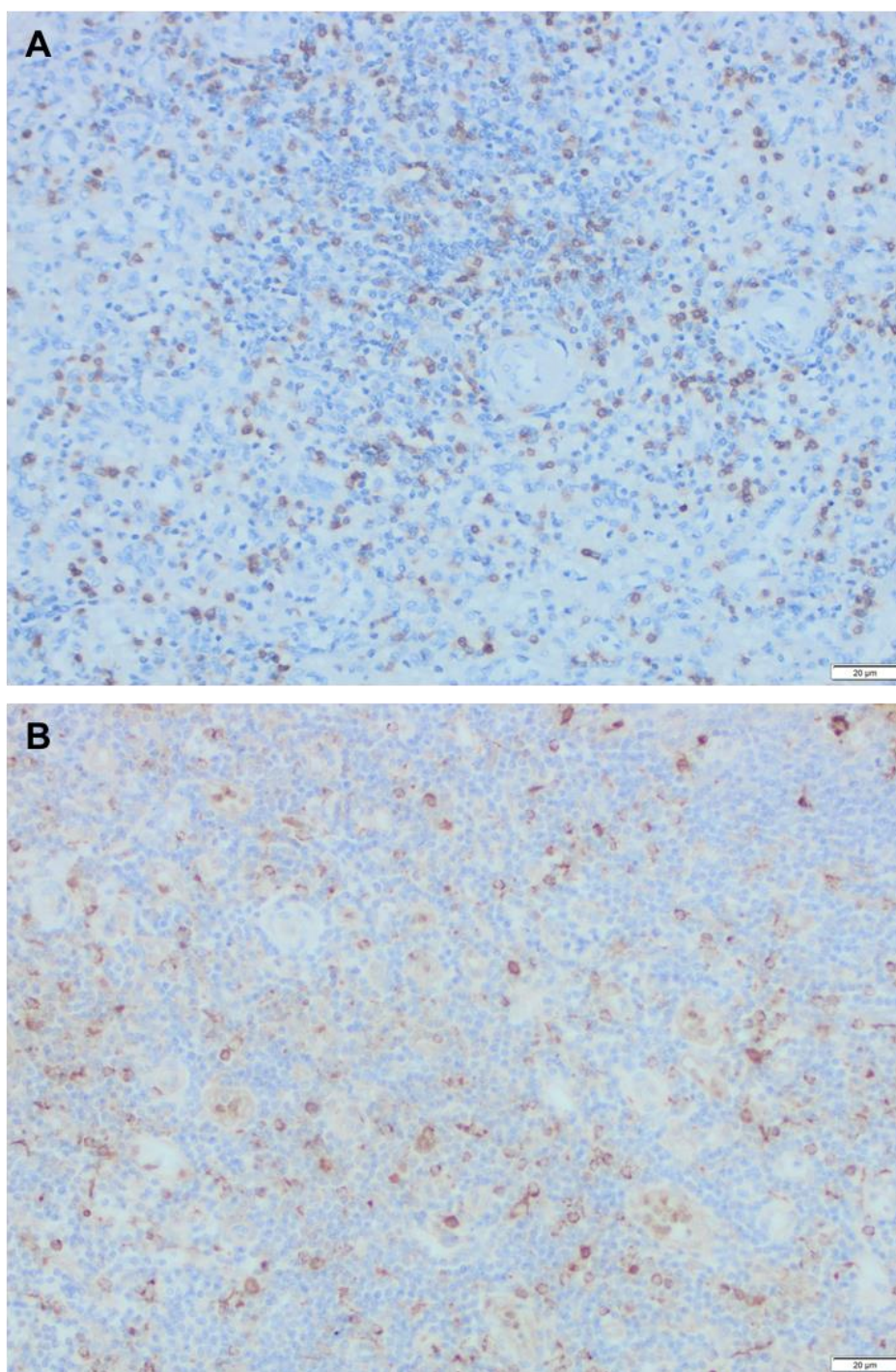


Figure B.1. Immunohistochemistry staining on control tonsil tissue

Immunohistochemistry staining showing positive CD3 (T cells) **(A)** and CD68 (macrophages) **(B)** in control tonsil tissue.

Publications, presentations and awards

Lawrence, H, **Mawdesley AE**, Holland JP, Kirby JA, Deehan DJ, Tyson-Capper AJ. Targeting Toll-like receptor 4 prevents cobalt-mediated inflammation. *Oncotarget*. 2016, 7(7): 7578-85. (joint 1st author)

Lawrence, H, Deehan DJ, Holland JP, Anjum SA, **Mawdesley AE**, Kirby JA, Tyson-Capper AJ. Cobalt ions recruit inflammatory cells *in vitro* through human Toll-like receptor 4. *Biochemistry and Biophysics Reports*. 2016, 7: 374-378.

Mawdesley AE, Davidson L, Anjum SA, Kirby JA, Tyson-Capper AJ. Effect of Cobalt Ions on Chemokine Expression: Case Report of Immune Cell Infiltration in Patient Undergoing Revision of Metal-On-Metal Implant. *Journal of Orthopaedic Research and Therapy* 2020, 5: 1154

Jamieson, S, **Mawdesley AE**, Deehan DJ, Holland, JP, Kirby JA, Tyson-Capper AJ. Orthopaedic biological responses: a TLR4-mediated inflammatory response to metal oxide ceramic nanopowders. **Publication currently under review with Scientific Reports, June 2020** (joint 1st author)

Mawdesley AE. Clinically relevant cobalt-chromium particles can increase inflammatory chemokine expression in macrophages. **Manuscript in preparation**

Conferences and Presentations

Oral Presentation, *European Orthopaedic Research Society*, Bristol, September 2015

Oral Presentation, *North East Postgraduate Conference*, Newcastle upon Tyne, October 2015

Oral Presentation, *ICM Seminar Programme*, Newcastle University, February 2018

Oral Presentation, *MRC DTP Conference*, University of Manchester, May 2018

Oral Presentation, *Immunology North East Symposium*, Durham University, June 2018

Oral Presentation, *British Orthopaedic Research Society*, University of Leeds, September 2018

Oral Presentation, *North East Postgraduate Conference*, Newcastle upon Tyne, November 2018

Oral and Poster Presentation, *Keystone Symposium: Innate Immune Receptors*, Taipei, Taiwan, March 2019

1 hour Public Lecture 'Tricked: Can metal hip replacements confuse our immune system?', *Explore Perspectives*, Joseph Cowen Lifelong Learning Centre, Newcastle upon Tyne, December 2019

Prizes and Awards

European Orthopaedic Research Society, Bristol, September 2015 – 2nd Prize, *Bristol Orthopaedic Trust Travel Grant*

North East Postgraduate Conference, Newcastle upon Tyne, October 2015 – *Best Immunology Talk*

Faculty of Medical Sciences Travel Award, January 2019 – for travel to *Keystone Symposium*, Taipei, Taiwan

References

- Abdel-Gadir, A., Berber, R., Porter, J.B., Quinn, P.D., Suri, D., Kellman, P., Hart, A.J., Moon, J.C., Manisty, C. and Skinner, J.A. (2016) 'Detection of metallic cobalt and chromium liver deposition following failed hip replacement using T2* and R2 magnetic resonance', *J Cardiovasc Magn Reson*, 18(1), p. 29.
- Adam, C., Wohlfarth, J., Haussmann, M., Sennefelder, H., Rodin, A., Maler, M., Martin, S.F., Goebeler, M. and Schmidt, M. (2017) 'Allergy-Inducing Chromium Compounds Trigger Potent Innate Immune Stimulation Via ROS-Dependent Inflammasome Activation', *J Invest Dermatol*, 137(2), pp. 367-376.
- Ahlstrom, M.G., Thyssen, J.P., Menne, T. and Johansen, J.D. (2017) 'Prevalence of nickel allergy in Europe following the EU Nickel Directive - a review', *Contact Dermatitis*, 77(4), pp. 193-200.
- Akbar, M., Brewer, J.M. and Grant, M.H. (2011) 'Effect of chromium and cobalt ions on primary human lymphocytes in vitro', *J Immunotoxicol*, 8(2), pp. 140-9.
- Akbar, M., Fraser, A.R., Graham, G.J., Brewer, J.M. and Grant, M.H. (2012) 'Acute inflammatory response to cobalt chromium orthopaedic wear debris in a rodent air-pouch model', *Journal of the Royal Society Interface*, 9(74), pp. 2109-2119.
- Al-Hajjar, M., Jennings, L.M., Begand, S., Oberbach, T., Delfosse, D. and Fisher, J. (2013) 'Wear of novel ceramic-on-ceramic bearings under adverse and clinically relevant hip simulator conditions', *J Biomed Mater Res B Appl Biomater*, 101(8), pp. 1456-62.
- Alarifi, S., Ali, D., Y, A.O., Ahamed, M., Siddiqui, M.A. and Al-Khedhairi, A.A. (2013) 'Oxidative stress contributes to cobalt oxide nanoparticles-induced cytotoxicity and DNA damage in human hepatocarcinoma cells', *Int J Nanomedicine*, 8, pp. 189-199.
- Alinovi, R., Goldoni, M., Pinelli, S., Campanini, M., Aliatis, I., Bersani, D., Lottici, P.P., Iavicoli, S., Petyx, M., Mozzoni, P. and Mutti, A. (2015) 'Oxidative and pro-inflammatory effects of cobalt and titanium oxide nanoparticles on aortic and venous endothelial cells', *Toxicol In Vitro*, 29(3), pp. 426-37.
- Amarasekera, D.S., Yun, H., Kim, S., Lee, N., Kim, H. and Rho, J. (2018) 'Regulation of Osteoclast Differentiation by Cytokine Networks', *Immune Netw*, 18(1), p. e8.
- Amarasekera, H. and Griffin, D.R. (2012) 'Surface Replacement of Hip Joint', *Recent Advances in Hip and Knee Arthroplasty*.
- Anand, R.J., Kohler, J.W., Cavallo, J.A., Li, J., Dubowski, T. and Hackam, D.J. (2007) 'Toll-like receptor 4 plays a role in macrophage phagocytosis during peritoneal sepsis', *J Pediatr Surg*, 42(6), pp. 927-32; discussion 933.
- Anjum, S.A., Lawrence, H., Holland, J.P., Kirby, J.A., Deehan, D.J. and Tyson-Capper, A.J. (2016) 'Effect of cobalt-mediated Toll-like receptor 4 activation on inflammatory responses in endothelial cells', *Oncotarget*, 7(47), pp. 76471-76478.
- Bauernfeind, F.G., Horvath, G., Stutz, A., Alnemri, E.S., MacDonald, K., Speert, D., Fernandes-Alnemri, T., Wu, J., Monks, B.G., Fitzgerald, K.A., Hornung, V. and Latz, E. (2009) 'Cutting edge: NF-kappaB activating pattern recognition and cytokine receptors license NLRP3 inflammasome activation by regulating NLRP3 expression', *J Immunol*, 183(2), pp. 787-91.

- Behl, B., Papageorgiou, I., Brown, C., Hall, R., Tipper, J.L., Fisher, J. and Ingham, E. (2013) 'Biological effects of cobalt-chromium nanoparticles and ions on dural fibroblasts and dural epithelial cells', *Biomaterials*, 34(14), pp. 3547-58.
- Bendre, M.S., Montague, D.C., Peery, T., Akel, N.S., Gaddy, D. and Suva, L.J. (2003) 'Interleukin-8 stimulation of osteoclastogenesis and bone resorption is a mechanism for the increased osteolysis of metastatic bone disease', *Bone*, 33(1), pp. 28-37.
- Bernthal, N.M., Celestre, P.C., Stavrakis, A.I., Ludington, J.C. and Oakes, D.A. (2012) 'Disappointing short-term results with the DePuy ASR XL metal-on-metal total hip arthroplasty', *J Arthroplasty*, 27(4), pp. 539-44.
- Bertrand, J., Delfosse, D., Mai, V., Awiszus, F., Harnisch, K. and Lohmann, C.H. (2018) 'Ceramic prosthesis surfaces induce an inflammatory cell response and fibrotic tissue changes', *Bone Joint J*, 100-B(7), pp. 882-890.
- Bijukumar, D.R., Salunkhe, S., Zheng, G., Barba, M., Hall, D.J., Pourzal, R. and Mathew, M.T. (2020) 'Wear particles induce a new macrophage phenotype with the potential to accelerate material corrosion within total hip replacement interfaces', *Acta Biomater*, 101, pp. 586-597.
- Blander, J.M. and Medzhitov, R. (2004) 'Regulation of phagosome maturation by signals from toll-like receptors', *Science*, 304(5673), pp. 1014-8.
- Blumenfeld, T.J., Bargar, W.L. and Campbell, P.A. (2010) 'A painful metal-on-metal total hip arthroplasty. A diagnostic dilemma', *Journal of Arthroplasty*, 25(7), pp. 1168.e1-1168.e4.
- Bohme, S., Stark, H.J., Meissner, T., Springer, A., Reemtsma, T., Kuhnel, D. and Busch, W. (2014) 'Quantification of Al₂O₃ nanoparticles in human cell lines applying inductively coupled plasma mass spectrometry (neb-ICP-MS, LA-ICP-MS) and flow cytometry-based methods', *J Nanopart Res*, 16(9), p. 2592.
- Bornhorst, J.A. and Falke, J.J. (2000) 'Purification of proteins using polyhistidine affinity tags', *Methods Enzymol*, 326, pp. 245-54.
- Bosker, B.H., Ettema, H.B., Boomsma, M.F., Kollen, B.J., Maas, M. and Verheyen, C.C.P.M. (2012) 'High incidence of pseudotumour formation after large-diameter metal-on-metal total hip replacement: A prospective cohort study', *Journal of Bone and Joint Surgery - Series B*, 94 B(6), pp. 755-761.
- Bosshart, H. and Heinzelmann, M. (2016) 'THP-1 cells as a model for human monocytes', *Ann Transl Med*, 4(21), p. 438.
- Brough, D. and Rothwell, N.J. (2007) 'Caspase-1-dependent processing of pro-interleukin-1beta is cytosolic and precedes cell death', *J Cell Sci*, 120(Pt 5), pp. 772-81.
- Brown, C., Williams, S., Tipper, J.L., Fisher, J. and Ingham, E. (2007) 'Characterisation of wear particles produced by metal on metal and ceramic on metal hip prostheses under standard and microseparation simulation', *J Mater Sci Mater Med*, 18(5), pp. 819-27.
- Brown, S.R., Davies, W.A., DeHeer, D.H. and Swanson, A.B. (2002) 'Long-term survival of McKee-Farrar total hip prostheses', *Clin Orthop Relat Res*, (402), pp. 157-63.
- Caicedo, M.S., Desai, R., McAllister, K., Reddy, A., Jacobs, J.J. and Hallab, N.J. (2009) 'Soluble and particulate Co-Cr-Mo alloy implant metals activate the inflammasome

danger signaling pathway in human macrophages: a novel mechanism for implant debris reactivity', *J Orthop Res*, 27(7), pp. 847-54.

Caicedo, M.S., Samelko, L., McAllister, K., Jacobs, J.J. and Hallab, N.J. (2013) 'Increasing both CoCrMo-alloy particle size and surface irregularity induces increased macrophage inflammasome activation in vitro potentially through lysosomal destabilization mechanisms', *J Orthop Res*, 31(10), pp. 1633-42.

Callaghan, J.J., O'Rourke M, R. and Saleh, K.J. (2004) 'Why knees fail: lessons learned', *J Arthroplasty*, 19(4 Suppl 1), pp. 31-4.

Campbell, J., Rajaei, S., Brien, E. and Paiement, G.D. (2017) 'Inflammatory pseudotumor after ceramic-on-ceramic total hip arthroplasty', *Arthroplast Today*, 3(2), pp. 83-87.

Campbell, P., Ebramzadeh, E., Nelson, S., Takamura, K., De Smet, K. and Amstutz, H.C. (2010) 'Histological features of pseudotumor-like tissues from metal-on-metal hips', *Clin Orthop Relat Res*, 468(9), pp. 2321-7.

Carli, A., Reuven, A., Zukor, D.J. and Antoniou, J. (2011) 'Adverse soft-tissue reactions around non-metal-on-metal total hip arthroplasty: A systematic review of the literature', *Bulletin of the NYU Hospital for Joint Diseases*, 69(SUPPL. 1), pp. S47-S51.

Case, C.P., Langkamer, V.G., Lock, R.J., Perry, M.J., Palmer, M.R. and Kemp, A.J. (2000) 'Changes in the proportions of peripheral blood lymphocytes in patients with worn implants', *J Bone Joint Surg Br*, 82(5), pp. 748-54.

Catelas, I., Bobyn, J.D., Medley, J.B., Krygier, J.J., Zukor, D.J. and Huk, O.L. (2003) 'Size, shape, and composition of wear particles from metal-metal hip simulator testing: effects of alloy and number of loading cycles', *J Biomed Mater Res A*, 67(1), pp. 312-27.

Catelas, I., Bobyn, J.D., Medley, J.B., Krygier, J.J., Zukor, D.J., Petit, A. and Huk, O.L. (2001) 'Effects of digestion protocols on the isolation and characterization of metal-metal wear particles. I. Analysis of particle size and shape', *J Biomed Mater Res*, 55(3), pp. 320-9.

Catelas, I., Lehoux, E.A., Hurda, I., Baskey, S.J., Gala, L., Foster, R., Kim, P.R. and Beaulé, P.E. (2015) 'Do Patients With a Failed Metal-on-metal Hip Implant With a Pseudotumor Present Differences in Their Peripheral Blood Lymphocyte Subpopulations?', *Clinical Orthopaedics and Related Research*.

Catelas, I., Petit, A., Vali, H., Fragiskatos, C., Meilleur, R., Zukor, D.J., Antoniou, J. and Huk, O.L. (2005) 'Quantitative analysis of macrophage apoptosis vs. necrosis induced by cobalt and chromium ions in vitro', *Biomaterials*, 26(15), pp. 2441-53.

Chanput, W., Mes, J.J., Savelkoul, H.F. and Wichers, H.J. (2013) 'Characterization of polarized THP-1 macrophages and polarizing ability of LPS and food compounds', *Food Funct*, 4(2), pp. 266-76.

Chen, D., Zhang, X., Guo, Y., Shi, S., Mao, X., Pan, X. and Cheng, T. (2012) 'MMP-9 inhibition suppresses wear debris-induced inflammatory osteolysis through downregulation of RANK/RANKL in a murine osteolysis model', *Int J Mol Med*, 30(6), pp. 1417-23.

Chen, X.X., Wang, T., Li, J. and Kang, H. (2016) 'Relationship between Inflammatory Response and Estimated Complication Rate after Total Hip Arthroplasty', *Chin Med J (Engl)*, 129(21), pp. 2546-2551.

- Chigae, A. and Sklar, L.A. (2012) 'Aspects of VLA-4 and LFA-1 regulation that may contribute to rolling and firm adhesion', *Front Immunol*, 3, p. 242.
- Choi, J.K., Geller, J.A., Yoon, R.S., Wang, W. and Macaulay, W. (2012) 'Comparison of total hip and knee arthroplasty cohorts and short-term outcomes from a single-center joint registry', *J Arthroplasty*, 27(6), pp. 837-41.
- Chowdhury, M.H., Ray, K., Gray, S.K., Pond, J. and Lakowicz, J.R. (2010) 'The use of aluminum nanostructures as platforms for metal enhanced fluorescence of the intrinsic emission of biomolecules in the ultra-violet', *Proc SPIE Int Soc Opt Eng*, 7577, p. 757700.
- Christiansen, R.J., Munch, H.J., Bonefeld, C.M., Thyssen, J.P., Sloth, J.J., Geisler, C., Soballe, K., Jellesen, M.S. and Jakobsen, S.S. (2019) 'Cytokine Profile in Patients with Aseptic Loosening of Total Hip Replacements and Its Relation to Metal Release and Metal Allergy', *J Clin Med*, 8(8).
- Colognato, R., Bonelli, A., Ponti, J., Farina, M., Bergamaschi, E., Sabbioni, E. and Migliore, L. (2008) 'Comparative genotoxicity of cobalt nanoparticles and ions on human peripheral leukocytes in vitro', *Mutagenesis*, 23(5), pp. 377-82.
- Craven, R. (2016) *The Effect of Nanoscale and Micron Sized Alumina and Cobalt Chromium Particles on Plasma Membrane Integrity*. University of Leeds.
- Cuckler, J.M. (2005) 'The rationale for metal-on-metal total hip arthroplasty', *Clin Orthop Relat Res*, 441, pp. 132-6.
- Cvetanovich, G.L., Schairer, W.W., Haughom, B.D., Nicholson, G.P. and Romeo, A.A. (2015) 'Does resident involvement have an impact on postoperative complications after total shoulder arthroplasty? An analysis of 1382 cases', *J Shoulder Elbow Surg*, 24(10), pp. 1567-73.
- D'Antonio, J.A., Capello, W.N. and Naughton, M. (2012) 'Ceramic bearings for total hip arthroplasty have high survivorship at 10 years', *Clin Orthop Relat Res*, 470(2), pp. 373-81.
- Dalal, A., Pawar, V., McAllister, K., Weaver, C. and Hallab, N.J. (2012) 'Orthopedic implant cobalt-alloy particles produce greater toxicity and inflammatory cytokines than titanium alloy and zirconium alloy-based particles in vitro, in human osteoblasts, fibroblasts, and macrophages', *J Biomed Mater Res A*, 100(8), pp. 2147-58.
- Dapunt, U., Giese, T., Lasitschka, F., Reinders, J., Lehner, B., Kretzer, J.P., Ewerbeck, V. and Hansch, G.M. (2014a) 'On the inflammatory response in metal-on-metal implants', *Journal of Translational Medicine*, 12(1).
- Dapunt, U., Maurer, S., Giese, T., Gaida, M.M. and Hansch, G.M. (2014b) 'The macrophage inflammatory proteins MIP1alpha (CCL3) and MIP2alpha (CXCL2) in implant-associated osteomyelitis: linking inflammation to bone degradation', *Mediators Inflamm*, 2014, p. 728619.
- Davda, K., Lali, F.V., Sampson, B., Skinner, J.A. and Hart, A.J. (2011) 'An analysis of metal ion levels in the joint fluid of symptomatic patients with metal-on-metal hip replacements', *Journal of Bone and Joint Surgery - Series B*, 93 B(6), pp. 738-745.
- Davies, A.P., Willert, H.G., Campbell, P.A., Learmonth, I.D. and Case, C.P. (2005) 'An unusual lymphocytic perivascular infiltration in tissues around contemporary metal-on-metal joint replacements', *Journal of Bone and Joint Surgery - Series A*, 87(1), pp. 18-27.

- De Pablo, R., Monserrat, J., Reyes, E., Díaz, D., Rodríguez-Zapata, M., De La Hera, A., Prieto, A. and Álvarez-Mon, M. (2013) 'Circulating sICAM-1 and sE-Selectin as biomarker of infection and prognosis in patients with systemic inflammatory response syndrome', *European Journal of Internal Medicine*, 24(2), pp. 132-138.
- De Smet, K., De Haan, R., Calistri, A., Campbell, P.A., Ebrahimzadeh, E., Pattyn, C. and Gill, H.S. (2008) 'Metal ion measurement as a diagnostic tool to identify problems with metal-on-metal hip resurfacing', *Journal of Bone and Joint Surgery - Series A*, 90(SUPPL. 4), pp. 202-208.
- Den Haan, J.M.M., Kraal, G. and Bevan, M.J. (2007) 'Cutting edge: Lipopolysaccharide induces IL-10-producing regulatory CD4⁺ T cells that suppress the CD8⁺ T cell response', *Journal of Immunology*, 178(9), pp. 5429-5433.
- Deng, J.C., Cheng, G., Newstead, M.W., Zeng, X., Kobayashi, K., Flavell, R.A. and Standiford, T.J. (2006) 'Sepsis-induced suppression of lung innate immunity is mediated by IRAK-M', *J Clin Invest*, 116(9), pp. 2532-42.
- Di, A., Xiong, S., Ye, Z., Malireddi, R.K.S., Kometani, S., Zhong, M., Mittal, M., Hong, Z., Kanneganti, T.D., Rehman, J. and Malik, A.B. (2018) 'The TWIK2 Potassium Efflux Channel in Macrophages Mediates NLRP3 Inflammasome-Induced Inflammation', *Immunity*, 49(1), pp. 56-65 e4.
- Doorn, P.F., Campbell, P.A., Worrall, J., Benya, P.D., McKellop, H.A. and Amstutz, H.C. (1998) 'Metal wear particle characterization from metal on metal total hip replacements: transmission electron microscopy study of periprosthetic tissues and isolated particles', *J Biomed Mater Res*, 42(1), pp. 103-11.
- Drynda, A., Drynda, S., Kekow, J., Lohmann, C.H. and Bertrand, J. (2018a) 'Differential Effect of Cobalt and Chromium Ions as Well as CoCr Particles on the Expression of Osteogenic Markers and Osteoblast Function', *Int J Mol Sci*, 19(10).
- Drynda, S., Drynda, A., Feuerstein, B., Kekow, J., Lohmann, C.H. and Bertrand, J. (2018b) 'The effects of cobalt and chromium ions on transforming growth factor-beta patterns and mineralization in human osteoblast-like MG63 and SaOs-2 cells', *J Biomed Mater Res A*, 106(8), pp. 2105-2115.
- Du, Z., Wang, S., Yue, B., Wang, Y. and Wang, Y. (2018) 'Effects of wear particles of polyether-ether-ketone and cobalt-chromium-molybdenum on CD4⁺ and CD8⁺-T-cell responses', *Oncotarget*, 9(13), pp. 11197-11208.
- Dutta, D.K., Potnis, P.A., Rhodes, K. and Wood, S.C. (2015) 'Wear particles derived from metal hip implants induce the generation of multinucleated giant cells in a 3-dimensional peripheral tissue-equivalent model', *PLoS One*, 10(4), p. e0124389.
- Erridge, C. (2010) 'Endogenous ligands of TLR2 and TLR4: agonists or assistants?', *J Leukoc Biol*, 87(6), pp. 989-99.
- Faye, P.A., Roualdes, O., Rossignol, F., Hartmann, D.J. and Desmouliere, A. (2017) 'Engulfment of ceramic particles by fibroblasts does not alter cell behavior', *Biomed Mater*, 12(1), p. 015023.
- Ferko, M.A. and Catelas, I. (2018) 'Effects of metal ions on caspase-1 activation and interleukin-1beta release in murine bone marrow-derived macrophages', *PLoS One*, 13(8), p. e0199936.
- Fox, R.J., Coffey, C.S., Conwit, R., Cudkowicz, M.E., Gleason, T., Goodman, A., Klawiter, E.C., Matsuda, K., McGovern, M., Naismith, R.T., Ashokkumar, A., Barnes,

J., Ecklund, D., Klingner, E., Koeppe, M., Long, J.D., Natarajan, S., Thornell, B., Yankey, J., Bermel, R.A., Debbins, J.P., Huang, X., Jagodnik, P., Lowe, M.J., Nakamura, K., Narayanan, S., Sakaie, K.E., Thoomukuntla, B., Zhou, X., Krieger, S., Alvarez, E., Apperson, M., Bashir, K., Cohen, B.A., Coyle, P.K., Delgado, S., Dewitt, L.D., Flores, A., Giesser, B.S., Goldman, M.D., Jubelt, B., Lava, N., Lynch, S.G., Moses, H., Ontaneda, D., Perumal, J.S., Racke, M., Repovic, P., Riley, C.S., Severson, C., Shinnar, S., Suski, V., Weinstock-Guttman, B., Yadav, V., Zabeti, A. and Investigators, N.S.-M.T. (2018) 'Phase 2 Trial of Ibudilast in Progressive Multiple Sclerosis', *N Engl J Med*, 379(9), pp. 846-855.

Gallo, J., Goodman, S.B., Lostak, J. and Janout, M. (2012) 'Advantages and disadvantages of ceramic on ceramic total hip arthroplasty: a review', *Biomed Pap Med Fac Univ Palacky Olomouc Czech Repub*, 156(3), pp. 204-12.

Germain, M.A., Hatton, A., Williams, S., Matthews, J.B., Stone, M.H., Fisher, J. and Ingham, E. (2003) 'Comparison of the cytotoxicity of clinically relevant cobalt-chromium and alumina ceramic wear particles in vitro', *Biomaterials*, 24(3), pp. 469-79.

Gibon, E., Ma, T., Ren, P.G., Fritton, K., Biswal, S., Yao, Z., Smith, L. and Goodman, S.B. (2012) 'Selective inhibition of the MCP-1-CCR2 ligand-receptor axis decreases systemic trafficking of macrophages in the presence of UHMWPE particles', *J Orthop Res*, 30(4), pp. 547-53.

Goode, A.E., Perkins, J.M., Sandison, A., Karunakaran, C., Cheng, H., Wall, D., Skinner, J.A., Hart, A.J., Porter, A.E., McComb, D.W. and Ryan, M.P. (2012) 'Chemical speciation of nanoparticles surrounding metal-on-metal hips', *Chem Commun (Camb)*, 48(67), pp. 8335-7.

Grammatopoulos, G., Pandit, H., Kwon, Y.M., Gundle, R., McLardy-Smith, P., Beard, D.J., Murray, D.W. and Gill, H.S. (2009) 'Hip resurfacings revised for inflammatory pseudotumour have a poor outcome', *J Bone Joint Surg Br*, 91(8), pp. 1019-24.

Green, T.R., Fisher, J., Matthews, J.B., Stone, M.H. and Ingham, E. (2000) 'Effect of size and dose on bone resorption activity of macrophages by in vitro clinically relevant ultra high molecular weight polyethylene particles', *J Biomed Mater Res*, 53(5), pp. 490-7.

Guijarro-Munoz, I., Compte, M., Alvarez-Cienfuegos, A., Alvarez-Vallina, L. and Sanz, L. (2014) 'Lipopolysaccharide activates Toll-like receptor 4 (TLR4)-mediated NF-kappaB signaling pathway and proinflammatory response in human pericytes', *J Biol Chem*, 289(4), pp. 2457-68.

Hailer, N.P., Blaheta, R.A., Dahlstrand, H. and Stark, A. (2011) 'Elevation of circulating HLA DR(+) CD8(+) T-cells and correlation with chromium and cobalt concentrations 6 years after metal-on-metal hip arthroplasty', *Acta Orthop*, 82(1), pp. 6-12.

Hallab, N.J., Caicedo, M., Epstein, R., McAllister, K. and Jacobs, J.J. (2010) 'In vitro reactivity to implant metals demonstrates a person-dependent association with both T-cell and B-cell activation', *J Biomed Mater Res A*, 92(2), pp. 667-82.

Hart, A.J., Satchithananda, K., Liddle, A.D., Sabah, S.A., McRobbie, D., Henckel, J., Cobb, J.P., Skinner, J.A. and Mitchell, A.W. (2012) 'Pseudotumors in association with well-functioning metal-on-metal hip prostheses: a case-control study using three-dimensional computed tomography and magnetic resonance imaging', *J Bone Joint Surg Am*, 94(4), pp. 317-25.

- Hart, A.J., Skinner, J.A., Winship, P., Faria, N., Kulinskaya, E., Webster, D., Muirhead-Allwood, S., Aldam, C.H., Anwar, H. and Powell, J.J. (2009) 'Circulating levels of cobalt and chromium from metal-on-metal hip replacement are associated with CD8+ T-cell lymphopenia', *J Bone Joint Surg Br*, 91(6), pp. 835-42.
- Hashimoto, M. and Imazato, S. (2015) 'Cytotoxic and genotoxic characterization of aluminum and silicon oxide nanoparticles in macrophages', *Dent Mater*, 31(5), pp. 556-64.
- Hatton, A., Nevelos, J.E., Matthews, J.B., Fisher, J. and Ingham, E. (2003) 'Effects of clinically relevant alumina ceramic wear particles on TNF-alpha production by human peripheral blood mononuclear phagocytes', *Biomaterials*, 24(7), pp. 1193-204.
- Haynes, D.R., Crotti, T.N., Loric, M., Bain, G.I., Atkins, G.J. and Findlay, D.M. (2001) 'Osteoprotegerin and receptor activator of nuclear factor kappaB ligand (RANKL) regulate osteoclast formation by cells in the human rheumatoid arthritic joint', *Rheumatology (Oxford)*, 40(6), pp. 623-30.
- He, W., Qu, T., Yu, Q., Wang, Z., Lv, H., Zhang, J., Zhao, X. and Wang, P. (2013) 'LPS induces IL-8 expression through TLR4, MyD88, NF-kappaB and MAPK pathways in human dental pulp stem cells', *International Endodontic Journal*, 46(2), pp. 128-136.
- Hidalgo, A., Chilvers, E.R., Summers, C. and Koenderman, L. (2019) 'The Neutrophil Life Cycle', *Trends Immunol*, 40(7), pp. 584-597.
- Holding, C.A., Findlay, D.M., Stamenkov, R., Neale, S.D., Lucas, H., Dharmapatni, A.S., Callary, S.A., Shrestha, K.R., Atkins, G.J., Howie, D.W. and Haynes, D.R. (2006) 'The correlation of RANK, RANKL and TNFalpha expression with bone loss volume and polyethylene wear debris around hip implants', *Biomaterials*, 27(30), pp. 5212-9.
- Holland, J.P., Langton, D.J. and Hashmi, M. (2012) 'Ten-year clinical, radiological and metal ion analysis of the Birmingham Hip Resurfacing from: A single, non-designer surgeon', *Journal of Bone and Joint Surgery - Series B*, 94 B(4), pp. 471-476.
- Honda, K., Takaoka, A. and Taniguchi, T. (2006) 'Type I interferon [corrected] gene induction by the interferon regulatory factor family of transcription factors', *Immunity*, 25(3), pp. 349-60.
- Hornung, V., Bauernfeind, F., Halle, A., Samstad, E.O., Kono, H., Rock, K.L., Fitzgerald, K.A. and Latz, E. (2008) 'Silica crystals and aluminum salts activate the NALP3 inflammasome through phagosomal destabilization', *Nat Immunol*, 9(8), pp. 847-56.
- Hosokawa, Y., Hosokawa, I., Ozaki, K., Nakae, H. and Matsuo, T. (2006) 'Cytokines differentially regulate ICAM-1 and VCAM-1 expression on human gingival fibroblasts', *Clinical and Experimental Immunology*, 144(3), pp. 494-502.
- Hughes, C.E. and Nibbs, R.J.B. (2018) 'A guide to chemokines and their receptors', *FEBS J*, 285(16), pp. 2944-2971.
- Huk, O.L., Catelas, I., Mwale, F., Antoniou, J., Zukor, D.J. and Petit, A. (2004) 'Induction of apoptosis and necrosis by metal ions in vitro', *J Arthroplasty*, 19(8 Suppl 3), pp. 84-7.
- li, M., Matsunaga, N., Hazeki, K., Nakamura, K., Takashima, K., Seya, T., Hazeki, O., Kitazaki, T. and Iizawa, Y. (2006) 'A Novel Cyclohexene Derivative, Ethyl (6R)-6-[(2-Chloro-4-fluorophenyl)sulfamoyl]cyclohex-1-ene-1-carboxylate (TAK-242), Selectively Inhibits Toll-Like Receptor 4-Mediated

- Cytokine Production through Suppression of Intracellular Signaling', *Molecular Pharmacology*, 69(4), pp. 1288-1295.
- Iwami, K.I., Matsuguchi, T., Masuda, A., Kikuchi, T., Musikachoen, T. and Yoshikai, Y. (2000) 'Cutting edge: naturally occurring soluble form of mouse Toll-like receptor 4 inhibits lipopolysaccharide signaling', *J Immunol*, 165(12), pp. 6682-6.
- Jameson, S.S., Baker, P.N., Mason, J., Porter, M.L., Deehan, D.J. and Reed, M.R. (2012) 'Independent predictors of revision following metal-on-metal hip resurfacing: a retrospective cohort study using National Joint Registry data', *J Bone Joint Surg Br*, 94(6), pp. 746-54.
- Jamsen, E., Kouri, V.P., Ainola, M., Goodman, S.B., Nordstrom, D.C., Eklund, K.K. and Pajarinen, J. (2017) 'Correlations between macrophage polarizing cytokines, inflammatory mediators, osteoclast activity, and toll-like receptors in tissues around aseptically loosened hip implants', *J Biomed Mater Res A*, 105(2), pp. 454-463.
- Jamsen, E., Pajarinen, J., Kouri, V.P., Rahikkala, A., Goodman, S.B., Manninen, M., Nordstrom, D.C., Eklund, K.K. and Nurmi, K. (2020) 'Tumor necrosis factor primes and metal particles activate the NLRP3 inflammasome in human primary macrophages', *Acta Biomater*, 108, pp. 347-357.
- Jin, Z.M., Firkins, P., Farrar, R. and Fisher, J. (2000) 'Analysis and modelling of wear of cobalt-chrome alloys in a pin-on-plate test for a metal-on-metal total hip replacement', *Proc Inst Mech Eng H*, 214(6), pp. 559-68.
- Jonitz-Heincke, A., Lochner, K., Schulze, C., Pohle, D., Pustlauk, W., Hansmann, D. and Bader, R. (2016) 'Contribution of human osteoblasts and macrophages to bone matrix degradation and proinflammatory cytokine release after exposure to abrasive endoprosthetic wear particles', *Mol Med Rep*, 14(2), pp. 1491-500.
- Jonitz-Heincke, A., Sellin, M.L., Seyfarth, A., Peters, K., Mueller-Hilke, B., Fiedler, T., Bader, R. and Klinder, A. (2019) 'Analysis of Cellular Activity Short-Term Exposure to Cobalt and Chromium Ions in Mature Human Osteoblasts', *Materials (Basel)*, 12(17).
- Jonitz-Heincke, A., Tillmann, J., Klinder, A., Krueger, S., Kretzer, J.P., Hol, P.J., Paulus, A.C. and Bader, R. (2017) 'The Impact of Metal Ion Exposure on the Cellular Behavior of Human Osteoblasts and PBMCs: In Vitro Analyses of Osteolytic Processes', *Materials (Basel)*, 10(7).
- Junttila, I.S. (2018) 'Tuning the Cytokine Responses: An Update on Interleukin (IL)-4 and IL-13 Receptor Complexes', *Front Immunol*, 9, p. 888.
- Kapellos, T.S., Taylor, L., Lee, H., Cowley, S.A., James, W.S., Iqbal, A.J. and Greaves, D.R. (2016) 'A novel real time imaging platform to quantify macrophage phagocytosis', *Biochem Pharmacol*, 116, pp. 107-19.
- Karam, J.A., Tokarski, A.T., Ciccotti, M., Austin, M.S. and Deirmengian, G.K. (2012) 'Revision total hip arthroplasty in younger patients: indications, reasons for failure, and survivorship', *Phys Sportsmed*, 40(4), pp. 96-101.
- Kaufman, A.M., Alabre, C.I., Rubash, H.E. and Shanbhag, A.S. (2008) 'Human macrophage response to UHMWPE, TiAlV, CoCr, and alumina particles: Analysis of multiple cytokines using protein arrays', *Journal of Biomedical Materials Research - Part A*, 84(2), pp. 464-474.

- Kawamoto, T., Ii, M., Kitazaki, T., Iizawa, Y. and Kimura, H. (2008) 'TAK-242 selectively suppresses Toll-like receptor 4-signaling mediated by the intracellular domain', *Eur J Pharmacol*, 584(1), pp. 40-8.
- Kayagaki, N., Wong, M.T., Stowe, I.B., Ramani, S.R., Gonzalez, L.C., Akashi-Takamura, S., Miyake, K., Zhang, J., Lee, W.P., Muszynski, A., Forsberg, L.S., Carlson, R.W. and Dixit, V.M. (2013) 'Noncanonical inflammasome activation by intracellular LPS independent of TLR4', *Science*, 341(6151), pp. 1246-9.
- Khan, U.A., Hashimi, S.M., Bakr, M.M., Forwood, M.R. and Morrison, N.A. (2016) 'CCL2 and CCR2 are Essential for the Formation of Osteoclasts and Foreign Body Giant Cells', *J Cell Biochem*, 117(2), pp. 382-9.
- Kiraly, E. and Gondos, T. (2014) 'The effect of functional movement ability on the quality of life after total hip replacement', *J Clin Nurs*, 23(1-2), pp. 124-31.
- Klinder, A., Seyfarth, A., Hansmann, D., Bader, R. and Jonitz-Heincke, A. (2018) 'Inflammatory Response of Human Peripheral Blood Mononuclear Cells and Osteoblasts Incubated With Metallic and Ceramic Submicron Particles', *Front Immunol*, 9, p. 831.
- Knight, S.R., Aujla, R. and Biswas, S.P. (2011) 'Total Hip Arthroplasty - over 100 years of operative history', *Orthopedic Reviews*, 3(2), p. e16.
- Kobayashi, K., Hernandez, L.D., Galan, J.E., Janeway, C.A., Jr., Medzhitov, R. and Flavell, R.A. (2002) 'IRAK-M is a negative regulator of Toll-like receptor signaling', *Cell*, 110(2), pp. 191-202.
- Kolaczowska, E. and Kubes, P. (2013) 'Neutrophil recruitment and function in health and inflammation', *Nat Rev Immunol*, 13(3), pp. 159-75.
- Kolatat, K., Perino, G., Wilner, G., Kaplowitz, E., Ricciardi, B.F., Boettner, F., Westrich, G.H., Jerabek, S.A., Goldring, S.R. and Purdue, P.E. (2015) 'Adverse local tissue reaction (ALTR) associated with corrosion products in metal-on-metal and dual modular neck total hip replacements is associated with upregulation of interferon gamma-mediated chemokine signaling', *Journal of Orthopaedic Research*, 33(10), pp. 1487-1497.
- Konan, S., Duncan, C.P., Masri, B.S. and Garbuz, D.S. (2017) 'What Is the Natural History of Asymptomatic Pseudotumors in Metal-on-metal THAs at Mid-term Followup?', *Clin Orthop Relat Res*, 475(2), pp. 433-441.
- Kopesky, P., Tiedemann, K., Alkekhia, D., Zechner, C., Millard, B., Schoeberl, B. and Komarova, S.V. (2014) 'Autocrine signaling is a key regulatory element during osteoclastogenesis', *Biol Open*, 3(8), pp. 767-76.
- Koulouvaris, P., Ly, K., Ivashkiv, L.B., Bostrom, M.P., Nestor, B.J., Sculco, T.P. and Purdue, P.E. (2008) 'Expression profiling reveals alternative macrophage activation and impaired osteogenesis in periprosthetic osteolysis', *J Orthop Res*, 26(1), pp. 106-16.
- Kubo, M. and Motomura, Y. (2012) 'Transcriptional regulation of the anti-inflammatory cytokine IL-10 in acquired immune cells', *Front Immunol*, 3, p. 275.
- Kwon, Y.M., Ostlere, S.J., McLardy-Smith, P., Athanasou, N.A., Gill, H.S. and Murray, D.W. (2011) "'Asymptomatic' Pseudotumors After Metal-on-Metal Hip Resurfacing Arthroplasty. Prevalence and Metal Ion Study', *Journal of Arthroplasty*, 26(4), pp. 511-518.

- Kwon, Y.M., Thomas, P., Summer, B., Pandit, H., Taylor, A., Beard, D., Murray, D.W. and Gill, H.S. (2010) 'Lymphocyte proliferation responses in patients with pseudotumors following metal-on-metal hip resurfacing arthroplasty', *Journal of Orthopaedic Research*, 28(4), pp. 444-450.
- Kwon, Y.M., Xia, Z., Glyn-Jones, S., Beard, D., Gill, H.S. and Murray, D.W. (2009) 'Dose-dependent cytotoxicity of clinically relevant cobalt nanoparticles and ions on macrophages in vitro', *Biomedical Materials*, 4(2).
- Lal, S., Hall, R.M. and Tipper, J.L. (2016) 'A novel method for isolation and recovery of ceramic nanoparticles and metal wear debris from serum lubricants at ultra-low wear rates', *Acta Biomater*, 42, pp. 420-428.
- Langton, D.J., Jameson, S.S., Joyce, T.J., Gandhi, J.N., Sidaginamale, R., Mereddy, P., Lord, J. and Nargol, A.V. (2011a) 'Accelerating failure rate of the ASR total hip replacement', *J Bone Joint Surg Br*, 93(8), pp. 1011-6.
- Langton, D.J., Jameson, S.S., Joyce, T.J., Hallab, N.J., Natu, S. and Nargol, A.V. (2010) 'Early failure of metal-on-metal bearings in hip resurfacing and large-diameter total hip replacement: A consequence of excess wear', *J Bone Joint Surg Br*, 92(1), pp. 38-46.
- Langton, D.J., Joyce, T.J., Jameson, S.S., Lord, J., Van Orsouw, M., Holland, J.P., Nargol, A.V. and De Smet, K.A. (2011b) 'Adverse reaction to metal debris following hip resurfacing: the influence of component type, orientation and volumetric wear', *J Bone Joint Surg Br*, 93(2), pp. 164-71.
- Langton, D.J., Sidaginamale, R.P., Joyce, T.J., Natu, S., Blain, P., Jefferson, R.D., Rushton, S. and Nargol, A.V. (2013) 'The clinical implications of elevated blood metal ion concentrations in asymptomatic patients with MoM hip resurfacings: a cohort study', *BMJ Open*, 3(3).
- Lassus, J., Waris, V., Xu, J.W., Li, T.F., Hao, J., Nietosvaara, Y., Santavirta, S. and Konttinen, Y.T. (2000) 'Increased interleukin-8 (IL-8) expression is related to aseptic loosening of total hip replacement', *Archives of Orthopaedic and Trauma Surgery*, 120(5-6), pp. 328-332.
- Laumonier, T., Ruffieux, E., Paccaud, J., Kindler, V. and Hannouche, D. (2019) 'In vitro evaluation of human myoblast function after exposure to cobalt and chromium ions', *J Orthop Res*.
- Laumonier, T., Ruffieux, E., Paccaud, J., Kindler, V. and Hannouche, D. (2020) 'In vitro evaluation of human myoblast function after exposure to cobalt and chromium ions', *J Orthop Res*, 38(6), pp. 1398-1406.
- Lawrence, H., Deehan, D., Holland, J., Kirby, J. and Tyson-Capper, A. (2014) 'The immunobiology of cobalt: Demonstration of a potential aetiology for inflammatory pseudotumours after metal-on-metal replacement of the hip', *Bone and Joint Journal*, 69B(9), pp. 1172-1177.
- Lawrence, H., Deehan, D.J., Holland, J.P., Anjum, S.A., Mawdesley, A.E., Kirby, J.A. and Tyson-Capper, A.J. (2016a) 'Cobalt ions recruit inflammatory cells in vitro through human Toll-like receptor 4', *Biochem Biophys Res*, 7, pp. 374-378.
- Lawrence, H., Mawdesley, A.E., Holland, J.P., Kirby, J.A., Deehan, D.J. and Tyson-Capper, A.J. (2016b) 'Targeting Toll-like receptor 4 prevents cobalt-mediated inflammation', *Oncotarget*, 7(7), pp. 7578-85.

- Lee, D., Shin, K.J., Kim, D.W., Yoon, K.A., Choi, Y.J., Lee, B.N.R. and Cho, J.Y. (2018) 'CCL4 enhances preosteoclast migration and its receptor CCR5 downregulation by RANKL promotes osteoclastogenesis', *Cell Death Dis*, 9(5), p. 495.
- Lee, J.H., Kim, H.N., Kim, K.O., Jin, W.J., Lee, S., Kim, H.H., Ha, H. and Lee, Z.H. (2012) 'CXCL10 promotes osteolytic bone metastasis by enhancing cancer outgrowth and osteoclastogenesis', *Cancer Research*, 72(13), pp. 3175-3186.
- Li, J. and Wang, H.M. (2014) 'Effects of cobalt chloride on phenotypes of normal human saphenous vein smooth muscle cells', *Int J Clin Exp Med*, 7(12), pp. 4933-41.
- Li, X. and Zhong, F. (2014) 'Nickel induces interleukin-1beta secretion via the NLRP3-ASC-caspase-1 pathway', *Inflammation*, 37(2), pp. 457-66.
- Li, Y. and Boraschi, D. (2016) 'Endotoxin contamination: a key element in the interpretation of nanosafety studies', *Nanomedicine (Lond)*, 11(3), pp. 269-87.
- Liden, C., Skare, L. and Vahter, M. (2008) 'Release of nickel from coins and deposition onto skin from coin handling--comparing euro coins and SEK', *Contact Dermatitis*, 59(1), pp. 31-7.
- Lima, H., Jr., Jacobson, L.S., Goldberg, M.F., Chandran, K., Diaz-Griffero, F., Lisanti, M.P. and Brojatsch, J. (2013) 'Role of lysosome rupture in controlling Nlrp3 signaling and necrotic cell death', *Cell Cycle*, 12(12), pp. 1868-78.
- Lin, P.S., Chang, H.H., Yeh, C.Y., Chang, M.C., Chan, C.P., Kuo, H.Y., Liu, H.C., Liao, W.C., Jeng, P.Y., Yeung, S.Y. and Jeng, J.H. (2017) 'Transforming growth factor beta 1 increases collagen content, and stimulates procollagen I and tissue inhibitor of metalloproteinase-1 production of dental pulp cells: Role of MEK/ERK and activin receptor-like kinase-5/Smad signaling', *J Formos Med Assoc*, 116(5), pp. 351-358.
- Liu, T., Zhang, L., Joo, D. and Sun, S.C. (2017) 'NF-kappaB signaling in inflammation', *Signal Transduct Target Ther*, 2.
- Lochner, K., Fritsche, A., Jonitz, A., Hansmann, D., Mueller, P., Mueller-Hilke, B. and Bader, R. (2011) 'The potential role of human osteoblasts for periprosthetic osteolysis following exposure to wear particles', *Int J Mol Med*, 28(6), pp. 1055-63.
- Lodowski, D.T. and Palczewski, K. (2009) 'Chemokine receptors and other G protein-coupled receptors', *Curr Opin HIV AIDS*, 4(2), pp. 88-95.
- Lohmann, C.H., Schwartz, Z., Koster, G., Jahn, U., Buchhorn, G.H., MacDougall, M.J., Casasola, D., Liu, Y., Sylvia, V.L., Dean, D.D. and Boyan, B.D. (2000) 'Phagocytosis of wear debris by osteoblasts affects differentiation and local factor production in a manner dependent on particle composition', *Biomaterials*, 21(6), pp. 551-61.
- Long, W., Quan, J., Liu, Y., Li, J., Gong, Q. and Jiang, H. (2020) '7ND protein exerts inhibitory effects on both osteoclast differentiation in vitro and lipopolysaccharide-induced bone erosion in vivo', *Mol Med Rep*, 22(1), pp. 97-104.
- Lopez-Castejon, G. and Brough, D. (2011) 'Understanding the mechanism of IL-1beta secretion', *Cytokine Growth Factor Rev*, 22(4), pp. 189-95.
- Lu, Y.C., Yeh, W.C. and Ohashi, P.S. (2008) 'LPS/TLR4 signal transduction pathway', *Cytokine*, 42(2), pp. 145-151.
- Lucarelli, M., Gatti, A.M., Savarino, G., Quattroni, P., Martinelli, L., Monari, E. and Boraschi, D. (2004) 'Innate defence functions of macrophages can be biased by nano-sized ceramic and metallic particles', *Eur Cytokine Netw*, 15(4), pp. 339-46.

- Mahendra, G., Pandit, H., Kliskey, K., Murray, D., Gill, H.S. and Athanasou, N. (2009) 'Necrotic and inflammatory changes in metal-on-metal resurfacing hip arthroplasties: Relation to implant failure and pseudotumor formation', *Acta Orthopaedica*, 80(6), pp. 653-659.
- Malem, D., Nagy, M.T., Ghosh, S. and Shah, B. (2013) 'Catastrophic failure of ceramic-on-ceramic total hip arthroplasty presenting as squeaking hip', *BMJ Case Rep*, 2013.
- Mariathasan, S., Weiss, D.S., Newton, K., McBride, J., O'Rourke, K., Roose-Girma, M., Lee, W.P., Weinrauch, Y., Monack, D.M. and Dixit, V.M. (2006) 'Cryopyrin activates the inflammasome in response to toxins and ATP', *Nature*, 440(7081), pp. 228-32.
- Matharu, G.S., Pandit, H.G., Murray, D.W. and Judge, A. (2016) 'Adverse reactions to metal debris occur with all types of hip replacement not just metal-on-metal hips: a retrospective observational study of 3340 revisions for adverse reactions to metal debris from the National Joint Registry for England, Wales, Northern Ireland and the Isle of Man', *BMC Musculoskelet Disord*, 17(1), p. 495.
- Matsunaga, N., Tsuchimori, N., Matsumoto, T. and Ii, M. (2011) 'TAK-242 (resatorvid), a small-molecule inhibitor of Toll-like receptor (TLR) 4 signaling, binds selectively to TLR4 and interferes with interactions between TLR4 and its adaptor molecules', *Molecular Pharmacology*, 79(1), pp. 34-41.
- Matthies, A.K., Skinner, J.A., Osmani, H., Henckel, J. and Hart, A.J. (2012) 'Pseudotumors are common in well-positioned low-wearing metal-on-metal hips', *Clin Orthop Relat Res*, 470(7), pp. 1895-906.
- Mattila, L., Kilpelainen, M., Terho, E.O., Koskenvuo, M., Helenius, H. and Kalimo, K. (2001) 'Prevalence of nickel allergy among Finnish university students in 1995', *Contact Dermatitis*, 44(4), pp. 218-23.
- Maurer-Ertl, W., Pränckh-Matzke, D., Friesenbichler, J., Bratschitsch, G., Holzer, L.A., Maier, M. and Leithner, A. (2017) 'Clinical Results and Serum Metal Ion Concentrations following Ceramic-on-Metal Total Hip Arthroplasty at a Mean Follow-Up of 60 Months', *Biomed Res Int*, 2017, p. 3726029.
- McEver, R.P. (2015) 'Selectins: initiators of leucocyte adhesion and signalling at the vascular wall', *Cardiovasc Res*, 107(3), pp. 331-9.
- Milosev, I., Kovac, S., Trebse, R., Levasic, V. and Pisot, V. (2012) 'Comparison of ten-year survivorship of hip prostheses with use of conventional polyethylene, metal-on-metal, or ceramic-on-ceramic bearings', *J Bone Joint Surg Am*, 94(19), pp. 1756-63.
- Mochida, Y., Boehler, M., Salzer, M. and Bauer, T.W. (2001) 'Debris from failed ceramic-on-ceramic and ceramic-on-polyethylene hip prostheses', *Clin Orthop Relat Res*, (389), pp. 113-25.
- Modi, W.S. and Yoshimura, T. (1999) 'Isolation of novel GRO genes and a phylogenetic analysis of the CXC chemokine subfamily in mammals', *Mol Biol Evol*, 16(2), pp. 180-93.
- Monnet, E., Choy, E.H., McInnes, I., Kobakhidze, T., de Graaf, K., Jacqmin, P., Lapeyre, G. and de Min, C. (2020) 'Efficacy and safety of NI-0101, an anti-toll-like receptor 4 monoclonal antibody, in patients with rheumatoid arthritis after inadequate response to methotrexate: a phase II study', *Ann Rheum Dis*, 79(3), pp. 316-323.

- Montesi, M., Beraudi, A., Stea, S., Ancarani, C., Traina, F. and Toni, A. (2012) 'Monocyte chemoattractant protein 1 expression in synovial fluid of patients with total hip arthroplasty', *Artif Organs*, 36(5), pp. 487-91.
- Munoz-Vega, M., Masso, F., Paez, A., Carreon-Torres, E., Cabrera-Fuentes, H.A., Fragoso, J.M., Perez-Hernandez, N., Martinez, L.O., Najib, S., Vargas-Alarcon, G. and Perez-Mendez, O. (2018) 'Characterization of immortalized human dermal microvascular endothelial cells (HMEC-1) for the study of HDL functionality', *Lipids Health Dis*, 17(1), p. 44.
- Munro, J.T., Masri, B.A., Duncan, C.P. and Garbuz, D.S. (2014) 'High complication rate after revision of large-head metal-on-metal total hip arthroplasty', *Clin Orthop Relat Res*, 472(2), pp. 523-8.
- Nakashima, Y., Sun, D.H., Trindade, M.C., Chun, L.E., Song, Y., Goodman, S.B., Schurman, D.J., Maloney, W.J. and Smith, R.L. (1999) 'Induction of macrophage C-C chemokine expression by titanium alloy and bone cement particles', *J Bone Joint Surg Br*, 81(1), pp. 155-62.
- National Joint Registry for England, W., Northern Ireland and the Isle of Man (2019) 'National Joint Registry for England and Wales 16th Annual Report 2019'.
- Nich, C., Takakubo, Y., Pajarinen, J., Ainola, M., Salem, A., Sillat, T., Rao, A.J., Raska, M., Tamaki, Y., Takagi, M., Konttinen, Y.T., Goodman, S.B. and Gallo, J. (2013) 'Macrophages - Key cells in the response to wear debris from joint replacements', *Journal of Biomedical Materials Research - Part A*, 101(10), pp. 3033-3045.
- Nich, C., Takakubo, Y., Pajarinen, J., Gallo, J., Konttinen, Y.T., Takagi, M. and Goodman, S.B. (2016) 'The Role of Macrophages in the Biological Reaction to Wear Debris from Artificial Joints', *J Long Term Eff Med Implants*, 26(4), pp. 303-309.
- Nilsdotter, A.K. and Isaksson, F. (2010) 'Patient relevant outcome 7 years after total hip replacement for OA - a prospective study', *BMC Musculoskelet Disord*, 11, p. 47.
- Nine, M.J., Choudhury, D., Hee, A.C., Mootanah, R. and Osman, N.A.A. (2014) 'Wear Debris Characterization and Corresponding Biological Response: Artificial Hip and Knee Joints', *Materials (Basel)*, 7(2), pp. 980-1016.
- Ninomiya, J.T., Kuzma, S.A., Schnettler, T.J., Krolikowski, J.G., Struve, J.A. and Weihrauch, D. (2013) 'Metal Ions Activate Vascular Endothelial Cells and Increase Lymphocyte Chemotaxis and Binding', *Journal of Orthopaedic Research*, 31(9), pp. 1484-1491.
- Nishanth, R.P., Jyotsna, R.G., Schlager, J.J., Hussain, S.M. and Reddanna, P. (2011) 'Inflammatory responses of RAW 264.7 macrophages upon exposure to nanoparticles: role of ROS-NFkappaB signaling pathway', *Nanotoxicology*, 5(4), pp. 502-16.
- Nyga, A., Hart, A. and Tetley, T.D. (2015) 'Importance of the HIF pathway in cobalt nanoparticle-induced cytotoxicity and inflammation in human macrophages', *Nanotoxicology*, 9(7), pp. 905-17.
- Obando-Pereda, G.A., Fischer, L. and Stach-Machado, D.R. (2014) 'Titanium and zirconia particle-induced pro-inflammatory gene expression in cultured macrophages and osteolysis, inflammatory hyperalgesia and edema in vivo', *Life Sci*, 97(2), pp. 96-106.
- Oblak, A., Pohar, J. and Jerala, R. (2015) 'MD-2 determinants of nickel and cobalt-mediated activation of human TLR4', *PLoS ONE*, 10(3).

- Olivier, V., Duval, J.L., Hindie, M., Pouletaut, P. and Nagel, M.D. (2003) 'Comparative particle-induced cytotoxicity toward macrophages and fibroblasts', *Cell Biol Toxicol*, 19(3), pp. 145-59.
- Oostingh, G.J., Casals, E., Italiani, P., Colognato, R., Stritzinger, R., Ponti, J., Pfaller, T., Kohl, Y., Ooms, D., Favilli, F., Leppens, H., Lucchesi, D., Rossi, F., Nelissen, I., Thielecke, H., Puentes, V.F., Duschl, A. and Boraschi, D. (2011) 'Problems and challenges in the development and validation of human cell-based assays to determine nanoparticle-induced immunomodulatory effects', *Part Fibre Toxicol*, 8(1), p. 8.
- Opal, S.M., Laterre, P.F., Francois, B., LaRosa, S.P., Angus, D.C., Mira, J.P., Wittebole, X., Dugernier, T., Perrotin, D., Tidswell, M., Jauregui, L., Krell, K., Pacht, J., Takahashi, T., Peckelsen, C., Cordasco, E., Chang, C.S., Oeyen, S., Aikawa, N., Maruyama, T., Schein, R., Kalil, A.C., Van Nuffelen, M., Lynn, M., Rossignol, D.P., Gogate, J., Roberts, M.B., Wheeler, J.L., Vincent, J.L. and Group, A.S. (2013) 'Effect of eritoran, an antagonist of MD2-TLR4, on mortality in patients with severe sepsis: the ACCESS randomized trial', *JAMA*, 309(11), pp. 1154-62.
- Opitz, B., Puschel, A., Beermann, W., Hocke, A.C., Forster, S., Schmeck, B., van Laak, V., Chakraborty, T., Suttorp, N. and Hippenstiel, S. (2006) 'Listeria monocytogenes activated p38 MAPK and induced IL-8 secretion in a nucleotide-binding oligomerization domain 1-dependent manner in endothelial cells', *J Immunol*, 176(1), pp. 484-90.
- Orlowski, G.M., Colbert, J.D., Sharma, S., Bogoy, M., Robertson, S.A. and Rock, K.L. (2015) 'Multiple Cathepsins Promote Pro-IL-1beta Synthesis and NLRP3-Mediated IL-1beta Activation', *J Immunol*, 195(4), pp. 1685-97.
- Oyajobi, B.O., Franchin, G., Williams, P.J., Pulkrabek, D., Gupta, A., Munoz, S., Grubbs, B., Zhao, M., Chen, D., Sherry, B. and Mundy, G.R. (2003) 'Dual effects of macrophage inflammatory protein-1alpha on osteolysis and tumor burden in the murine 5TGM1 model of myeloma bone disease', *Blood*, 102(1), pp. 311-9.
- Painter, K.J. (2009) 'Modelling cell migration strategies in the extracellular matrix', *J Math Biol*, 58(4-5), pp. 511-43.
- Pajarinen, J., Cenni, E., Savarino, L., Gomez-Barrena, E., Tamaki, Y., Takagi, M., Salo, J. and Konttinen, Y.T. (2010) 'Profile of toll-like receptor-positive cells in septic and aseptic loosening of total hip arthroplasty implants', *Journal of Biomedical Materials Research - Part A*, 94(1), pp. 84-92.
- Pandit, H., Glyn-Jones, S., McLardy-Smith, P., Gundle, R., Whitwell, D., Gibbons, C.L., Ostlere, S., Athanasou, N., Gill, H.S. and Murray, D.W. (2008) 'Pseudotumours associated with metal-on-metal hip resurfacings', *J Bone Joint Surg Br*, 90(7), pp. 847-51.
- Papageorgiou, I., Abberton, T., Fuller, M., Tipper, J.L., Fisher, J. and Ingham, E. (2014) 'Biological Effects of Clinically Relevant CoCr Nanoparticles in the Dura Mater: An Organ Culture Study', *Nanomaterials (Basel)*, 4(2), pp. 485-504.
- Papageorgiou, I., Brown, C., Schins, R., Singh, S., Newson, R., Davis, S., Fisher, J., Ingham, E. and Case, C.P. (2007) 'The effect of nano- and micron-sized particles of cobalt-chromium alloy on human fibroblasts in vitro', *Biomaterials*, 28(19), pp. 2946-58.
- Park, B.S. and Lee, J.O. (2013) 'Recognition of lipopolysaccharide pattern by TLR4 complexes', *Exp Mol Med*, 45, p. e66.

- Park, E.K., Jung, H.S., Yang, H.I., Yoo, M.C., Kim, C. and Kim, K.S. (2007) 'Optimized THP-1 differentiation is required for the detection of responses to weak stimuli', *Inflamm Res*, 56(1), pp. 45-50.
- Paukkeri, E.L., Korhonen, R., Hamalainen, M., Pesu, M., Eskelinen, A., Moilanen, T. and Moilanen, E. (2016) 'The Inflammatory Phenotype in Failed Metal-On-Metal Hip Arthroplasty Correlates with Blood Metal Concentrations', *PLoS One*, 11(5), p. e0155121.
- Paulus, A.C., Ebinger, K., Cheng, X., Hasselt, S., Weber, P., Kretzer, J.P., Bader, R. and Utzschneider, S. (2019) 'Local Biological Reactions and Pseudotumor-Like Tissue Formation in relation to Metal Wear in a Murine In Vivo Model', *Biomed Res Int*, 2019, p. 3649838.
- Perera, A.P., Fernando, R., Shinde, T., Gundamaraju, R., Southam, B., Sohal, S.S., Robertson, A.A.B., Schroder, K., Kunde, D. and Eri, R. (2018) 'MCC950, a specific small molecule inhibitor of NLRP3 inflammasome attenuates colonic inflammation in spontaneous colitis mice', *Sci Rep*, 8(1), p. 8618.
- Perino, G., Ricciardi, B.F., Jerabek, S.A., Martignoni, G., Wilner, G., Maass, D., Goldring, S.R. and Purdue, P.E. (2014) 'Implant based differences in adverse local tissue reaction in failed total hip arthroplasties: A morphological and immunohistochemical study', *BMC Clinical Pathology*, 14(1).
- Perregaux, D. and Gabel, C.A. (1994) 'Interleukin-1 beta maturation and release in response to ATP and nigericin. Evidence that potassium depletion mediated by these agents is a necessary and common feature of their activity', *J Biol Chem*, 269(21), pp. 15195-203.
- Persson, A., Eisler, T., Boden, H., Krupic, F., Skoldenberg, O. and Muren, O. (2018) 'Revision for Symptomatic Pseudotumor After Primary Metal-on-Polyethylene Total Hip Arthroplasty with a Standard Femoral Stem', *J Bone Joint Surg Am*, 100(11), pp. 942-949.
- Petit, A., Catelas, I., Antoniou, J., Zukor, D.J. and Huk, O.L. (2002) 'Differential apoptotic response of J774 macrophages to alumina and ultra-high-molecular-weight polyethylene particles', *J Orthop Res*, 20(1), pp. 9-15.
- Petit, A., Mwale, F., Tkaczyk, C., Antoniou, J., Zukor, D.J. and Huk, O.L. (2005) 'Induction of protein oxidation by cobalt and chromium ions in human U937 macrophages', *Biomaterials*, 26(21), pp. 4416-22.
- Petrilli, V., Dostert, C., Muruve, D.A. and Tschopp, J. (2007) 'The inflammasome: a danger sensing complex triggering innate immunity', *Curr Opin Immunol*, 19(6), pp. 615-22.
- Phillips, E.A., Klein, G.R., Cates, H.E., Kurtz, S.M. and Steinbeck, M. (2014) 'Histological characterization of periprosthetic tissue responses for metal-on-metal hip replacement', *J Long Term Eff Med Implants*, 24(1), pp. 13-23.
- Posada, O.M., Gilmour, D., Tate, R.J. and Grant, M.H. (2014) 'CoCr wear particles generated from CoCr alloy metal-on-metal hip replacements, and cobalt ions stimulate apoptosis and expression of general toxicology-related genes in monocyte-like U937 cells', *Toxicology and Applied Pharmacology*, 281(1), pp. 125-135.
- Posada, O.M., Tate, R.J. and Grant, M.H. (2015) 'Toxicity of cobalt-chromium nanoparticles released from a resurfacing hip implant and cobalt ions on primary human lymphocytes in vitro', *Journal of Applied Toxicology*, 35(6), pp. 614-622.

- Potnis, P.A., Dutta, D.K. and Wood, S.C. (2013) 'Toll-like receptor 4 signaling pathway mediates proinflammatory immune response to cobalt-alloy particles', *Cellular Immunology*, 282(1), pp. 53-65.
- Radziun, E., Dudkiewicz Wilczynska, J., Ksiazek, I., Nowak, K., Anuszevska, E.L., Kunicki, A., Olszyna, A. and Zabkowski, T. (2011) 'Assessment of the cytotoxicity of aluminium oxide nanoparticles on selected mammalian cells', *Toxicol In Vitro*, 25(8), pp. 1694-700.
- Raghavan, B., Martin, S.F., Esser, P.R., Goebeler, M. and Schmidt, M. (2012) 'Metal allergens nickel and cobalt facilitate TLR4 homodimerization independently of MD2', *EMBO Reports*, 13(12), pp. 1109-1115.
- Rajpura, A., Porter, M.L., Gambhir, A.K., Freemont, A.J. and Board, T.N. (2011) 'Clinical experience of revision of metal on metal hip arthroplasty for aseptic lymphocyte dominated vasculitis associated lesions (ALVAL)', *Hip Int*, 21(1), pp. 43-51.
- Rengarajan, M., Hayer, A. and Theriot, J.A. (2016) 'Endothelial Cells Use a Formin-Dependent Phagocytosis-Like Process to Internalize the Bacterium *Listeria monocytogenes*', *PLoS Pathog*, 12(5), p. e1005603.
- Renner, L., Schmidt-Braekling, T., Faschingbauer, M. and Boettner, F. (2016) 'Do cobalt and chromium levels predict osteolysis in metal-on-metal total hip arthroplasty?', *Arch Orthop Trauma Surg*, 136(12), pp. 1657-1662.
- Rice, T.W., Wheeler, A.P., Bernard, G.R., Vincent, J.L., Angus, D.C., Aikawa, N., Demeyer, I., Sainati, S., Amlot, N., Cao, C., Li, M., Matsuda, H., Mouri, K. and Cohen, J. (2010) 'A randomized, double-blind, placebo-controlled trial of TAK-242 for the treatment of severe sepsis', *Crit Care Med*, 38(8), pp. 1685-94.
- Rodrigo, A., Valles, G., Saldana, L., Rodriguez, M., Martinez, M.E., Munuera, L. and Vilaboa, N. (2006) 'Alumina particles influence the interactions of cocultured osteoblasts and macrophages', *J Orthop Res*, 24(1), pp. 46-54.
- Rony, L., de Sainte Hermine, P., Steiger, V., Mallet, R., Hubert, L. and Chappard, D. (2018) 'Characterization of wear debris released from alumina-on-alumina hip prostheses: Analysis of retrieved femoral heads and peri-prosthetic tissues', *Micron*, 104, pp. 89-94.
- Rosales, C. and Uribe-Querol, E. (2017) 'Phagocytosis: A Fundamental Process in Immunity', *Biomed Res Int*, 2017, p. 9042851.
- Roualdes, O., Duclos, M.E., Gutknecht, D., Frappart, L., Chevalier, J. and Hartmann, D.J. (2010) 'In vitro and in vivo evaluation of an alumina-zirconia composite for arthroplasty applications', *Biomaterials*, 31(8), pp. 2043-54.
- Samelko, L., Caicedo, M.S., Lim, S.J., Della-Valle, C., Jacobs, J. and Hallab, N.J. (2013) 'Cobalt-Alloy Implant Debris Induce HIF-1 α Hypoxia Associated Responses: A Mechanism for Metal-Specific Orthopedic Implant Failure', *PLoS ONE*, 8(6).
- Samelko, L., Landgraeber, S., McAllister, K., Jacobs, J. and Hallab, N.J. (2016) 'Cobalt Alloy Implant Debris Induces Inflammation and Bone Loss Primarily through Danger Signaling, Not TLR4 Activation: Implications for DAMP-ening Implant Related Inflammation', *PLoS One*, 11(7), p. e0160141.

- Samelko, L., Landgraeber, S., McAllister, K., Jacobs, J. and Hallab, N.J. (2017) 'TLR4 (not TLR2) dominate cognate TLR activity associated with CoCrMo implant particles', *J Orthop Res*, 35(5), pp. 1007-1017.
- Sampson, B. and Hart, A. (2012) 'Clinical usefulness of blood metal measurements to assess the failure of metal-on-metal hip implants', *Ann Clin Biochem*, 49(Pt 2), pp. 118-31.
- Sargeant, A., Goswami, T. and Swank, M. (2006) 'Ion concentrations from hip implants', *J Surg Orthop Adv*, 15(2), pp. 113-4.
- Sato, N., Kinbara, M., Kuroishi, T., Kimura, K., Iwakura, Y., Ohtsu, H., Sugawara, S. and Endo, Y. (2007) 'Lipopolysaccharide promotes and augments metal allergies in mice, dependent on innate immunity and histidine decarboxylase', *Clin Exp Allergy*, 37(5), pp. 743-51.
- Savarino, L., Greco, M., Cenni, E., Cavasinni, L., Rotini, R., Baldini, N. and Giunti, A. (2006) 'Differences in ion release after ceramic-on-ceramic and metal-on-metal total hip replacement. Medium-term follow-up', *J Bone Joint Surg Br*, 88(4), pp. 472-6.
- Sawa, Y., Ueki, T., Hata, M., Iwasawa, K., Tsuruga, E., Kojima, H., Ishikawa, H. and Yoshida, S. (2008) 'LPS-induced IL-6, IL-8, VCAM-1, and ICAM-1 expression in human lymphatic endothelium', *Journal of Histochemistry and Cytochemistry*, 56(2), pp. 97-109.
- Scharf, B., Clement, C.C., Zolla, V., Perino, G., Yan, B., Elci, S.G., Purdue, E., Goldring, S., Macaluso, F., Cobelli, N., Vachet, R.W. and Santambrogio, L. (2014) 'Molecular analysis of chromium and cobalt-related toxicity', *Sci Rep*, 4, p. 5729.
- Schmidt, M., Raghavan, B., Muller, V., Vogl, T., Fejer, G., Tchaptchet, S., Keck, S., Kalis, C., Nielsen, P.J., Galanos, C., Roth, J., Skerra, A., Martin, S.F., Freudenberg, M.A. and Goebeler, M. (2010) 'Crucial role for human Toll-like receptor 4 in the development of contact allergy to nickel', *Nat Immunol*, 11(9), pp. 814-9.
- Schutte, R.J., Parisi-Amon, A. and Reichert, W.M. (2009) 'Cytokine profiling using monocytes/macrophages cultured on common biomaterials with a range of surface chemistries', *J Biomed Mater Res A*, 88(1), pp. 128-39.
- Scully, W.F. and Teeny, S.M. (2013) 'Pseudotumor associated with metal-on-polyethylene total hip arthroplasty', *Orthopedics*, 36(5), pp. e666-70.
- Serda, R.E., Gu, J., Burks, J.K., Ferrari, K., Ferrari, C. and Ferrari, M. (2009) 'Quantitative mechanics of endothelial phagocytosis of silicon microparticles', *Cytometry A*, 75(9), pp. 752-60.
- Serrano, P.M., Rodrigues, C., M, S.S., Coelho, R., Cardoso, P. and Oliveira, V. (2018) 'Pseudotumor complicating a well-fixed ceramic-on-polyethylene total hip arthroplasty', *Clin Case Rep*, 6(9), pp. 1756-1760.
- Sidaginamale, R.P., Joyce, T.J., Lord, J.K., Jefferson, R., Blain, P.G., Nargol, A.V. and Langton, D.J. (2013) 'Blood metal ion testing is an effective screening tool to identify poorly performing metal-on-metal bearing surfaces', *Bone Joint Res*, 2(5), pp. 84-95.
- Skjesol, A., Yurchenko, M., Bosl, K., Gravastrand, C., Nilsen, K.E., Grovdal, L.M., Agliano, F., Patane, F., Lentini, G., Kim, H., Teti, G., Kumar Sharma, A., Kandasamy, R.K., Sporsheim, B., Starheim, K.K., Golenbock, D.T., Stenmark, H., McCaffrey, M., Espevik, T. and Husebye, H. (2019) 'The TLR4 adaptor TRAM controls the

phagocytosis of Gram-negative bacteria by interacting with the Rab11-family interacting protein 2', *PLoS Pathog*, 15(3), p. e1007684.

Song, M., Jin, J., Lim, J.E., Kou, J., Pattanayak, A., Rehman, J.A., Kim, H.D., Tahara, K., Lalonde, R. and Fukuchi, K. (2011) 'TLR4 mutation reduces microglial activation, increases Abeta deposits and exacerbates cognitive deficits in a mouse model of Alzheimer's disease', *J Neuroinflammation*, 8, p. 92.

Song, N., Liu, Z.S., Xue, W., Bai, Z.F., Wang, Q.Y., Dai, J., Liu, X., Huang, Y.J., Cai, H., Zhan, X.Y., Han, Q.Y., Wang, H., Chen, Y., Li, H.Y., Li, A.L., Zhang, X.M., Zhou, T. and Li, T. (2017) 'NLRP3 Phosphorylation Is an Essential Priming Event for Inflammasome Activation', *Mol Cell*, 68(1), pp. 185-197 e6.

Stein, N.C., Kreuzmann, C., Zimmermann, S.P., Niebergall, U., Hellmeyer, L., Goettsch, C., Schoppet, M. and Hofbauer, L.C. (2008) 'Interleukin-4 and interleukin-13 stimulate the osteoclast inhibitor osteoprotegerin by human endothelial cells through the STAT6 pathway', *J Bone Miner Res*, 23(5), pp. 750-8.

Sterner, T., Schutze, N., Saxler, G., Jakob, F. and Rader, C.P. (2004) '[Effects of clinically relevant alumina ceramic, zirconia ceramic and titanium particles of different sizes and concentrations on TNF-alpha release in a human macrophage cell line]', *Biomed Tech (Berl)*, 49(12), pp. 340-4.

Thierse, H.J., Gamedinger, K., Junkes, C., Guerreiro, N. and Weltzien, H.U. (2005) 'T cell receptor (TCR) interaction with haptens: Metal ions as non-classical haptens', *Toxicology*, 209(2), pp. 101-107.

Tipper, J.L., Firkins, P.J., Ingham, E., Fisher, J., Stone, M.H. and Farrar, R. (1999) 'Quantitative analysis of the wear and wear debris from low and high carbon content cobalt chrome alloys used in metal on metal total hip replacements', *J Mater Sci Mater Med*, 10(6), pp. 353-62.

Tipper, J.L., Hatton, A., Nevelos, J.E., Ingham, E., Doyle, C., Streicher, R., Nevelos, A.B. and Fisher, J. (2002) 'Alumina-alumina artificial hip joints. Part II: characterisation of the wear debris from in vitro hip joint simulations', *Biomaterials*, 23(16), pp. 3441-8.

Tsaousi, A., Jones, E. and Case, C.P. (2010) 'The in vitro genotoxicity of orthopaedic ceramic (Al₂O₃) and metal (CoCr alloy) particles', *Mutat Res*, 697(1-2), pp. 1-9.

Tyson-Capper, A.J., Lawrence, H., Holland, J.P., Deehan, D.J. and Kirby, J.A. (2013) 'Metal-on-metal hips: Cobalt can induce an endotoxin-like response', *Annals of the Rheumatic Diseases*, 72(3), pp. 460-461.

Underwood, R.J., Zografos, A., Sayles, R.S., Hart, A. and Cann, P. (2012) 'Edge loading in metal-on-metal hips: low clearance is a new risk factor', *Proc Inst Mech Eng H*, 226(3), pp. 217-26.

Urban, R.M., Jacobs, J.J., Tomlinson, M.J., Gavrilovic, J., Black, J. and Peoc'h, M. (2000) 'Dissemination of wear particles to the liver, spleen, and abdominal lymph nodes of patients with hip or knee replacement', *J Bone Joint Surg Am*, 82(4), pp. 457-76.

van Lingen, C.P., Ettema, H.B., Timmer, J.R., de Jong, G. and Verheyen, C.C. (2013) 'Clinical manifestations in ten patients with asymptomatic metal-on-metal hip arthroplasty with very high cobalt levels', *Hip Int*, 23(5), pp. 441-4.

Vaure, C. and Liu, Y. (2014) 'A comparative review of toll-like receptor 4 expression and functionality in different animal species', *Front Immunol*, 5, p. 316.

- Videm, V. and Albrigtsen, M. (2008) 'Soluble ICAM-1 and VCAM-1 as markers of endothelial activation', *Scand J Immunol*, 67(5), pp. 523-31.
- Viemann, D., Schmidt, M., Tenbrock, K., Schmid, S., Muller, V., Klimmek, K., Ludwig, S., Roth, J. and Goebeler, M. (2007) 'The contact allergen nickel triggers a unique inflammatory and proangiogenic gene expression pattern via activation of NF-kappaB and hypoxia-inducible factor-1alpha', *J Immunol*, 178(5), pp. 3198-207.
- Walter, L.R., Marel, E., Harbury, R. and Wearne, J. (2008) 'Distribution of chromium and cobalt ions in various blood fractions after resurfacing hip arthroplasty', *J Arthroplasty*, 23(6), pp. 814-21.
- Wang, C.T., Lin, Y.T., Chiang, B.L., Lee, S.S. and Hou, S.M. (2010) 'Over-expression of receptor activator of nuclear factor-kappaB ligand (RANKL), inflammatory cytokines, and chemokines in periprosthetic osteolysis of loosened total hip arthroplasty', *Biomaterials*, 31(1), pp. 77-82.
- Wang, Y., Wu, N.N., Mou, Y.Q., Chen, L. and Deng, Z.L. (2013) 'Inhibitory effects of recombinant IL-4 and recombinant IL-13 on UHMWPE-induced bone destruction in the murine air pouch model', *J Surg Res*, 180(2), pp. e73-81.
- Wang, Z., Yan, Y., Su, Y. and Qiao, L. (2016) 'Effect of proteins on the surface microstructure evolution of a CoCrMo alloy in bio-tribocorrosion processes', *Colloids Surf B Biointerfaces*, 145, pp. 176-184.
- Waterson, H.B., Whitehouse, M.R., Greidanus, N.V., Garbuz, D.S., Masri, B.A. and Duncan, C.P. (2018) 'Revision for adverse local tissue reaction following metal-on-polyethylene total hip arthroplasty is associated with a high risk of early major complications', *Bone Joint J*, 100-B(6), pp. 720-724.
- Wei, Z., Chen, L., Thompson, D.M. and Montoya, L.D. (2014) 'Effect of particle size on in vitro cytotoxicity of titania and alumina nanoparticles', *Journal of Experimental Nanoscience*, 9(6), pp. 625-638.
- Weighardt, H., Jusek, G., Mages, J., Lang, R., Hoebe, K., Beutler, B. and Holzmann, B. (2004) 'Identification of a TLR4- and TRIF-dependent activation program of dendritic cells', *European Journal of Immunology*, 34(2), pp. 558-564.
- Whitehouse, M.R., Endo, M., Zachara, S., Nielsen, T.O., Greidanus, N.V., Masri, B.A., Garbuz, D.S. and Duncan, C.P. (2015) 'Adverse local tissue reactions in metal-on-polyethylene total hip arthroplasty due to trunnion corrosion: the risk of misdiagnosis', *Bone Joint J*, 97-B(8), pp. 1024-30.
- Witzleb, W.C., Ziegler, J., Krummenauer, F., Neumeister, V. and Guenther, K.P. (2006) 'Exposure to chromium, cobalt and molybdenum from metal-on-metal total hip replacement and hip resurfacing arthroplasty', *Acta Orthop*, 77(5), pp. 697-705.
- Xia, Z., Kwon, Y.M., Mehmood, S., Downing, C., Jurkschat, K. and Murray, D.W. (2011) 'Characterization of metal-wear nanoparticles in pseudotumor following metal-on-metal hip resurfacing', *Nanomedicine*, 7(6), pp. 674-81.
- Xia, Z., Ricciardi, B.F., Liu, Z., von Ruhland, C., Ward, M., Lord, A., Hughes, L., Goldring, S.R., Purdue, E., Murray, D. and Perino, G. (2017) 'Nano-analyses of wear particles from metal-on-metal and non-metal-on-metal dual modular neck hip arthroplasty', *Nanomedicine*, 13(3), pp. 1205-1217.
- Yang, S., Zhang, K., Jiang, J., James, B. and Yang, S.Y. (2019) 'Particulate and ion forms of cobalt-chromium challenged preosteoblasts promote osteoclastogenesis and

osteolysis in a murine model of prosthesis failure', *J Biomed Mater Res A*, 107(1), pp. 187-194.

Yarrow-Wright, L.E. (2018) *Development of a novel 3D in vitro model to measure cellular response to antioxidant doped highly cross-linked ultra high molecular weight polyethylene wear debris* University of Leeds.

Zhang, J., Alcaide, P., Liu, L., Sun, J., He, A., Luscinskas, F.W. and Shi, G.P. (2011) 'Regulation of endothelial cell adhesion molecule expression by mast cells, macrophages, and neutrophils', *PLoS One*, 6(1), p. e14525.

Zijlstra, W.P., Bulstra, S.K., Van Raay, J.J.A.M., Van Leeuwen, B.M. and Kuijer, R. (2012) 'Cobalt and chromium ions reduce human osteoblast-like cell activity in vitro, reduce the OPG to RANKL ratio, and induce oxidative stress', *Journal of Orthopaedic Research*, 30(5), pp. 740-747.

Zlotnik, A. and Yoshie, O. (2012) 'The chemokine superfamily revisited', *Immunity*, 36(5), pp. 705-16.